On Soft Limits of Large-Scale Structure Correlation Functions

Dissertation

zur Erlangung des Doktorgrades

an der Fakultät für Mathematik,

Informatik und Naturwissenschaften,

Fachbereich Physik

der Universität Hamburg

vorgelegt von

Laura Sagunski

aus

Schleswig

Hamburg

2016

Folgende Gutachter empfehlen die Annahme der Dissertation:

Gutachter der Dissertation und Disputation:	Dr. Thomas Konstandin
	Prof. Dr. Günter Sigl
Gutachter der Disputation:	Dr. Kai Schmidt-Hoberg
	Prof. Dr. Géraldine Servant
Vorsitzender der Prüfungskommission:	Prof. Dr. Dieter Horns
Tag der Disputation:	5. Juli 2016

To those who mean the world to me,

my amazing family,

and

my great love,
Timo.

Summary

Large-scale structure surveys have the potential to become the leading probe for precision cosmology in the next decade. To extract valuable information on the cosmological evolution of the Universe from the observational data, it is of major importance to derive accurate theoretical predictions for the statistical large-scale structure observables, such as the power spectrum and the bispectrum of (dark) matter density perturbations. Hence, one of the greatest challenges of modern cosmology is to theoretically understand the non-linear dynamics of large-scale structure formation in the Universe from first principles. While analytic approaches to describe the large-scale structure formation are usually based on the framework of non-relativistic cosmological perturbation theory, we pursue another road in this thesis and develop methods to derive generic, non-perturbative statements about large-scale structure correlation functions. We study unequal- and equal-time correlation functions of density and velocity perturbations in the limit where one of their wavenumbers becomes small, that is, in the soft limit.

In the soft limit, it is possible to link $(\mathcal{N}+1)$-point and $\mathcal{N}$-point correlation functions to non-perturbative 'consistency conditions'. These provide in turn a powerful tool to test fundamental aspects of the underlying theory at hand. In this work, we first rederive the (resummed) consistency conditions at *unequal times* by using the so-called eikonal approximation. The main appeal of the unequal-time consistency conditions is that they are solely based on symmetry arguments and thus are universal. Proceeding from this, we direct our attention to consistency conditions at *equal times*, which, on the other hand, depend on the interplay between soft and hard modes. We explore the existence and validity of equal-time consistency conditions within and beyond perturbation theory. For this purpose, we investigate the predictions for the soft limit of the bispectrum of density and velocity perturbations in two different approaches, namely in the perturbative time-flow approach and in a non-perturbative background method. This background method, which relies on absorbing a spherically symmetric soft mode into a locally curved background cosmology, has recently inspired a proposal for an (allegedly non-perturbative) angular-averaged equal-time consistency condition for the bispectrum of density perturbations (henceforth referred to as VKPR proposal). We demonstrate explicitly for an Einstein–de Sitter universe that the time-flow relations as well as the VKPR proposal are only fulfilled at leading order in perturbation theory, but are not exact beyond it. Since the VKPR proposal still leads to qualitatively accurate predictions for the bispectrum of density perturbations beyond the linear perturbative order, it can nevertheless be regarded as a reasonable *empirical* approximation in this case. However, transferring the VKPR proposal to the velocity perturbations significantly fails beyond linear order in perturbation theory. In consequence, we generalize the background method to properly account for the effect of local curvature both in the density and velocity perturbations on short distance scales. This allows us not only to identify the discrepancies of the VKPR proposal, but also to formulate a proper generalization of it which includes both the density

and velocity perturbations. In addition, we use the background method to deduce a generic, non-perturbative angular-averaged bispectrum consistency condition, which depends on the density power spectrum of hard modes in the presence of local curvature.

Building upon this, we proceed by deriving a non-perturbative equation for the power spectrum in the soft limit. To this end, we perform an operator product expansion, on the one hand, and deduce a non-perturbative *angular-dependent* bispectrum consistency condition, on the other hand. We obtain the latter from extending the background method to the case of a directional soft mode, being absorbed into a locally curved anisotropic background cosmology. The resulting non-perturbative power spectrum equation encodes the coupling to ultraviolet (UV) modes in two time-dependent coefficients. These can most generally be inferred from response functions to geometrical parameters, such as spatial curvature, in the locally curved anisotropic background cosmology. However, we can determine one coefficient by use of the angular-averaged bispectrum consistency condition together with the generalized VKPR proposal, and we show that the impact of the other one is subleading. Neglecting the latter in consequence, we confront the non-perturbative power spectrum equation against numerical simulations and find indeed a very good agreement within the expected error bars. Moreover, we argue that both coefficients and thus the non-perturbative power spectrum in the soft limit depend only weakly on UV modes deep in the non-linear regime. This non-perturbative finding allows us in turn to derive important implications for perturbative approaches to large-scale structure formation. First, it leads to the conclusion that the UV dependence of the power spectrum found in explicit computations within standard perturbation theory is an artifact. Second, it implies that in the Eulerian (Lagrangian) effective field theory (EFT) approach, where UV divergences are canceled by counter-terms, the renormalized leading-order coefficient(s) receive most contributions from modes close to the non-linear scale. The non-perturbative approach we developed can in principle be used to precisely infer the size of these renormalized leading-order EFT coefficient(s) by performing small-volume numerical simulations within an anisotropic 'separate universe' framework. Our results suggest that the importance of these coefficient(s) is a $\sim 10\%$ effect at most.

Zusammenfassung

Rotverschiebungssurveys zur Durchmusterung der großräumigen Struktur des Universums haben das Potential, innerhalb des nächsten Jahrzehnts die führende kosmologische Präzisionsmessung zu werden. Um aus den Beobachtungsdaten wertvolle Informationen über die kosmologische Entwicklung des Universums gewinnen zu können, ist es von größter Bedeutung präzise theoretische Vorhersagen für die statistischen Observablen der großräumigen Struktur des Universums, wie zum Beispiel das Leistungsspektrum und das Bispektrum der (Dunkle-) Materiedichtefluktuationen, zu machen. Eine der größten Herausforderungen der modernen Kosmologie ist es daher, die nicht-lineare Dynamik der kosmologischen Strukturbildung von Grund auf theoretisch zu verstehen. Während analytische Methoden zur Beschreibung der kosmologischen Strukturbildung in der Regel auf den Grundlagen der nicht-relativistischen kosmologischen Störungstheorie basieren, verfolgen wir in dieser Dissertation einen anderen Ansatz und entwickeln Methoden, um generelle, nicht-perturbative Aussagen über Korrelationsfunktionen der großräumigen Struktur des Universum herzuleiten. Hierfür untersuchen wir Korrelationen von Dichte- und Geschwindigkeitsfluktuationen ungleicher und gleicher Zeiten in dem Limes, in dem eine ihrer Wellenzahlen sehr klein wird, das heißt im sogenannten 'weichen' Limes.

In diesem weichen Limes ist es möglich, $(\mathcal{N}+1)$-Punkts- und $\mathcal{N}$-Punktskorrelationsfunktionen zu nicht-perturbativen 'Konsistenzbedingungen' zu verknüpfen. Diese bilden ihrerseits ein mächtiges Handwerkszeug, um fundamentale Aspekte der zugrundliegenden physikalischen Theorie zu testen. Im Rahmen dieser Arbeit leiten wir zunächst die (resummierten) Konsistenzbedingungen für ungleiche Zeiten her, indem wir die sogenannte Eikonalnäherung verwenden. Der größte Reiz dieser Konsistenzbedingungen für ungleiche Zeiten besteht darin, dass sie auschließlich auf Symmetrieargumenten beruhen und daher universell sind. Danach wenden wir uns den Konsistenzbedingungen für gleiche Zeiten zu, die andererseits von der Wechselwirkung zwischen weichen und harten Moden abhängen. Wir erforschen die Existenz und Gültigkeit von Konsistenzbedingungen für gleichen Zeiten innerhalb der Störungstheorie sowie über sie hinausgehend. Zu diesem Zweck untersuchen wir die Vorhersagen zweier verschiedener Methoden für den weichen Limes des Bispektrums der Dichte- und Geschwindigkeitsfluktuationen, nämlich zum einen der perturbativen 'time-flow'-Methode und zum anderen einer nicht-perturbativen Hintergrundmethode. Diese Hintergrundmethode, die auf der Absorbierung einer sphärisch symmetrischen weichen Mode in eine lokal gekrümmte Hintergrundkosmologie basiert, hat kürzlich zu einem (vermeintlich nicht-perturbativen) Vorschlag einer winkelgemittelten Konsistenzbedingung gleicher Zeiten für das Bispektrum der Dichtefluktuationen (fortan als VKPR-Vorschlag bezeichnet) geführt. Wir weisen explizit für ein Einstein-de-Sitter-Universum nach, dass die 'time-flow'-Relationen ebenso wie der VKPR-Vorschlag nur in Stöhrungstheorie erster Ordnung, nicht aber darüber hinaus, exakt sind. Da der VKPR-Vorschlag jenseits der Störungstheorie erster Ordnung dennoch zu qualitativ korrekten Vorhersagen für das Bispektrum der Dichtefluktuationen führt, kann er jedoch als eine

vernünftige *empirische* Näherung betrachtet werden. Wird der VKPR-Vorschlag allerdings auf die Geschwindigkeitsfluktuationen übertragen, ergeben sich signifikante Abweichungen jenseits der Störungstheorie erster Ordnung. Aufgrund dessen verallgemeinern wir die Hintergrundmethode, um den Effekt lokaler Krümmung auf die Dichte- und Geschwindigkeitsfluktuationen auf kurzen Distanzskalen physikalisch richtig zu beschreiben. Dadurch ist es uns möglich, nicht nur die Unstimmigkeiten des VKPR-Vorschlags auszumachen, sondern auch eine geeignete Verallgemeinerung des letzteren, die sowohl Dichte- als auch Geschwindigkeitsfluktuationen einbezieht, zu formulieren. Zusätzlich verwenden wir die Hintergrundmethode, um eine generelle, nicht-perturbative winkelgemittelte Bispektrumkonsistenzbedingung herzuleiten, die vom Dichteleistungsspektrum harter Moden in Gegenwart von lokaler Krümmung abhängt.

Wir fahren anschließend fort, indem wir eine nicht-perturbative Gleichung für das Leistungsspektrum im weichen Limes herleiten. Dafür führen wir einerseits eine Operator-Produkt-Entwicklung durch und ermitteln andererseits eine nicht-perturbative *winkelabhängige* Bispektrumkonsistenzbedingung. Wir erhalten diese, indem wir die Hintergrundmethode für den Fall einer gerichteten weichen Mode, die in eine lokal gekrümmte anisotrope Hintergrundkosmologie absorbiert wird, erweitern. Die resultierende nicht-perturbative Leistungsspektrumgleichung beinhaltet die Kopplung an ultraviolette (UV-)Moden durch zwei zeitabhängige Koeffizienten. Diese können am allgemeinsten durch Antwortfunktionen ('response functions') bezüglich geometrischer Parameter, wie etwa räumlicher Krümmung, in der lokal gekrümmten anisotropen Hintergrundkosmologie abgeleitet werden. Allerdings können wir einen Koeffizienten mithilfe der winkelgemittelten Bispektrumkonsistenzbedingung sowie des verallgemeinerten VKPR-Vorschlags bestimmen. Wir zeigen zudem, dass der andere Koeffizienten nur einen geringfügigen Einfluss hat. Daher vergleichen wir, unter Vernachlässigung des letzteren, die nicht-perturbative Leistungsspektrumgleichung mit numerischen Simulationen und stellen in der Tat eine sehr gute Übereinstimmung innerhalb der erwarteten Fehlergrenzen fest. Darüber hinaus erörtern wir, dass beide Koeffizienten und folglich das nicht-perturbative Leistungsspektrum im weichen Limes nur schwach von UV-Moden weit im nicht-linearen Bereich abhängen. Diese nicht-perturbative Erkenntnis ermöglicht es uns ihrerseits, wichtige Implikationen für perturbative Methoden der kosmologischen Strukturbildung abzuleiten. Zum einen führt sie zu der Schlussfolgerung, dass die UV-Abhängigkeit des Leistungsspektrums, die in expliziten Berechnungen innerhalb der perturabtiven Standardmethode ('standard perturbation theory') auftritt, ein Artefakt ist. Zum anderen impliziert sie, dass in der Eulerschen (Lagrangeschen) Methode der effektiven Feldtheorie (EFT), in der die UV-Divergenzen durch Gegenterme ('counter-terms') aufgehoben werden, die renormierten Koeffizient(en) führender Ordnung die größten Beiträge von Moden nahe des nicht-linearen Bereiches erhalten. Die von uns entwickelte nicht-perturbative Methode kann im Prinzip verwendet werden, um die Größe der renormierten EFT-Koeffizient(en) präzise mithilfe von numerischen Simulationen eines anisotropen unabhängigen Unversums ('separate universe') zu bestimmen. Unsere Ergebnissen nach entspricht die Relevanz dieser Koeffizient(en) allenfalls einem $\sim 10\%$-Effekt.

The results presented in this thesis are based on the following publications:

[1] I. Ben-Dayan, T. Konstandin, R. A. Porto, and L. Sagunski, "On Soft Limits of Large-Scale Structure Correlation Functions," *JCAP* **1502** no. 02, (2015) 026, `arXiv:1411.3225 [astro-ph.CO]`.

[2] M. Garny, T. Konstandin, R. A. Porto, and L. Sagunski, "On the Soft Limit of the Large Scale Structure Power Spectrum: UV Dependence," *JCAP* **1511** no. 11, (2015) 032, `arXiv:1508.06306 [astro-ph.CO]`.

Contents

Contents

Contents

List of Figures

Nomenclature

ΛCDM universe .... Universe with cosmological constant Λ and CDM

2dFGRS .... 2-degree Field Galaxy Redshift Survey

BAO .... Baryon acoustic oscillations

BBGKY hierarchy .... Bogoliubov–Born–Green–Kirkwood–Yvon hierarchy

BICEP .... Background Imaging of Cosmic Extragalactic Polarization

BOSS .... Baryon Oscillation Spectroscopic Survey

CAMB .... Code for Anisotropies in the Microwave Background

CDM .... Cold dark matter

CMB .... Cosmic microwave background

COBE .... COsmic Background Explorer

COLA .... COmoving Lagrangian Acceleration

DES .... Dark Energy Survey

DESI .... Dark Energy Spectroscopic Instrument

DM .... Dark matter

e.g. .... From Latin 'exempli gratia', for example

EAGLE .... Evolution and Assembly of GaLaxies and their Environments

eBOSS .... enhanced BOSS

EdS universe .... Einstein–de Sitter universe

Nomenclature

EFT .... Effective field theory

ESA .... European Space Agency

FRW metric .... Friedmann–Robertson–Walker metric

GADGET .... GAlaxies with Dark matter and Gas intEracT

GW .... Gravitational wave

i.e. .... From Latin 'id est', that is

IR .... Infrared

LEFT .... Lagrangian-space EFT

LIGO .... Laser Interferometer Gravitational-Wave Observatory

LO .... Leading order

LPT .... Lagrangian perturbation theory

LSS .... Large-scale structure

LSST .... Large Synoptic Survey Telescope

NL .... Non-linear

NLO .... Next-to-leading order

NNLO .... Next-to-next-to-leading order

OPE .... Operator product expansion

PT .... Perturbation theory

RG .... Renormalization group

RGPT .... Renormalization group perturbation theory

RPT .... Renormalized perturbation theory

SDSS .... Sloan Digital Sky Survey

SNe .... Supernovae

SPT .... Standard perturbation theory

TF .... Trace-free

TRG approach .... Time-renormalization group approach

UV .... Ultraviolet

VKPR proposal .... Proposal by Valageas, and also by Kehagias, Perrier and Riotto

WFIRST .... Wide Field Infrared Survey Telescope

WMAP .... Wilkinson Microwave Anisotropy Probe

ZA .... Zel'dovich approximation

Chapter 1

Introduction

> *"I, however, believe that there is at least one philosophical problem in which all thinking men are interested. It is the problem of cosmology: the problem of understanding the world – including ourselves, and our knowledge, as part of the world. All science is cosmology, I believe, and for me the interest of philosophy, no less than that of science, lies solely in the contributions which it has made to it."*
>
> — Sir Karl Raimund Popper, *The Logic of Scientific Discovery* [3]

Preface

The recent first direct detection of gravitational waves (GW) from a merging black hole binary system by the Laser Interferometer Gravitational-Wave Observatory (LIGO) [4] is not only a confirmation of a century-old major prediction of Einstein's general relativity [5], but marks the dawn of new era for testing the fundamental properties of the theory of gravitation [6–8]. Moreover, it paves the way for establishing direct GW detection as an unprecedented window into the Universe with the potential to probe gravitational waves both from astrophysical sources and of (primordial) cosmological origin in the near future (see for instance [9, 10]).

Cosmology itself – as the study of the beginning, evolution and composition of the physical Universe – has already reached a 'golden age' [11] at this present time. Within the last decades, tremendous observational progress accompanied by a spectacular amount of high-accuracy data has heralded an era of precision cosmology. Thereby, measurements of the temperature fluctuations in the cosmic microwave background (CMB) by the COsmic Background Explorer (COBE) [12], the Wilkinson Microwave Anisotropy Probe (WMAP) [13] and more recently by

1. Introduction

the Planck satellite[1] [16, 17], as well as the imprint of the baryon acoustic oscillations (BAOs) in the large-scale structure (LSS) observed by galaxy redshift surveys such as the ground-based Sloan Digital Sky Survey (SDSS) [18, 19] (see Figure 1.1) and distance measurements based on type Ia supernovae (SNe) [20, 21] are probably the most eminent examples for observational probes that contributed to the establishment of a 'concordance model' of the Hot Big Bang cosmology, the ΛCDM model.

In this standard cosmological model, the Universe is homogeneous and isotropic on its largest scales, spatially flat ($\Omega_K \simeq 0$), with a mass-energy density being dominated not by baryonic matter ('b'), but by cold dark matter (CDM) and dark energy in form of a cosmological constant Λ (with density parameters $\Omega_{b,0} \simeq 0.05$, $\Omega_{DM,0} \simeq 0.26$, $\Omega_{\Lambda,0} \simeq 0.69$ at present time) [17]. Moreover, the cosmological observations offer powerful evidence in favor of simple (single-field) inflationary models [22], providing an attractive mechanism for generating the nearly scale-invariant (with spectral index $n_s \simeq 0.97$) primordial power spectrum of highly Gaussian, adiabatic (scalar) seed perturbations [23].

The measurements of the anisotropies in the CMB by the Planck satellite have provided invaluable information about the origin of the seeds of structure [17, 22], which have plausibly been created out of quantum fluctuations during an inflationary phase of accelerated, exponential expansion in the very Early Universe [24–26] (for reviews see [27–29]), as well as about their development throughout the cosmological ages into the present large-scale structure. While this is a remarkable achievement, many issues regarding the nature of an inflationary cosmology remain unresolved. Perhaps the most outstanding one is whether a slowly-rolling, weakly coupled fundamental scalar field played the role of the Higgs mechanism for the Early Universe or if the Universe chose a different path, such as dynamics of strong coupling or supersymmetry [30–32]. These possibilities remain viable candidates to play a role in the Early Universe and have not been considerably hindered by the Planck data [30]. In particular, the currently existing bounds on (equilateral) non-Gaussianity [23] lie still above certain well-motivated theoretical thresholds (see e.g., [30–36]). A venue to improve on our present understanding of cosmological evolution of the Universe and address the origin of both its late and its (very plausibly) early phase of accelerated expansion is provided by the study of the large-scale structure of the Universe [37].

Large-scale structure surveys are due to become the next leading probe for precision cosmology in the next decade. Through ambitious observational programs, the currently under way and upcoming galaxy redshift surveys will be able to constrain the cosmological model and

---

[1]In addition to these satellite missions, a new generation of ground-based observatories, among them the BICEP (Background Imaging of Cosmic Extragalactic Polarization) experiment [14] and the Keck Array [15] provide an unprecedented sensitivity to measure the B-mode polarization of the CMB.
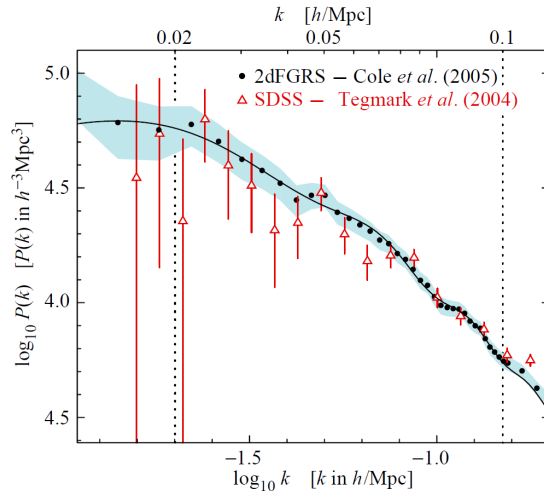
Fig. 1.1.: Power spectrum of the galaxy distribution from the 2-degree Field Galaxy Redshift Survey (2dFGRS) [38] and the Sloan Digital Sky Survey (SDSS) [18] (reprinted from [39]). While the 2dFGRS galaxy power spectrum is shown by the black circles with a shaded 1σ-error band, the SDSS galaxy power spectrum is displayed by the red triangles and error bars. The solid curve corresponds to the best theoretical fit for the ΛCDM concordance model and is normalized to the 2dFGRS galaxy power spectrum [38]. The power spectrum of the galaxy number density fluctuations is related to the dark matter density power spectrum by a bias parameter (see e.g., [40]). For wavenumbers $k \gtrsim 0.05\,h/\mathrm{Mpc}$, one can see the characteristic signature which has been imprinted in the galaxy distribution by sound waves of the baryon-photon fluid in the Early Universe. These are the so-called baryon acoustic oscillations (BAOs) [41, 42].

the nature of dark energy with remarkable accuracy. Since the turn of the century, galaxy redshift surveys, as for instance SDSS (see before) or the 2-degree Field Galaxy Redshift Survey (2dFGRS) [38, 43], have confirmed the rich variety of the large-scale structure in the Universe (see Figure 1.2). Besides groups, clusters and superclusters of galaxies, the observed three-dimensional distribution of galaxies shows walls, filaments and voids. Recently, the Baryon Oscillation Spectroscopic Survey (BOSS) [44, 45], as a part of the SDSS-III project [46], has provided the largest volume of the low-redshift Universe ever surveyed, with a galaxy density valuable for precision cosmology.[2]

---

[2]BOSS has mapped $1.5 \cdot 10^6$ luminous galaxies covering a survey area of $10^4\,\mathrm{deg}^2$ to measure the scale of the baryon-acoustic oscillations in the clustering of matter up to redshifts $z < 0.7$ [44]. Here, the unit of square degrees 'deg^2' constitutes a measure of the solid angle, with the whole sphere being equal to $4\pi\,(180/\pi)^2\,\mathrm{deg}^2 \simeq 4.12 \cdot 10^4\,\mathrm{deg}^2$.

1. Introduction
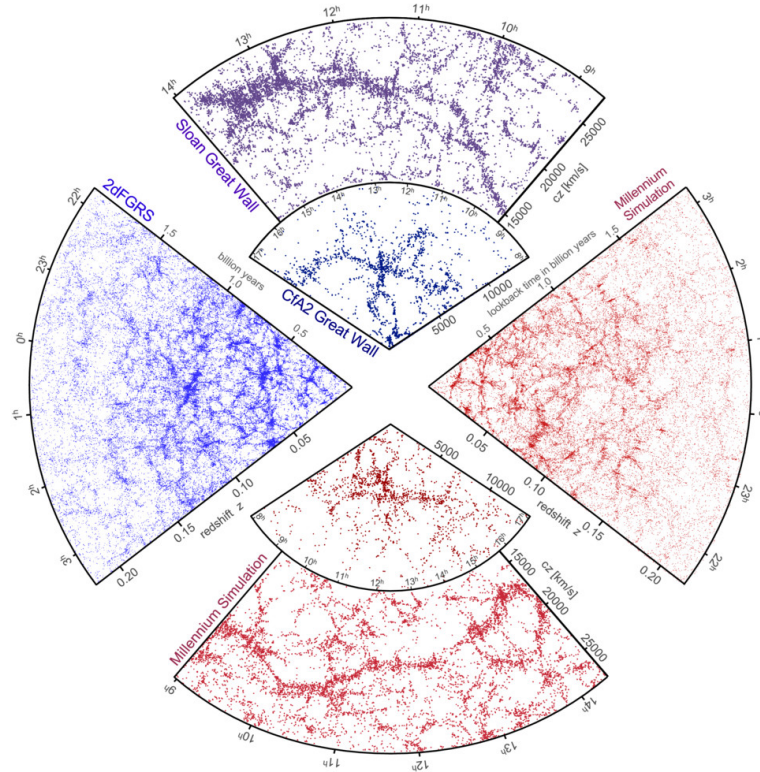
Fig. 1.2.: Galaxy distribution map from the 2-degree Field Galaxy Redshift Survey (2dFGRS) [38, 43] and the Sloan Digital Sky Survey (SDSS) [18, 19] as well as from 'mock' catalogs based on the Millenium simulation [47–49] (reprinted from [50]). The radial direction indicates the redshift, whereas the polar angle is the right ascension.

Here, the two slices at the top show the Great Wall [51], with the Coma Cluster at the center, and the Sloan Great Wall, which has been identified by SDSS [52]. The latter is one of the largest observed structures in the Universe, stretching over more than $\sim 10^9$ ly (light years) and containing more than $\sim 10^4$ galaxies. Besides, the cone on the left shows a part of the galaxy distribution map from 2dFGRS, which has in total determined the distances of more than 220 000 galaxies.

At the bottom and on the right, mock catalogs of the galaxy distribution, selected according the maps of the surveys, are depicted. These have been constructed with semi-analytic techniques to describe the formation and distribution of galaxies within the dark matter evolution modeled by the Millenium simulation.

In the next decade, the advent of additional ground-based galaxy redshift surveys, such as the Dark Energy Survey (DES) [53, 54], the enhanced Baryon Oscillation Spectroscopic Survey (eBOSS) [55], the Dark Energy Spectroscopic Instrument (DESI) [56] and the Large Synoptic

Survey Telescope (LSST) [57], as well as complementary spaceborne surveys like the Wide Field Infrared Survey Telescope (WFIRST) [58] or the ESA Euclid satellite mission [59, 60] will revolutionize observational cosmology by measuring the distribution of galaxies with unprecedented accuracy. Thus, they will be able to address the very fundamental open questions of cosmology, namely the physics of inflation as origin of the seeds of structure, the properties of dark matter, the nature of dark energy or alternatively modifications of gravity on cosmological scales [59, 61].

While CMB measurements primarily supply two-dimensional data from the last-scattering surface, large-scale structure surveys map the three-dimensional distribution of galaxies in the Universe and hence contain more, potentially richer cosmological information [62]. In principle, they provide roughly a 1000-fold increase in the number of modes available compared to the CMB [63]. However, extracting this information is a daunting task due to the currently more limited theoretical understanding of LSS physics in the low-redshift universe, which is additionally complicated by the non-linear nature of dark matter clustering. In fact, according to the nowadays widely accepted physical picture, the present large-scale structure grew in the expanding Universe out of the small primordial seed fluctuations in the matter density through the dynamics of gravitational instability, driven by the dominant dark matter density component. Thus, one of the main goals of present cosmology is to theoretically understand the dynamics of large-scale structure formation and derive reliable theoretical predictions for the LSS observables from it.

To date, most cosmological implications from large-scale structure data have been drawn by confronting it against the theoretical predictions for the power spectrum, i.e., the (connected) two-point correlation function, of (dark) matter density perturbations. This statistical LSS observable encodes all the information available if the primordial random density fluctuations are Gaussian distributed. However, in order to fully exploit the wealth of information contained in the large-scale structure data, it is also important to study higher-order statistical correlation functions, such as the bispectrum, the (connected) three-point correlation function, of density perturbations. For instance, since the density bispectrum is initially zero for Gaussian-distributed density perturbations and subsequently generated only due to the non-linear dynamics of dark matter clustering [64], theoretical predictions of the latter directly allow to constrain primordial non-Gaussianity [65–71] (for constraints from the density power spectrum see [72–77]).

However, providing sufficiently accurate theoretical predictions for the large-scale structure observables even in the simplest cosmological models is a challenging task due to the non-linear nature of dark matter clustering. Due to this, the traditional approach to model the

dynamics of gravitational instability consists in performing numerical N-body simulations of collisionless cold dark matter particles (for an introduction to different N-body methods and a review of the latest numerical techniques, we refer to [40] and [78], respectively). Using numerical simulations to model the dynamics of gravitational instability has a long and distinguished history, dating back to the year 1960 where the first computer calculations were performed with a number of $N = 16$ collisionless particles [79]. By comparison, current state-of-the-art simulations, such as Millenium Simulation [47–49] carried out with the N-body code GADGET [80, 81] [3], involve more than $N = 10^{10}$ particles (see also Figure 1.2). For other advanced numerical simulations see e.g., [82–84]. While these N-body simulations model the gravitational clustering of pure dark matter particles, the challenge however lies in including the baryonic matter component to predict the formation and distribution of observable luminous galaxies. In fact, appropriate hydrodynamic simulations which account for the fluid motion (hydrodynamic evolution) of the baryons as well as the dynamics of gravitational instability, such as the Illustris or EAGLE (Evolution and Assembly of GaLaxies and their Environments) project [85, 86], are computationally very expensive and thus only applicable for a limited range of distance scales. Due to this limitation, one uses instead algorithms, as for instance COLA (COmoving Lagrangian Acceleration) [87, 88] or PTHalos, that combine N-body simulations for small distance scales with analytic approaches of cosmological perturbation theory (PT) for large distance scales, to generate 'mock' catalogs of the galaxy distribution and extract the statistical large-scale structure observables thereof.

Even though these numerical methods provide fairly accurate theoretical predictions for the large-scale structure observables, the considerations above reveal a number of reasons to resort instead – when possible – to analytic approaches [89]. First of all, it is currently challenging to perform hydrodynamic simulations including baryonic matter. Moreover, simultaneously scanning over a large set of cosmological parameters or models and a wide dynamical range of scales becomes computationally expensive and time consuming the higher the precision is targeted (for a critical analysis of the ultimate level of accuracy and feasibility of numerical simulations see [90]). Finally and most importantly, the development of analytic approaches to assess the dynamics of large-scale structure formation allows to gain a fundamental understanding of the underlying physics from first principles.

Since the very early days of modern cosmology [40, 91, 92], analytic approaches within the framework of non-relativistic cosmological perturbation theory, both in Eulerian and Lagrangian space, have been developed with the aim to describe the formation of the large-scale structure in the Universe from first principles. By far the most studied analytic approach to

---

[3]The abbreviation GADGET stands for 'GAlaxies with Dark matter and Gas intEracT'.

model the dynamics of LSS formation is the so-called standard perturbation theory (SPT) in Eulerian space (see for instance [40, 92–102]). It is based on solving the non-linear perfect fluid equations of the dark matter clustering in Fourier space by a perturbative expansion in terms of the linearly evolved matter density contrast. This perturbative ansatz is well justified as long as the real-space density contrast, describing the relative deviation of the matter density from the spatially-averaged mean matter density, is very small compared to unity. This is the case on large distance scales (corresponding to small momentum scales in Fourier space) and at early times (or high redshifts).

While the density contrast is the fundamental physical quantity in the Eulerian framework of perturbation theory, Lagrangian perturbation theory (hereafter LPT) implements a displacement vector field as basic dynamical variable [103–127]. In particular, by proceeding from the linear perturbative order of this displacement field, the Zel'dovich approximation (ZA) [91] derives an approximate solution to the fluid equations (for its applications see e.g., [105, 128–137]). Both the perturbative approaches of SPT and LPT have certain advantages, but reveal shortcomings as well [138–141]. However, LPT has received less attention in the past than SPT as its Eulerian counterpart, partly because it has – in addition to the shortcomings of SPT – the drawback that the Lagrangian picture breaks down once shell-crossing occurs in the clustering process.

Although SPT as a perturbative method provides valuable insights in the dynamics of LSS formation [40], it has been realized soon that its shortcomings lead to a fundamental limitation of its predictive power. For instance, its perturbative predictions for the power spectrum of matter density perturbations possess only a small range of validity beyond linear order at late times (or equivalently at low redshifts) and show poor convergence properties due to the appearance of UV-divergent integrals (see [102]). Hence, a lot of effort has been devoted in the last decade to the development of alternative perturbative LSS approaches with the aim to overcome the intrinsic limitations of SPT and extend the range of reliable perturbative predictions for the density power spectrum from the weakly to the mildly non-linear regime. Thereby, predicting the power spectrum of density perturbations accurately in the mildly non-linear regime is of particular interest since it contains invaluable information about the cosmological evolution encoded in the features of the baryon acoustic oscillations.

The first significant progress in this direction was made by the pioneering work of the renormalized perturbation theory (RPT) approach [142–144] (see also [142–146] in this context). Based on the observation that large perturbative contributions arising from soft, long-wavelength effects can be resummed in SPT, it reorganized the perturbative expansion using techniques of quantum field theory and the theory of turbulence in hydrodynamics [147]. Compared to SPT, the method of RPT leads indeed to an improvement of the convergence

properties of the power spectrum on intermediate scales. This success of RPT motivated the development of a plethora of resummation schemes in the years that followed [114, 116, 148–163]. Among others, two interesting approaches are the so-called closure theory [149] and the time-flow approach [156], also referred to as time-renormalization group approach (TRG). Their particular characteristic consists in extending the fluid equations to an infinite hierarchical system of evolution equations directly formulated in terms of the final quantities of interest, namely correlation functions such as the power spectrum and the bispectrum. One then relies on truncating the infinite hierarchy of evolution equations to a closed system of equations by an appropriate 'closure approximation' to derive a perturbative solution of the correlation functions in these approaches. In general, all of the resummation techniques lead to relatively accurate perturbative predictions on the onset of non-linearity, but fail on sufficiently large momentum scales. A detailed overview of the different resummation schemes can be found in the review articles [100, 138–141, 164].

The main recent focus of analytic studies in the field of LSS formation can be broadly classified in two categories [89, 100]. On the one hand, the impact of *soft, long-wavelength (IR)* perturbations on modes around the scale of the baryon acoustic oscillations has been addressed from different directions, for instance comprising symmetry arguments, such as (extended) Galilean invariance and the equivalence principle [165–177], or by applying the eikonal approximation [101, 159, 160].

On the other hand, considerable efforts have been directed towards understanding the influence of *hard, short-wavelength (UV)* perturbations. Their treatment is further complicated by the inherently non-linear process of dark matter clustering on short momentum scales. In this regard, the semi-analytic effective field theory (EFT) approach to large-scale structure [49, 63, 178–207] and its formulation in Lagrangian space (LEFT) [89, 208] has emerged as a useful tool to parameterize the imprint of UV modes on long-distance observables and push the validity of perturbation theory towards short(er) distance scales. In the EFT approach, corrective terms with effective parameters are added to the perturbative expansion in SPT (see e.g., [63, 178, 208]). These EFT parameters are split into a counter-term to cancel possible UV divergences of the perturbative expansion in SPT and a (physical) renormalized piece that accounts for deviations from the perfect-fluid approximation on short distance scales. Subsequently, the renormalized parameters are determined from observational data and numerical simulations. In addition, partly motivated by results from N-body simulations [209, 210], complementary analytic approaches have been put forward with the aim to circumvent the intrinsic limitations of SPT from first principles [102, 211–216].

Motivation

In this thesis, however, we pursue another road. To check the consistency of different perturbative approaches and, in greater depth, to test the fundamental aspects of the underlying theory against observations or numerical simulations, it is of major importance to gain non-perturbative and method-independent information on large-scale structure observables. Given the complexity of correlation functions in the theory of structure formation as such, examples of these non-perturbative statements are rare. A case in which the derivation of non-perturbative predictions is possible is the so-called squeezed or *soft limit* of large-scale structure correlation functions, that is, the limit where one of their wavenumbers becomes small. For this reason, our motivation in this thesis consists in investigating large-scale structure correlation functions in the soft limit. We develop methods to derive correlation functions of the matter density and velocity perturbations, such as the power spectrum and the bispectrum, in the soft limit non-perturbatively. In turn, we use these non-perturbative relations to address shortcomings in perturbation theory and explore implications within and beyond it.

In the soft limit, it is for instance possible to link $(\mathcal{N} + 1)$-point and $\mathcal{N}$-point correlation functions of density and velocity perturbations to so-called 'consistency conditions'. These consistency conditions do not only allow to derive non-perturbative statements, but are also independent of the details of the physics on short distance scales, which can be highly nonlinear. Hence, they provide a powerful tool for probing basic aspects of the underlying theory at hand. Due to the huge amount of data that future large-scale structure surveys will deliver, the consistency conditions in the context of structure formation might be possibly even more valuable than the inflationary ones (see e.g., [33, 217–227]). Indeed, large-scale structure consistency conditions have recently received significant attention [167–171, 173–176, 228–234]. They can be derived for correlation functions of density and velocity fields evaluated at equal or unequal times.

The main appeal of the consistency conditions for *unequal-time* correlation functions lies in the fact that they can be deduced solely from symmetry arguments and hence are universal. They are only based on the general assumption of a single-field inflationary background, providing the initial conditions for the seeds of structure, and the diffeomorphism invariance (general covariance) of general relativity. For this reason, the unequal-time consistency conditions provide fairly generic, non-perturbative predictions about the dynamics on short distance scales, which can serve as a probe of the underlying assumptions and the fundamental aspects of the theory [165–171, 228, 235]. Hence, confronted against observations of forthcoming large-scale structure surveys, they will allow to test single-field inflation as the theory

providing the initial seed perturbations, as well as the equivalence principle in gravitational theories, especially since fluctuations enter the non-linear regime at small redshift.

In this work, we (re-)derive the consistency conditions for unequal-time correlation functions of both density and velocity perturbations. For this purpose, we work in the Eulerian framework of cosmological perturbation theory and use the compact notation of the large-scale structure fluid equations, simultaneously including the density and velocity perturbation fields (see for instance [40, 236]). One crucial aspect in the derivation of the unequal-time consistency conditions is the factorization of soft and hard modes. Here, we apply the eikonal approximation which naturally accounts for the resummation of the soft mode into a so-called eikonal phase [159, 160, 237]. Moreover, it allows to derive consistency conditions for unequal-time correlation functions of both the density and velocity fluctuations in a straightforward and transparent way.

However, these consistency conditions become degenerate for the observationally most interesting case of *equal-time* correlation functions, in the sense that they vanish at leading order in the soft momentum (the long-wavelength mode) q. In order to gain information about equal-time correlation functions, one thus needs to investigate next-to-leading order (NLO). Beyond leading order, the equal-time correlators depend, on the other hand, on the interplay between soft and hard modes so that dynamical information starts to become relevant [165, 166, 224]. Hence, it is important to investigate the existence and validity of equal-time consistency conditions even for short-distance modes deep in the non-linear regime. In fact, allegedly non-perturbative (angular-averaged) consistency conditions have been advocated in the recent literature [173, 174].

To explore under which circumstances consistency conditions for equal-time correlation functions exist beyond a perturbative treatment of the hard modes, we first compute the soft limit of the angular-averaged connected three-point function, namely the bispectrum, up to next-to-leading order in SPT. This serves us as a benchmark for subsequently comparing different perturbative and non-perturbative methods. We investigate the predictions for the soft-limit of the bispectrum in two different approaches, namely in the perturbative time-flow approach (also known as time-renormalization group (TRG) approach) [156], and in a non-perturbative background method where the soft mode is absorbed into a locally curved cosmology, on the other hand.

The time-flow approach constitutes a perturbative method which is based on truncating a hierarchical system of differential evolution equations for equal-time correlation functions, the flow equations, by applying a 'closure' approximation. In general, perturbative statements can be derived in the time-flow approach only by imposing a suitable closure approximation.

Usually, the closure approximation truncating the infinite hierarchy of flow equations consists in neglecting the connected four-point correlation function, i.e., the trispectrum. However, we show that the latter plays an important role in assessing the validity of an equal-time consistency condition for the angular-averaged bispectrum in the soft limit derived from the time-flow approach.

The non-perturbative background method, on the other hand, implements a map between the dynamics on short distance scales within a flat Friedmann–Robertson–Walker (FRW) cosmology in the presence of a spherically symmetric long-wavelength perturbation and a locally curved FRW universe. Thereby, the soft mode is absorbed into the locally curved background cosmology. This background method, first discussed in [165, 166], is referred to as 'separate universe' approach in the context of N-body simulations where it is used to determine the so-called power spectrum response function [238–241]. It is exactly this equivalence between a soft, long-wavelength perturbation in a flat universe and a locally curved background which has inspired a proposal for an (allegedly non-perturbative) 'equal-time consistency condition' for the angular-averaged bispectrum of density perturbations by Valageas, and also by Kehagias, Perrier and Riotto (VKPR) in [173, 174].

Since the VKPR proposal is advocated in [173, 174] as being valid even in the non-linear regime, we compare its predictions for the bispectrum of density perturbations up to one-loop order with the ones derived in SPT. This gives us a first insight into the validity and quantitative accuracy of the VKPR proposal within the realm of perturbation theory.

For assessing the validity of the VKPR proposal beyond perturbation theory, we subsequently derive a non-perturbative angular-averaged consistency relation for the bispectrum in the soft limit from first principles. For this purpose, we develop a straightforward and shortened derivation of the relevant transformations in the background method. Building upon that, we use these transformations to relate the bispectrum of density perturbations in the soft limit to the variation of the power spectrum on short distance scales in the presence of local curvature. As a result, we obtain a generic, non-perturbative angular-averaged bispectrum consistency condition. In turn, we confront this non-perturbative bispectrum relation against the VKPR proposal. Thereby, we identify the differences between these relations and work out the reasons behind them. This allows us to draw a final conclusion about the validity of the VKPR proposal within and beyond perturbation theory. In addition, we derive a generalization of the background method to properly incorporate the effect of local curvature not only in the density perturbations on short distance scales but also in the respective velocity fluctuations. Thereby, we reveal that the velocity fluctuations react differently (by a factor of the order one) to the presence of local curvature than the density perturbations. Based on this, we formulate a generalization of the VKPR proposal that includes both the density and

1. Introduction

velocity perturbation fields.

Building upon the derivation of the non-perturbative relation for the bispectrum in the soft limit, we proceed in the same direction afterwards. In fact, our aim consists in deducing a non-perturbative equation for the power spectrum in the soft limit.

To arrive at such a power spectrum equation, a rather sophisticated procedure is required. For instance, one needs to include information deduced from an *angular-dependent* non-perturbative relation for the bispectrum in the soft limit. Hence, we first use an operator product expansion (OPE) to infer the structure of such a bispectrum relation and to parameterize its angular dependence in terms of Legendre polynomials. Based on the fluid equations, we then derive a non-perturbative differential evolution equation for the power spectrum in the soft limit which includes two-non linear contributions depending on the bispectrum. However, on the basis of the overall momentum dependence of each of the non-linear contributions, we can subsequently deduce the bispectrum contributions remaining after performing the loop integral. This allows us finally to formulate the non-perturbative equation for the power spectrum in the soft limit solely in terms of two time-dependent coefficients, encoding in particular the dependence of the ultraviolet (UV) modes.

To extract these coefficients, we subsequently need to determine the non-perturbative angular-dependent consistency condition for the bispectrum in the soft limit explicitly. Thus, we generalize the background method from the case of a spherically symmetric soft mode to the one of a *directional* long-wavelength perturbation. Thereby, we implement a map between a flat FRW cosmology in the presence of a directional soft mode and a locally curved anisotropic universe. From the resulting angular-dependent bispectrum consistency condition we determine the coefficients entering in the non-perturbative power spectrum equation. These constitute a function of the variance of the 'displacement fields' on short distance scales or equivalently the momentum integrated power spectrum of hard modes, albeit to some extent in a locally curved anisotropic universe. However, since one of the coefficients is suppressed compared to the other, we perform a truncation of the non-perturbative power spectrum equation. We demonstrate that the remaining contribution can be determined by use of the angular-averaged bispectrum consistency condition only and use the generalized VKPR proposal to evaluate its curvature dependence.

In the numerical analysis performed afterwards, we solve the truncated equation for the power spectrum in the soft limit and show that it fares relatively well against numerical simulations. Besides, we estimate the overall error in the non-perturbative power spectrum equation induced by neglecting the impact of one coefficient and approximating the curvature dependence of the other one by the generalized VKPR proposal. Furthermore, we study

12

the dependence of the non-perturbative power spectrum in the soft limit on the hard modes beyond the non-linear scale. Since their impact on the non-perturbative power spectrum is encoded in the momentum integral of variance of the displacement fields, we evaluate the latter by introducing a cutoff scale. From the conclusions we draw about the dependence of the non-perturbative power spectrum on hard modes deep in the non-linear regime, we finally deduce important ramifications for the power spectrum in perturbation theory. To be precise, our findings allow us to address the UV dependence of the power spectrum observed in explicit computations within SPT as well as to derive implications for the renormalized leading-order coefficient(s) in the effective field theory (EFT) approach of large-scale structure.

Outline of the thesis

The remainder of this thesis is structured as follows. After this introductory chapter, we develop in Chapter 2 the theoretical framework to analytically describe the formation of the large-scale structure in the Universe. We first discuss the dynamics of gravitational instability in the expanding Universe and derive the large-scale structure fluid equations of the dark matter evolution. These are exactly the fluid equations which one aims to solve by a perturbative expansion in terms of the linear density contrast within the Eulerian framework of cosmological perturbation theory. In Chapter 3, we review the basic concept of the standard perturbation theory approach to solve the fluid equations perturbatively, proceeding from the linear to the non-linear solutions and accounting for different cosmological models. To go beyond that, we rewrite the non-linear fluid equations in a compact form which allows for a diagrammatic interpretation of the perturbative solutions in SPT.

Based on these perturbative solutions of the fluid equations, we derive in Chapter 4 the perturbative predictions for the statistical large-scale structure observables such as the power spectrum and the bispectrum, which we define as connected parts of correlation functions. Moreover, we extend the diagrammatic representation of SPT to present the perturbative contributions to the correlation functions in terms of tree-level and loop diagrams. By the example of the perturbative predictions for the power spectrum in SPT, we point out the qualitative and quantitative shortcomings of SPT afterwards (see Chapter 5). Subsequently, we present an overview of different approaches in cosmological perturbation theory aiming at addressing these drawbacks and improving the perturbative predictions for the large-scale structure observables. Subsequently, we discuss a few specific perturbative approaches in further detail, namely the framework of renormalized perturbation theory (RPT), the eikonal approximation as well as the time-flow approach.

We refer to these particular perturbative approaches or make use of their characteristic

properties in the chapters that follow. For instance, we apply the eikonal approximation in Chapter 6 to (re-)derive the consistency conditions for unequal-time correlation functions in the soft limit. Moreover, to explore the existence of equal-time consistency conditions, we first investigate the perturbative predictions of the time-flow approach for the angular-averaged bispectrum in the soft limit, before proceeding to the non-perturbative background method. By use of this, we then derive a non-perturbative angular-averaged bispectrum consistency condition to assess the validity of the VKPR proposal and additionally deduce a generalization of the latter. It turns out that these are the two ingredients needed to evaluate the truncated non-perturbative power spectrum equation in the soft limit that we derive in Chapter 7. The numerical analysis of this non-perturbative power spectrum allows us in turn to derive implications for the power spectrum in perturbation theory, in particular with regard to SPT and the EFT of LSS. Finally, in Chapter 8 we summarize the main conclusions of this thesis and presents an outlook with interesting aspects for future work.

For computational details, we refer to Appendix A which contains, our calculation of the SPT bispectrum at one-loop order in the soft limit as well as an estimate for the impact of the coefficient neglected in the truncated non-perturbative power spectrum equation.

Unless marked otherwise, the results in this thesis have been worked out by myself. Chapter 6 and Chapter 7 are based on the publications [1] and [2], respectively.

Notations and conventions

Throughout this thesis, we choose the signature of the spacetime metric to be $(-+++)$ and use the Einstein summation convention to implicitly sum over repeated indices. Thereby, the range of the sum is dictated by the nature of the indices. In detail, spacetime indices are denoted by small Greek letters, e.g., $\mu, \nu = \{0, 1, 2, 3\}$, whereas Latin indices, such as $i, j = \{1, 2, 3, \ldots\}$, refer to conventional summations. (Particularly in this work, we label the power spectrum and the bispectrum usually by indices a, b, c which are either 1 or 2, indicating the density or velocity perturbations, respectively.) Furthermore, we denote three-dimensional vectors, such as the comoving momentum $\boldsymbol{k}$, in boldface and their magnitudes by $|\boldsymbol{k}| \equiv k$.

To account for the expansion of the Universe, we usually work in comoving spacetime coordinates $(\boldsymbol{x}, \tau)$, which are related to the physical coordinates $(\boldsymbol{r}, t)$ by the scale factor $a(\tau)$. Since the scale factor is a universal function of time τ, we also take $a(\tau)$ itself, its logarithm $\ln a(\tau)$ (related to the parameter η) and the cosmological redshift z,

$$1 + z = \frac{a_0}{a(\tau)} \tag{1.1}$$

with present-time value $a_0 \equiv 1$, as a measure of time.

Furthermore, we work in natural units where the speed of light c and the reduced Planck constant $\hbar$ are equal to unity,

$$c = \hbar \equiv 1 \,. \tag{1.2}$$

In cosmology, distances which are measured via redshift z and converted to physical length scales by Hubble's law [242] incorporate the uncertainty of the present value of the Hubble parameter, the so-called Hubble constant H_0.[4] The uncertainty in the Hubble constant is usually expressed by the dimensionless Hubble parameter h (not to be confused with the Planck constant), defined as [243]

$$H_0 = 100 \, h \, \frac{\mathrm{km}}{\mathrm{s} \cdot \mathrm{Mpc}} \simeq \frac{1}{3000} \, h/\mathrm{Mpc} \tag{1.3}$$

with $1\,\mathrm{pc} \simeq 3.086 \cdot 10^{16}\,\mathrm{m} = 3.262\,\mathrm{ly}$ (see e.g., [244]). Here, we have used $c = 1$ in the last equality. To indicate this uncertainty, distances (momenta) are traditionally expressed in units of length (inverse length) as

$$[\text{distance}] = 1\,\mathrm{Mpc}/h\,, \qquad [\text{momentum}] = 1\,h/\mathrm{Mpc} \tag{1.4}$$

(see Figure 1.1). For instance, the characteristic length scale of the (observable) Universe, namely the Hubble radius R_H, which is defined as the distance light has traveled during the characteristic age of the Universe, the Hubble time $t_H = 1/H_0$, then arises as (see (1.3)) [245]

$$R_H \equiv \frac{c}{H_0} \simeq 3000\,\mathrm{Mpc}/h\,. \tag{1.5}$$

Finally, our conventions for the 3-dimensional Fourier transform of a space- and time-dependent field $f(\boldsymbol{x}, \tau)$ are

$$\tilde{f}(\boldsymbol{k}, \tau) \equiv \int \frac{d^3 x}{(2\pi)^3}\, e^{-i\boldsymbol{k}\cdot\boldsymbol{x}}\, f(\boldsymbol{x}, \tau)\,, \qquad f(\boldsymbol{x}, \tau) \equiv \int d^3 k\, e^{i\boldsymbol{k}\cdot\boldsymbol{x}}\, \tilde{f}(\boldsymbol{k}, \tau)\,, \tag{1.6}$$

where the Fourier transform $\tilde{f}(\boldsymbol{k}, \tau)$ includes a dependence on the comoving wavenumber (momentum) $\boldsymbol{k}$. For reasons of better readability, we usually omit the tilde symbol of the Fourier transform.

Moreover, we denote the Laplace transform of a time-dependent function $g(\tau)$ by [246]

$$\hat{g}(\omega) \equiv \int d\tau\, e^{-\omega\tau} g(\tau)\,, \qquad g(\tau) \equiv \oint_{c-i\infty}^{c+i\infty} \frac{d\omega}{2\pi i}\, e^{\omega\tau}\, \hat{g}(\omega)\,. \tag{1.7}$$

---

[4]In the latest data release of the Planck collaboration, the value for the Hubble constant, representing the present expansion rate of the Universe, is given by $H_0 = (67.8 \pm 0.9)\,\mathrm{km}\,\mathrm{s}^{-1}\,\mathrm{Mpc}^{-1}$ [17].

Here, ω refers to a complex number frequency parameter, whereas c constitutes a real number such that the contour path of integration lies within the region of convergence of $\hat{g}(\omega)$. Besides, we use the following differentiation property of the Laplace transform

$$\int_{\tau_0}^{\infty} d\tau\, e^{-\omega\tau}\, \frac{dg(\tau)}{d\tau} = \omega\,\hat{g}(\omega) - g(\tau_0)\,. \tag{1.8}$$

Chapter 2

Eulerian Dynamics of Gravitational Instability

Contents

2.1. Dark matter evolution on large distance scales

Galaxy redshift surveys such as the Sloan Digital Sky Survey (SDSS) [18, 19] or the 2-degree Field Galaxy Redshift Survey (2dFGRS) [38, 43] have revealed a rich variety of the large-scale structure in the Universe. Besides groups, clusters and superclusters of galaxies, the observed galaxy distribution shows walls, filaments and voids. Walls and filaments are stretched regions with a high galaxy density which form the boundaries between voids, vast regions of nearly empty space. A map of the galaxy distribution from 2dFGRS can be seen in Figure 2.1.

One of the largest known structures is the Sloan Great Wall [248], shown in Figure 1.2. It has a length (proper size at the present epoch) of [249]

$$r \simeq 100 \, \mathrm{Mpc}/h \, . \tag{2.1}$$

One of the main goals of present cosmology is to understand the formation process of these large-scale structures in the Universe. The idea that the large-scale structure, seen in galaxy
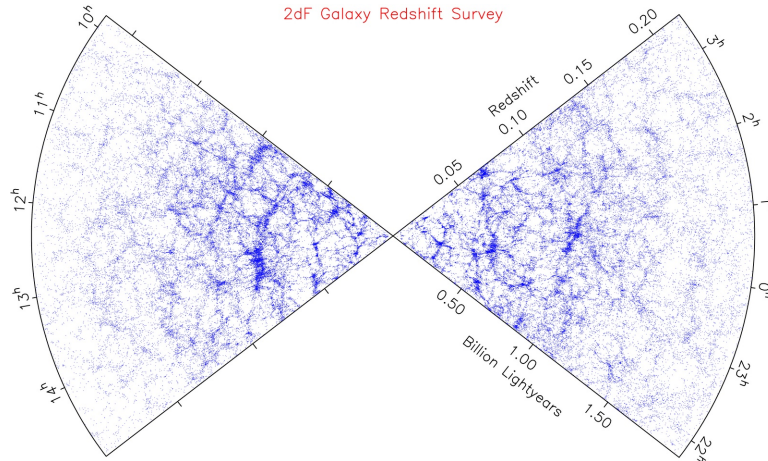
Fig. 2.1.: Galaxy distribution map from the complete 2-degree Field Galaxy Redshift Survey (1997-2002) [38, 43] (reprinted from [247]). In the radial direction the redshift is plotted, while the polar angle is the right ascension. Since the redshift is directly related to the distance of an object by the Hubble law, redshift surveys map the three-dimensional distribution of galaxies. Our Galaxy is in the center of the figure. Here, the distribution of more than 200 000 galaxies is plotted [245] (see also Figure 1.2).

surveys, grew out of small (primordial) inhomogeneities in the matter density through gravitational instability [250, 251] has become widely accepted in the last three decades. In the framework of gravitational instability, one assumes that *on large distance scales* gravity is the only agent responsible for the formation of structures, and that the growth and the evolution of the matter density fluctuations is dominated by its dark matter (DM) component [40, 92].

According to the current cosmological paradigm, the observed baryonic mass constitutes just a small fraction of the total mass in the Universe. The main component, however, is expected to be a form of *non-relativistic* and *collisionless* matter, called *cold dark matter* (CDM) [252–255]. The large-scale structure seen in galaxy surveys arises from the primordial fluctuations in the matter density, which are generated out of quantum fluctuations during inflation. When in the matter-dominated era of the Universe, CDM becomes the dominant form of energy, the primordial fluctuations are amplified due to gravitational interactions of CDM particles. Moreover, the distribution of CDM in the expanding Universe forms potential wells where stars, galaxies and galaxy clusters develop by hierarchical growth and clustering. This leads finally to the large-scale structure we observe in the Sky today.

No evidence for structures with a linear dimension much larger than $r \simeq 100\,\mathrm{Mpc}/h$ has

been found. This homogeneity scale has to be compared to the Hubble radius at present time, as defined in (1.5),

$$R_H \simeq 3000 \, \text{Mpc}/h \, . \tag{2.2}$$

The fact that $r \ll R_H$ justifies the Cosmological Principle, i.e., the Universe can been seen as homogeneous and isotropic on large Hubble scales.

Consequently, on spheres of size much than larger the typical size of galaxy clusters, the galaxy number density corresponds to the mean density of the Universe modified by small fluctuations. One assumes that this characteristic also holds for the dark matter density distribution. Hence, on sufficiently large distance scales, the formation of structures can be modeled by using perturbative techniques in terms of the small matter density fluctuations. This perturbative description of LSS formations is denoted as cosmological perturbation theory. However, when approaching smaller distance scales and later times, the density fluctuations become larger and the validity of perturbative methods starts to break down.

Throughout this thesis, we assume the framework that the LSS formed due to gravitational instabilities and discuss how perturbation theory can be used to understand the physics of gravitational instability and to test this hypothesis against observations.

2.1.1. Summary of approximations

To study the process of LSS formation with analytic methods, we have to rely on certain assumptions and approximations [123]. These restrictions are valid when we consider the dark matter evolution on sufficiently large scales. They can be summarized as follows:

- The LSS is formed due to gravitational instability only.

- CDM dominates the dynamics of gravitational instability.

- CDM is collisionless and non-relativistic at decoupling.

- On subhorizon scales, CDM can be described by non-relativistic Newtonian gravity.

- In the early stages of gravitational instability, CDM behaves like a pressureless perfect fluid.

- The velocity dispersion is negligible so that the single-stream approximation can be used.

- There is neither primordial vorticity, nor vorticities on sufficient large distance scales.

The last three points are further discussed in Section 2.4 and Chapter 3 where we derive the non-linear fluid equations of LSS and motivate the single-flow approximation. In the following section, we consider the remaining points in detail.

2.1.2. Approximations in detail

Dynamics of gravitational instability

According to the ΛCDM model, the evolution of the Universe after the Big Bang up to the present time can be divided in four global phases [256], namely inflation ($\sim 10^{-36} \dots 10^{-32}$ s), radiation domination ($\sim 10^{-32} \dots 10^{11}$ s), matter domination ($\sim 10^{11} \dots 10^{17}$ s) and dark energy domination ($\sim 10^{17}$ s to today). Since matter decouples from the primordial plasma in the early stages of matter domination, modeling the LSS formation thus amounts to describe gravitational instabilities in the two phases of matter and dark energy domination.[1] During both phases, the energy composition of the Universe shows a significant higher amount of dark matter than of baryonic matter (atoms). As a consequence, we can neglect the baryonic contribution to the total matter density in the Universe and approximate it by its dark matter component only. Consequently, we solve the evolution equations of gravitational instability just in terms of the dark matter density. Compared to typical masses of galaxies with particle number densities of at least 10^{50} particles per Mpc^3 [257], the mass of all possible DM candidates is extremely small. In this limit where the number of particles $N \gg 1$, discreteness effects such as two-body relaxation (important for instance in globular clusters [258]) are negligible.[2] Note that this means that we can describe DM as a (pressureless) fluid since internal effects within the fluid should not significantly affect the evolution on large distance scales.

Moreover, on sufficiently large distance scales, thermal effects of the intergalactic medium (hot gas) can be neglected. Thus, on those scales, it is justified to assume that the LSS is formed only due to gravitational self-interaction of CDM particles.

Properties of CDM

There is substantial evidence (though, no direct detection yet) that the Universe contains a large amount of non-baryonic dark matter (for a review on DM see e.g., [261]). Usually, one assumes that there must be at least some CDM, composed of particles with non-relativistic velocities when decoupling takes place during the early stages of the matter domination epoch [243, 262, 263]. Apart from CDM, there might be also some hot or warm dark matter particles that decouple having relativistic velocities.

---

[1] Galaxy formation started roughly at $\sim 6 \cdot 10^8$ yrs $\simeq 2 \cdot 10^{15}$ s (at about redshift $z \sim 10$) after the Big Bang [27].

[2] See for instance [259, 260] for studies of discreteness effects in N-body simulations.

The details of how large-scale structures evolve from primordial density fluctuations depend on the nature of dark matter. Hot and warm dark matter, for instance, cannot cluster on galaxy scales until it has cooled down to relativistic speeds and so gives rise to a considerably different primordial power spectrum. CDM, on the other hand, explains the observed properties of galaxies quite well [252–255] (see also [264]). In particular, the measured two-point correlation function of galaxies indicates that there exists a large amount of power on small distance scales, of order of a few kpc. If the dark matter particles had significant velocities, i.e., if they were hot or warm, the structures on small scales would be erased [262]. This is why one usually assumes that large-scale structure formation is driven mainly by CDM.[3]

In addition, CDM has to be nearly collisionless. Collisions would lead to halos which are round, in contrast to data that indicates triaxiality, e.g in clusters [267]. The limit of this constraint is that there might be dark matter self-interactions (for details see e.g., [265, 266, 268, 269]) which may serve to erase small-scale structures in galaxy halos as well as density cusps expected in the cores of galaxies.

Non-relativistic Newtonian gravity

Current galaxy surveys are focused on distance scales of the order $\mathcal{O}\left(100\,\mathrm{Mpc}/h\right)$ [270]. On those scales much smaller than the Hubble radius, in the sub-horizon regime, CDM particles can be treated as non-relativistic so that the equations of motion reduce to those of Newtonian gravity.[4] Thus, we can use Newtonian dynamical laws to study LSS formation.

On the other hand, future LSS surveys will probe larger and larger volumes and access scales comparable to the Hubble horizon. On those ultra-large distance scales, it is important to take general relativistic effects into account. In general, relativistic corrections to the Newtonian approximation scale like the ratio of the physical wavenumber k/a and the Hubble parameter H [63, 179]

$$\frac{\text{Relativistic corrections}}{\text{Newtonian approximation}} \sim \left(\frac{aH}{k}\right)^2 \tag{2.3}$$

with $(aH)/k \ll 1$ on subhorizon scales and $(aH)/k > 1$ on superhorzion scales (see (1.5)) [27].

All relativistic effects can be interpreted as projection effects. They comprise, for instance, weak gravitational lensing, redshift-space distortions or gravitational redshift, and have been treated consistently in [274–279]. On extremely large distance scales, relativistic effects can

---

[3]Some of the existing problems in the CDM model may, however, be overcome by considering DM that is not completely cold [265, 266].

[4]For a proper justification of the Newtonian treatment starting from the general relativistic equations see e.g., [92]. A detailed description of gravitational instability in relativistic perturbation theory is given in [271–273].

substantially modify the power spectrum of the number density of galaxies from the usual Newtonian predictions. However, they are strongly sub-dominant on distance scales of the order $\mathcal{O}\left(100\,\mathrm{Mpc}/h\right)$, where current galaxy surveys are focused on [270].

In this thesis, we investigate LSS formation on scales on which relativistic corrections are negligible. Thus, we restrict our considerations to the Newtonian description of gravitational instabilities in what follows.

2.2. Particle dynamics in the expanding Universe

We use the *Eulerian* framework to describe the dynamics of gravitational instability. This amounts in studying the dynamics of density and velocity fields in terms of fixed time and space coordinates, t and $\boldsymbol{r}$. In contrast to this, there exists the so-called *Lagrangian* scheme following the trajectories of particles or fluid elements [91, 103, 104] (see also the discussion in Section 5.2).

To describe the formation of large-scale structure by the Eulerian dynamics of gravitational instability, let us model the matter content of the Universe as a sea of identical dust-like particles of mass m interacting only gravitationally. This means that collisions between them are rare and the mean free path is large. Moreover, let us assume that the particles move in a smoothly varying Newtonian gravitational potential Φ induced by the local mass density due to the particle distribution in the Universe.

In order to study the dynamics of particles in the expanding Universe in terms of the departure from the homogeneous and isotropic background expansion, it is convenient to use comoving coordinates $\boldsymbol{x}$. These are related to the physical coordinates $\boldsymbol{r}$ by the cosmological scale factor $a(\tau)$,

$$\boldsymbol{r} = a(\tau)\,\boldsymbol{x}\,. \tag{2.4}$$

At present time, $\boldsymbol{x}$ and $\boldsymbol{r}$ are equal since $a_0 = 1$. Due to homogeneity and isotropy of the Universe, the scale factor $a(\tau)$ is a universal function of time. Here, we have defined it with respect to conformal time τ, which is connected to physical time by

$$dt = a(\tau)\,d\tau\,. \tag{2.5}$$

In the following, we only use conformal time as our time variable and comoving coordinates as space variable. All spatial derivatives are taken with respect to $\boldsymbol{x}$ so that $\nabla \equiv \nabla_{\boldsymbol{x}}$.

The equations of motion that we derive in the following are valid in a homogeneous and isotropic Universe, which evolves according to the Friedmann equations [280, 281]

$$\mathcal{H}^2 = \frac{8\pi G}{3}a^2\bar{\rho} + \frac{\Lambda}{3}a^2 - K\,, \qquad \frac{\partial\mathcal{H}}{\partial\tau} = -\frac{4\pi G}{3}a^2\left(\bar{\rho} + 3p\right) + \frac{\Lambda}{3}a^2\,. \tag{2.6}$$

Here, the quantity $\mathcal{H}$ denotes the conformal expansion rate which is related to the Hubble parameter H as [40]

$$\mathcal{H}(\tau) \equiv \frac{d \ln a(\tau)}{d\tau} = Ha \,. \tag{2.7}$$

Besides, $\bar{\rho}$ and p denote the mean energy density and the pressure, respectively. Note that in the phase of matter and dark energy domination, relevant to describe large-scale structure formation, the contribution of radiation to the energy density is negligible so that $\bar{\rho}$ is equivalent to the mean matter density. Moreover, notice that in the matter-dominated phase, the pressure p can be neglected as well. Finally, in the Friedmann equations above, G refers to the gravitational constant, Λ to the cosmological one and $K = \{-1, 0, 1\}$ to the curvature parameter representing an 'open', a 'flat' or a 'closed' Universe, respectively.

If we then define the cosmological density parameters

$$\Omega_m(\tau) \equiv \frac{8\pi G a^2 \bar{\rho}}{3\mathcal{H}^2} = \frac{\bar{\rho}}{\rho_c} \,, \qquad \Omega_\Lambda(\tau) \equiv \frac{a^2 \Lambda}{3\mathcal{H}^2} \,, \qquad \Omega_k(\tau) \equiv -\frac{K}{\mathcal{H}^2} \tag{2.8}$$

with the critical density $\rho_c(\tau)$, we can rewrite the Friedmann equations as [40]

$$\left(\Omega_{\text{tot}}(\tau) - 1\right) \mathcal{H}^2(\tau) = K \,, \qquad \frac{\partial \mathcal{H}}{\partial \tau} = \left(-\frac{\Omega_m(\tau)}{2} + \Omega_\Lambda(\tau)\right) \mathcal{H}^2 \tag{2.9}$$

where

$$\Omega_{\text{tot}}(\tau) \equiv \Omega_m(\tau) + \Omega_\Lambda(\tau) = 1 - \Omega_k(\tau) \tag{2.10}$$

by neglecting the radiation density as well as the pressure p. In particular, the first Friedmann equation implies that $\Omega_{\text{tot}} < 1$, $\Omega_{\text{tot}} = 1$ and $\Omega_{\text{tot}} > 1$ for $K = \{-1, 0, 1\}$, that is, for an 'open', a 'flat' or a 'closed' Universe, respectively.

Proceeding from this, let us derive the equations of motion for particles in the expanding Universe whose evolution follows the Friedmann equations. We first define the proper particle velocity $\boldsymbol{v} \equiv d\boldsymbol{r}/dt$ in comoving coordinates (and conformal time). Using (2.4) and (2.7), we see that it splits up into two terms,

$$\boldsymbol{v}(\boldsymbol{x}, \tau) = \mathcal{H}\boldsymbol{x} + \boldsymbol{u} \,, \qquad \boldsymbol{u} \equiv \frac{d\boldsymbol{x}}{d\tau} \,. \tag{2.11}$$

The first term represents the contribution from the background expansion, whereas the second term defines the peculiar velocity $\boldsymbol{u}$, the motion of the particle relative to an observer comoving with the background.

Hence, the Lagrangian of a particle with mass m and velocity $\boldsymbol{v}$ moving in a smooth Newtonian gravitational potential $\Phi(\boldsymbol{x}, t)$ reads [92, 280]

$$\mathcal{L} = \frac{1}{2} m \left(\mathcal{H}\boldsymbol{x} + \boldsymbol{u}\right)^2 - m \, \Phi(\boldsymbol{x}, t) \,. \tag{2.12}$$

By a canonical transformation, preserving the form of the equations of motion, of the form $\mathcal{L} \to \mathcal{L} - d\psi/d\tau$ with $\psi = m\,\mathcal{H}x^2/2$, the Lagrangian reduces to

$$\mathcal{L} = \frac{1}{2}m\,u^2 - m\,\phi(\boldsymbol{x}, \tau)\,, \tag{2.13}$$

where we defined the cosmological gravitational potential $\phi(\boldsymbol{x}, \tau)$ as

$$\phi(\boldsymbol{x}, \tau) \equiv \frac{1}{2}\frac{\partial \mathcal{H}}{\partial \tau}x^2 + \Phi(\boldsymbol{x}, \tau)\,. \tag{2.14}$$

As we derive in the next section, the cosmological gravitation potential is sourced only by fluctuations around the mean mass density in the Universe and hence describes the deviation from the Newtonian background potential $\Phi(\boldsymbol{x}, \tau)$.

Based on Lagrangian mechanics, it follows from (2.11) and (2.13), that the canonical momentum, defined as $\boldsymbol{p} \equiv \partial \mathcal{L}/\partial \dot{\boldsymbol{x}}$ with $\dot{\boldsymbol{x}} = d\boldsymbol{x}/dt \equiv \boldsymbol{u}/a$, is given by

$$\boldsymbol{p} = m\,a\,\boldsymbol{u}\,. \tag{2.15}$$

Consequently, the Newtonian equation of motion, derived from the Euler-Lagrange equations $dp_i/dt = \partial \mathcal{L}/\partial x_i$, arises in comoving coordinates as

$$\frac{d\boldsymbol{p}}{d\tau} = -\,m\,a\,\nabla\phi\,. \tag{2.16}$$

In general, one derives the time variation of the momentum from the geodesic equation. However, assuming that the metric perturbations are small and for distance scales much below the Hubble scale, the previous Newtonian equation holds. A detailed derivation of the Newtonian limit from general relativity can be found in [92].

2.3. The Vlasov-Poisson equation

In the theory of cosmological structure formation, the distribution of matter is described as a continuous field. In other words, cosmological perturbations on sufficiently large distance scales allow for a fluid description. The transition from a microscopic system of N point-like particles in form of a discrete distribution in phase space, described by the Klimontovich equation (for a detailed discussion see [211, 212, 282]), to a smoothed coarse-grained system can be seen as the continuum (or thermodynamical) limit. In this limit, where the discrete character or particles is lost, one formally takes the limit of an infinite number of particles, $N \to \infty$. As a consequence, the individual masses are negligible, $m \to 0$, while the total mass density $\propto Nm$ is kept constant. In this continuum limit, the Klimontovich equation becomes the so-called Vlasov equation [283]. Combining the Vlasov with the Poisson equation for the cosmological

gravitational potential, the Vlasov equation yields the Vlasov-Poisson equation. This constitutes the fundamental equation to describes the dynamics of gravitational instability. All subsequent calculations are derived from this equation.

Before regarding the Poisson equation, let us derive the Vlasov equation. For this purpose, we consider the number of particles per unit volume in phase space,

$$dN = f(\boldsymbol{x}, \boldsymbol{p}, \tau) \, d^3x \, d^3p \,, \tag{2.17}$$

which defines the phase-space distribution function $f(\boldsymbol{x}, \boldsymbol{p}, \tau)$. According to Liouville's theorem, which is a key theorem in classical statistical and Hamiltonian mechanics, the phase-space density f is constant along each particle trajectory in phase space. In other words, its total time derivative vanishes, $df/d\tau = 0$. By using the equations of motion (2.15) and (2.16), this leads to the expression [40, 284]

$$\frac{df}{d\tau} = \frac{\partial f}{\partial \tau} + \frac{\boldsymbol{p}}{m \, a} \cdot \nabla f - a \, m \, \nabla \phi \cdot \frac{\partial f}{\partial \boldsymbol{p}} = 0 \,. \tag{2.18}$$

This equation, corresponding to the collisionless Boltzmann equation, is referred to as Vlasov equation. It describes the conservation of particle number, i.e., the rate of change in particle number per unit phase-space volume is equal to the net flux of particles across its surface.

Based on the definition of the particle distribution function in (2.17), the comoving number density of particles equals $n(\boldsymbol{x}, \tau) \equiv \int d^3p \, f(\boldsymbol{x}, \boldsymbol{p}, \tau)$ so that the proper mass density is given by

$$\rho(\boldsymbol{x}, \tau) \equiv \frac{m}{a^3} \int d^3p \, f(\boldsymbol{x}, \boldsymbol{p}, \tau) \,. \tag{2.19}$$

Here, the factor a^{-3} is the conversion to proper space density (per volume $d^3r = d^3x/a^3$). The mass density can be decomposed in a homogeneous and an inhomogeneous part to account for global and local effects,

$$\rho(\boldsymbol{x}, \tau) \equiv \bar{\rho}(\tau) \, [1 + \delta(\boldsymbol{x}, \tau)] \,, \tag{2.20}$$

where $\bar{\rho}(\tau)$ denotes the spatial average of $\rho(\boldsymbol{x}, t)$, i.e., the mean mass density (see (2.6)), scaling like a^{-3} for non-relativistic particles during the matter-domination era, and $\delta(\boldsymbol{x}, \tau)$ is the dimensionless *density contrast*.

The mass density $\rho(\boldsymbol{x}, \tau)$ is related to the Newtonian gravitational potential $\Phi(\boldsymbol{x}, t)$ by the Poisson equation

$$\nabla^2 \Phi(\boldsymbol{x}, \tau) = 4\pi G a^2 \, (\rho + 3p) - a^2 \Lambda \,, \tag{2.21}$$

which has been modified compared to the usual Poisson equation by a pressure term and a term accounting for the presence of a cosmological constant Λ. Note that the pressure term

has been added for completeness. Since we are concerned with a pressureless perfect fluid, the pressure term vanishes in our considerations.

For the cosmological gravitational potential $\phi(\boldsymbol{x}, \tau)$, defined in (2.14), we obtain, on the other hand, the following field equation,

$$
\begin{aligned}
\nabla^2 \phi(\boldsymbol{x}, \tau) &= 4\pi G a^2 \left(\rho + 3p\right) - a^2 \Lambda + 3 \frac{\partial \mathcal{H}}{\partial \tau} \\
&= 4\pi G a^2 \left(\rho - \bar{\rho}\right) \\
&= \frac{3}{2} \Omega_m \mathcal{H}^2 \, \delta \,,
\end{aligned}
\tag{2.22}
$$

where we used the second Friedmann equation in (2.6) and the definition of the matter density parameter Ω_m for the second and third equality. From the last equality, we can see that the gravitational cosmological potential ϕ is only sourced by density fluctuations δ.

The cosmological potential ϕ depends through the Poisson equation (2.22) on the density field ρ, which in turn is the integral of the particle distribution function over momentum (see (2.19)). Due to this, ϕ induces a non-linearity in the Vlasov equation (2.18). Thus, the system of equations (2.18) and (2.22) can be combined to a non-linear partial differential equation, the so-called Vlasov-Poisson equation.

2.3.1. Velocity moments of the Vlasov-Poisson hierarchy

Solving the Vlasov-Poisson equation analytically is a prohibitive task as it is a non-linear differential equation with seven variables. Thus, we seek for approximate solutions.

Usually, one is not interested in solving the full phase-space dynamics, but to determine the evolution of the spatial distribution. For this reason, a convenient way to solve the Vlasov-Poisson equation is to integrate out the (unknown) momentum dependence by taking an increasing number of 'velocity moments', and then close the infinite hierarchy of evolution equations in a consistent but approximate way.

From the first three moments of the Vlasov-Poisson equation, we can derive the basic conservation equations for the description of gravitational instabilities. Let us define the zeroth, first and second velocity moments as follows.

The zeroth-order velocity moment simply relates the phase-space density f to the proper mass density field according to the definition (2.17) in the previous section,

$$
\rho(\boldsymbol{x}, \tau) \equiv \frac{m}{a^3} \int d^3 p \, f(\boldsymbol{x}, \boldsymbol{p}, \tau) \,.
\tag{2.23}
$$

Subsequently, the first- and second-order moments define the peculiar velocity $\boldsymbol{u}(\boldsymbol{x}, \tau)$ (see

also (2.11)),

$$\boldsymbol{u}(\boldsymbol{x}, \tau) \equiv \frac{1}{\int d^3 p \, f(\boldsymbol{x}, \boldsymbol{p}, \tau)} \int d^3 p \, \frac{\boldsymbol{p}}{ma} f(\boldsymbol{x}, \boldsymbol{p}, \tau) \,, \tag{2.24}$$

and the velocity dispersion tensor $\sigma_{ij}(\boldsymbol{x}, \tau)$,

$$u_i(\boldsymbol{x}, \tau) \, u_j(\boldsymbol{x}, \tau) + \sigma_{ij}(\boldsymbol{x}, \tau) = \frac{1}{\int d^3 p \, f(\boldsymbol{x}, \boldsymbol{p}, \tau)} \int d^3 p \, \frac{p_i}{ma} \frac{p_j}{ma} \, f(\boldsymbol{x}, \boldsymbol{p}, \tau) \,. \tag{2.25}$$

The latter is related to the stress-energy tensor by $T_{ij} \equiv (1 + \delta) \, \sigma_{ij}$ [209] and describes isotropic as well as anisotropic velocity dispersion.

The evolution equations for the matter density $\rho(\boldsymbol{x}, \tau)$ or the density contrast $\delta(\boldsymbol{x}, \tau)$, as well as for the peculiar velocity $\boldsymbol{u}(\boldsymbol{x}, \tau)$ and the velocity dispersion tensor $\sigma_{ij}(\boldsymbol{x}, \tau)$ follow then from taking moments of the Vlasov equation (2.18). By this procedure, we finally arrive at the fluid equations for large-scale structure allowing us to study the dynamics of dark matter fluctuations on large distance scales purely in terms of these three quantities.

2.4. Closing the infinite Vlasov-Poisson hierarchy

2.4.1. Fluid equations

Taking the nth-order moment of the Vlasov equation yields the equation of motion of the nth-order moment of the particle distribution function $f(\boldsymbol{x}, \boldsymbol{p}, \tau)$.

For the zeroth-order moment, the matter density $\rho(\boldsymbol{x}, \tau)$, we get the following evolution equation

$$\frac{\partial \rho(\boldsymbol{x}, \tau)}{\partial \tau} + 3 \, \mathcal{H} \, \rho(\boldsymbol{x}, \tau) + \nabla \cdot \{\rho(\boldsymbol{x}, \tau) \, \boldsymbol{u}(\boldsymbol{x}, \tau)\} = 0 \,, \tag{2.26}$$

where we have integrated the Vlasov equation (2.18) over momentum and used the equations (2.23) and (2.24) defining $\rho(\boldsymbol{x}, \tau)$ and $\boldsymbol{u}(\boldsymbol{x}, \tau)$. The last term of the Vlasov equation (2.18) vanishes due to integration by parts, while the Poisson equation is not needed yet.

The equation above is referred to as *continuity equation.* Since the Vlasov equation describes particle number conservation in phase-space, its integral over momentum simply leads to the real space expression. In terms of the matter density it thus imposes conservation of mass. Note the continuity equation corresponds exactly to the Navier-Stokes equation, for a pressureless perfect fluid.[5]

Written in terms of the density contrast, defined in (2.20), and the peculiar velocity, the continuity equation reads

$$\frac{\partial \delta(\boldsymbol{x}, \tau)}{\partial \tau} + \nabla \cdot \{[1 + \delta(\boldsymbol{x}, \tau)] \, \boldsymbol{u}(\boldsymbol{x}, \tau)\} = 0 \,. \tag{2.27}$$

---

[5]The Navier-Stokes equation describes the motion of viscous fluids with pressure. In general, it is not a conservation equation, but rather describes a dissipative system [285].

Thereby, we have used the fact that the mean density scales like $\bar{\rho}(\tau) \propto a^{-3}$. Notice moreover that we have integrated out the phase-space information completely as well as eliminated the particle masses m.

For convenience, it is useful to have quantities with a vanishing statistical average (in particular for considering correlation functions). By construction of $\boldsymbol{u}$ as the peculiar velocity field and of the cosmological gravitational potential ϕ as the source of the deviation from the background density, these two fields have already zero mean. It is only natural to follow the relative deviation of the density from the background field, namely the density contrast δ, instead of the mass density itself. That is why we use $\boldsymbol{u}$, ϕ and δ as variables in the equations that follow.

From the next-order momentum of the Vlasov equation, we obtain the evolution equation of the peculiar velocity $\boldsymbol{u}(\boldsymbol{x}, \tau)$. For this purpose, we take the first moment of (2.18) and subtract $\boldsymbol{u}(\boldsymbol{x}, \tau)$ times the continuity equation (2.27). This gives us the *Euler equation*,

$$\frac{\partial \boldsymbol{u}(\boldsymbol{x}, \tau)}{\partial \tau} + \mathcal{H}(\tau)\, \boldsymbol{u}(\boldsymbol{x}, \tau) + [\boldsymbol{u}(\boldsymbol{x}, \tau) \cdot \nabla]\, \boldsymbol{u}(\boldsymbol{x}, \tau) = -\nabla \phi(\boldsymbol{x}, \tau) - \frac{1}{\rho}\, \boldsymbol{e}_i \nabla_j (\rho\, \sigma_{ij}) \qquad (2.28)$$

with unit vector $\boldsymbol{e}_i$, which states conservation of momentum. The first term on the right-hand side of this equation corresponds to a gravitational force, while the second one is due to a pressure force which in general can be anisotropic.

Note that the continuity equation (2.27) couples the zeroth-order moment ρ to the first-order moment $\boldsymbol{u}$ and the Euler equation in turn relates $\boldsymbol{u}$ to the second-order moment σ_{ij}, and so on. By taking successively higher-order moments of the Vlasov equation, one hence produces an infinite hierarchy of evolution equations describing physics on smaller and smaller distance scales with increasing order.

2.4.2. Single-flow approximation

The next step to solve these evolution equations is then to close the hierarchy in a consistent way. The hierarchy can be truncated from the Euler equation (2.28), either if the underlying microphysics dictates a relation for the velocity dispersion tensor σ_{ij} (the equation of state of the cosmological fluid), or if the higher-order moments become negligible.

In standard fluid dynamics [286], for instance, the equation of state is given by

$$\sigma_{ij} = -p\, \delta_{ij} + \eta \left(\nabla_i u_j + \nabla_j u_i - \frac{2}{3} \delta_{ij} \nabla \cdot \boldsymbol{u} \right) + \zeta\, \delta_{ij} \nabla \cdot \boldsymbol{u} \qquad (2.29)$$

with pressure p and viscosity coefficients η and ζ, respectively. The equation of state basically relies on the assumption that cosmological structure formation is driven by matter with negligible velocity dispersion or pressure, as for example cold dark matter (CDM). In the context
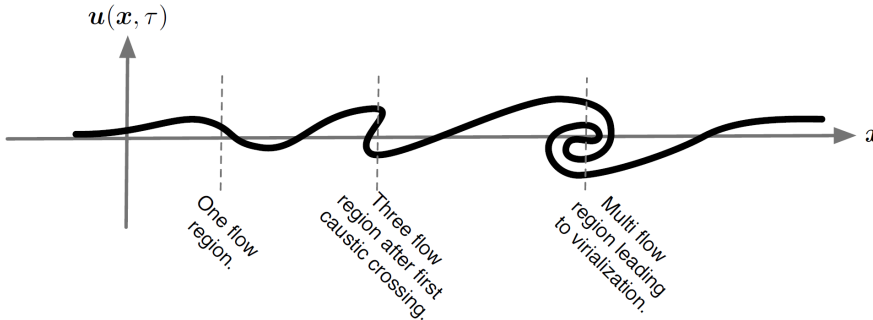
Fig. 2.2.: Schematic plot of the one-dimensional phase-space diagram depicting the first shell crossings and the emergence of multi-flow regions (adapted and reprinted from [100]).

of gravitational instabilities we are interested in, this is indeed the case. In the early phase of gravitational dynamics, until the formation of the first caustics, the velocity dispersion tensor is negligible as we discuss next.

From its definition in (2.25), one can deduce that the velocity dispersion tensor σ_{ij} characterizes the deviation of particle motions from a single coherent flow (single stream), which is described by the first term in this equation. In the early stages of gravitational instability, before structures start to collapse and virialize, until the formation of the first caustics, the velocity dispersion is negligible. Hence, the approximation to set

$$\sigma_{ij}(\boldsymbol{x}, \tau) \simeq 0 \tag{2.30}$$

holds with good accuracy, since the velocity dispersion is much smaller than the velocity gradient induced by the density fluctuations. This is the *single-flow approximation* where there are no deviations from a coherent fluid low. It simply assumes that all particles at a given point $\boldsymbol{x}$ move together with the same velocity $\boldsymbol{u}(\boldsymbol{x}, \tau)$. This amounts to demanding that

$$f(\boldsymbol{x}, \boldsymbol{p}, \tau) = \frac{a^3 \, \rho(\boldsymbol{x}, \tau)}{m} \, \delta^{\mathrm{D}}(\boldsymbol{p} - m \, a \, \boldsymbol{u}(\boldsymbol{x}, \tau)) \,, \tag{2.31}$$

where $\delta^{\mathrm{D}}(\ldots)$ denotes the three-dimensional Dirac delta distribution. Note that by neglecting the velocity dispersion σ_{ij}, the Euler equation (2.28) describes a pressureless perfect fluid, i.e., a dust universe [282]. Thus, the dynamics of gravitational instability in the single-flow approximation simply reduce to the dynamics of a pressureless perfect fluid. Although, the single-flow approximation breaks down on progressively larger distance scales as time proceeds, it is still sufficient at present time on scales relevant to LSS to use this simple approximation for investigating a great deal of effects. The breakdown of $\sigma_{ij} \simeq 0$ implies the generation of velocity dispersion due to multiple streams. The velocity dispersion is only

different from zero in points where the trajectories of particles, pulled towards one-another by gravity, cross each other. This process is known as caustics or shell-crossing (see Figure 2.2). The name 'shell-crossing' originates from the analysis of spherical gravitational collapse where the crossing of two particles implies entire shells to become congruent at the same time due to spherical symmetry. During LSS formation, multi-streaming occurs first when large caustics cross the first singularity, creating a three-flow region where vorticity can be generated (see Figure 2.2) [287]. After shell-crossing in the multi-flow regions, only very few analytic results exists and one should rely on N-body simulations.

Throughout this work, we study the Vlasov-Poisson equations in the single-flow approximation describing the dynamics of gravitational instability by a pressureless perfect fluid. As a next step, we investigate the solutions of the Poisson, continuity and Euler equations, (2.22), (2.27) and (2.28), respectively, for vanishing velocity dispersion $\sigma_{ij} \simeq 0$ in a systematic way. These equations build the basis for our description of large-scale structure formation.

Chapter 3

Standard Cosmological Perturbation Theory

Contents

In this chapter, our intention is to systematically investigate the analytic solutions for the fluid equations of large-scale structure, namely the Poisson, continuity and Euler equation, in the single-flow approximation. To solve these coupled non-linear differential equations, one has to resort to perturbative methods. Here, we present the basic method within the Eulerian framework of cosmological perturbation theory, the so-called *standard perturbation theory (SPT)* approach [40, 92–102].

Following [40, 100], we discuss the concept of SPT and its fundamental assumptions that lead to perturbative solutions of the non-linear fluid equations. We derive these solutions by proceeding successively from linear order to non-linear higher orders in perturbation theory. As a starting point, let us explore the linear solutions to the evolution equations of dark matter clustering.

3.1. Linear perturbation theory

If we consider sufficiently large distance scales, the Universe becomes smooth. Then, the fluctuation fields $\boldsymbol{u}(\boldsymbol{x}, \tau)$, $\phi(\boldsymbol{x}, \tau)$ and $\delta(\boldsymbol{x}, \tau)$ in (2.11), (2.14) and (2.20) can be assumed to

be small compared to the homogeneous contributions from the Hubble flow and the mean density $\bar{\rho}(\tau)$, respectively. Consequently, we can linearize the single-flow continuity and Euler equations, (2.27) and (2.28), to study the evolution of gravitational instability in the linear regime.

One linearizes the evolution equations (2.27) and (2.28) with respect to $\delta(\boldsymbol{x}, \tau)$ and $\boldsymbol{u}(\boldsymbol{x}, \tau)$ by neglecting the terms $\nabla \cdot [\delta(\boldsymbol{x}, \tau)\boldsymbol{u}(\boldsymbol{x}, \tau)]$ and $[\boldsymbol{u}(\boldsymbol{x}, \tau) \cdot \nabla] \boldsymbol{u}(\boldsymbol{x}, \tau)$ in the continuity and the Euler equation, respectively. The linearized system of equations then reads

$$\frac{\partial \delta(\boldsymbol{x}, \tau)}{\partial \tau} + \nabla \cdot \boldsymbol{u}(\boldsymbol{x}, \tau) \;=\; 0 \,, \tag{3.1}$$

$$\frac{\partial \boldsymbol{u}(\boldsymbol{x}, \tau)}{\partial \tau} + \mathcal{H}(\tau) \, \boldsymbol{u}(\boldsymbol{x}, \tau) \;=\; -\nabla \phi(\boldsymbol{x}, \tau) \,. \tag{3.2}$$

These equations are straightforward to solve. As follows from the Helmholtz decomposition [288], also known as the fundamental theorem of vector calculus, the peculiar velocity $\boldsymbol{u}(\boldsymbol{x}, \tau)$, as any vector field, can be completely (up to a constant) described by its divergence and its vorticity, denoted here as

$$\theta(\boldsymbol{x}, \tau) \equiv \nabla \cdot \boldsymbol{u}(\boldsymbol{x}, \tau) \,, \qquad \boldsymbol{w}(\boldsymbol{x}, \tau) \equiv \nabla \times \boldsymbol{u}(\boldsymbol{x}, \tau) \,. \tag{3.3}$$

By taking the curl of the linearized equation (3.2), its right-hand side vanishes. Thus, we directly obtain the linearized evolution equation for the vorticity,

$$\frac{\partial \boldsymbol{w}(\boldsymbol{x}, \tau)}{\partial \tau} + \mathcal{H}(\tau) \, \boldsymbol{w}(\boldsymbol{x}, \tau) = 0 \,. \tag{3.4}$$

From the solution of this equation, scaling like $\boldsymbol{w}(\tau) \propto a^{-1}$, we deduce that in the *linear* regime, any initial vorticity decays in time due to the expansion of the Universe.

Thus, we can neglect the contribution of the vorticity in the linearized evolution equations (3.1) and (3.2). As a consequence, this allows us to express them in terms of two scalar quantities, namely the density contrast $\delta(\boldsymbol{x}, \tau)$ and the velocity divergence $\theta(\boldsymbol{x}, \tau)$, as defined in (3.3). After taking the divergence of (3.2) and making use of the Poisson equation (2.22) and the definition of the velocity divergence in (3.3), we obtain the following two evolution equations for δ and θ,

$$\frac{\partial \delta(\boldsymbol{x}, \tau)}{\partial \tau} + \theta(\boldsymbol{x}, \tau) \;=\; 0 \,, \tag{3.5}$$

$$\frac{\partial \theta(\boldsymbol{x}, \tau)}{\partial \tau} + \mathcal{H}(\tau) \, \theta(\boldsymbol{x}, \tau) + \frac{3}{2} \Omega_m(\tau) \mathcal{H}^2(\tau) \delta(\boldsymbol{x}, \tau) \;=\; 0 \,. \tag{3.6}$$

In order to solve this system of differential equations, we use the first equation to express the velocity divergence as a time derivative of the density contrast and then insert it into

the second equation. Doing so, we eliminate the velocity divergence and get a second-order differential equation for the density contrast,

$$\frac{\partial^2 \delta(\boldsymbol{x}, \tau)}{\partial \tau^2} + \mathcal{H}(\tau) \frac{\partial \delta(\boldsymbol{x}, \tau)}{\partial \tau} - \frac{3}{2} \Omega_m(\tau) \mathcal{H}^2(\tau) \delta(\boldsymbol{x}, \tau) = 0 \,. \tag{3.7}$$

Notice that no operator acting on the spatial coordinates, but only time derivatives enter in this equation. This is a characteristic feature of the growth of instabilities in a pressureless fluid which implies in particular that the linear growth rate of the fluctuations does not depend on the scale. In other words, we can rewrite the density contrast as a product of a time-dependent linear growth factor $D_1(\tau)$ and a space-dependent initial density contrast $\delta_0(\boldsymbol{x}) \equiv \delta(\boldsymbol{x}, \tau = 0)$ so that $\delta(\boldsymbol{x}, \tau) = D_1(\tau) \delta_0(\boldsymbol{x})$. Inserting this relation in (3.7) yields a differential equation for the linear growth factor $D_1(\tau)$

$$\frac{\partial^2 D_1(\tau)}{\partial \tau^2} + \mathcal{H}(\tau) \frac{\partial D_1(\tau)}{\partial \tau} + \frac{3}{2} \Omega_m(\tau) \mathcal{H}^2(\tau) D_1(\tau) = 0 \,. \tag{3.8}$$

As it constitutes a second-order differential equation, it has two independent specific solutions, one that is growing with time, denoted by $D_1^+(\tau)$, and a second one decaying in time, referred to as $D_1^-(\tau)$. The explicit solution for the growing mode $D_1^+(\tau)$ is given by an integral representation as a function of Ω_m and the conformal expansion rate $\mathcal{H}$ [289],

$$D_1^+(\tau) = \frac{5}{2} \Omega_m \, \mathcal{H}_0^2 \, \frac{\mathcal{H}}{a} \int\limits_0^a \frac{da'}{[\mathcal{H}(a')]^3} \,, \tag{3.9}$$

where $\mathcal{H}_0 \equiv \mathcal{H}(a_0)$ denotes the conformal expansion rate today and where we normalized the scale factor such that $a_0 \equiv 1$ at present time. For the decaying mode, on the other hand, a simple analytic solution exists (see [289]),

$$D_1^-(\tau) = \frac{H}{H_0} = \frac{1}{a} \frac{\mathcal{H}}{\mathcal{H}_0} \,. \tag{3.10}$$

Consequently, the generic solution for the density contrast is given by the linear combination of the growing and the decaying mode solution,

$$\delta^L(\boldsymbol{x}, \tau) = D_1^+(\tau) \, \delta_0^+(\boldsymbol{x}) + D_1^-(\tau) \, \delta_0^-(\boldsymbol{x}) \,, \tag{3.11}$$

where $\delta_0^+(\boldsymbol{x})$ and $\delta_0^-(\boldsymbol{x})$ are two functions of space describing the initial field configuration. Inserting this solution in the linearized continuity equation (3.5) allows in turn to solve this equation for the velocity divergence θ. The resulting relation,

$$\theta^L(\boldsymbol{x}, \tau) = -\mathcal{H}(\tau) \left[f(\tau) \, \delta_0^+(\boldsymbol{x}) + g(\tau) \, \delta_0^-(\boldsymbol{x}) \right] \,, \tag{3.12}$$

can be expressed in terms of the growth rates

$$f(\tau) \equiv \frac{1}{\mathcal{H}(\tau)} \frac{d \ln D_1^+(\tau)}{d\tau} = \frac{d \ln D_1^+}{d \ln a} \,, \qquad g(\tau) = \frac{1}{\mathcal{H}(\tau)} \frac{d \ln D_1^-(\tau)}{d\tau} \,. \tag{3.13}$$

The simple solution for the decaying mode $D_1^-(\tau)$ even allows to derive a generally valid explicit solution for the growth rate $g(\tau)$. By inserting the decaying-mode solution (3.10) in the definition of the growth rate (3.13) and using the second Friedmann equation (2.9), we deduce

$$g(\tau) = \frac{1}{\mathcal{H}^2} \frac{d\mathcal{H}}{d\tau} - 1 = \Omega_\Lambda - \frac{\Omega_m}{2} - 1 \,. \tag{3.14}$$

Note that this result is valid for arbitrary Ω_m and Ω_Λ.

The specific solutions for the growth factors $D_1^\pm(\tau)$ and subsequently for the growth functions $f(\tau)$ and $g(\tau)$ depend on the background cosmology through the density parameters Ω_m and Ω_Λ, the scale factor a and hence the conformal expansion rate $\mathcal{H}(a)$. The form of $\mathcal{H}(a)$ is explicitly determined by the first Friedmann equation (2.9). Written in terms of the cosmological parameters at present time, which we denote by the subscript '0', this equation reads

$$\mathcal{H}(a) = \mathcal{H}_0 \sqrt{\Omega_{m,0}\, a^{-1} + (1 - \Omega_{m,0} - \Omega_{\Lambda,0}) + \Omega_{\Lambda,0}\, a^2} \,, \tag{3.15}$$

where we used the fact that the mean matter density scales like $\bar{\rho}(\tau) \propto a^{-3}$.

In the following, we discuss the form of the growth factors for those cosmological models which are relevant for our further considerations. A detailed overview of the specific solutions of $D_1^\pm(\tau)$ in different cosmological models can be found in [40, 92].

3.1.1. Linear solutions for an Einstein–de Sitter cosmology

Let us first consider the case of an Einstein–de Sitter (EdS) cosmological model. An EdS cosmology describes a flat ($K = 0$) universe containing matter only ($\Omega_m = 1$, $\Omega_\Lambda = 0$). It can be considered as a good description of our Universe after matter-radiation equality with the largest deviations arising at late times when dark energy starts to dominate. By solving the Friedmann equations (2.9) for an EdS cosmology, the scale factor $a(\tau)$ in conformal time and the conformal expansion rate $H(\tau)$, defined in (2.7), can be determined in this case as[1]

$$a(\tau) = \left(\frac{H_0}{2} \tau \right)^2 \propto \tau^2 \,, \qquad \mathcal{H} = \mathcal{H}_0\, a^{-1/2} = \frac{2}{\tau} \,. \tag{3.16}$$

Note that at present time, $\mathcal{H}_0 \equiv H_0$ since $a_0 \equiv 1$.

---

[1] In comparison, for an EdS cosmology, the scale factor $a(t)$ and the Hubble parameter $H(t)$ with respect to physical time t, related to conformal time by (2.5), read $a(t) = \left(\frac{3}{2} H_0\, t \right)^{2/3} \propto t^{2/3}$ and $H = H_0\, a^{-3/2} = \frac{2}{3t}$.

The equations (3.9), (3.10), (3.13) and (7.40) then yield the following simple solutions for the growth factors and the growth rates in the EdS case,

$$D_1^+(\tau) = a\,, \qquad D_1^-(\tau) = a^{-3/2}\,, \qquad f(\tau) = 1\,, \qquad g(\tau) = -\frac{3}{2}\,. \qquad (3.17)$$

Hence, for an EdS background cosmology, the growth rates are constant. Moreover, the growing mode $D_1^+(\tau)$ is equal to the scale factor a so that the density contrast (3.11) grows as a as well. This gives the time scale of LSS formation and allows to compare the amplitude of the metric perturbations at recombination to the local density perturbations. Moreover, the scaling $\delta^L(\boldsymbol{x}, \tau) \propto a$ in the growing mode implies that the cosmological gravitational potential in the Poisson equation (2.22) for the corresponding mode is constant in time, at least for an EdS universe. This fact becomes important later on and we discuss its consequences in detail in Section 6.3.

In contrast, the decaying mode $D_1^-(\tau)$ scales like $a^{-3/2}$ so that all density perturbations which have initially been in the decaying mode disappear fast and become subdominant after a short period of time. Hence, for an EdS cosmology, we can neglect the decaying mode solution and consider only the growing-mode solution for the density contrast and the velocity divergence.

3.1.2. Linear solutions for a ΛCDM cosmology

As a second example, we discuss the observationally favored case of a ΛCDM cosmological model, corresponding to a (not necessarily flat) universe with (dark) matter ($\Omega_m \neq 0$), and dark energy in form of a cosmological constant Λ, such that $\Omega_\Lambda \neq 0$. For a ΛCDM background cosmology, the linear growth factor $D_1^+(\tau)$ cannot be determined exactly since solving the integral (3.9) by use of the general expression for the conformal expansion rate $\mathcal{H}(a)$ in (3.15) is not possible by analytic means. However, it is well approximated by the expression [290, 291]

$$D_1^+(\tau) \simeq \left(\frac{5}{2}\right) \frac{a\,\Omega_{m,0}}{\Omega_{m,0}^{4/7} - \Omega_{\Lambda,} + (1 + \Omega_{m,0}/2)(1 + \Omega_{\Lambda,0}/70)}\,, \qquad (3.18)$$

so that the growth rate $f(\tau)$ becomes approximately [281]

$$f(\tau) \simeq \left[1 - (\Omega_{m,0} + \Omega_{\Lambda,0} - 1)\,a + \Omega_{\Lambda,0}\,a^3\right]^{-4/7}\,. \qquad (3.19)$$

To calculate the decaying mode $D_1^-(\tau)$ and the corresponding growth rate $g(\tau)$ in the case of a ΛCDM universe, no approximation formulae are necessary since one just uses the simple analytic solutions (3.10) with (3.15) and (3.14), respectively.

3.2. Non-linear perturbation theory

Proceeding from the linear approximation of the evolution equations for the density and velocity fields, our next step consists in studying the full representation of the evolution equations including the non-linear terms neglected so far.

In order to do so, we make the self-consistent approximation to characterize the velocity field $\boldsymbol{u}(\boldsymbol{x}, \tau)$ by its divergence $\theta(\boldsymbol{x}, \tau)$ and neglect its vorticity component $\boldsymbol{w}(\boldsymbol{x}, \tau)$ (see (3.3)). This approximation can be justified as follows. By taking the curl of the Euler equation in (2.28), we obtain the non-linear evolution equation for the vorticity

$$\frac{\partial \boldsymbol{w}(\boldsymbol{x}, \tau)}{\partial \tau} + \mathcal{H}(\tau)\, \boldsymbol{w}(\boldsymbol{x}, \tau) - \nabla \times [\boldsymbol{u}(\boldsymbol{x}, \tau) \times \boldsymbol{w}(\boldsymbol{x}, \tau)] = \nabla \times \left(\frac{1}{\rho}\, \boldsymbol{e}_i \nabla_j\, \sigma_{ij} \right)\,, \qquad (3.20)$$

where we have reintroduced the velocity dispersion tensor σ_{ij} for the moment. The equation above reveals that in the single-flow approximation and if the initial vorticity vanishes, the vorticity remains zero at all times. On the other hand, if the initial vorticity is not equal to zero, it decays at linear order due to the expansion of the Universe, as we deduced from (3.4). However, it can be amplified in the non-linear regime through the third term on the left-hand side in (3.20).

In our following considerations, we assume that the initial vorticity vanishes, i.e., that the initial velocity field is irrotational. Then, the single-flow approximation $\sigma_{ij} \simeq 0$ together with the vorticity evolution equation (3.20) ensures that the vorticity remains zero throughout the evolution. Note, however, that this assumption is only self-consistent as long as the single-flow approximation is valid. In particular, on small enough distance scales (in the strongly non-linear regime), multi-streaming and shocks can generate an anisotropic velocity dispersion and in turn induce vorticity (see e.g., [129, 209, 287, 292]). We take this point up again in Section 5.1.

Assuming the initial velocity field to be irrotational allows us in consequence to describe the linear as well as non-linear evolution of gravitational instability purely in terms of the density contrast $\delta(\boldsymbol{x}, \tau)$ and the velocity divergence $\theta(\boldsymbol{x}, \tau)$.

3.2.1. Non-linear evolution equations in Fourier space

In order to compute the non-linear corrections to the solutions of the linear evolution equations, let us study the two non-linear evolution equations in terms of the density contrast $\delta(\boldsymbol{x}, \tau)$ and the velocity divergence $\theta(\boldsymbol{x}, \tau)$. While the first one is just given by the continuity equation (2.27), one obtains the second one by taking the divergence of the Euler equation (2.28)

and inserting the Poisson equation (2.22) afterwards,

$$\frac{\partial \delta(\boldsymbol{x}, \tau)}{\partial \tau} + \theta(\boldsymbol{x}, \tau) = - \nabla \cdot [\delta(\boldsymbol{x}, \tau) \boldsymbol{u}(\boldsymbol{x}, \tau)] \,,$$

$$\frac{\partial \theta(\boldsymbol{x}, \tau)}{\partial \tau} + \mathcal{H}(\tau)\theta(\boldsymbol{x}, \tau) + \frac{3}{2}\Omega_m(\tau)\mathcal{H}(\tau)^2 \, \delta(\boldsymbol{x}, \tau) = - \nabla \cdot \{ [\boldsymbol{u}(\boldsymbol{x}, \tau) \cdot \nabla] \, \boldsymbol{u}(\boldsymbol{x}, \tau) \} \,. \tag{3.21}$$

The non-linear contributions to the evolution equations are given by the terms on the right-hand side of the previous equations (see the linear equations (3.5) and (3.6)).

For studying the non-linearities in the evolution equations, it is convenient to work in Fourier space. The reason for this is that on large distance scales in the linear regime, different Fourier modes evolve independently and thus conserve the primordial statistics, whereas on small distance scales non-linear corrections induce a coupling of different Fourier modes. Hence, our next step consists in performing a Fourier transform of the non-linear evolution equations (3.21). Our conventions for the Fourier transform are given in (1.6). By using the relation between the velocity and the velocity divergence in Fourier space, $\tilde{\boldsymbol{u}}(\boldsymbol{k}, \tau) = -i\boldsymbol{k}\,\tilde{\theta}(\boldsymbol{k}, \tau)/k^2$, we obtain the Fourier transform of the non-linear contributions on the right-hand side of the equations (3.21) as

$$\nabla \cdot [\delta(\boldsymbol{x}, \tau)\boldsymbol{u}(\boldsymbol{x}, \tau)] = \int d^3q \, d^3p \, e^{i(\boldsymbol{q}+\boldsymbol{p})\cdot\boldsymbol{x}} \, \alpha(\boldsymbol{q}, \boldsymbol{p}) \cdot \tilde{\theta}(\boldsymbol{q}, \tau)\tilde{\delta}(\boldsymbol{p}, \tau) \,,$$

$$\nabla \cdot \{[\boldsymbol{u}(\boldsymbol{x}, \tau) \cdot \nabla] \, \boldsymbol{u}(\boldsymbol{x}, \tau)\} = \int d^3q \, d^3p \, e^{i(\boldsymbol{q}+\boldsymbol{p})\cdot\boldsymbol{x}} \, \beta(\boldsymbol{q}, \boldsymbol{p}) \cdot \tilde{\theta}(\boldsymbol{q}, \tau) \, \tilde{\theta}(\boldsymbol{p}, \tau) \,, \tag{3.22}$$

where the two time-independent functions

$$\alpha(\boldsymbol{q}, \boldsymbol{p}) \equiv \frac{(\boldsymbol{q} + \boldsymbol{p}) \cdot \boldsymbol{q}}{q^2} \,, \qquad \beta(\boldsymbol{q}, \boldsymbol{p}) \equiv \frac{(\boldsymbol{q} + \boldsymbol{p})^2 \, \boldsymbol{q} \cdot \boldsymbol{p}}{2q^2p^2} \tag{3.23}$$

encode the non-linearity of the evolution equations by coupling the different Fourier modes $\boldsymbol{q}$ and $\boldsymbol{p}$ together. This mode-coupling in Fourier space is characteristic for non-linear theories. Subsequently, we perform the Fourier transform of the non-linear evolution equations (3.21), insert the relations (3.22) on the right-hand side and introduce a three-dimensional Dirac delta distribution $\delta^{\mathrm{D}}(\ldots)$,

$$\frac{\partial \tilde{\delta}(\boldsymbol{k}, \tau)}{\partial \tau} + \tilde{\theta}(\boldsymbol{k}, \tau) = - \int d^3q \, d^3p \, \delta^{\mathrm{D}}(\boldsymbol{k} - \boldsymbol{q} - \boldsymbol{p}) \, \alpha(\boldsymbol{q}, \boldsymbol{p}) \cdot \tilde{\theta}(\boldsymbol{q}, \tau)\tilde{\delta}(\boldsymbol{p}, \tau) \,, \tag{3.24}$$

$$\frac{\partial \tilde{\theta}(\boldsymbol{k}, \tau)}{\partial \tau} + \mathcal{H}(\tau)\tilde{\theta}(\boldsymbol{k}, \tau) + \frac{3}{2}\Omega_m \mathcal{H}^2(\tau)\tilde{\delta}(\boldsymbol{k}, \tau)$$
$$= - \int d^3q \, d^3p \, \delta^{\mathrm{D}}(\boldsymbol{k} - \boldsymbol{q} - \boldsymbol{p}) \, \beta(\boldsymbol{q}, \boldsymbol{p}) \cdot \tilde{\theta}(\boldsymbol{q}, \tau)\tilde{\theta}(\boldsymbol{p}, \tau) \,. \tag{3.25}$$

Notice that while the density contrast $\delta(\boldsymbol{x}, \tau)$ and the velocity divergence $\theta(\boldsymbol{x}, \tau)$ are real variables, their Fourier transforms $\tilde{\delta}(\boldsymbol{k}, \tau)$ and $\tilde{\theta}(\boldsymbol{k}, \tau)$ are complex [40].

The previous equations show that the evolution of $\tilde{\delta}(\boldsymbol{k}, \tau)$ and $\tilde{\theta}(\boldsymbol{k}, \tau)$ is determined by the mode coupling of these fields for all pairs of wavevectors $\boldsymbol{q}$ and $\boldsymbol{p}$ whose sum is $\boldsymbol{k}$, as is required by translation invariance in a spatially homogeneous Universe. Note that due to the definition of the functions α and β in (3.23), the mode-coupling integrals vanish for $\boldsymbol{k} = 0$ so that the linear theory is always valid for momenta close to $\boldsymbol{k} = 0$, even at late times.

In what follows, we omit the tilde symbol for the Fourier transform for better readability.

3.2.2. Standard formulation of perturbation theory

At this stage, we are able to investigate the solutions to the non-linear evolution equations in Fourier space, (3.24) and (3.25). Due to the non-linearity, these equations cannot be solved by analytic means so that we have to proceed with perturbative methods in the following. In standard perturbation theory [40, 92–102], one assumes that the *amplitude* of the density and velocity perturbations is small. In this case, it is possible to expand the density and velocity fields about their linear solutions [40]. As we derived in Section 3.1, the linear solutions for the density contrast and the velocity divergence correspond to simple time-dependent scalings of the initial density contrast (see (3.11) and (3.12)). If we only take the growing-mode solution

$$D_1(\tau) \equiv D_1^+(\tau), \qquad \delta_0^+(\boldsymbol{k}) \equiv \delta_0(\boldsymbol{k}) \tag{3.26}$$

into account (the decaying mode solution becomes negligible after a short period of time), the linear solutions for the density contrast and the velocity divergence read

$$\delta^L(\boldsymbol{k}, \tau) = D_1(\tau)\, \delta_0(\boldsymbol{k})\,, \qquad \theta^L(\boldsymbol{k}, \tau) = -\mathcal{H}(\tau) f(\tau) D_1(\tau)\, \delta_0(\boldsymbol{k})\,. \tag{3.27}$$

Consequently, the characteristic assumption of SPT implies that one can perform a series expansion of the density contrast $\delta(\boldsymbol{k}, \tau)$ and the velocity divergence $\theta(\boldsymbol{k}, \tau)$,

$$\delta(\boldsymbol{k}, \tau) = \sum_{n=1}^{\infty} \delta^{(n)}(\boldsymbol{k}, \tau)\,, \qquad \theta(\boldsymbol{k}, \tau) = \sum_{n=1}^{\infty} \theta^{(n)}(\boldsymbol{k}, \tau)\,, \tag{3.28}$$

in the nth-order perturbative contributions $\delta^{(n)}(\boldsymbol{k}, \tau)$ and $\theta^{(n)}(\boldsymbol{k}, \tau)$ scaling like the nth power of the initial density contrast $\delta_0(\boldsymbol{k})$, but evolving differently in time. Thereby, $\delta^{(1)}(\boldsymbol{k}, \tau) \equiv \delta^L(\boldsymbol{k}, \tau)$ and $\theta^{(1)}(\boldsymbol{k}, \tau) \equiv \theta^L(\boldsymbol{k}, \tau)$ correspond to the linear solutions in (3.27).

3.2.3. Non-linear solutions for an Einstein–de Sitter cosmology

As a first example, let us discuss the perturbative solutions to the non-linear evolution equations in the case of an EdS Universe. As we derived in Section 3.1, the linear growing mode in

EdS just equals the scale factor of the Universe, $D_1(\tau) = a(\tau)$, so that the linear growing-mode solutions for the density contrast and the velocity divergence read (see (3.17)),

$$\delta^L(\boldsymbol{k}, \tau) = a(\tau)\, \delta_0(\boldsymbol{k})\,, \qquad \theta^L(\boldsymbol{k}, \tau) = -\mathcal{H}(\tau)\, a(\tau)\, \delta_0(\boldsymbol{k})\,. \tag{3.29}$$

Based on the functional form of these equations, we make the following ansatz for the perturbative expansion in (3.28) to solve the non-linear evolution equations for EdS cosmology [96–98],

$$\delta(\boldsymbol{k}, \tau) = \sum_{n=1}^{\infty} a^n(\tau)\delta_n(\boldsymbol{k})\,, \qquad \theta(\boldsymbol{k}, \tau) = -\mathcal{H}(\tau)\sum_{n=1}^{\infty} a^n(\tau)\theta_n(\boldsymbol{k})\,, \tag{3.30}$$

where we only take the growing-mode solutions into account (see (3.26)). This perturbative expansion corresponds to an expansion in terms of the linear solution $\propto a(\tau)$ with time-independent coefficients $\delta_n(\boldsymbol{k})$ and $\theta_n(\boldsymbol{k})$, respectively. Due to this, the perturbative solutions to the non-linear evolution equations for an EdS cosmology are separable in their time and momentum dependence. We can make use of this fact to determine the form of the time-independent coefficients $\delta_n(\boldsymbol{k})$ and $\theta_n(\boldsymbol{k})$. For this purpose, we insert the perturbative expansion (3.30) into the non-linear evolution equations (3.24) and (3.25). Then, we use the relation (3.16) for the conformal expansion rate in an EdS cosmology, $\mathcal{H} = \mathcal{H}_0\, a^{-1/2}$, to perform the derivatives with respect to conformal time. This allows us to scale out overall factors of $\mathcal{H}$ and $\mathcal{H}^2$ in the evolution equations (3.24) and (3.25), respectively. Consequently, these take a homogeneous form in $a(\tau)$ so that we obtain the governing equations for the coefficients $\delta_n(\boldsymbol{k})$ and $\theta_n(\boldsymbol{k})$. These can be formally solved in terms of the initial density contrast $\delta_0(\boldsymbol{k})$ and constitute mode-coupling integrals over n powers of the initial density contrast,

$$\begin{aligned}
\delta_n(\boldsymbol{k}) &= \int d^3q_1 \ldots \int d^3q_n\, \delta^{\mathrm{D}}(\boldsymbol{k} - \boldsymbol{q}_{1\ldots n})\, F_n(\boldsymbol{q}_1, \ldots, \boldsymbol{q}_n) \cdot \delta_0(\boldsymbol{q}_1)\ldots\delta_0(\boldsymbol{q}_n)\,, \\
\theta_n(\boldsymbol{k}) &= \int d^3q_1 \ldots \int d^3q_n\, \delta^{\mathrm{D}}(\boldsymbol{k} - \boldsymbol{q}_{1\ldots n})\, G_n(\boldsymbol{q}_1, \ldots, \boldsymbol{q}_n) \cdot \delta_0(\boldsymbol{q}_1)\ldots\delta_0(\boldsymbol{q}_n)
\end{aligned} \tag{3.31}$$

with $\boldsymbol{q}_{1\ldots n} \equiv \boldsymbol{q}_1 + \ldots + \boldsymbol{q}_n$. These solution contain the kernels $F_n(\boldsymbol{q}_1, \ldots, \boldsymbol{q}_n)$ and $G_n(\boldsymbol{q}_1, \ldots, \boldsymbol{q}_n)$ which are dimensionless, scalar functions of the wave vectors $\boldsymbol{q}_1, \ldots, \boldsymbol{q}_n$. They are constructed recursively from the fundamental mode-coupling functions $\alpha(\boldsymbol{q}, \boldsymbol{p})$ and $\beta(\boldsymbol{q}, \boldsymbol{p})$, as we discuss now.

Since, for $n = 1$, the mode-coupling integrals have to reproduce the linear solution (3.29) from the perturbative expansion (3.30), i.e., $\delta_1(\boldsymbol{k}) = \theta_1(\boldsymbol{k}) = \delta_0(\boldsymbol{k})$, the first-order kernels simply equal

$$F_1(\boldsymbol{q}_1) = G_1(\boldsymbol{q}_1) \equiv 1\,. \tag{3.32}$$

3. Standard Cosmological Perturbation Theory

This means that at very early times, where the scale factor $a(\tau)$ was small and the linear contribution dominates the perturbative expansion (3.30), $\delta_0(\boldsymbol{k})$ completely characterizes the linear fluctuations.

For the higher-order kernels $n \geq 2$, one can derive recursion relations by using combinatorics [96, 98],

$$
\begin{aligned}
F_n(\boldsymbol{q}_1, \dots, \boldsymbol{q}_n) = \sum_{m=1}^{n-1} \frac{G_m(\boldsymbol{q}_1, \dots, \boldsymbol{q}_m)}{(2n+3)(n-1)} &\Big[(2n+1)\alpha(\boldsymbol{k}_1, \boldsymbol{k}_2) F_{n-m}(\boldsymbol{q}_{m+1}, \dots, \boldsymbol{q}_n) \\
&+ 2\beta(\boldsymbol{k}_1, \boldsymbol{k}_2) G_{n-m}(\boldsymbol{q}_{m+1}, \dots, \boldsymbol{q}_n) \Big] ,
\end{aligned}
\tag{3.33}
$$

$$
\begin{aligned}
G_n(\boldsymbol{q}_1, \dots, \boldsymbol{q}_n) = \sum_{m=1}^{n-1} \frac{G_m(\boldsymbol{q}_1, \dots, \boldsymbol{q}_m)}{(2n+3)(n-1)} &\Big[3\,\alpha(\boldsymbol{k}_1, \boldsymbol{k}_2) F_{n-m}(\boldsymbol{q}_{m+1}, \dots, \boldsymbol{q}_n) \\
&+ 2n\,\beta(\boldsymbol{k}_1, \boldsymbol{k}_2) G_{n-m}(\boldsymbol{q}_{m+1}, \dots, \boldsymbol{q}_n) \Big]
\end{aligned}
\tag{3.34}
$$

with

$$
\boldsymbol{k}_1 \equiv \sum_{i=1}^{m} \boldsymbol{q}_i , \qquad \boldsymbol{k}_2 \equiv \sum_{i=m+1}^{n} \boldsymbol{q}_i .
\tag{3.35}
$$

Note that momentum conservation holds for the different modes $\boldsymbol{q}_1, \dots, \boldsymbol{q}_n$ contributing to the kernels F_n and G_n, enforced by the Dirac delta distribution in the mode-coupling integrals (3.31), such that $\boldsymbol{k} = \boldsymbol{k}_1 + \boldsymbol{k}_2 = \boldsymbol{q}_1 + \dots + \boldsymbol{q}_n$. The explicit expressions for the kernels up to order $n = 4$ can be found in [96]. In order to calculate correlation functions of the density contrast, such as the power spectrum, later on, it is easier to symmetrize the kernels F_n and G_n with respect to their momenta $\boldsymbol{q}_1, \dots, \boldsymbol{q}_n$. We obtain the symmetrized kernels, denoted by F_n^s and G_n^s, by performing the sum over F_n and G_n with all possible $n!$ permutations of their n momenta and diving by $n!$ afterwards,

$$
\begin{aligned}
F_n^s(\boldsymbol{q}_1, \dots, \boldsymbol{q}_n) &= \frac{1}{n!} \sum_{\pi} F_n(\boldsymbol{q}_{\pi(1)}, \dots, \boldsymbol{q}_{\pi(n)}) , \\
G_n^s(\boldsymbol{q}_1, \dots, \boldsymbol{q}_n) &= \frac{1}{n!} \sum_{\pi} G_n(\boldsymbol{q}_{\pi(1)}, \dots, \boldsymbol{q}_{\pi(n)}) ,
\end{aligned}
\tag{3.36}
$$

where π denotes the permutations of the set $\{1, \dots, n\}$. Note that one can use the symmetrized kernels F_n^s and G_n^s instead of F_n and G_n in the mode-coupling integrals (3.31) without changing the result since their arguments are dummy variables of integration. Due to their symmetry properties, one usually uses the kernels F_n^s and G_n^s for calculations of large-scale structure observables (see 4.4).

As an example, the explicit symmetrized expressions for the second-order kernels are computed by inserting the first-order kernels (3.32) and the definitions of the mode mode-coupling

functions α and β (see (3.23)) in the recursion relations (3.33) and (3.34) and by symmetrizing them according to (3.36) afterwards. The resulting equations for the symmetrized kernels have a simple and intuitive form,

$$
\begin{aligned}
F_2^s(\boldsymbol{q}_1, \boldsymbol{q}_2) &= \frac{5}{7} + \frac{1}{2}\left(\frac{\boldsymbol{q}_1 \cdot \boldsymbol{q}_2}{q_1^2} + \frac{\boldsymbol{q}_1 \cdot \boldsymbol{q}_2}{q_2^2}\right) + \frac{2}{7}\frac{(\boldsymbol{q}_1 \cdot \boldsymbol{q}_2)^2}{q_1^2 q_2^2}, \\
G_2^s(\boldsymbol{q}_1, \boldsymbol{q}_2) &= \frac{3}{7} + \frac{1}{2}\left(\frac{\boldsymbol{q}_1 \cdot \boldsymbol{q}_2}{q_1^2} + \frac{\boldsymbol{q}_1 \cdot \boldsymbol{q}_2}{q_2^2}\right) + \frac{4}{7}\frac{(\boldsymbol{q}_1 \cdot \boldsymbol{q}_2)^2}{q_1^2 q_2^2}.
\end{aligned}
\tag{3.37}
$$

From this we can see that the mode-coupling to second-order reaches its maximum if the momenta $\boldsymbol{q}_1$ and $\boldsymbol{q}_2$ are aligned, whereas the kernels vanish in the case where the momenta are anti-parallel.

In general, the symmetrized kernels F_n^s and G_n^s have the following characteristic properties [96, 293, 294]. First, if the overall momentum $\boldsymbol{k} = \boldsymbol{q}_1 + \ldots + \boldsymbol{q}_n$ is small, but the individual momenta $\boldsymbol{q}_i$ with $i \in \{1, \ldots, n\}$ are not, the symmetrized kernel grows as the second power of the overall momentum $\boldsymbol{k}$,

$$
F_n^s(\boldsymbol{q}_1, \ldots, \boldsymbol{q}_n)_{k \to 0} \propto k^2.
\tag{3.38}
$$

Second, if, in contrast, the overall momentum $\boldsymbol{k}$ stays fixed, but one argument of F_n^s, which we call $\boldsymbol{p}$, gets large, the symmetrized kernels scale as the inverse square of this momentum,

$$
F_n^s(\boldsymbol{q}_1, \ldots, \boldsymbol{q}_{n-2}, \boldsymbol{p}, -\boldsymbol{p})_{p \gg q_i} \propto \frac{k^2}{p^2}.
\tag{3.39}
$$

This behavior is equivalent for G_n^s. Furthermore, if one of the arguments $\boldsymbol{q}_i$ of the symmetrized kernels F_n^s or G_n^s goes to zero, one finds an infrared divergence $\propto \boldsymbol{q}_i/q_i^2$, originating from the infrared behavior of the mode-coupling functions $\alpha(\boldsymbol{q}, \boldsymbol{p})$ and $\beta(\boldsymbol{q}, \boldsymbol{p})$. However, if the partial sum of several momenta goes to zero, no infrared divergences occur. Finally, the kernels are F_n^s and G_n^s are symmetric under $\boldsymbol{q}_i \leftrightarrow \boldsymbol{q}_j$ with $i, j \in \{1, \ldots, n\}$ so that

$$
F_n^s(\ldots, \boldsymbol{q}_i, \ldots, \boldsymbol{q}_j, \ldots) = F_n^s(\ldots, \boldsymbol{q}_j, \ldots, \boldsymbol{q}_i, \ldots),
\tag{3.40}
$$

which is equivalently valid for G_n^s. This property often allows to reduce analytic expressions containing several kernels of different momentum structure to simpler relations. This becomes in particular important when calculating large-scale structure observables, as we show explicitly in Section 4.4.

3.2.4. Approximate non-linear solutions for arbitrary cosmologies

In general, for cosmological models other than EdS, the perturbative expansion is more complicated since the solutions at each order are functions whose dependence on conformal time τ

and momentum $\boldsymbol{k}$ is not separable and thus cannot be directly integrated [107, 295–297]. Furthermore, the growing-mode solutions at order n are not proportional to $[D_1(\tau)]^n$ or $a^n(\tau)$, respectively, as in the case of an EdS cosmology (see (3.30)). There exist no recursion relations for the perturbative kernels as (3.33) and (3.34) for arbitrary Friedmann-Robertson-Walker (FRW) cosmological models with $\Omega_m \neq 1$ and/or $\Omega_\Lambda \neq 0$. However, once the growth factors have been scaled out, one finds that the perturbative solutions only depend extremely weak on the cosmological parameters Ω_m and Ω_Λ [282, 295, 296]. Due to this very weak dependence it is possible to apply a simple approximation to the non-linear evolution equations for general Ω_m and Λ which leads to separable solutions at each order in perturbation theory and yields the same recursion relation as for an EdS Universe [298]. Hence, the dependence of the perturbative solutions on the cosmological parameters Ω_m and Ω_Λ is completely encoded in the linear growth factor $D_1(\tau)$. Let us now consider this approximation in detail.

Our aim is to solve the non-linear evolution equations (3.24) and (3.25) in Fourier space approximately for arbitrary cosmological models by imposing a perturbative expansion with a separable time and momentum dependence. Since the growing-mode solutions of the linear evolution equations (3.8) are in general of the form (3.27), our ansatz for the corresponding separable perturbative expansion reads [298]

$$\delta(\boldsymbol{k},\tau) = \sum_{n=1}^{\infty} D_n(\tau)\delta_n(\boldsymbol{k})\,, \qquad \theta(\boldsymbol{k},\tau) = -\mathcal{H}(\tau)f(\tau)\sum_{n=1}^{\infty} E_n(\tau)\theta_n(\boldsymbol{k})\,. \qquad (3.41)$$

This is a generalization of the perturbative expansions (3.30) in an EdS cosmology where we have $D_n(\tau) = E_n(\tau) = [D_1(\tau)]^n$ with $D_1(\tau) = a(\tau)$ and $f(\tau) = 1$.

If we insert the perturbative expansions (3.41) into the non-linear evolution equations (3.24) and (3.25), we can use the definition of the linear growth rate $f(\tau)$ as well as the differential equation (3.8) for the linear growth factor $D_1(\tau)$, to replace the time derivative by a derivative with respect to D_1. This allows to scale out an overall factor $(\mathcal{H}f)$ in (3.24) and a factor $-(\mathcal{H}f)^2$ in (3.25). The resulting equations for the nth order of the perturbative expansion then read

$$\frac{\partial D_n(\tau)}{\partial \ln D_1}\delta_n(\boldsymbol{k}) - E_n(\tau)\theta_n(\boldsymbol{k})$$
$$= \int d^3q\, d^3p\, \delta^{\mathrm{D}}(\boldsymbol{k}-\boldsymbol{q}-\boldsymbol{p})\, \alpha(\boldsymbol{q},\boldsymbol{p}) \cdot \sum_{m=1}^{n-1} E_m(\tau)D_{n-m}(\tau)\, \theta_m(\boldsymbol{q})\delta_{n-m}(\boldsymbol{p})\,, \qquad (3.42)$$

$$\frac{\partial E_n(\tau)}{\partial \ln D_1}\theta_n(\boldsymbol{k}) + \left(\frac{3}{2}\frac{\Omega_m}{f^2}-1\right)E_n(\tau)\theta_n(\boldsymbol{k}) - \frac{3}{2}\frac{\Omega_m}{f^2}D_n(\tau)\delta_n(\boldsymbol{k})$$
$$= \int d^3q\, d^3p\, \delta^{\mathrm{D}}(\boldsymbol{k}-\boldsymbol{q}-\boldsymbol{p})\, \beta(\boldsymbol{q},\boldsymbol{p}) \cdot \sum_{m=1}^{n-1} E_m(\tau)E_{n-m}(\tau)\, \theta_m(\boldsymbol{q})\theta_{n-m}(\boldsymbol{p})\,. \qquad (3.43)$$

The time and momentum dependence of this system of evolution equations becomes separable if we set

$$D_n(\tau) \;=\; E_n(\tau) = [D_1(\tau)]^n \;, \tag{3.44}$$

$$f(\tau) \;=\; \Omega_m^{1/2} \tag{3.45}$$

The latter condition, which has been first noted in the context of second-order perturbation theory in [299] and was generalized in [298], leads indeed to separable solutions at any order in perturbation theory. Furthermore, after scaling out an overall factor $[D_1(\tau)]^n$, the purely momentum-dependent evolution equations arising from (3.42) and (3.43) reduce to the same equations as in the EdS case with $\Omega_m = 1$ and $\Omega_\Lambda = 0$. Consequently, their formal solution is given by the mode-coupling integrals (3.31) and the corresponding recursion relations (3.32) and (3.33).

This behavior makes the solution of the non-linear evolution equations for arbitrary cosmologies very convenient. Actually, it turns out that (3.45) is a highly accurate approximation to the exact solutions of the non-linear evolution equations for arbitrary cosmologies. For instance, the precise solution for the second-order growth factor in cosmological models with $\Omega_\Lambda = 0$ is given by $D_2(\tau)/D_1(\tau)^2 = 1 + 3/17 \left(\Omega_m^{-2/63} - 1 \right)$ and hence extremely insensitive to Ω_m [40].

3.3. Diagrammatic formulation of perturbation theory

In the standard formulation of perturbation theory that we discussed in the previous Section 3.2, one describes the non-linear dynamics as a collection of linear waves which interact through the mode-coupling functions α and β. Thus, even if one chooses growing-mode initial conditions, after scattering due to non-linear interactions, the waves do not remain purely in the growing mode but sub-dominant time dependencies arise. In the standard treatment of perturbation theory, these are neglected and only the fastest growing mode, proportional to $[D_1(\tau)]^n$ at the perturbative order n is taken into account. In this section, we introduce the diagrammatic formulation of standard perturbation theory which generalizes the results discussed in Section 3.2 by including the full time dependence of the non-linear solutions at every order in perturbation theory [236, 300]. This formulation has the advantage that it allows to write the non-linear evolution equations in a more compact form and that it allows for an interpretation of the non-linear solutions in terms of diagrams.

3.3.1. Fluid equations in a compact notation

Our aim is to express the non-linear evolution equations in Fourier space, (3.24) and (3.25), in a compact, more symmetric form [40, 100, 142, 143, 236]. For this purpose, we replace the time derivative in the non-linear evolution equations by a logarithmic derivative with respect to the linear growth factor $D_1(\tau)$. In order to do so, we follow the same procedure as for deriving the equations (3.42) and (3.43), but do not perform a perturbative expansion yet. Then, the non-linear evolution equations (3.24) and (3.25) can be recast as follows (see (3.42)-(3.43)),

$$\frac{\partial \delta(\boldsymbol{k}, \tau)}{\partial \ln D_1} + \Theta(\boldsymbol{k}, \tau) = \int d^3q \, d^3p \, \delta^{\mathrm{D}}(\boldsymbol{k} - \boldsymbol{q} - \boldsymbol{p}) \, \alpha(\boldsymbol{q}, \boldsymbol{p}) \cdot \Theta(\boldsymbol{q}, \tau) \, \delta(\boldsymbol{p}, \tau) \,, \tag{3.46}$$

$$\begin{aligned} \frac{\partial \Theta(\boldsymbol{k}, \tau)}{\partial \ln D_1} &+ \left(\frac{3}{2}\frac{\Omega_m}{f^2} - 1\right)\Theta(\boldsymbol{k}, \tau) - \frac{3}{2}\frac{\Omega_m}{f^2}\delta(\boldsymbol{k}, \tau) \\ &= \int d^3q \, d^3p \, \delta^{\mathrm{D}}(\boldsymbol{k} - \boldsymbol{q} - \boldsymbol{p}) \, \beta(\boldsymbol{q}, \boldsymbol{p}) \cdot \Theta(\boldsymbol{q}, \tau) \, \Theta(\boldsymbol{p}, \tau) \,, \end{aligned} \tag{3.47}$$

where we have defined the quantity

$$\Theta(\boldsymbol{k}, \eta) \equiv -\frac{\theta(\boldsymbol{k}, \eta)}{\mathcal{H}f} \,. \tag{3.48}$$

Note that this equation is valid for arbitrary cosmological models since we have not specified the background evolution here.

For rewriting these equations in a compact form (see [236, 300]), we first replace the conformal time τ by introducing a new time variable η, which we define as the logarithm of the linear growth factor $D_1(\tau)$,

$$\eta \equiv \ln D_1(\tau) \,. \tag{3.49}$$

In terms of this new time variable, the growth rate f then reads (see (3.13))

$$f(\eta) \equiv \frac{1}{\mathcal{H}}\frac{d\eta}{d\tau} = \frac{d\eta}{d\ln a} \,. \tag{3.50}$$

As a second step, we write the density contrast $\delta(\boldsymbol{k}, \eta)$ and the velocity divergence $\theta(\boldsymbol{k}, \eta)$, contained in the definition of $\Theta(\boldsymbol{k}, \eta)$ in (3.48), as a doublet $\psi_a(\boldsymbol{k}, \eta)$ with index $a \in \{1, 2\}$,

$$\psi_a(\boldsymbol{k}, \eta) \equiv \begin{pmatrix} \delta(\boldsymbol{k}, \eta) \\ \Theta(\boldsymbol{k}, \eta) \end{pmatrix} \,. \tag{3.51}$$

Next, we encode the dependence of the non-linear equations (3.46) and (3.47) on the cosmological model, parametrized by the linear growth rate $f(\eta)$ and the matter density parameter $\Omega_m(\eta)$, in a matrix [100]

$$\Omega_{ab}(\eta) = \begin{pmatrix} 0 & -1 \\ -\frac{3}{2}\frac{\Omega_m}{f^2} & \frac{3}{2}\frac{\Omega_m}{f^2} - 1 \end{pmatrix} \,. \tag{3.52}$$

Note that the generalized, most generic form of this matrix [156] involves as well a momentum dependence, $\Omega_{ab}(\boldsymbol{k}, \eta)$.[2] However, since our following considerations merely comprise cosmological models where the background-encoding matrix is momentum independent and thus of the form (3.52), we omit the momentum dependence of the latter henceforth.

Proceeding from this, we finally summarize the non-linear terms on the right-hand side of the equations (3.46) and (3.47), characterized by the mode-coupling functions $\alpha(\boldsymbol{q}, \boldsymbol{p})$ and $\beta(\boldsymbol{q}, \boldsymbol{p})$ (see (3.23)), by introducing a vertex function $\gamma_{abc}(\boldsymbol{k}, \boldsymbol{q}, \boldsymbol{p})$ with $a, b, c \in \{1, 2\}$. The only independent, non-vanishing elements of γ_{abc} are products of the Dirac delta distribution and the mode-coupling functions α and β,

$$
\begin{aligned}
\gamma_{121}(\boldsymbol{k}, \boldsymbol{q}, \boldsymbol{p}) = \gamma_{112}(\boldsymbol{k}, \boldsymbol{p}, \boldsymbol{q}) &= \frac{1}{2}\, \delta^{\mathrm{D}}(\boldsymbol{k} - \boldsymbol{q} - \boldsymbol{p}) \cdot \alpha(\boldsymbol{q}, \boldsymbol{p})\,, \\
\gamma_{222}(\boldsymbol{k}, \boldsymbol{q}, \boldsymbol{p}) &= \delta^{\mathrm{D}}(\boldsymbol{k} - \boldsymbol{q} - \boldsymbol{p}) \cdot \beta(\boldsymbol{q}, \boldsymbol{p})\,.
\end{aligned}
\tag{3.53}
$$

All other elements of the vertex function γ_{abc} are equal to zero. Furthermore, it is symmetric in the sense that $\gamma_{abc}(\boldsymbol{k}, \boldsymbol{q}, \boldsymbol{p}) = \gamma_{acb}(\boldsymbol{k}, \boldsymbol{p}, \boldsymbol{q})$. Note that γ_{abc} does not depend on time, but only on momentum and encodes all non-linear couplings of the system of evolution equations.

At this point, we can rewrite the non-linear evolution equations (3.46) and (3.47) as compact equations in matrix form. For this, we use the definitions of the doublet $\psi_a(\boldsymbol{k}, \eta)$, the matrix $\Omega_{ab}(\eta)$ and the vertex functions $\gamma_{abc}(\boldsymbol{k}, \boldsymbol{q}, \boldsymbol{p})$ in (3.51), (3.52) and (3.53), to combine (3.46) and (3.47) into a compact expression for non-linear fluid equations [236, 300],

$$
\partial_\eta \psi_a(\boldsymbol{k}, \eta) + \Omega_{ab}(\eta)\, \psi_b(\boldsymbol{k}, \eta) = \gamma_{abc}(\boldsymbol{k}, \boldsymbol{q}, \boldsymbol{p})\, \psi_b(\boldsymbol{q}, \eta)\, \psi_c(\boldsymbol{p}, \eta)\,.
\tag{3.54}
$$

Here and henceforth, we use the convention to sum repeated indices implicitly and integrate over internal momenta whenever the vertex function $\gamma_{abc}(\boldsymbol{k}, \boldsymbol{q}, \boldsymbol{p})$ appears.

3.3.2. Linear propagator

For solving the non-linear fluid equations (3.54), the basic assumption in the framework of SPT is that the amplitude of the perturbations ψ_a is small (see Section 3.2.2). As a consequence, one can solve the fluid equations perturbatively by treating the non-linear contribution on the right-hand side of (3.54) as a perturbation to the linearized equations,

$$
\partial_\eta \psi_a^L(\boldsymbol{k}, \eta) + \Omega_{ab}(\eta)\, \psi_b^L(\boldsymbol{k}, \eta) = 0\,,
\tag{3.55}
$$

where the index L indicates the linear approximation. The formal solution of the linearized fluid equations is given in terms of a Green's function $g_{ab}(\eta, \eta_0)$ and the initial conditions

---

[2]The momentum dependence of the background-encoding matrix $\Omega_{ab}(\boldsymbol{k}, \eta)$ has to be taken into account to treat, e.g., scalar-tensor modifications of gravity or cosmological models containing massive neutrinos (see [301–303] as well as Section 5.5).

$\psi_a(\boldsymbol{k}, \eta_0)$ [101]. It reads

$$\psi_a^L(\boldsymbol{k}, \eta) = \exp\left[\int_{\eta_0}^{\eta} d\eta' \, \Omega_{ab}(\eta')\right] \Theta^{\mathrm{H}}(\eta - \eta_0) \, \psi_b(\boldsymbol{k}, \eta_0) \equiv g_{ab}(\eta, \eta_0) \, \psi_b(\boldsymbol{k}, \eta_0) \,. \tag{3.56}$$

Here, we denoted the Heaviside step function by $\Theta^{\mathrm{H}}(\eta)$ to avoid confusion with the velocity divergence field $\Theta(\boldsymbol{k}, \eta)$, as defined in (3.48). Note that if the cosmology-encoding matrix Ω_{ab} is momentum dependent, as it is the case in its most general form, the Green's function involves a momentum dependence as well, such that $g_{ab}(\boldsymbol{k}, \eta, \eta_0)$. The explicit form of the momentum-dependent linear propagator for generic cosmological models is given in the appendix of [156]. If the matrix Ω_{ab} is independent of $\boldsymbol{k}$ and η and thus constant, the Green's function depends on the difference $\eta - \eta_0$ only. This is for instance the case for an EdS cosmology, as we show explicitly in the next section.

The Green's function $g_{ab}(\eta, \eta_0)$ is referred to as the linear retarded propagator [142, 143]. It gives the time evolution of the linear density or velocity perturbation ψ_a^L from a point of time η', for example the initial time η_0, to a later point of time η [148, 304],

$$\psi_a^L(\boldsymbol{k}, \eta) = g_{ab}(\eta, \eta') \, \psi_b^L(\boldsymbol{k}, \eta') \tag{3.57}$$

with $\eta' \geq \eta$. By inserting the linear solution above in the linearized fluid equations (3.55), we derive that the linear propagator satisfies the differential equation

$$[\delta_{ab} \partial_\eta + \Omega_{ab}(\eta)] \, g_{bc}(\eta, \eta') = 0 \tag{3.58}$$

with the causal boundary condition

$$g_{ab}(\eta, \eta) = \delta_{ab} \,, \tag{3.59}$$

where δ_{ab} represents the Kronecker delta symbol. Moreover, the linear propagator possess the property

$$g_{ab}(\eta, \eta') \, g_{bc}(\eta', \eta'') = g_{ac}(\eta, \eta'') \,, \tag{3.60}$$

which allows to decompose its time evolution.

Since the definition of the linear propagator via (3.56) constituted the last missing ingredient for solving the non-linear fluid equations, we can now continue with deriving their solutions for different cosmological models.

3.3.3. Approximate solutions of the fluid equations for arbitrary cosmologies

In order to solve the non-linear fluid equations (3.54) explicitly, we have to specify the cosmological model determining the background evolution of the Universe. Since the complete dependence on the background cosmology is encoded in the matrix $\Omega_{ab}(\eta)$, defined in (3.52), this

amounts in determining the matter density parameter $\Omega_m(\eta)$ and the linear growth rate $f(\eta)$. As discussed in Section 3.2.4, the condition (see (3.45))

$$f(\eta) \simeq \Omega_m^{1/2}\,, \tag{3.61}$$

leading to separable solutions for the non-linear evolution equations, is a very good approximation to the exact numerical solutions. Due to this, one uses this approximation to determine the matrix $\Omega_{ab}(\eta)$ in (3.52), which then just contains constant elements and coincides with the one in the case of an EdS cosmology where $\Omega_m = 1$,

$$\Omega_{ab}(\eta) \simeq \Omega_{ab}^{\mathrm{EdS}}(\eta)\,. \tag{3.62}$$

We discuss the explicit solution for an EdS cosmology below. The phenomenologically interesting cases of a ΛCDM universe or a universe with (non-clustering) quintessence [142–144, 148, 304] are then treated by using the matrix $\Omega_{ab}^{\mathrm{EdS}}(\eta)$, but taking the time dependence $\eta = \ln D_1(\tau)$ in terms of the linear growth factor $D_1(\tau)$ correctly into account, i.e., $D_1(\tau) \neq a(\tau)$. For a ΛCDM cosmology, the linear growth factor is explicitly given in (3.18).

If we approximate the dependence of the non-linear solutions on the underlying cosmological model in this way, the growing mode of the perturbations $\psi_a(\boldsymbol{k}, \eta)$ is treated correctly. However, the decaying mode arises with a wrong time dependence [156]. Since the growing and decaying modes mix due to mode-coupling through the vertex functions γ_{abc}, this approximation works well in the linear regime, but breaks down when non-linearities become important. A comparison of the non-linear solutions for general cosmological models obtained with and without approximating the matrix $\Omega_{ab}(\eta)$ by the one in the EdS case, (3.62), can be found in [156].

In this section, we discussed the solutions to the fluid equations (3.54) for different cosmological models. These correspond to generalizations of the results in Section 3.2 which yield the growing-mode solutions. The matrix formulation of SPT, however, allows to include the full time dependence of the non-linear solutions at each order in perturbation theory. As a starting point, let us derive the solutions of the fluid equations for the simplest case of a flat, matter-dominated EdS universe.

3.3.4. Solutions of the fluid equations for an Einstein–de Sitter cosmology

In an EdS cosmology, describing a flat ($k = 0$) universe with matter only ($\Omega_m = 1, \Omega_\Lambda = 0$), the linear growth factor of density perturbations in the growing mode, $D_1(\tau)$, equals the scale factor $a(\tau)$ (see (3.17)) so that the time variable η of the fluid equations, as defined in (3.49), simply reads

$$\eta = \ln a(\tau)\,. \tag{3.63}$$

Moreover, the linear growth rate for an EdS universe, (3.17), is given by $f(\tau) = 1$. By taking this into account, using $\Omega_{\text{tot}} = 1$ as well as the second Friedmann equation with $\Omega_\Lambda = 0$ (see (2.9)-(2.10)), the cosmology-encoding matrix $\Omega_{ab}(\eta)$ in (3.52) reduces in the EdS case to

$$\Omega_{ab}^{\text{EdS}}(\eta) = \begin{pmatrix} 0 & -1 \\ -\frac{3}{2}\,\Omega_m & 1 + \frac{1}{\mathcal{H}^2}\frac{\partial\mathcal{H}}{\partial\tau} \end{pmatrix} = \begin{pmatrix} 0 & -1 \\ -3/2 & 1/2 \end{pmatrix} \tag{3.64}$$

with $\Omega_m = 1$. From the second equality, we see explicitly that this matrix contains in fact constant elements only and hence is time independent, $\Omega_{ab}^{\text{EdS}}(\eta) = \Omega_{ab}^{\text{EdS}}$. Due to this time independence of the matrix Ω_{ab}^{EdS}, it is possible to derive an implicit integral solution of the non-linear fluid equations (3.54). This solution is determined by performing a Laplace transform of (3.54) with respect to the time variable η. We denote the Laplace transform of the doublet (3.51) by $\hat{\psi}_a(\mathbf{k}, \omega)$, where the new time variable ω constitutes the complex number frequency. The definition of the Laplace transform, its inverse as well as its differentiation property are given in the equations (1.7)-(1.8).

We evaluate the Laplace transform of the fluid equations by first using the differentiation property (1.8) to eliminate the η-derivative on the left-hand side of (3.54). On the right-hand side of the equations, we first perform the inverse Laplace transform of $\psi_b(\mathbf{k}_1, \eta)$ in order to evaluate the overall Laplace transform with respect to $\psi_c(\mathbf{k}_2, \eta)$ afterwards. This allows us to write the fluid equations purely in terms of Laplace-transformed quantities,

$$\sigma_{ab}^{-1}(\omega)\,\hat{\psi}_b(\mathbf{k}, \omega) = \psi_a(\mathbf{k}, \eta_0) + \gamma_{abc}(\mathbf{k}, \mathbf{q}, \mathbf{p}) \oint_{c-i\infty}^{c+i\infty} \frac{d\omega_1}{2\pi i}\,\hat{\psi}_b(\mathbf{q}, \omega_1)\,\hat{\psi}_c(\mathbf{p}, \omega - \omega_1)\,, \tag{3.65}$$

where the initial time is denoted by η_0. Notice that, due to the differentiation property (1.8), the doublet $\psi_a(\mathbf{k}, \eta_0)$, which sets the initial conditions, is not a Laplace-transformed quantity. Furthermore, we have combined the second term we get from the differentiation equation and the one containing the matrix Ω_{ab}^{EdS} into the matrix $\sigma_{ab}^{-1}(\omega) \equiv \omega\,\delta_{ab} + \Omega_{ab}^{\text{EdS}}$.

Next, we multiply the expression (3.65) by the inverse of the matrix $\sigma_{ab}^{-1}(\omega)$, yielding

$$\sigma_{ab}(\omega) = \frac{1}{(2\omega + 3)(\omega - 1)} \begin{pmatrix} 2\omega + 1 & 2 \\ 3 & 2\omega \end{pmatrix}. \tag{3.66}$$

Then, we evaluate the inverse Laplace transformation with a similar procedure as before in order to regain a relation solely in terms of the doublet (3.51). This finally yields the formal integral solution of the non-linear fluid equations (3.54) [142, 236, 300]. In the case of an EdS Universe, this solution can be expressed in terms of the linear propagator,

$$\psi_a(\mathbf{k}, \eta) = g_{ab}(\eta, \eta_0)\psi_b(\mathbf{k}, \eta_0) + \int_{\eta_0}^{\eta} d\eta'\,g_{ab}(\eta, \eta')\gamma_{bcd}(\mathbf{k}, \mathbf{q}, \mathbf{p})\psi_c(\mathbf{q}, \eta')\psi_d(\mathbf{p}, \eta')\,, \tag{3.67}$$

by defining

$$g_{ab}(\eta, \eta') \equiv \oint\limits_{c-i\infty}^{c+i\infty} \frac{d\omega}{2\pi i}\, \sigma_{ab}(\omega)\, e^{\omega(\eta-\eta')} = \left[B\, e^{(\eta-\eta')} + A\, e^{-\frac{3}{2}(\eta-\eta')} \right]_{ab} \Theta^{\mathrm{H}}(\eta - \eta') \qquad (3.68)$$

with

$$B = \frac{1}{5} \begin{pmatrix} 3 & 2 \\ 3 & 2 \end{pmatrix}, \qquad A = \frac{1}{5} \begin{pmatrix} 2 & -2 \\ -3 & 3 \end{pmatrix}. \qquad (3.69)$$

Note that for an EdS universe, it is possible to derive an explicit solution for the linear propagator. Thereby, one chooses $c > 1$ to pick out the standard retarded propagator [300]. The Heaviside step function $\Theta^{\mathrm{H}}(\eta - \eta')$ ensures causality by requiring $\eta \geq \eta'$ for $g_{ab}(\eta, \eta') \neq 0$, whereas $g_{ab}(\eta, \eta') = 0$ for $\eta < \eta'$.

Up to this point, we have not specified any particular initial conditions. From a physical point of view, the most interesting initial conditions are those where the initial density and velocity perturbations $\psi_a(\boldsymbol{k}, \eta_0)$ are not independent, but proportional to Gaussian random fields. In this case, one can write the initial conditions as

$$\psi_a(\boldsymbol{k}, \eta_0) = u_a\, \delta_0(\boldsymbol{k}), \qquad (3.70)$$

where u_a denotes a constant two-component 'vector' and $\delta_0(\boldsymbol{k}) \equiv \delta(\boldsymbol{k}, \eta_0)$ corresponds to a Gaussian-distributed initial density field. Thus, we effectively reduce the non-Gaussianity of the initial conditions to a Gaussian problem where the linear solutions are Gaussian random fields. For the sake of simplicity, we consider only initial conditions of the form (3.70) throughout this thesis.

From the time dependence of the linear propagator $g_{ab}(\eta, \eta_0)$ in (3.68) we can readily identify the growing- and decaying-mode initial conditions. Since the first term in (3.68) represents the propagation of linear growing-mode solutions and the second one corresponds to linear decaying-mode propagation, the growing ($\psi_a(\boldsymbol{k}, \eta) \propto \exp(\eta - \eta_0)$) and the decaying ($\psi_a(\boldsymbol{k}, \eta) \propto \exp[-3/2\,(\eta - \eta_0)]$) modes can be selected by considering initial fields $\psi_a(\boldsymbol{k}, \eta_0)$ proportional to (see (3.70))

$$u_a^+ = \begin{pmatrix} 1 \\ 1 \end{pmatrix} \qquad \text{and} \qquad u_a^- = \begin{pmatrix} 1 \\ -3/2 \end{pmatrix}. \qquad (3.71)$$

If we set the initial conditions in the growing mode, $\psi_a(\boldsymbol{k}, \eta_0) = u_a^+\, \delta_0(\boldsymbol{k}) \propto (1, 1)$, the linear solution of the fluid equations, $\psi_a^L(\boldsymbol{k}, \eta) = g_{ab}(\eta, \eta_0)\, \psi_b(\boldsymbol{k}, \eta_0)$ (see (3.67)) recovers the standard time scaling. This is due to the fact that the second term of the linear propagator $g_{ab}(\eta, \eta_0)$ in (3.68) vanishes upon contraction with $\psi_a(\boldsymbol{k}, \eta_0)$, while the first term reproduces the usual growing-mode time dependence $\psi_a^L(\boldsymbol{k}, \eta) = e^\eta \psi_a(\boldsymbol{k}, 0) = D_1(\tau)\, \psi_a(\boldsymbol{k}, 0)$ with $\eta_0 = 0$ and $D_1(\tau) = a(\tau)$.

3.3.5. Perturbative solutions of the fluid equations

The formal integral solution (3.67) can be interpreted as an equation for $\psi_a(\boldsymbol{k}, \eta)$ in the presence of an 'external source' $\psi_b(\boldsymbol{k}, \eta_0)$ with prescribed statistics given by the initial conditions [300]. It contains the full time dependence of the non-linear solutions. While the first term in (3.67) describes the linear propagation from the initial conditions, the second term contains information about the non-linear mode couplings. This non-linear contribution comes from the interaction of all pairs of waves $\boldsymbol{q}$ and $\boldsymbol{p}$ (whose sum is $\boldsymbol{k} = \boldsymbol{q} + \boldsymbol{p}$ due to translation invariance) at all intermediate times η' (with $0 \leq \eta' \leq \eta$). The interaction is characterized by the matrix γ_{abc} and then linearly evolved in time from η' to η by the propagator $g_{ab}(\eta, \eta')$. Even if growing-mode initial conditions are imposed, the waves do not purely remain in the growing mode after the scattering, but there is also a contribution from the decaying-mode propagation. Thus, at the time η, the non-linear contribution depends on all scattering processes that happened between $\eta' = \eta_0$, where the initial conditions are set, and $\eta' = \eta$.

This interpretation of the solution (3.67) to the non-linear fluid equations is essentially a field-theoretical description of gravitational instability [236]. One can understand the non-linear corrections as loop corrections to the linear propagator and the matrix γ_{abc} as interaction vertex. In Section 3.3.6, we see that this simple interpretation leads to a graphical representation in terms of diagrams if the solution $\psi_a(\boldsymbol{k}, \eta)$ is determined recursively by means of perturbation theory.

Proceeding from the formal integral solution of the fluid equations (3.67), we seek for an explicit perturbative solution for $\psi_a(\boldsymbol{k}, \eta)$ in form of a series expansion (see (3.28) and (3.31)),

$$\psi_a(\boldsymbol{k}, \eta) = \sum_{n=1}^{\infty} \psi_a^{(n)}(\boldsymbol{k}, \eta), \tag{3.72}$$

where [143]

$$\psi_a^{(n)}(\boldsymbol{k}, \eta) = \int d^3 q_1 \ldots \int d^3 q_n \, \delta^{\mathrm{D}}(\boldsymbol{k} - \boldsymbol{q}_{1\ldots n})$$
$$\cdot \bar{\mathcal{F}}_{a a_1 a_2 \ldots a_n}^{(n)}(\boldsymbol{q}_1, \ldots, \boldsymbol{q}_n, \eta) \cdot \psi_{a_1}(\boldsymbol{q}_1, \eta_0) \ldots \psi_{a_n}(\boldsymbol{q}_n, \eta_0) \tag{3.73}$$

with $\boldsymbol{k}_{1\ldots n} \equiv \boldsymbol{k}_1 + \ldots + \boldsymbol{k}_n$. Note that in contrast to (3.31), the kernels $\mathcal{F}_{a a_1 a_2 \ldots a_n}^{(n)}(\boldsymbol{q}_1, \ldots, \boldsymbol{q}_n, \eta)$ defined above depend on the time η. Moreover, their dependence on time is non-trivial since it does not only include the fastest growing mode like the kernels $F_n(\boldsymbol{q}_1, \ldots, \boldsymbol{q}_n)$ and $G_n(\boldsymbol{q}_1, \ldots, \boldsymbol{q}_n)$ but also sub-leading η-dependent terms.

However, the standard recursion relations for the kernels $F_n(\boldsymbol{q}_1, \ldots, \boldsymbol{q}_n)$ and $G_n(\boldsymbol{q}_1, \ldots, \boldsymbol{q}_n)$, given in (3.33) and (3.34), can be easily derived in the diagrammatic formulation of SPT. For

this purpose, we first assume Gaussian-distributed growing-mode initial conditions, $\psi_a(\boldsymbol{k}, \eta_0) = u_a^+ \delta_0(\boldsymbol{k})$ (see (3.70) and (3.71)) so that (3.73) reduces to

$$\psi_a^{(n)}(\boldsymbol{k}, \eta) = \int d^3 q_1 \ldots \int d^3 q_n \, \delta^{\mathrm{D}}(\boldsymbol{k} - \boldsymbol{q}_{1\ldots n}) \, \mathcal{F}_a^{(n)}(\boldsymbol{q}_1, \ldots, \boldsymbol{q}_n, \eta) \cdot \delta_0(\boldsymbol{q}_1) \ldots \delta_0(\boldsymbol{q}_n) \quad (3.74)$$

with

$$\mathcal{F}_a^{(n)}(\boldsymbol{q}_1, \ldots, \boldsymbol{q}_n, \eta) \equiv \bar{\mathcal{F}}_{a a_1 \ldots a_n}^{(n)}(\boldsymbol{q}_1, \ldots, \boldsymbol{q}_n, \eta) \, u_{a_1}^+ \ldots u_{a_{2n}}^+ \,. \quad (3.75)$$

Inserting the perturbative expansion (3.72) and the simplified expressions (3.74) into the formal integral solution (3.67) allows us to determine the recursion relations satisfied by the kernels $\bar{\mathcal{F}}_a^{(n)}(\boldsymbol{q}_1, \ldots, \boldsymbol{q}_n, \eta)$ at any order in perturbation theory. For the first-order kernel at $n = 1$ we can read off the relation

$$\mathcal{F}_a^{(1)}(\boldsymbol{q}_1, \eta) \, \delta_{\mathrm{D}}(\boldsymbol{k} - \boldsymbol{q}_1) = g_{ab}(\eta, \eta_0) \, u_b^+ = e^{(\eta - \eta_0)} \, u_a^+ \,, \quad (3.76)$$

where we used (3.68) and (3.71) for the last equality. Here, we see that the first-order kernel, in contrast to the higher-order ones, does not depend on momentum, but only on time. Furthermore, at order n with $n > 1$, we find the equality

$$\psi_a^{(n)}(\boldsymbol{k}, \eta) = \sum_{m=1}^{n-1} \int_{\eta_0}^{\eta} d\eta' \, g_{ab}(\eta, \eta') \, \gamma_{bcd}(\boldsymbol{k}, \boldsymbol{q}, \boldsymbol{p}) \, \psi_c^{(m)}(\boldsymbol{q}, \eta') \psi_d^{(n-m)}(\boldsymbol{p}, \eta') \,, \quad (3.77)$$

which by comparison with (3.74) determines the recursion relation for the nth-order kernel [300]

$$\mathcal{F}_a^{(n)}(\boldsymbol{q}_1, \ldots, \boldsymbol{q}_n, \eta) \, \delta_{\mathrm{D}}(\boldsymbol{k} - \boldsymbol{q}_{1\ldots n}) = \sum_{m=1}^{n-1} \int_{\eta_0}^{\eta} d\eta'' \, g_{ab}(\eta, \eta'') \, \gamma_{bcd}(\boldsymbol{k}, \boldsymbol{q}_{1\ldots m}, \boldsymbol{q}_{m+1\ldots n})$$
$$\cdot \mathcal{F}_c^{(m)}(\boldsymbol{q}_1, \ldots, \boldsymbol{q}_m, \eta'') \, \mathcal{F}_d^{(n-m)}(\boldsymbol{q}_{m+1}, \ldots, \boldsymbol{q}_n, \eta'') \quad (3.78)$$

with $\boldsymbol{k} = \boldsymbol{q}_{1\ldots n}$ due to translation invariance. Here, we have replaced the integration variable by η'' to distinguish the internal integration determining the kernels $\mathcal{F}_a^{(n)}(\boldsymbol{q}_1, \ldots, \boldsymbol{q}_n, \eta)$ from the time integration over η' in the perturbative solution (3.77). To compute the perturbative solution (3.77) for higher and higher orders, one has to successively reinsert the doublet on the left-hand side of the equation into the doublets within the integral on its right-hand side.

The recursion relations (3.78) in the diagrammatic formulation of SPT reduce to the standard recursion relations, given by (3.33) and (3.34), in the limit where the initial conditions are imposed in the infinite past. This is realized by replacing the lower limit of integration, $\eta'' = \eta_0$, in (3.78) by $\eta'' = -\infty$. In this case, (3.78) yields the standard recursion relations [300],

$$\mathcal{F}_a^{(n)}(\boldsymbol{q}_1, \ldots, \boldsymbol{q}_n, \eta) = e^{n(\eta - \eta_0)} \begin{pmatrix} F_n(\boldsymbol{q}_1, \ldots, \boldsymbol{q}_n) \\ G_n(\boldsymbol{q}_1, \ldots, \boldsymbol{q}_n) \end{pmatrix} \,, \quad (3.79)$$

where only the fastest growing mode is taken into account at each order n in perturbation theory.

If we are not imposing the initial conditions in the infinite past, the recursion relations (3.78) and hence the perturbative expansion (3.72) with (3.74) preserves the full time dependence, including all transients from initial conditions (see [142, 300]). This feature plays a key role in allowing the process of resummation of the non-linear propagator. For a detailed discussion of this point see e.g., [142].

3.3.6. Diagrammatic representation of the perturbative solution

Although the recursion relations for the kernels in (3.78) allow us to calculate an explicit analytic expression for the perturbative solution $\psi_a^{(n)}(\boldsymbol{k}, \eta)$ of the non-linear fluid equations by use of (3.74), the computational effort increases considerably with the perturbative order n. However, since all perturbative solutions are derived successively from the recursion relations and hence share the same building blocks, they have the characteristic features allowing to construct a diagrammatic representation in a way similar to Feynman diagrams. This graphical interpretation, based on ideas in [96, 236, 305, 306] and worked out in detail in [142] (compare with [148] for an alternative formulation), helps in addition to understand the physical meaning of the different contributions in the infinite perturbative series.

In the first approach to develop a diagrammatic representation of the perturbative solutions [96, 305, 306], the diagrams are constructed from the kernels $\mathcal{F}_a^{(n)}(\boldsymbol{q}_1, \ldots, \boldsymbol{q}_n, \eta)$ as basic objects. However, this has the disadvantage that, at order n of perturbation theory, the diagrams possess a number of n lines representing the different momenta.

Compared to this, the graphical representation based on ideas in [236] and worked out in detail in [142] (see also [148] for an alternative formulation) yields simpler diagrams. Since the diagrams in this formulation are constructed from three basic building blocks rather than from derived quantities such as the kernels, the non-linear interactions are represented by vertices which always involve a fixed number of three lines. The complication in this formulation is, however, that the time evolution has not been 'integrated out' as it is the case when using the kernels (see (3.78)), but that one has to integrate over intermediate times η'' whenever non-linear interactions occur. Thus, one effectively sums over all possible interactions which occur between the initial time η_0 and the final time η. This procedure allows in fact the resummation of diagrams in [142].

In the following, we discuss the diagrammatic formulation of [142, 236] by introducing the three building blocks and explain the rules to combine them to diagrams (see e.g., [100]). This allows us to build sets of diagrams for solutions $\psi_a^{(n)}(\boldsymbol{k}, \eta)$ at each order in perturbation

$$\psi_a(\boldsymbol{k}, \eta_0) \qquad\qquad g_{ab}(\eta, \eta') \qquad\qquad \gamma_{abc}(\boldsymbol{k}, \boldsymbol{q}, \boldsymbol{p})$$

$$(b, \boldsymbol{q})$$

$$k = q + p$$

$$(a, \boldsymbol{k}) \qquad\qquad (a, \eta) \qquad\qquad (b, \eta') \qquad (a, \boldsymbol{k})$$
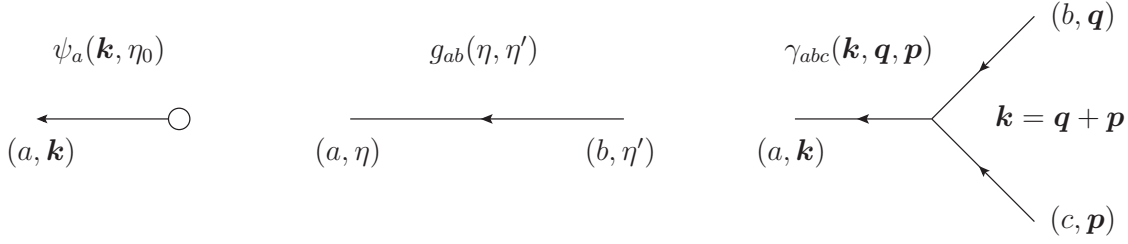
$$(c, \boldsymbol{p})$$

Fig. 3.1.: Diagrammatic representation of the three basic building blocks to construct the perturbative solutions of the non-linear fluid equations. These are the initial field $\psi_a(\boldsymbol{k}, \eta_0)$, the linear propagator $g_{ab}(\eta, \eta')$ and the vertex $\gamma_{bcd}(\boldsymbol{k}, \boldsymbol{q}, \boldsymbol{p})$.

theory.

From (3.74) and (3.78), it is obvious that the perturbative solutions $\psi_a^{(n)}(\boldsymbol{k}, \eta)$ are constructed from three basic building blocks, which have to be translated into the language of Feynman diagrams, namely the *initial field* $\psi_a(\boldsymbol{k}, \eta_0)$, the *linear propagator* $g_{ab}(\eta, \eta')$ as well as the *vertex* $\gamma_{abc}(\boldsymbol{k}, \boldsymbol{q}, \boldsymbol{p})$.

The graphical representation of these three basic objects is shown in Figure 3.1. Therein, the initial fields $\psi_a(\boldsymbol{k}, \eta_0)$ are represented by an open circle with a line emerging from it that carries a momentum $\boldsymbol{k}$. Thus, each initial field is characterized by a momentum $\boldsymbol{k}$. The lines have a time direction, which is indicated by an arrow. Note that all arrows point away from the initial fields and hence indicate the direction of an evolution forward in time. Furthermore, the lines are labeled with different indices at both ends, e.g., with a and b as in the second diagram in Figure 3.1. There, the line represents the linear evolution in time from η' to η, described by the linear propagator $g_{ab}(\eta, \eta')$. Hence, the graphical representation of the linear solution, $\psi_a^{(L)}(\boldsymbol{k}, \eta) = \psi_a^{(1)}(\boldsymbol{k}, \eta) = g_{ab}(\eta, \eta_0)\psi_b(\boldsymbol{k}, \eta_0)$ (see (3.67)), is given by the first diagram shown in Figure 3.2.

Moreover, each non-linear interaction between modes is represented by a vertex $\gamma_{abc}(\boldsymbol{k}, \boldsymbol{q}, \boldsymbol{p})$ in form of a branching. Each vertex is the convergence point of two incoming lines with momenta $\boldsymbol{q}$ and $\boldsymbol{p}$ which couple to one outgoing line that carries the momentum $\boldsymbol{k} = \boldsymbol{q} + \boldsymbol{p}$ (due to the quadratic non-linearities in the fluid equations). Each interaction conserves momentum and occurs at a time η' with $0 \leq \eta' \leq \eta$ (see (3.77)). Furthermore, the branches correspond to linear propagators which represent the linear evolution of a given mode from the time η' to the time η. Finally, one has to sum up the internal indices, integrate over the internal momenta, e.g., $\boldsymbol{q}$ and $\boldsymbol{p}$, as well as the intermediate interaction times η', each over the full time interval $[\eta_0, \eta]$. Figure 3.2 shows the diagrams contributing up to order $n = 4$ in perturbation theory.
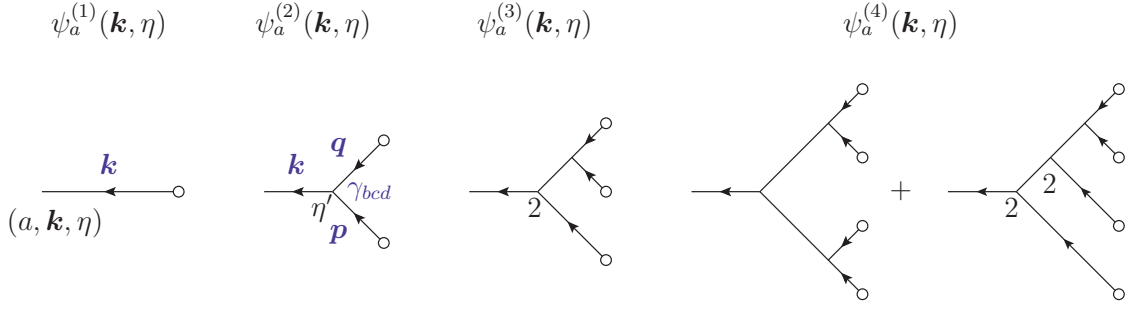
Fig. 3.2.: Diagrams representing the solutions $\psi_a^{(n)}(\boldsymbol{k}, \eta)$ in (3.74) up to order $n = 4$ in perturbation theory.

To illustrate this procedure, let us consider Figure 3.2, where the diagrams contributing up to order $n = 4$ in perturbation theory are shown. As an example, we can explicitly deduce the second- and third-order perturbative solutions, $\psi_a^{(2)}(\boldsymbol{k}, \eta)$ and $\psi_a^{(3)}(\boldsymbol{k}, \eta)$, from the corresponding diagrams in the figure. They are given by

$$\psi_a^{(2)}(\boldsymbol{k}, \eta) = \int d^3q \int d^3p \int_{\eta_0}^{\eta} d\eta'\, g_{ab}(\eta, \eta')\gamma_{bcd}(\boldsymbol{k}, \boldsymbol{q}, \boldsymbol{p})\, g_{ce}(\eta', \eta_0)\psi_e(\boldsymbol{q}, \eta_0)\, g_{df}(\eta, \eta_0)\psi_f(\boldsymbol{p}, \eta_0)\,,$$

$$\psi_a^{(3)}(\boldsymbol{k}, \eta) = 2 \int d^3q \int d^3p \int_{\eta_0}^{\eta} d\eta'\, g_{ab}(\eta, \eta')\gamma_{bcd}(\boldsymbol{k}, \boldsymbol{q}, \boldsymbol{p})\, g_{ce}(\eta', \eta_0)\psi_e(\boldsymbol{q}, \eta_0)\, \psi_d^{(2)}(\boldsymbol{p}, \eta)\,.$$

$$(3.80)$$

These equations read off from the diagrams in Figure 3.2 correspond exactly to the relations we get by inserting the kernels (3.76) and (3.78) in the integral representation (3.74).

In order to construct the set of diagrams representing the nth-order solution $\psi_a^{(n)}(\boldsymbol{k}, \eta)$ in (3.77), one has to all topologically different trees which possess $n - 1$ vertices in form of branchings and n initial fields (circles). Each tree is constructed from the final time η by drawing a line backwards up to a vertex. At the vertex, the line splits into two branches. Subsequently, each of these two lines lines continues until the reach another vertex or an initial field at $\eta = 0$. One has to repeat this procedure at each vertex until all branches end up in initial fields. Note that if the branching is asymmetric, it is assigned a factor of 2. As we can deduce from (3.77), all different diagrams with $n - 1$ vertices and n initial fields represent an integral contribution and have to be summed up to obtain the perturbative solution $\psi_a^{(n)}(\boldsymbol{k}, \eta)$ at order n.

Diagrammatic representations like the one we applied here to describe the non-linear evolution in the growth of the large-scale structure can be derived for any field theory with quadratic non-linearities. In particular, in the case of turbulence very similar methods ex-

ist [147, 307, 308]. Besides, also path-integral methods have been applied to the dynamics of gravitational clustering. For details, we refer to [148, 153, 154, 158].

In the following chapter, we use the perturbative solution $\psi_a^{(n)}(\boldsymbol{k}, \eta)$ of the non-linear fluid equations and its diagrammatic representation to derive theoretical predictions for large-scale structure observables, such as the power spectrum and the bispectrum, from perturbation theory. Since the characteristic of large-scale structure observables is their statistical nature, we first illustrate why a statistical approach is needed to model the cosmological evolution of the large-scale structure.

Chapter 4

Statistical Large-Scale Structure Observables

Contents

4.1. The need for a statistical approach

According to the current physical explanation, the present large-scale structure arises from the growth of primordial seed fluctuations in the matter density, which are amplified by gravitational instability, in an otherwise homogeneous universe [40]. An attractive explanation of the physical origin of these primordial fluctuations is the inflationary paradigm [24–26]. In models of inflation, the primordial fluctuations originate from quantum fluctuations of a scalar field, the so-called inflaton. Since it is beyond the scope of this thesis to discuss models of inflation in any detail, we refer instead to the reviews [243, 309–311] for an overview on this topic. However, it is worth recalling that the simplest single-field inflationary models predict, in agreement with observations of the Planck satellite, that the primordial fluctuations originate from scalar perturbations which are predominantly adiabatic, almost scale-invariant [17, 22], and very close to Gaussian [23, 72]. For this reason, we assume in this work that the primordial (initial) fluctuations are Gaussian. In other words, our description of the evolution

in time of the density contrast and the velocity divergence fields will rely on *Gaussian initial conditions.*

The primordial fluctuations cannot be probed directly by observations. This would in fact provide definite initial conditions for the deterministic evolution equations. Moreover, the time scale of the cosmological evolution is much bigger than any possible observation period so that it is not possible to follow the complete evolution of a single system in time. Through our past light cone, we observe instead various objects at different stages of their evolution. As a consequence, it is only possible to describe and also probe the time evolution of the perturbations, leading to the observed large-scale structure of the Universe, by a *statistical approach.*

For statistically approaching the cosmological evolution of the large-scale structure, one models the observable universe as a stochastic realization of a statistical ensemble of possibilities. To probe this evolution, one then has to make theoretical predictions of statistical quantities which in turn depend on the statistical properties of the primordial perturbations. In general, the statistical characterization of the perturbations is done using joint ensemble averages of a number $\mathcal{N}$ of fields in real or Fourier space, which we refer to as $\mathcal{N}$-point correlation functions or correlators. We will restrict our consideration to Fourier space by considering correlation functions of the doublet field $\psi_a(\boldsymbol{k}, \eta)$. In case of Gaussian initial conditions, this approach has the advantage that all information is encoded in the two-point correlation function $\langle \psi_a(\boldsymbol{k}, \eta) \, \psi_b(\boldsymbol{q}, \eta) \rangle$.

By the assumption of Gaussian initial conditions, all non-Gaussian features will be generated, gradually from small to larger momentum scales, only due to the subsequent non-linear evolution of the system through gravitational clustering. In consequence, non-Gaussianities are generated as a function of scale and time in all $\mathcal{N}$-point correlation functions. However, on small momentum scales on which perturbation theory applies, the $\mathcal{N}$-point correlation functions still scale as the power of the two-point correlation functions and hence can be used to make theoretical predictions to constrain the cosmological evolution. In this thesis, we will mainly focus on the power spectrum and the bispectrum which are closely related to the two- and three-point correlation functions in Fourier space. Our intention in this chapter is to make predictions for statistical quantities, such as the power spectrum and the bispectrum, in the framework of SPT, introduced in Chapter 3.

4.2. Definition of the power spectrum

Based on the Cosmological Principle, we assume that the fluctuation fields (in real space) are statistically homogeneous and isotropic. In general, one refers to a random field as statistically

homogeneous and isotropic if all ensemble averages of products of the field remain the same under translations in space and spatial rotations [40]. However, the validity of this assumption has to be tested against observations. Significant deviations from statistical homogeneity and isotropy are, for instance, generated by redshift-space distortions in galaxy surveys (see [275, 276, 312] for details). Hence, the redshift-space density field is an example for a field where the assumption of statistical homogeneity and isotropy is not valid. In this thesis, we will, however, proceed on the assumption of statistically homogeneous and isotropic fields.

Statistical homogeneity and isotropy implies that the two-point correlation function of the density contrast or the velocity divergence in real space, defined as the ensemble average of the respective fields at two different locations $\boldsymbol{x}$ and $\boldsymbol{x}+\boldsymbol{r}$ (in comoving coordinates), depends on the separation r, only. As a consequence, its Fourier transform, the two-point correlation in Fourier space, can be expressed in terms of a quantity $P_{ab}(k, \eta)$ which depends only on the norm k [101],

$$\left\langle \psi_a(\boldsymbol{k}, \eta) \, \psi_b(\boldsymbol{q}, \eta) \right\rangle \equiv \delta^{\mathrm{D}}(\boldsymbol{k} + \boldsymbol{q}) \, P_{ab}(k, \eta) \tag{4.1}$$

with the three-dimensional Dirac delta distribution $\delta^{\mathrm{D}}(\ldots)$. This quantity is the so-called *power spectrum.* Note that there are basically two conventions in the literature to define the power spectrum. Apart from the convention (4.1) which we use, it is also convenient to reverse the role of the factors $(2\pi)^3$ in the Fourier transforms (1.6) so that the definition of the power spectrum (4.1) is consequently modified to $\left\langle \psi_a(\boldsymbol{k}, \eta) \, \psi_b(\boldsymbol{q}, \eta) \right\rangle \equiv (2\pi)^3 \delta^{\mathrm{D}}(\boldsymbol{k} + \boldsymbol{q}) \, P_{ab}(k, \eta)$.

To determine the general form of the power spectrum, we have to insert the formal integral solution for $\psi_a(\boldsymbol{k}, \eta)$, given in (3.67), into the definition of the power spectrum (4.1). As we discussed in 3.3.5, the formal integral solution can be interpreted as an equation for $\psi_a(\boldsymbol{k}, \eta)$ in the presence of an 'external source' given by the initial conditions $\psi_a(\boldsymbol{k}, \eta_0)$. Since we assume Gaussian initial conditions, the statistical properties of the random variables $\psi_a(\boldsymbol{k}, \eta_0)$ in (3.70) are then completely characterized by its two-point correlator

$$\left\langle \psi_a(\boldsymbol{k}, \eta_0) \, \psi_b(\boldsymbol{q}, \eta_0) \right\rangle \equiv \delta^{\mathrm{D}}(\boldsymbol{k} + \boldsymbol{q}) \, P_{ab}(k, \eta_0) \,. \tag{4.2}$$

Here, $P_{ab}(k, \eta_0) \equiv P_{ab,0}(k)$ denotes the initial power spectrum. Since all pairs of initial doublet fields can be replaced by the initial power spectrum $P_{ab,0}(k)$, it constitutes one of the basic building blocks for statistical calculations. Its diagrammatic representation, which arises from 'gluing' a pair of initial fields from Figure 3.1 together, is shown in Figure 4.1.

Furthermore, for Gaussian-distributed initial conditions (see (3.70)), the initial power spectrum

$$P_{ab,0}(k) = u_a u_b P_0(k) \tag{4.3}$$

can be expressed in terms of the initial power spectrum of density perturbations $P_0(k)$, which

$$P_{ab,0}(k)$$

$(a, \boldsymbol{k})$ $(b, -\boldsymbol{k})$
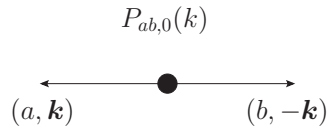
Fig. 4.1.: Diagrammatic representation of the initial power spectrum $P_{ab,0}(k)$.

is defined as

$$\left\langle \delta_0(\boldsymbol{k}) \, \delta_0(\boldsymbol{q}) \right\rangle \equiv \delta^{\mathrm{D}}(\boldsymbol{k} + \boldsymbol{q}) \, P_0(k) \,. \tag{4.4}$$

Note that the 'initial' power spectrum $P_0(k)$ derives from the linear evolution of the primordial density fluctuations through the radiation-dominated era and the resulting decoupling of matter from radiation in the cosmological evolution of the Universe. In general, one uses numerical codes of the relativistic Boltzmann equation [284, 313–315] to model this evolution, whereas analytic techniques allow to understand the results at least qualitatively (see e.g., [316, 317].) The initial power spectrum $P_0(k)$ then arises as [40]

$$P_0(k) = k^{n_s} \, T^2(k) \,, \tag{4.5}$$

where n_s denotes the primordial spectral index and $T(k)$ corresponds to the transfer function describing the evolution of density perturbation through decoupling (with $T(k = 0) \equiv 1$). The transfer depends on the cosmological parameters in a complicated way. However, in the simplest cases with negligible baryon contributions, it can be approximated by a fitting formula [314, 318]. In the adiabatic CDM case, for instance, the transfer functions scales like $T^2(k) \to \ln^2(k)/k^4$ as $k \to \infty$, due to the suppression of the growth of perturbations during the radiation-dominated era (see [319]).

4.3. Higher-order correlation functions

4.3.1. The Wick theorem for Gaussian random fields

Although the power spectrum is well defined for almost all homogeneous random fields, it gains a fundamental role if we require the doublets $\psi_a(\boldsymbol{k}, \eta)$ to be Gaussian random fields. In this case, we can apply the Wick theorem which is a fundamental theorem for classical and quantum field theories [320]. It states that any ensemble average of Gaussian random variables can be obtained by products of ensemble averages of pairs. Written explicitly in terms of the fields $\psi_a(\boldsymbol{k}, \eta)$ and by omitting the η-dependence of the fields for better readability, the Wick

theorem reads

$$\left\langle \psi_{a_1}(\boldsymbol{k}_1) \dots \psi_{a_{2p+1}}(\boldsymbol{k}_{2p+1}) \right\rangle = 0\,,$$

$$\left\langle \psi_{a_1}(\boldsymbol{k}_1) \dots \psi_{a_{2p}}(\boldsymbol{k}_{2p}) \right\rangle = \sum_{\text{all pair associations}} \prod_{p \text{ pairs } (i,j)} \left\langle \psi_{a_i}(\boldsymbol{k}_i)\, \psi_{a_j}(\boldsymbol{k}_j) \right\rangle \tag{4.6}$$

with $p \in \mathbb{N}$ being an integer. Hence, all ensemble averages consisting of an odd number $(2p+1)$ of fields vanish, whereas correlators of an even number $2p$ of fields can always be decomposed into $(2p-1)!!$ contributions corresponding to all different pairs p of the $2p$ fields. These pairs can in turn be expressed in terms of the power spectrum (4.1). As a consequence, this implies that for Gaussian random fields, one can construct all higher-order correlation functions entirely from the power spectrum (4.1). Moreover, due to the fact that we assume Gaussian initial conditions, the statistical characteristics of these correlation functions are then completely determined by the initial power spectrum $P_0(k)$, defined in (4.2).

4.3.2. Connected parts of correlation functions

Apart from the power spectrum, it is generally possible to introduce higher-order correlators, e.g., the so-called bispectrum and trispectrum. These higher-order correlation functions are defined as the *connected* part (denoted with a subscript 'c') of the joint ensemble average of an arbitrary number $\mathcal{N}$ of fields, $\left\langle \psi_{a_1}(\boldsymbol{k}_1) \dots \psi_{a_\mathcal{N}}(\boldsymbol{k}_\mathcal{N}) \right\rangle_c$. They are of particular importance for a statistical description since, in contrast to unconnected correlation functions, each connected correlator provides independent information. Formally, the connected part of a correlation function of $\mathcal{N}$ fields is defined as [40]

$$\left\langle \psi_{a_1}(\boldsymbol{k}_1) \dots \psi_{a_\mathcal{N}}(\boldsymbol{k}_\mathcal{N}) \right\rangle_c \equiv \left\langle \psi_{a_1}(\boldsymbol{k}_1) \dots \psi_{a_\mathcal{N}}(\boldsymbol{k}_\mathcal{N}) \right\rangle \\ - \sum_{\mathcal{S} \in \mathcal{P}(\{\boldsymbol{k}_1, \dots, \boldsymbol{k}_\mathcal{N}\})} \prod_{s_i \in \mathcal{S}} \left\langle \psi_{a_{s_i(1)}}(\boldsymbol{k}_{s_i(1)}) \dots \psi_{a_{s_i(\#s_i)}}(\boldsymbol{k}_{s_i(\#s_i)}) \right\rangle_c\,, \tag{4.7}$$

where the sum is taken over the proper partitions $\mathcal{S}$ of $\{\boldsymbol{k}_1, \dots, \boldsymbol{k}_\mathcal{N}\}$, that is, over any partition except the set itself. Consequently, s_i indicates a subset of $\{\boldsymbol{k}_1, \dots, \boldsymbol{k}_\mathcal{N}\}$ contained in partition $\mathcal{S}$. One can visualize this decomposition in an illustrative way by defining diagrammatic representations of the connected parts as in Figure 4.2. From this one can directly construct the decomposition of the connected correlation functions according to (4.7). This is exemplarily shown for the three-point correlation function in Figure 4.3.

If the average of $\psi_a(\boldsymbol{k}, \eta)$ is equal to zero, $\left\langle \psi_a \right\rangle = 0$, only partitions without singlets $\left\langle \psi_a \right\rangle$ contribute to the decomposition (4.7). In this case, the connected parts of the correlation

4. Statistical Large-Scale Structure Observables

$$\langle\psi_{a_1}\rangle_c \qquad\qquad \langle\psi_{a_1}\psi_{a_2}\rangle_c \qquad\qquad\qquad \langle\psi_{a_1}\psi_{a_2}\psi_{a_3}\rangle_c \qquad\qquad\qquad \langle\psi_{a_1}\psi_{a_2}\psi_{a_3}\psi_{a_4}\rangle_c$$
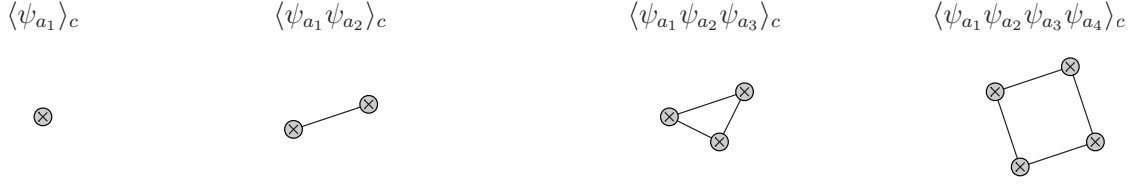
Fig. 4.2.: Diagrammatic representation of the connected parts of the correlation functions of up to $\mathcal{N} = 4$ fields.

Fig. 4.3.: Decomposition of the three-point correlation function into its connected parts.

functions of up to $\mathcal{N} = 4$ fields simply read

$$
\begin{aligned}
\langle\psi_a\rangle_c &= 0\,,\\
\langle\psi_a\psi_b\rangle_c &= \langle\psi_a\psi_b\rangle\,,\\
\langle\psi_a\psi_b\psi_c\rangle_c &= \langle\psi_a\psi_b\psi_c\rangle\,,\\
\langle\psi_a\psi_b\psi_c\psi_d\rangle_c &= \langle\psi_a\psi_b\psi_c\psi_d\rangle - \langle\psi_a\psi_b\rangle_c\langle\psi_c\psi_d\rangle_c - \langle\psi_a\psi_c\rangle_c\langle\psi_b\psi_d\rangle_c - \langle\psi_a\psi_d\rangle_c\langle\psi_b\psi_c\rangle_c\,,
\end{aligned}
\tag{4.8}
$$

where the correlation functions are symmetric under the exchange of the indices a, b, c, d, as for instance $\langle\psi_a\psi_b\rangle = \langle\psi_b\psi_a\rangle$. Here, we omitted the momentum dependence of the doublet fields to clarify the decomposition in connected and unconnected parts.

If we assume the doublets to be Gaussian fields, as it is the case for the initial fields $\psi_a(\boldsymbol{k}, \eta_0)$, we can apply the Wick theorem to (4.7) and decompose the unconnected correlation functions into pairs associations of the doublet fields, i.e., in unconnected two-point correlation functions. Since the connected and unconnected two-point correlation functions are equal (see (4.8)), all higher-order connected correlation functions subsequently vanish. Thus, in the case of Gaussian random fields, the two-point correlation function or equivalently the power spectrum remains the only non-vanishing statistical quantity. For Gaussian initial fields $\psi_a(\boldsymbol{k}, \eta_0)$, this is then the initial power spectrum $P_{ab}(k, \eta_0)$ in (4.3).

However, in the case where the doublet fields have non-Gaussian features, e.g., in the non-linear regime, the fields $\psi_a(\boldsymbol{k}, \eta)$ exhibit non-trivial connected higher-order correlation functions $\langle\psi_{a_1}(\boldsymbol{k}_1)\ldots\psi_{a_\mathcal{N}}(\boldsymbol{k}_\mathcal{N})\rangle_c$ which cannot be reconstructed by use of the Wick theorem from the two-point correlators only. Due to statistical homogeneity and isotropy of the fields $\psi_a(\boldsymbol{k}, \eta)$, these connected $\mathcal{N}$-point functions are always proportional to $\delta^{\mathrm{D}}(\boldsymbol{k}_1 + \cdots + \boldsymbol{k}_\mathcal{N})$

(see (4.1)). Hence, we can redefine them by introducing the quantity $P_\mathcal{N}(\boldsymbol{k}_1, \ldots, \boldsymbol{k}_\mathcal{N})$,

$$\left\langle \psi_{a_1}(\boldsymbol{k}_1, \eta) \ldots \psi_{a_\mathcal{N}}(\boldsymbol{k}_\mathcal{N}, \eta) \right\rangle_c = \delta^{\mathrm{D}}(\boldsymbol{k}_1 + \ldots + \boldsymbol{k}_\mathcal{N}) \, P^\mathcal{N}_{a_1 \ldots a_\mathcal{N}}(\boldsymbol{k}_1, \ldots, \boldsymbol{k}_\mathcal{N}, \eta) \, . \qquad (4.9)$$

Here, all the fields are evaluated at the same time η. Note that this has not necessarily to be the case. It is also possible to define unequal-time correlation functions. We consider correlation functions at unequal times explicitly in Section 6.1.1. The equal-time correlation function $P^\mathcal{N}_{a_1 \ldots a_\mathcal{N}}(\boldsymbol{k}_1, \ldots, \boldsymbol{k}_\mathcal{N}, \eta)$ corresponds to the power spectrum $P_{ab}(k, \eta)$, defined in (4.1), for the case $\mathcal{N} = 2$, since the connected and the unconnected two-point correlation function are equal (see (4.8)). Furthermore, for $\mathcal{N} = 3$ and $\mathcal{N} = 4$ one refers to the correlation functions $P^\mathcal{N}_{a_1 \ldots a_\mathcal{N}}(\boldsymbol{k}_1, \ldots, \boldsymbol{k}_\mathcal{N}, \eta)$ as bispectrum and trispectrum, respectively. Following [156], we denote the bispectrum and the trispectrum by

$$\begin{aligned}
\left\langle \psi_a(\boldsymbol{k}, \eta) \, \psi_b(\boldsymbol{q}, \eta) \, \psi_c(\boldsymbol{p}, \eta) \right\rangle_c &\equiv \delta^{\mathrm{D}}(\boldsymbol{k} + \boldsymbol{q} + \boldsymbol{p}) \, B_{abc}(\boldsymbol{k}, \boldsymbol{q}, \boldsymbol{p}, \eta) \, , \\
\left\langle \psi_a(\boldsymbol{k}, \eta) \, \psi_b(\boldsymbol{q}, \eta) \, \psi_c(\boldsymbol{p}, \eta) \, \psi_c(\boldsymbol{w}, \eta) \right\rangle_c &\equiv \delta^{\mathrm{D}}(\boldsymbol{k} + \boldsymbol{q} + \boldsymbol{p} + \boldsymbol{w}) \, Q_{abcd}(\boldsymbol{k}, \boldsymbol{q}, \boldsymbol{p}, \boldsymbol{w}, \eta) \, .
\end{aligned} \qquad (4.10)$$

Proceeding from the definition of correlation functions, our goal is now to determine these correlation functions explicitly by use of the perturbative solution for the doublet field $\psi_a(\boldsymbol{k}, \eta)$.

4.4. Power spectrum and bispectrum in SPT

In general, the perturbative solution for $\psi_a(\boldsymbol{k}, \eta)$ in (3.72) and (3.74) can be used to determine (connected) $\mathcal{N}$-point correlation functions for arbitrary numbers of fields $\mathcal{N}$. In this thesis, however, we focus on the computation of the connected two- and three-point correlation functions, i.e., the power spectrum and the bispectrum (see (4.1) and (4.10)). We start with the computation of the power spectrum within the perturbative framework of SPT.

4.4.1. Perturbative expansion of the power spectrum

Similar to the perturbative expansion for the doublet field $\psi_a(\boldsymbol{k}, \eta)$ in (3.72)-(3.74) in terms of integrals of the initial field $\psi_a(\boldsymbol{k}, \eta_0)$ (or the initial density contrast $\delta_0(\boldsymbol{k})$ for growing-mode initial conditions), our aim is to develop a perturbative expansion for the power spectrum $P_{ab}(k, \eta)$ in (4.1) in terms of integrals of the initial power spectrum $P_0(k)$ in (4.4).

For this purpose, we replace both doublet fields in the two-point function $\left\langle \psi_a(\boldsymbol{k}, \eta) \, \psi_b(\boldsymbol{q}, \eta) \right\rangle$, defining the power spectrum in (4.1), by their series expansions (3.72). According to (3.73), the nth-order contribution of each series expansion contains n powers of initial fields. Since we assume the initial fields to be Gaussian random fields, the Wick theorem (4.6) dictates that only those correlation functions do not vanish for which the total number of initial fields from

the series expansion of both fields is even. Thus, the perturbative expansion of the two-point correlation function is given by

$$
\begin{aligned}
\left\langle \psi_a \psi_b \right\rangle_c = {} & \left\langle \psi_a^{(1)} \psi_b^{(1)} \right\rangle_c \\
& + \left\langle \psi_a^{(1)} \psi_b^{(3)} \right\rangle_c + \left\langle \psi_a^{(2)} \psi_b^{(2)} \right\rangle_c + \left\langle \psi_a^{(3)} \psi_b^{(1)} \right\rangle_c \\
& + \left\langle \psi_a^{(1)} \psi_b^{(5)} \right\rangle_c + \left\langle \psi_a^{(2)} \psi_b^{(4)} \right\rangle_c + \left\langle \psi_a^{(3)} \psi_b^{(3)} \right\rangle_c + \left\langle \psi_a^{(4)} \psi_b^{(2)} \right\rangle_c + \left\langle \psi_a^{(5)} \psi_b^{(1)} \right\rangle_c \\
& + \dots \,,
\end{aligned}
\tag{4.11}
$$

where we omitted the time and momentum dependence of the doublet fields for better readability. In general, for Gaussian initial conditions, the first non-vanishing perturbative contribution to a connected $\mathcal{N}$-point correlation function requires perturbation theory of order $n = \mathcal{N} - 1$ [95].

If we next expand the power spectrum in a perturbative series, a so-called loop expansion in the diagrammatic language, of the form [40]

$$
P_{ab}(k, \eta) = \sum_{\ell=0}^{\infty} P_{ab}^{(\ell)}(k, \eta) \,,
\tag{4.12}
$$

and insert it into the power spectrum in (4.1), we can deduce by comparison with (4.11) that the ℓth-order term (the ℓ-loop contribution) in the series expansion of the power spectrum satisfies the relation [142]

$$
\delta^{\mathrm{D}}(\boldsymbol{k} + \boldsymbol{q}) \, P_{ab}^{(\ell)}(k, \eta) = \sum_{m=1}^{2\ell+1} \left\langle \psi_a^{(m)}(\boldsymbol{k}, \eta) \, \psi_b^{(2\ell+2-m)}(\boldsymbol{q}, \eta) \right\rangle_c .
\tag{4.13}
$$

Thus, the tree-level power spectrum indicating the loop order $\ell = 0$, which is equivalent to the *linear* power spectrum,

$$
P_{ab}^{(0)}(k, \eta) \equiv P_{ab}^{L}(k, \eta) \,,
\tag{4.14}
$$

is given by the first contribution on the right-hand side of (4.11). Notice that we indicate the loop order of correlation functions generally with a superscript '(l)', such as $P_{ab}^{(0)}(k, \eta)$ in the equation above. In contrast to this, we denote initial configurations by a subscript '0', like the initial power spectrum $P_{ab,0}(k)$ in (4.3).

By assuming Gaussian-distributed growing-mode initial conditions, $\psi_a(\boldsymbol{k}, \eta_0) = u_a \, \delta_0(\boldsymbol{k})$, and setting (see (3.70)-(3.71))

$$
u_a \equiv u_a^+ = \begin{pmatrix} 1 \\ 1 \end{pmatrix} \,,
\tag{4.15}
$$

we can use the series contributions $\psi_a^{(n)}(\boldsymbol{k}, \eta)$ in terms of the kernels $\mathcal{F}_a^{(n)}(\boldsymbol{q}_1, \dots, \boldsymbol{q}_n, \eta)$ (in (3.74), (3.76) and (3.78)) and the definition of the initial power spectrum $P_0(k)$ in (4.4)

to determine the linear power spectrum explicitly,

$$P_{ab}^L(k,\eta) = g_{ac}(\eta,\eta_0)\, u_c\, P_0(k)\, g_{bd}(\eta,\eta_0)\, u_d = e^{2(\eta-\eta_0)}\, u_a u_b P_0(k)\,. \tag{4.16}$$

Note that for $\eta_0 = 0$, the linear power spectrum scales like $\propto e^{2\eta} = D_1(\tau)^2$ (see (3.49)) with $D_1(\tau)$ being the growing mode of the linear growth factor and $D_1(\tau) = a(\tau)$ in the case of an EdS universe (see (3.17)). Consequently, in the linear regime the power spectrum of the density and velocity fields simply corresponds to a time-dependent scaling of the initial power spectrum $P_0(k)$. For the discussion that follows, we introduce in addition the notation

$$P_{11}^L(k,\eta) \equiv P^L(k,\eta) = e^{2(\eta-\eta_0)}\, P_0(k) \tag{4.17}$$

for the linear power spectrum of density fluctuations.

The next-to-leading order corrections in the perturbative expansion of the power spectrum for $\ell = 1$ yield the one-loop power spectrum. The one-loop contributions to the power spectrum have been extensively studied in the literature, see e.g., [93, 94, 97, 306, 321–325]. As we can deduce from the perturbative expansion of the two-point correlation function in (4.13), the one-loop power spectrum,

$$P_{ab}^{(1)}(k,\eta) \equiv P_{ab}^{1-\text{loop}}(k,\eta)\,, \tag{4.18}$$

consists of three contributions. These correspond to the terms in the second line on the right-hand side of (4.11). After substituting the perturbative solutions $\psi_a^{(n)}(\boldsymbol{k},\eta)$ of (3.74) in (4.13) and accounting for momentum conservation, we can summarizes the one-loop contributions to the power spectrum as follows (see e.g., [326]),

$$P_{ab}^{1-\text{loop}}(k,\eta) \;=\; P_{ab}^{(13)}(k,\eta) + P_{ab}^{(22)}(k,\eta)\,, \tag{4.19}$$

where

$$\begin{aligned}
P_{ab}^{(13)}(k,\eta) \equiv\; & 3\,P_0(k)\left[\mathcal{F}_a^{s(1)}(\boldsymbol{k},\eta) \int d^3l\, \mathcal{F}_b^{s(3)}(\boldsymbol{k},\boldsymbol{l},-\boldsymbol{l},\eta)\, P_0(l) \right.\\
& \left. + \mathcal{F}_b^{s(1)}(\boldsymbol{k},\eta) \int d^3l\, \mathcal{F}_a^{s(3)}(\boldsymbol{k},\boldsymbol{l},-\boldsymbol{l},\eta)\, P_0(l) \right]
\end{aligned} \tag{4.20}$$

and

$$P_{ab}^{(22)}(k,\eta) \equiv 2 \int d^3l\, \mathcal{F}_a^{s(2)}(\boldsymbol{k}-\boldsymbol{l},\boldsymbol{l},\eta)\, \mathcal{F}_b^{s(2)}(\boldsymbol{k}-\boldsymbol{l},\boldsymbol{l},\eta)\, P_0(|\boldsymbol{k}-\boldsymbol{l}|)\, P_0(l)\,. \tag{4.21}$$

Here, we have renamed the internal momenta, which arise from the perturbative solutions $\psi_a^{(n)}(\boldsymbol{k},\eta)$ in (3.74) and remain after accounting for momentum conservation. We refer to them as *loop momenta* $\boldsymbol{l}$. Moreover, we have used the symmetrized form of the kernels, which

we denote, in analogy to (3.36), by $\mathcal{F}_a^{s(n)}(\boldsymbol{q}_1, \ldots, \boldsymbol{q}_n, \eta)$. The kernels $\mathcal{F}_a^{s(n)}(\boldsymbol{q}_1, \ldots, \boldsymbol{q}_n, \eta)$ have the advantage that their symmetry in $\boldsymbol{q}_i \leftrightarrow -\boldsymbol{q}_i$ with $i \in \{1, \ldots, n\}$ (see (3.40)) can be exploited to simplify the momentum dependence of the overall expression. Finally, the prefactors 3 and 2 correspond to combinatorial factors counting the number of possibilities to choose the internal momenta $\boldsymbol{q}_i$ of the kernels.

Although the kernel $\mathcal{F}_a^{s(1)}(\boldsymbol{k}, \eta)$ of (3.76) is momentum independent, it is needed in this notation to account for the correct time dependence of the power spectrum. If we only consider the growing-mode time dependence of the kernels, given in (3.79), we can easily deduce that the one-loop power spectrum scales like $\propto e^{4\eta} = D_1(\tau)^4$ with $D_1(\tau) = a(\tau)$ for an EdS universe.

Note that the one-loop contributions $P_{ab}^{(13)}(k, \eta)$ and $P_{ab}^{(22)}(k, \eta)$ in (4.20) and (4.21) possess a rather different structure with regard to the momentum dependence of their kernels. The contribution $P_{ab}^{(22)}(k, \eta)$, on the one hand, is in general positive definite [40]. It describes the effects of mode-coupling between waves with momenta $\boldsymbol{k} - \boldsymbol{l}$ and $\boldsymbol{l}$, respectively. On the other hand, $P_{ab}^{(13)}(k, \eta)$ is always negative and describes the effect of previrialization which slows down the growth of structure. The dependence of its kernels on momentum indicates that this contribution to the one-loop power spectrum, in contrast to $P_{ab}^{(22)}(k, \eta)$, does not describe mode-coupling effects. However, since $P_{ab}^{(13)}(k, \eta)$, is proportional to the initial power spectrum $P_0(k)$ (see (4.20)), one can interpret this contribution as the one-loop correction to the linear propagator in (4.16) [236], that is, the non-linear correction to the standard linear growth $\propto e^{2\eta}$. This can in fact be interpreted as a sign of a resummable structure of the theory. In Chapter 5, we address the resummation of perturbative corrections in approaches other than SPT, for instance in the renormalized perturbation theory (RPT) approach [142–144], in detail.

In Figure 4.4, the perturbative SPT contributions up to one-loop order for the power spectrum of density perturbations $P_{11}(k, z = 0) \equiv P_{11}(k, \eta(z = 0))$, at present time or equivalently at redshift $z = 0$ (see (1.1)) and for a ΛCDM universe (see (3.49) and (3.18)), are compared with results from numerical simulations (blue squares) [327].[1] While positive contributions of the linear power spectrum $P_{11}^L(k, \eta) \equiv P^L(k, \eta)$, as defined in (4.17), and the one-loop correction $P_{11}^{(22)}(k, \eta)$ (see (4.21)) correspond to the solid red lines, the negative one-loop correction $P_{11}^{(13)}(k, \eta)$ of (4.20) is displayed by the dashed red line. The figure shows that a strong cancellation between the positive and negative one-loop correction occurs. Due to this, the overall one-loop correction to the full non-linear (NL) density power spectrum

---

[1] The cosmological parameters used for the N-body simulations are the density parameters $\Omega_{m,0} = 0.27$, $\Omega_{\Lambda,0} = 0.73$ and $\Omega_{b,0} = 0.046$, a dimensionless Hubble parameter of $h_0 = 0.72$ as well as the power spectrum renormalization $\sigma_8 = 0.9$ and the primordial spectral index $n_s = 1$ [327].
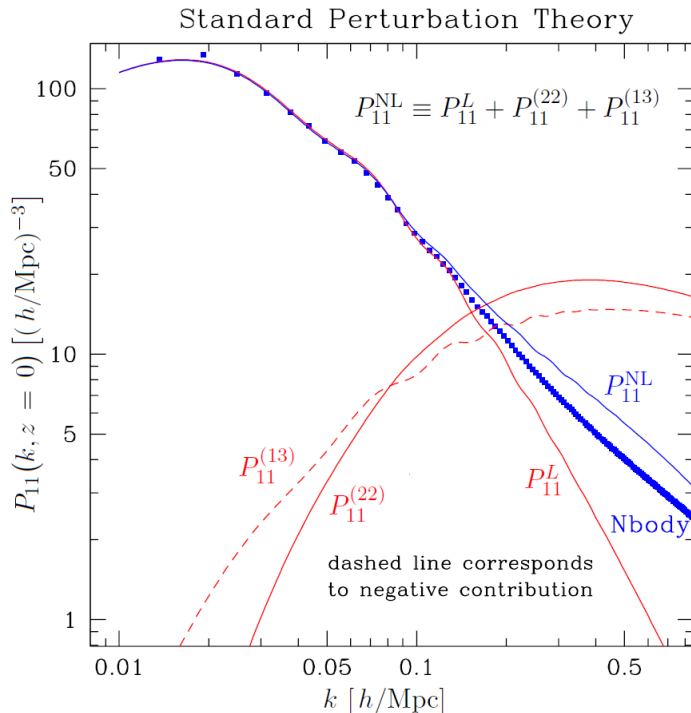
Fig. 4.4.: Perturbative contributions to the power spectrum of density perturbations $P_{11}(k, z = 0) \equiv P_{11}(k, \eta(z = 0))$, at present time (or equivalently at redshift $z = 0$) for a ΛCDM universe, up to one-loop order in SPT (adapted and reprinted from [327]). Here, the contributions of the linear power spectrum $P_{11}^L(k, \eta)$ and the one-loop power spectrum correction $P_{11}^{(22)}(k, \eta)$ (in solid red lines each) are positive, whereas the one-loop contribution $P_{11}^{(13)}(k, \eta)$ (dashed red line) to the density power spectrum is negative. Hence, a strong cancellation between $P_{11}^{(22)}(k, \eta)$ and $P_{11}^{(13)}(k, \eta)$ occurs so that the overall one-loop correction to the full non-linear (NL) power spectrum at this order $P_{11}^{\mathrm{NL}}(k, \eta) \equiv P_{11}^L(k, \eta) + P_{11}^{(22)}(k, \eta) + P_{11}^{(13)}(k, \eta)$ (solid blue line) is small. However, in comparison to the results for the density power spectrum obtained from numerical simulations (blue squares), the accuracy of this non-linear SPT power spectrum is rather poor and becomes worse for increasing wavenumbers k. To be precise, the SPT predictions overestimate the amount of power at high wavenumber. For instance, at $k \simeq 0.2\,h/\mathrm{Mpc}$ this overestimation is already of the order of $\sim 20\%$ [327].

at this order, here denoted by $P_{11}^{\mathrm{NL}}(k, \eta)$, (solid blue line) is small. However, confronted against the results from N-body simulations, the accuracy of the full one-loop power spectrum predictions $P_{11}^{\mathrm{NL}}(k, \eta)$ is rather poor. At $k \simeq 0.2\,h/\mathrm{Mpc}$, e.g., it overestimates the power

by about $\sim 20\%$ [327]. This 'overshoot phenomenon' [294] is characteristic for perturbative power spectrum predictions in SPT. We investigate the reasons behind it in Section 5.1.

Loop contributions higher than the one-loop corrections to the density power spectrum have been, for instance, considered in [305], including the full contributions up to two loops as well as the most important terms at three- and four-loop order in the case where the momentum k is large. Moreover, explicit computations for the power spectrum of density perturbations up to three-loop order have been performed and compared to the results from numerical simulations in [102] (see also Figure 5.1).

To summarize the results of this section, we can write the loop expansion of the power spectrum in SPT as (see (4.12), (4.16) and (4.20)-(4.21))

$$P_{ab}^{\mathrm{SPT}}(k,\eta) = P_{ab}^{L}(k,\eta) + P_{ab}^{(13)}(k,\eta) + P_{ab}^{(22)}(k,\eta) + \text{higher loop orders}. \tag{4.22}$$

Note that depending on the initial conditions (the form of the initial power spectrum), the integrals in the loop expansion of the power spectrum can be divergent when the loop momentum l becomes large, that is, in the UV limit. Consequently, the loop expansion can lead to divergent, non-physical results. This issue which constitutes one of the main drawbacks of SPT has been addressed, for instance, in the framework of the effective field theory of large-scale structure by implementing a renormalization procedure for the UV divergences (for details see [63, 178, 208]). We take this point up again in the Section 5.1 (see in particular in Section 5.1.2) where we discuss the shortcomings of SPT in detail.

Diagrammatic representation of the power spectrum

Based on the diagrammatic interpretation of the perturbative solution $\psi_a^{(n)}(\boldsymbol{k},\eta)$ in Section 3.3.6, we can now extend the graphical representation to describe the loop contributions to the power spectrum in terms of diagrams (for details see e.g., [142]). In order to diagrammatically represent each term which contributes to the power spectrum $P_{ab}^{(\ell)}$ of (4.13) at loop-order ℓ, we put one of the tree-like diagrams for $\psi_a^{(m)}(\boldsymbol{k},\eta)$, depicted in Figure 3.2, against one for $\psi_b^{(2\ell+2-m)}(\boldsymbol{q},\eta)$ such that the initial fields, corresponding to open circles in Figure 3.2, face each other. Then, we pair these initial fields in all possible ways and 'glue' them together afterwards. Like this, each pair of initial fields, e.g., $\psi_{a_i}(\boldsymbol{q}_i,\eta_0)$ and $\psi_{b_j}(\boldsymbol{q}_j,\eta_0)$ with $i \in \{1,\ldots,m\}$ and $j \in \{1,\ldots,2\ell+2-m\}$ (see (4.13) and (3.73)), is joined to an initial power spectrum according to (4.2), i.e., $\langle \psi_{a_i}(\boldsymbol{q}_i,\eta_0)\,\psi_{b_j}(\boldsymbol{q}_j,\eta_0)\rangle \equiv \delta^{\mathrm{D}}(\boldsymbol{q}_i + \boldsymbol{q}_j)\,u_{a_i}u_{b_j}\,P_0(q_i)$. In the following, we represent the initial power spectra diagrammatically in form of a filled circle.

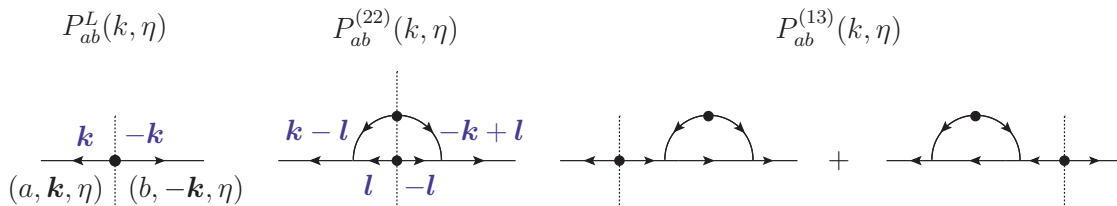Notice that for perturbative solutions $\psi_a^{(n)}(\boldsymbol{k},\eta)$ of order $n > 3$, we have to take into

Fig. 4.5.: Diagrammatic representation of the tree-level contribution $P_{ab}^L(k,\eta)$ as well as the one-loop corrections $P_{ab}^{(22)}(k,\eta)$ and $P_{ab}^{(13)}(k,\eta)$ to the power spectrum. The dashed lines, which cut only through initial power spectra and indicate the points where two tree-like diagrams of the perturbative solutions $\psi_a^{(n)}(\boldsymbol{k},\eta)$ of Figure 3.2 have been 'glued' together, define the so-called 'principle cross section'.

account that more than one tree-like diagram exists (see for instance the diagrams for $n = 4$ in Figure 3.2). Thus, we have to perform the procedure described above for all combinations of one tree-like diagram for $\psi_a^{(m)}(\boldsymbol{k},\eta)$ with one for $\psi_b^{(2\ell+2-m)}(\boldsymbol{q},\eta)$. Since this leads to a specific number of equal diagrams, we assign to each independent type of diagram the corresponding number as a weighing factor.

In Figure 4.5, we have depicted all diagrams contributing to the power spectrum $P_{ab}(k,\eta)$ up to one-loop order. The first diagram on the left shows the linear power spectrum $P_{ab}^L(k,\eta)$. According to its definition in (4.16), it is represented diagrammatically by a filled circle with two external lines. Thereby, the arrows indicate the direction of the momenta. The other diagrams in Figure 4.5 depict the one-loop contributions to the power spectrum. While the second diagram from left constitutes the diagrammatic interpretation of the contribution $P_{ab}^{(22)}(k,\eta)$ in (4.21), the remaining two diagrams correspond to the two terms summarized in $P_{ab}^{(13)}(k,\eta)$ (see (4.20)). In addition, we refer to [101, 142] where loop diagrams of the power spectrum up to order $\ell = 4$ can be found (see also [307] for a full account of loop diagrams in the case of turbulence).

Finally, let us focus our attention on the dashed lines in Figure 4.5, which split each diagram into two by cutting only through initial power spectra. They represent the points where two tree-like diagrams of the perturbative solutions $\psi_a^{(n)}(\boldsymbol{k},\eta)$ have been 'glued' together. Moreover, these lines define the 'principal cross section' that plays an important role in the process of resummation in RPT [142], as we discuss in Section 5.3 in further detail.

Since the diagrammatic representation of the loop contributions $P_{ab}^{(\ell)}(k,\eta)$ to the power spectrum is constructed from the perturbative solutions $\psi_a^{(n)}(\boldsymbol{k},\eta)$, the loop diagrams of the power spectrum are constructed of the same building blocks as the perturbative solutions. These are the initial fields $\psi_a(\boldsymbol{k},\eta_0)$ which are correlated to initial power spectra $P_0(k)$ ac-

cording to (4.2), the linear propagator $g_{ab}(\eta, \eta')$ and the vertices $\gamma_{bcd}(\boldsymbol{k}, \boldsymbol{q}, \boldsymbol{p})$. Thus, we read off the form of the loop contribution to the power spectrum directly from the diagrams in Figure 4.5 by using the same rules as described in Section 3.3.6. Each diagram in Figure 4.5 corresponds to a term $\langle \psi_a^{(m)} \psi_b^{(2\ell+2-m)} \rangle$ with $m \in \{1 \ldots, 2\ell + 1\}$ in the sum of contributions to the power spectrum at order ℓ (see (4.13)). While the first diagram in this figure yields the linear power spectrum in (4.16), the second leads to the one-loop contribution $P_{ab}^{(22)}(k, \eta)$ in (4.21). The third and fourth diagram, on the other hand, correspond to the two terms summarized in the remaining one-loop contribution $P_{ab}^{(13)}(k, \eta)$ in (4.20).

As an example for deducing the form of the loop contributions to the power spectrum from the diagrams in Figure 4.5 by application of the rules of Section 3.3.6, we consider the second diagram in the figure above corresponding to $P_{ab}^{(22)}(k, \eta)$. This gives the integral expression

$$
\begin{aligned}
P_{ab}^{(22)}(k, \eta) = 2 \int d^3 l \int_{\eta_0}^{\eta} d\eta' \int_{\eta_0}^{\eta} d\eta'' \Big[&g_{ac}(\eta, \eta') \, \gamma_{cde}^s(\boldsymbol{k}, \boldsymbol{l}, \boldsymbol{k} - \boldsymbol{l}) \, g_{df}(\eta', \eta_0) \, u_f \, g_{eg}(\eta', \eta_0) \, u_g \Big] \\
\times P_0(q) P_0(|\boldsymbol{k} - \boldsymbol{l}|) \Big[&g_{bc}(\eta, \eta'') \, \gamma_{cde}^s(-\boldsymbol{k}, -\boldsymbol{l}, -\boldsymbol{k} + \boldsymbol{l}) \, g_{df}(\eta'', \eta_0) \, u_f \, g_{eg}(\eta'', \eta_0) \, u_g \Big],
\end{aligned}
\tag{4.23}
$$

which corresponds exactly to the relation we obtain by inserting the (symmetrized) kernels (3.78) with (3.76) in the equation for $P_{ab}^{(22)}(k, \eta)$ in (4.21). Thus, both expressions for $P_{ab}^{(22)}(k, \eta)$ are equivalent.

4.4.2. Perturbative expansion of the bispectrum

As the next step, we consider the series expansion of the connected three-point correlation function, i.e., the bispectrum $B_{abc}(\boldsymbol{k}, \boldsymbol{q}, \boldsymbol{p}, \eta)$ as defined in (4.10), in terms of loop contributions. In order to determine the loop contributions to the bispectrum, we proceed in the same way as we did for deriving the loop expansion of the power spectrum in the previous section. Thus, insert the series expansion for the doublet fields $\psi_a(\boldsymbol{k}, \eta)$ in (3.72) into the connected three-point correlation function $\langle \psi_a(\boldsymbol{k}, \eta) \, \psi_b(\boldsymbol{q}, \eta) \, \psi_c(\boldsymbol{p}, \eta) \rangle_c$ which defines the bispectrum in (4.10). After applying the Wick theorem (4.6) under the assumption of Gaussian initial conditions, we obtain the following perturbative expansion for the connected three-point

correlation function

$$
\begin{aligned}
\left\langle \psi_a \psi_b \psi_c \right\rangle_c =\ & \left\langle \psi_a^{(1)} \psi_b^{(1)} \psi_c^{(2)} \right\rangle_c + \left\langle \psi_a^{(1)} \psi_b^{(2)} \psi_c^{(1)} \right\rangle_c + \left\langle \psi_a^{(2)} \psi_b^{(1)} \psi_c^{(1)} \right\rangle_c \\
& + \left\langle \psi_a^{(2)} \psi_b^{(2)} \psi_c^{(2)} \right\rangle_c \\
& + \left\langle \psi_a^{(1)} \psi_b^{(2)} \psi_c^{(3)} \right\rangle_c + \left\langle \psi_a^{(1)} \psi_b^{(3)} \psi_c^{(2)} \right\rangle_c + \left\langle \psi_a^{(2)} \psi_b^{(1)} \psi_c^{(3)} \right\rangle_c \\
& + \left\langle \psi_a^{(2)} \psi_b^{(3)} \psi_c^{(1)} \right\rangle_c + \left\langle \psi_a^{(3)} \psi_b^{(1)} \psi_c^{(2)} \right\rangle_c + \left\langle \psi_a^{(3)} \psi_b^{(2)} \psi_c^{(1)} \right\rangle_c \\
& + \left\langle \psi_a^{(1)} \psi_b^{(1)} \psi_c^{(4)} \right\rangle_c + \left\langle \psi_a^{(1)} \psi_b^{(4)} \psi_c^{(1)} \right\rangle_c + \left\langle \psi_a^{(4)} \psi_b^{(1)} \psi_c^{(1)} \right\rangle_c \\
& + \dots .
\end{aligned}
\tag{4.24}
$$

Here, we have again omitted the time and momentum dependence of the doublet fields for reasons of clarity.

Next, we perform a perturbative expansion of the bispectrum in terms of loop orders ℓ,

$$
B_{abc}(\boldsymbol{k}, \boldsymbol{q}, \boldsymbol{p}, \eta) = \sum_{\ell=0}^{\infty} B_{abc}^{(\ell)}(\boldsymbol{k}, \boldsymbol{q}, \boldsymbol{p}, \eta) ,
\tag{4.25}
$$

which we insert into the definition of the bispectrum in (4.10). By comparison with the perturbation series of the three-point correlation function in (4.24), we can infer that the ℓ-loop contribution of the bispectrum is determined by

$$
\begin{aligned}
& \delta^{\mathrm{D}}(\boldsymbol{k} + \boldsymbol{q} + \boldsymbol{p})\, B_{abc}^{(\ell)}(\boldsymbol{k}, \boldsymbol{q}, \boldsymbol{p}, \eta) \\
& \quad = \sum_{m_1=1}^{2\ell+2} \sum_{m_2=1}^{2\ell+3-m_1} \left\langle \psi_a^{(m_1)}(\boldsymbol{k}, \eta)\, \psi_b^{(m_2)}(\boldsymbol{q}, \eta)\, \psi_b^{(2\ell+4-m_1-m_2)}(\boldsymbol{q}, \eta) \right\rangle_c .
\end{aligned}
\tag{4.26}
$$

From this relation, we can directly derive the form of the bispectrum loop contributions. We use the perturbative solutions $\psi_a^{(n)}(\boldsymbol{k}, \eta)$ of (3.74), depending on the kernels $\mathcal{F}_a^{(n)}(\boldsymbol{q}_1, \dots, \boldsymbol{q}_n, \eta)$ in (3.76) and (3.78), as well as the definition of the initial power spectrum $P_0(k)$ in (4.2). Consequently, at loop order $\ell = 0$ the tree-level bispectrum, which we also refer to as linear bispectrum

$$
B_{abc}^{(0)}(\boldsymbol{k}, \boldsymbol{q}, \boldsymbol{p}, \eta) \equiv B_{abc}^{L}(\boldsymbol{k}, \boldsymbol{q}, \boldsymbol{p}, \eta) ,
\tag{4.27}
$$

arises as [328]

$$
\begin{aligned}
B_{abc}^{L}(\boldsymbol{k}, \boldsymbol{q}, \boldsymbol{p}, \eta) =\ & 2\, \mathcal{F}_a^{s(1)}(\boldsymbol{k}, \eta)\, \mathcal{F}_b^{s(1)}(\boldsymbol{q}, \eta)\, \mathcal{F}_c^{s(2)}(\boldsymbol{k}, \boldsymbol{q}, \eta)\, P_0(k) P_0(q) \\
& + 2\, \mathcal{F}_a^{s(1)}(\boldsymbol{k}, \eta)\, \mathcal{F}_b^{s(2)}(\boldsymbol{k}, \boldsymbol{p}, \eta)\, \mathcal{F}_c^{s(1)}(\boldsymbol{p}, \eta)\, P_0(k) P_0(p) \\
& + 2\, \mathcal{F}_a^{s(2)}(\boldsymbol{q}, \boldsymbol{p}, \eta)\, \mathcal{F}_b^{s(1)}(\boldsymbol{q}, \eta)\, \mathcal{F}_c^{s(1)}(\boldsymbol{p}, \eta)\, P_0(q) P_0(p) ,
\end{aligned}
\tag{4.28}
$$

and consequently corresponds to the contributions in the first line on the right-hand side of (4.24).

Note that due to the Dirac delta distribution in (4.26) arising from the definition of the bispectrum (4.10), the tree-level bispectrum is not a function of three independent vectors $\boldsymbol{k}$, $\boldsymbol{q}$ and $\boldsymbol{p}$. Instead, it is defined only for momentum configurations forming closed triangles, i.e., $\boldsymbol{k} + \boldsymbol{q} + \boldsymbol{p} = 0$. This is equivalently valid for the loop contributions of the bispectrum (see (4.30)-(4.34)). In order to display analytic results, however, it is convenient to remove the dependence on the third momentum by setting $\boldsymbol{p} = -\boldsymbol{k} - \boldsymbol{q}$ and express the bispectrum in terms of the absolute values k, q of the remaining two momenta as well as their respective angle θ_{kq} with $\cos\theta_{kq} \equiv (\boldsymbol{k} \cdot \boldsymbol{q})/(kq)$ [298] (see e.g., Section 6.2.1). In comparison to the power spectrum, that is a one-dimensional quantity because of statistical homogeneity and isotropy (see Section 4.2), the bispectrum is, due to the same reason, a three-dimensional quantity depending on two magnitudes and one angle.

In the case where we only take the growing-mode time dependence of the kernels into account (see (3.79)), the linear bispectrum scales like $\propto e^{4\eta} = D_1(\tau)^4$ and hence like $a^4(\tau)$ for an EdS universe. If we use the diagrammatic representation of the perturbative solution $\psi_a^n(\boldsymbol{k}, \eta)$ and transfer the techniques to construct loop diagrams which we discussed for the power spectrum to the case of the bispectrum, we can easily rederive the form of the tree-level bispectrum in (4.28). From the diagrammatic point of view, there is no possibility to connect three external points without invoking the three-point vertex of $\psi_a^{(2)}(\boldsymbol{k}, \eta)$. Consequently, the tree-level bispectrum (4.28) is represented by the first diagram in Figure 4.6.

As we can see from (4.26), the next-to-leading order of the bispectrum, the one-loop bispectrum,

$$B_{abc}^{(1)}(\boldsymbol{k}, \boldsymbol{q}, \boldsymbol{p}, \eta) \equiv B_{abc}^{1-\text{loop}}(\boldsymbol{k}, \boldsymbol{q}, \boldsymbol{p}, \eta), \tag{4.29}$$

comprises several contributions. These originate from the remaining terms written down in the perturbative expansion of the three-point correlation function in (4.24). For detailed discussions of the one loop bispectrum in SPT see for instance [40, 298, 328]. The one-loop contributions to the bispectrum can be summarized in the following way,

$$
\begin{aligned}
B_{abc}^{1-\text{loop}}(\boldsymbol{k}, \boldsymbol{q}, \boldsymbol{p}, \eta) = \; & B_{abc}^{(222)}(\boldsymbol{k}, \boldsymbol{q}, \boldsymbol{p}, \eta) + B_{abc}^{(321,\text{I})}(\boldsymbol{k}, \boldsymbol{q}, \boldsymbol{p}, \eta) + B_{abc}^{(321,\text{II})}(\boldsymbol{k}, \boldsymbol{q}, \boldsymbol{p}, \eta) \\
& + B_{abc}^{(411)}(\boldsymbol{k}, \boldsymbol{q}, \boldsymbol{p}, \eta),
\end{aligned}
\tag{4.30}
$$

where we have defined

$$
\begin{aligned}
B_{abc}^{(222)}(\boldsymbol{k}, \boldsymbol{q}, \boldsymbol{p}, \eta) \;\equiv\; & 8 \int d^3 l \, \mathcal{F}_a^{s(2)}(-\boldsymbol{l}, \boldsymbol{l} + \boldsymbol{k}, \eta) \, \mathcal{F}_b^{s(2)}(\boldsymbol{l} + \boldsymbol{k}, \boldsymbol{p} - \boldsymbol{l}, \eta) \, \mathcal{F}_c^{s(2)}(\boldsymbol{l}, \boldsymbol{p} - \boldsymbol{l}, \eta) \\
& \times P_0(l) P_0(|\boldsymbol{l} + \boldsymbol{k}|) P_0(|\boldsymbol{l} - \boldsymbol{p}|),
\end{aligned}
\tag{4.31}
$$

$$B_{abc}^L(\boldsymbol{k}, \boldsymbol{q}, \boldsymbol{p}, \eta) \qquad\qquad B_{abc}^{(222)}(\boldsymbol{k}, \boldsymbol{q}, \boldsymbol{p}, \eta) \qquad\qquad B_{abc}^{(231,\mathrm{I})}(\boldsymbol{k}, \boldsymbol{q}, \boldsymbol{p}, \eta)$$

$(a, \boldsymbol{k}, \eta)$

$$B_{abc}^{(231,\mathrm{II})}(\boldsymbol{k}, \boldsymbol{q}, \boldsymbol{p}, \eta) \qquad\qquad B_{abc}^{(411)}(\boldsymbol{k}, \boldsymbol{q}, \boldsymbol{p}, \eta)$$
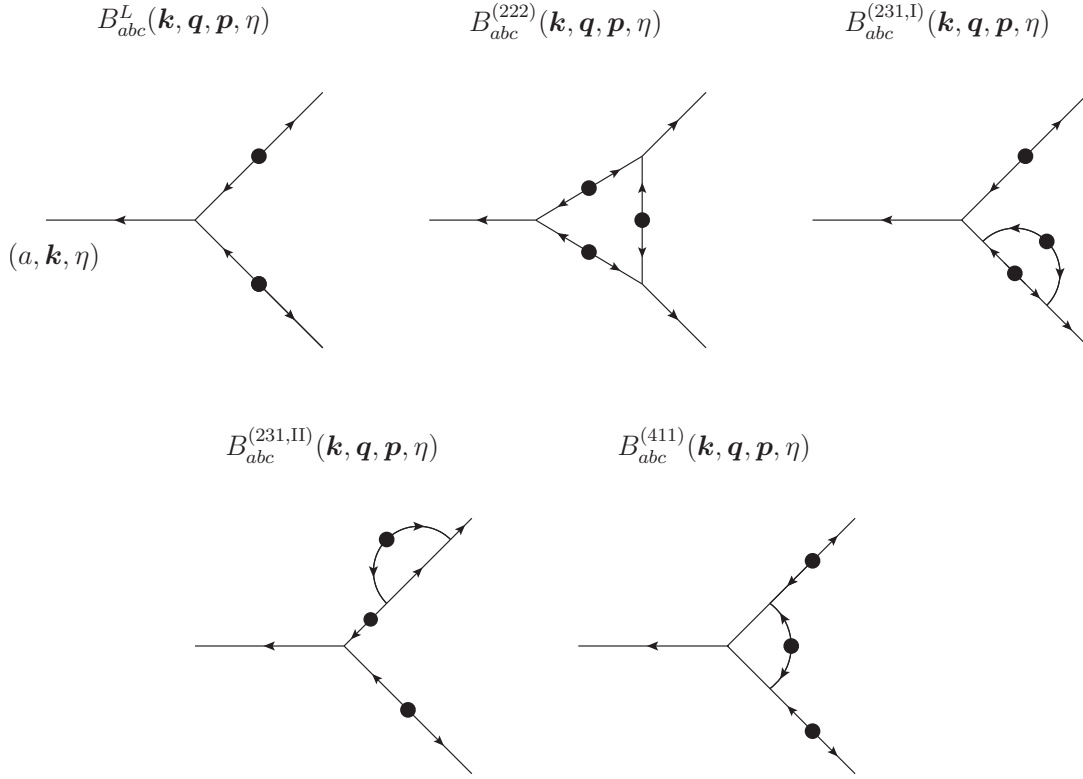
Fig. 4.6.: Diagrammatic representation of the tree-level contribution $B_{abc}^L(\boldsymbol{k}, \boldsymbol{q}, \boldsymbol{p}, \eta)$ as well as the one-loop corrections $B_{abc}^{(222)}(\boldsymbol{k}, \boldsymbol{q}, \boldsymbol{p}, \eta)$, $B_{abc}^{(321,\mathrm{I})}(\boldsymbol{k}, \boldsymbol{q}, \boldsymbol{p}, \eta)$, $B_{abc}^{(321,\mathrm{II})}(\boldsymbol{k}, \boldsymbol{q}, \boldsymbol{p}, \eta)$ and $B_{abc}^{(411)}(\boldsymbol{k}, \boldsymbol{q}, \boldsymbol{p}, \eta)$, to the bispectrum. Performing permutations of the indices a, b, c together with the associated momenta $\boldsymbol{k}$, $\boldsymbol{q}$, $\boldsymbol{p}$ for the individual diagrams yields the diagrammatic representation of all terms contributing to the full one-loop bispectrum (see (4.28) and (4.31)-(4.34)).

$$
\begin{aligned}
B_{abc}^{(321,\mathrm{I})}(\boldsymbol{k}, \boldsymbol{q}, \boldsymbol{p}, \eta) \;\equiv\; & 6\,\mathcal{F}_a^{s(1)}(\boldsymbol{k}, \eta)\,P_0(k) \\
& \times \int d^3l\,\mathcal{F}_b^{s(2)}(\boldsymbol{l}, \boldsymbol{q} - \boldsymbol{l}, \eta)\,\mathcal{F}_c^{s(3)}(-\boldsymbol{l}, \boldsymbol{l} - \boldsymbol{q}, -\boldsymbol{k}, \eta)\,P_0(l)P_0(|\boldsymbol{l} - \boldsymbol{q}|) \\
& + 5\ \text{permutations}\,,
\end{aligned}
\tag{4.32}
$$

$$
\begin{aligned}
B_{abc}^{(321,\mathrm{II})}(\boldsymbol{k}, \boldsymbol{q}, \boldsymbol{p}, \eta) \;\equiv\; & 6\,\mathcal{F}_a^{s(1)}(\boldsymbol{k}, \eta)\,\mathcal{F}_b^{s(2)}(\boldsymbol{k}, \boldsymbol{p}, \eta)\,P_0(k)P_0(p)\int d^3l\,\mathcal{F}_c^{s(3)}(\boldsymbol{p}, \boldsymbol{l}, -\boldsymbol{l}, \eta)\,P_0(l) \\
& + 5\ \text{permutations}\,,
\end{aligned}
\tag{4.33}
$$

$$
\begin{aligned}
B_{abc}^{(411)}(\boldsymbol{k}, \boldsymbol{q}, \boldsymbol{p}, \eta) \;\equiv\; & 12\,\mathcal{F}_a^{s(1)}(\boldsymbol{k}, \eta)\,\mathcal{F}_b^{s(1)}(\boldsymbol{q}, \eta)\,P_0(k)P_0(q)\int d^3l\,\mathcal{F}_c^{s(4)}(\boldsymbol{l}, -\boldsymbol{l}, -\boldsymbol{k}, -\boldsymbol{q}, \eta)\,P_0(l) \\
& + 2\ \text{permutations}\,.
\end{aligned}
\tag{4.34}
$$

Notice that in the case where $a = b = c$, the one-loop contribution $B_{abc}^{(321,\text{II})}(\boldsymbol{k}, \boldsymbol{q}, \boldsymbol{p}, \eta)$ to the bispectrum can be expressed in terms of the one-loop power spectrum contribution $P_{ab}^{(13)}(k, \eta)$ in (4.20),

$$B_{aaa}^{(321,\text{II})}(\boldsymbol{k}, \boldsymbol{q}, \boldsymbol{p}, \eta) = \mathcal{F}_a^{s(2)}(\boldsymbol{k}, \boldsymbol{p}, \eta)\, P_0(k)\, P_{aa}^{(13)}(p, \eta) +\ 5 \text{ permutations} \,. \tag{4.35}$$

By performing permutations of the indices a, b, c together with the momenta $\boldsymbol{k}, \boldsymbol{q}, \boldsymbol{p}$ associated to them, we obtain the other terms of the one-loop contributions (4.31)-(4.34), which are explicitly given in (4.24).

As an example, let us consider the one-loop contribution $B_{abc}^{(321,\text{I})}(\boldsymbol{k}, \boldsymbol{q}, \boldsymbol{p}, \eta)$ in (4.32). The term written down in this equation originates from the correlator $\left\langle \psi_a^{(1)}(\boldsymbol{k})\, \psi_b^{(2)}(\boldsymbol{q})\, \psi_c^{(3)}(\boldsymbol{p}) \right\rangle_c$ in the perturbative expansion of the connected three-point correlation function in (4.24). To derive the contribution to $B_{abc}^{(321,\text{I})}(\boldsymbol{k}, \boldsymbol{q}, \boldsymbol{p}, \eta)$ which is generated by the correlation function $\left\langle \psi_a^{(1)}(\boldsymbol{k})\, \psi_b^{(3)}(\boldsymbol{q}) \psi_c^{(2)}(\boldsymbol{p}) \right\rangle_c$, we permute the indices b and c and simultaneously the momenta $\boldsymbol{q}$ and $\boldsymbol{p}$. Thus, in this equation we have to replace the momentum $\boldsymbol{q}$ by $\boldsymbol{p}$. The other terms contributing to $B_{abc}^{(321,\text{I})}(\boldsymbol{k}, \boldsymbol{q}, \boldsymbol{p}, \eta)$ are obtained analogously.

Translated to the diagrammatic representation, the four one-loop contributions to the bispectrum correspond to the diagrams shown in Figure 4.6. In accordance to the procedure described above, permuting the indices a, b, c together with the respective momenta $\boldsymbol{k}, \boldsymbol{q}, \boldsymbol{p}$ of the four independent diagrams yields the other diagrammatic contributions to the one-loop bispectrum.

Besides, we can see from the dependence of the bispectrum contributions (4.31)-(4.34) on the kernels (see (3.79)) that the one-loop bispectrum in the growing mode scales like $\propto e^{6\eta} = D_1(\tau)^6$, where $D_1(\tau) = a(\tau)$ in the EdS case.

In summary, we can write the loop expansion of the bispectrum in SPT as (see (4.26) with (4.28) and (4.31)-(4.34))

$$\begin{aligned} B_{abc}(\boldsymbol{k}, \boldsymbol{q}, \boldsymbol{p}, \eta) = {}& B_{abc}^L(\boldsymbol{k}, \boldsymbol{q}, \boldsymbol{p}, \eta) \\ & + B_{abc}^{(222)}(\boldsymbol{k}, \boldsymbol{q}, \boldsymbol{p}, \eta) + B_{abc}^{(321,\text{I})}(\boldsymbol{k}, \boldsymbol{q}, \boldsymbol{p}, \eta) \\ & + B_{abc}^{(321,\text{II})}(\boldsymbol{k}, \boldsymbol{q}, \boldsymbol{p}, \eta) + B_{abc}^{(411)}(\boldsymbol{k}, \boldsymbol{q}, \boldsymbol{p}, \eta) + \text{higher loop orders} \,. \end{aligned} \tag{4.36}$$

As it is the case for the power spectrum (see Section 4.4.1), the bispectrum in SPT also suffers from the problem that the integrals in the loop expansion can become UV divergent. This problem has been addressed, for instance, in the context of the effective field theory approach of LSS in [186, 187]. Therein, the bispectrum up to one-loop order is studied and appropriate counter-terms to cancel the possible UV divergences are introduced. Moreover, a comparison of predictions for the one-loop bispectrum in different theoretical approaches, such as SPT, RPT and EFT, with numerical simulations can be found in [294].

Chapter 5

Overview of Perturbative Approaches

Contents

5.1. Shortcomings of standard perturbation theory

Standard perturbation theory (SPT) is by far the most studied analytic approach to describe the dynamics of large-scale structure formation in the Universe [40, 92–102]. As we have discussed in the Chapter 3 and 4, it is based on solving the non-linear pressureless and non-viscous perfect fluid equations of the dark matter evolution by a perturbative expansion in terms of the linearly evolved density field or equivalently the initial density contrast. This perturbative ansatz holds as long as the real-space density contrast $\delta(\boldsymbol{x}, \tau)$ is very small compared to unity, $|\delta| \ll 1$, namely on large distance scales and at early times. However, since the density contrast increases on smaller distance scales (corresponding to larger modes k in Fourier space) and later points of time (or equivalently at smaller redshifts z), its validity as an appropriate expansion parameter for a perturbative treatment of the dynamics of gravitational instability becomes questionable.

Indeed, while at high redshift, the perturbative SPT corrections to the linear density power spectrum yield already at one-loop order a very good agreement with numerical simulations

for a ΛCDM model, at redshift $z = 0$, the one-loop density power spectrum deviates from the N-body results up to $\sim 20\%$ for $k \leq 0.2\,h/$Mpc [142, 329] (see also Figure 4.4). A similar behavior is observed for the bispectrum [329].

In general, the non-linear power spectrum corrections in SPT only extend the range of validity of the linear theory by a small amount at low redshifts, whereas they quickly overpredict the amount of power on larger momentum scales. [294]. This overshoot phenomenon, which is clearly visible in Figure 4.4, appears since the loop corrections to the power spectrum in SPT are integrated over the entire range of momenta k and thus include the regime where the density contrast is not small any more. In numerical simulations, the contributions from this regime are actually strongly suppressed compared to SPT [137].

Moreover, the convergence properties of the SPT loop expansion for the power spectrum are problematic. As we discussed in Section 4.4.1, the perturbative expansion relies on intricate cancellations of large terms with opposite sign at the individual loop order. We have seen the cancellation of the contributions $P_{11}^{(13)}(k, \eta)$ and $P_{11}^{(22)}(k, \eta)$ to the one-loop density power spectrum explicitly in Figure 4.4. This behavior complicates not only the numerical evaluation of the power spectrum [101, 102, 182, 306], but also implies that increasing the loop order does not necessarily improve the accuracy of the perturbative predictions for the power spectrum, in particular at small redshifts. At high loop orders, it becomes additionally apparent that the perturbative SPT predictions are sensitive to UV modes. For particular sets of initial conditions, the loop contributions to the power spectrum in SPT even show a UV-divergent behavior. On top of that, for a ΛCDM cosmology, three-loop order computations indicate that the density power spectrum at redshift $z = 0$ does not even converge for small momenta (large distance scales) well within the linear regime (see Figure 5.1).

Based on these considerations, we conclude that SPT possesses a number of qualitative and quantitative shortcomings that can be summarized as follows [40, 180, 215]:

- SPT does not have a clear expansion parameter for a perturbative treatment of large-scale structure formation since the real-space density contrast is not small for all scales and points of time.

- Loop integrals in SPT are sensitive to UV modes. For particular sets of initial conditions, they even show a UV-divergent behavior.

- The perturbative expansion in SPT is plagued by the emergence of spurious IR enhanced contributions ('IR divergences').

- SPT does not consistently account for deviations from the perfect fluid assumption on short distance scales.
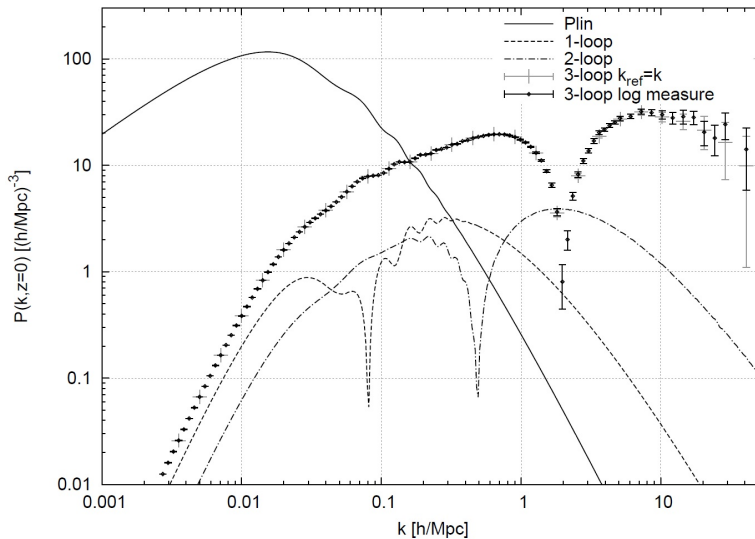
Fig. 5.1.: Perturbative contributions to the power spectrum of density perturbations, $P\big(k, z = 0\big) \equiv P_{11}\big(k, \eta(z = 0)\big)$, at present time (or equivalently at redshift $z = 0$) and for a ΛCDM universe up to three-loop order in SPT (reprinted from [102]). In [102], the linear density power spectrum (see (4.17)) has been computed from the initial power spectrum of the CAMB code [330] for a ΛCDM cosmological model with WMAP5 parameters [331]. Based on this, the power spectrum contributions up to three-loop order in SPT, defined by (4.12)-(4.13), have been determined by numerical Monte Carlo integration at $z = 0$. For the three-loop contribution, the black diamonds and gray crosses correspond to two different parameterizations of the absolute loop momenta, whereas the error bars show an estimate for the numerical error whose relative size is ≤ 0.002 for $k \leq 0.55\,h/\mathrm{Mpc}$.

For very small momenta k, the three-loop contribution is bigger even than the one-loop correction to the density power spectrum. Although the linear power spectrum contribution dominates over the loop-corrections in this regime, this indicates that at redshift $z = 0$ in the ΛCDM case, the loop expansion in SPT does not even converge for very small modes k well within the linear regime. However, the loop expansion exhibits properties compatible with an asymptotic series. Thus, in [102], a Padé resummation [332] has been established to restore its convergence in the limit of small momentum and improve it in the range of the baryon acoustic oscillations. Moreover, the figure shows that for momenta $k \gtrsim 0.16\,h/\mathrm{Mpc}$, the overall sum of the three-loop corrections, which is negative, becomes bigger than the linear power spectrum. Hence, SPT clearly does not converge neither on these scales. Finally, for even larger momentum k, the three-loop correction shows a logarithmic enhancement compared to the linear power spectrum (see also [101]). The loop expansion of the power spectrum shows a divergent behavior in this UV limit as well.

5. Overview of Perturbative Approaches

In the following, we discuss these drawbacks of SPT in further detail and illustrate them by giving examples.

5.1.1. Lack of a clear perturbative expansion parameter

Standard perturbation theory does not constitute a conventional perturbation theory in the sense of having a small coupling constant. On the contrary, since the real-space density contrast increases on smaller distance scales (for larger momenta k in Fourier space) and later points of time η, the validity of the perturbative solution to non-linear fluid equations depends – apart from the assumed underlying initial conditions – on the considered scale as well as on the point of time in the dark matter evolution.

For our Universe today, at redshift $z = 0$, the dark matter distribution on very large distance scales or equivalently in the regime of small momenta k is well modeled by the linear density power spectrum in SPT (see Figure 4.4). On intermediate, quasi-linear scales, the dark matter distribution may in principle be also described analytically by extending SPT beyond linear order. This is of particular interest since an accurate modeling of the baryon acoustic oscillations, which are imprinted on the power spectrum for small redshifts in the quasi-linear regime at [131]

$$0.05 \, h/\text{Mpc} \lesssim k_{\text{BAO}} \lesssim 0.15 \, h/\text{Mpc} \tag{5.1}$$

(see Figure 4.4 and Figure 5.1), would allow to constrain the parameters of the cosmological evolution and the nature of dark energy [333–335] (see also [142]).[1] However, as discussed before, the predictions for the one-loop density power spectrum in SPT at redshift $z = 0$ deviate from the numerical results up to $\sim 20\%$ already at weakly non-linear scales $k \leq 0.2 \, h/\text{Mpc}$. One obtains similar findings when considering the real-space two-point density correlation function in dependence of the distance scale r. For instance, in comparison to numerical simulations, the linear-order SPT predictions for the two-point density correlation function in real space around the BAO scale $r \simeq \mathcal{O}(100) \, \text{Mpc}/h$ reveal only an accuracy of $\sim 3\%$ at redshift $z \simeq 4$ [140]. Thus, even in this regime in real space where SPT is expected to be perturbative, one needs to include loop corrections for $z \lesssim 4$.

In [208], it has been shown using a simple toy model that at redshift $z = 0$, the one-loop SPT corrections to the linear two-point density correlation function in real space around the BAO peak are of the order $\mathcal{O}(1)$. This is an indication that the validity of the perturbative expansion

---

[1]In the real-space analog to the density power spectrum, namely the two-point correlation function depending on the comoving distance r, the baryon acoustic oscillations are imprinted on distance scales of the order $r \simeq \mathcal{O}(100) \, \text{Mpc}/h$ [138]. To be precise, the characteristic BAO peak arises at the scale $r_{\text{BAO}} \simeq 110 \, \text{Mpc}/h$ [216].

in SPT breaks down already at the weakly non-linear scale. Indeed, for a ΛCDM cosmology at redshift $z = 0$, it stops converging in Fourier space roughly at $k \simeq 0.1 \, h/\text{Mpc}$ [183, 188]

As soon as the real-space density contrast becomes of the order $\delta \sim \mathcal{O}(1)$, perturbation theory is not well-defined any longer. The characteristic scale at which this happens is referred to as the *non-linear scale* [40]. This non-linear scale, which is usually identified in momentum space with moments of the linear power spectrum of density perturbations [101],

$$k_{\text{NL}}^{-2} \sim \int dq \, P_{11}^L(q, \eta) \,. \tag{5.2}$$

separates the dynamics of gravitational instability into two regimes. For $k < k_{\text{NL}}$, the linear dynamics of large distance scales are dominant and its description by means of perturbation theory is justified. For $k \geq k_{\text{NL}}$, on the other hand, the fully non-linear dynamics of small distance scales makes perturbation theory inapplicable and it seems unavoidable to resort to non-perturbative methods. For cosmological purposes, such as constraining the cosmological parameters from the baryon acoustic oscillations, we are usually interested in the small-k regime. Thus, the ultimate goal of perturbative approaches is to find an accurate analytic description of the dynamics of gravitational instability in this mildly non-linear regime.

Treating the latter perturbatively requires caution since the two regimes separated by the non-linear scale k_{NL} are coupled by non-linearities. While at linear order in SPT, different Fourier modes of the density contrast (and the velocity divergence) evolve independently (see (3.56) with (3.51)), their evolution beyond linear order is not independent any more due to the impact of the mode-coupling terms in the fluid equations (3.54) (see also (3.77)). This implies that at the non-linear level, two hard, short-wavelength (UV) modes, can couple to produce a long-wavelength (IR) mode. As a consequence, beyond linear perturbation theory, UV modes can in principle affect the dynamics of the long-wavelength perturbations. In conclusion, SPT is successful in extending the validity of linear perturbation theory in a limited range, but does not constitute a perturbative approach yielding accurate predictions even for mildly non-linear scales. Due to this apparent lack of SPT, a variety of perturbative approaches aiming at a better control of perturbation theory in the mildly non-linear regime have been developed. We give an overview of the different perturbative methods in Section 5.2.

5.1.2. UV divergence

An additional drawback of SPT arises from the UV sensitivity of the loop integrals in the perturbative expansion [40, 102]. This UV sensitivity becomes apparent in the strong dependence of the perturbative predictions, e.g., for the density power spectrum, at high loop orders on the short-wavelength (UV) modes. For particular sets of initial conditions, these even exhibit a UV-divergent behavior (see Figure 5.1).

5. Overview of Perturbative Approaches

The emergence of UV divergences in SPT can be demonstrated by a illustrative example [40]. Let us consider the simplest case of an EdS cosmology with scale-free power-low initial conditions, $P_0(k) \propto k^{n_s}$ with n_s denoting the primordial spectral index (see (4.5)). In this case, already the one-loop density power spectrum shows a UV-divergent behavior for $k \to \infty$ if $n_s \geq -1$. In general, at one-loop order, the SPT loop integrals for these initial conditions are UV divergent if $n_s \geq -3 + 2/l$ for $k \to \infty$ [96, 100]. (Note that in case of $n_s \leq -1$, IR divergences occur in the loop integrals for $k \to 0$.) The UV divergence arises even in the case of very soft external momenta where the perturbative expansion in SPT is in principle expected to work. For obtaining finite predictions for the power spectrum beyond linear order in SPT, it is then required to introduce an (arbitrary) UV cutoff scale. This cutoff dependence of the perturbative predictions beyond leading order hence leads to a loss of predictability of the SPT approach. Notice that the sensitivity of the SPT predictions to the cutoff scale is also an indication that SPT fails to model the dynamics on the short distance scales properly and highlights some inconsistency in the perturbative method.

Despite this, the UV sensitivity of SPT has not been considered rigorously, with a few exceptions [336], until recently (see e.g., [101, 102]). The reason for this is that for the case of the phenomenologically favored ΛCDM cosmology, the perturbative predictions of SPT do not reveal a strong UV sensitivity. However, in the present era of precision cosmology, the infinite error, produced in the simplest case of an EdS cosmology, indicates that (finite) SPT predictions still do not correctly capture the imprint of non-linear hard modes in the dynamics of large-scale structure formation, and thus highlights some inconsistency in the perturbative approach [208]. This issues has been recently addressed by transferring concepts of effective field theory (EFT) approaches to the dynamics of large-scale structure formation (see e.g., [63, 178, 208]). However, the effective operators possess a non-local time dependence which makes the renormalization at high loop order more complicated [202].

On the other hand, numerical simulations indicate the actual sensitivity of the power spectrum to UV modes is smaller than suggested by SPT predictions [209, 210], in accordance to expectations from qualitative arguments in [92]. Thus, an accurate description of the dynamics of gravitational instability may be possible even under rather broad assumptions about the dynamics on short scales. This motivates the development of new perturbative approaches which allow to consistently isolate the UV contributions and systematically study their sensitivity to the underlying assumptions. As we discuss in Section 5.2, recent examples of such kind of approaches include [211, 213, 214].

To go beyond that, we pursue a different road in Chapter 7. There, we develop non-perturbative methods which allow us, among others, to further investigate the UV dependence of SPT (see in particular Section 7.4).

5.1.3. Spurious IR divergences

Apart from the sensitivity of its perturbative predictions to the impact of UV modes, SPT is plagued by the emergence of spurious infrared enhanced contributions. Qualitatively, these 'IR divergences' in SPT originate from using the initial distribution to evaluate late-time quantities. This generates a non-local time dependence to the large displacements of the fluid particles due to large-scale bulk flows [215]. These spurious IR divergences in SPT significantly complicate the computational performance, as well as the analysis of physical effects produced by the large-scale bulk flows.

However, in equal-time correlation functions, as for instance the power spectrum and the bispectrum, summing all diagrams contributing at a fixed loop order in perturbation theory [94] leads to a cancellation of the IR divergences. To be precise, for the leading IR divergences this cancellation has been formally proven to all perturbative orders in SPT [237] and can be ascribed to the equivalence principle [169, 306]. Moreover, it has been demonstrated that the subleading IR divergences which arise at two- and higher-loop orders cancel out as well [101, 125, 167, 168, 182]. Potentially, it might also be possible to explain the cancellation of the subleading IR effects by using symmetry arguments such as Galilean invariance [101, 167, 168, 306]. Furthermore, IR-safe integrands up to two-loop order and for an arbitrary loop order have been constructed in [101, 182] and [102], respectively.

Particularly in [101], the effects of soft (IR) modes on hard modes have been studied systematically not only in SPT, but also by use of the so-called eikonal approximation [159]. Within the eikonal approximation, which we review in Section 5.4, one can explicitly show that equal-time correlation functions, such as the power spectrum, on very large momentum scales are not affected by the impact of soft modes [160]. This indicates that the effects in the SPT power spectrum associated to the non-linear scale k_{NL} are spurious.

Although the effect of soft (IR) modes on very large momentum scales is absent for equal-time correlation functions, they can nevertheless affect the dynamics on intermediate scales, being important for a description of the baryon acoustic oscillations [144, 337] (see also [176, 189]). To overcome this problem, there have been attempts for adopting Galilean-invariant approaches, such as in [163]. Apart from this, it has been shown in [101] that the modification of the SPT density power spectrum due to the impact of soft modes corresponds at most to logarithmic corrections at any loop order.

Thus, although it is questionable if resummation techniques provide a systematic improvement in the determination of equal-time correlation functions on large momentum scales, they might resum the correct subdiagrams to treat soft-mode effects at intermediate scales and hence to predict accurate results in this regime.

We give an overview of different resummation schemes in Section 5.2, and subsequently take the former point up again in Section 5.4.

5.1.4. Deviations from the perfect fluid approximation

On small distance scales, SPT possesses not only the shortcoming that the real-space density contrast becomes large, but in addition that the perfect fluid approximation fails. Indeed, as we discussed in Section 2.4, on sufficiently small distance scales shell-crossing and thus multi-streaming occurs. Then, the single-flow approximation, on which the pressureless and non-viscous perfect fluid equations are based, becomes invalid (see also Section 2.1.1). Due to the non-linear nature of the dark matter evolution, the failure of the perfect fluid description on small distance scales can have a sizeable effect on the dynamics on large distance scales.

Since SPT is based on solving the perfect fluid equations perturbatively, it does – a priori – not account for deviations from the perfect fluid on small distance scales or equivalently for large momenta k. Thus, calculating its impact on small momentum scales is not possible within the framework of SPT.

To address this issue, two complementary strategies have been developed. The effective field theory approach (see e.g., [63, 178, 208]) takes deviations from the perfect fluid assumption into account by adding an effective pressure and effective viscosity coefficients to the perfect fluid equations. These compose in turn an effective velocity dispersion tensor σ_{ij} contributing to the fluid equations (see (2.29) and (2.28)). The effective coefficients are split into a counter-term to cancel possible UV divergences and a (physical) renormalized piece. Then, the resulting renormalized coefficients capture, among others, the deviations from the perfect fluid equations. They are inferred from observational data or numerical simulations. A different direction has been followed by the development of perturbative approaches which actually start from the viscous fluid dynamics [213, 214]. Thereby, the viscous fluid dynamics accounts for the deviations from the perfect fluid description in terms of a gradient expansion and shares some commonalities with the EFT approach (see for instance [214]).

To address the shortcomings of SPT discussed in this section and improve upon its perturbative predictions, a plethora of alternative perturbative approaches to LSS formation has been developed. We have mentioned some of these already in our previous considerations. In the following, we provide an overview of the different perturbative methods in the literature by pointing out their characteristics, similarities and differences.

5.2. Alternative perturbative approaches

The development of analytic approaches within cosmological perturbation theory to model the formation of the large-scale structure in the Universe, both in Eulerian and in Lagrangian space, dates back to the very early days of modern cosmology [40, 91, 92]. In the Eulerian description of cosmological perturbation theory, SPT constitutes by a good margin the most common perturbative approach to investigate the dynamics of LSS formation. While its perturbative solution of the non-linear fluid equations relies on the density contrast as fundamental quantity, its Lagrangian-space equivalent, the so-called *Lagrangian perturbation theory (LPT)*, introduces a displacement vector field as central dynamical variable [103–127]. In turn, proceeding from the linear perturbative order of this displacement field, the so-called *Zel'dovich approximation (ZA)* [91] deduces an approximate solution to the fluid equations (see e.g., [105, 128–137]). However, since LPT does not only suffer from the same shortcomings as SPT, but has the additional drawback that the Lagrangian picture breaks down once shell-crossing occurs, it has received less attention in the past than SPT as its Eulerian counterpart [138].

Although SPT as a perturbative method provides valuable insights in the dynamics of LSS formation (see e.g., [40]), the shortcomings it reveals lead to a fundamental limitation of its predictive power. In particular, it possesses only a small range of validity at low redshifts (see Section 5.1.1) and shows poor convergence properties due to the emergence of UV-divergent loop integrals (see Section 5.1.2). This UV-divergent behavior of the perturbative expansion in SPT has been confirmed to date by computations of the density power spectrum up to three-loop order [102, 338].

Due to these drawbacks of SPT, a lot of effort has been devoted in the recent years to the development of alternative perturbative LSS approaches with the aim to overcome the fundamental shortcomings of SPT and extend the range of reliable perturbative predictions from the weakly into the mildly non-linear regime. An accurate description of the dynamics in the mildly non-linear regime is of particular importance as it encodes invaluable cosmological information, provided for instance by the baryon acoustic oscillations [142, 334, 335] at low redshifts (see (5.1)).

To address these issues of SPT, two different directions have been followed in the literature. On the one hand, the results of [102, 209] suggest that the UV divergence of the perturbative SPT expansion originates from an unphysical treatment of modes well inside the regime of validity of the single-flow approximation in the framework of SPT [303]. Hence, one expects to achieve progress from better understanding the perturbative expansion itself and identifying the effects behind the failure of perturbation theory. Based on this motivation, a variety of

resummation techniques for the perturbative expansion, as for example renormalized perturbation theory (RPT) [142–144], have been developed. These focus on the resummation of higher-order contributions in the perturbative expansion in order to improve its convergence properties and extend its range of validity compared to SPT.

On the other hand, an alternative way to address the lack of convergence in SPT consists in considering corrections to the single-flow assumption and thus the perfect fluid approximation arising from non-linear hard modes. For this purpose, one proceeds to an effective fluid description which requires to extract information from observational data or numerical simulations. This is the idea behind the *effective field theory (EFT)* of large-scale structure [49, 63, 178–207] and its formulation in *Lagrangian space (LEFT)* [89, 208]. It is beyond the scope of this work to discuss the (semi-analytic) effective field theory approach in detail. Instead, we refer to [63, 178, 208] where the basic aspects of the EFT approach and its Lagrangian space formulation LEFT are introduced, as well as to [89] for a review of the latter. Other approaches using an effective description beyond the perfect fluid or accounting for deviations from the perfect fluid approximation (see Section 5.1.4) can be found in [209, 211, 212] and [213, 214], respectively.

5.2.1. Resummation schemes

It was in particular the development of resummation techniques that has resurfaced a renewed interest on analytic approaches in cosmological perturbation theory in the last decade. The pioneering work in this line is the *renormalized perturbation theory (RPT)* approach [142–144]. Based on the observation that large perturbative contributions arising from soft-mode effects can be resummed in SPT, it reorganized the perturbative expansion in terms of a non-linear propagator to improve its convergence. In the large-momentum limit, the non-linear propagator subsequently allows to resum infinite classes of subdiagrams in the perturbative expansion and leads to an exponential suppression of large soft-mode effects controlled by the non-linear scale k_{NL}. Remarkably, the result for the non-linear propagator fairs very well against numerical simulations [339]. This resummation also leads to an improvement of the convergence properties of the density power spectrum in comparison to SPT. A natural extension of the non-linear RPT (two-point) propagator is provided by the concept of multi-point propagators introduced in [339, 340]. We review the fundamental aspects of RPT and the multi-point propagator formulation in Section 5.3.

Motivated by the success of RPT, a large variety of resummation schemes mostly intending to resum large soft effects, has been developed (see e.g., [114, 116, 148–163]). Many of these perturbative approaches implement concepts from other fields, such as quantum field theory

(see Section 3.3.6) or the hydrodynamic theory of turbulence [147]. All of them provide relatively accurate predictions for the density power spectrum on the onset of non-linearity, but fail on sufficiently large momentum scales. In the following, we give an overview of a number of specific resummation schemes by pointing out their commonalities and differences and finally comparing their predictions for the density power spectrum. Detailed reviews of the different resummation schemes can be found in [100, 138–141, 164]).

While the perturbative approaches of SPT and also RPT aim to solve the non-linear fluid equations perturbatively with respect to the doublet field $\psi_a(\mathbf{k}, \eta)$ of density and velocity perturbations, an alternative strategy is to extend the fluid equations to an infinite hierarchy of evolution equations directly in terms of the correlation functions, such as the power spectrum and the bispectrum. In order to derive a perturbative solution for the correlation functions, one then truncates the infinite hierarchy of evolution equations to a closed system of equations through an appropriate 'closure approximation'. In the so-called *closure theory* [149], the hierarchical system of evolution equations is truncated by approximating the three-point correlation function by its leading-order expression in SPT. This allows in turn to explicitly determine the non-linear propagator, defined as in RPT, in the small- and large-momentum limit and to match it naturally in the intermediate regime. Proceeding from this, the power spectrum is derived order-by-order via a Born-like series expansion [341]. Apart from this, an attempt to solve the closure equations numerically without resorting to a Born-like expansion has appeared in [116].

A variant of the closure theory is the *time-flow approach* [156], which is also referred to as *time-renormalization group approach* since it can be interpreted as a specific formulation of the Wilsonian renormalization group (RG) [342–346] with the time being the flow parameter. Details about the time-flow approach can be found in Section 5.5. In the time-flow approach, the infinite hierarchy of evolution equations is truncating by neglecting the connected part of the four-point correlation function, the trispectrum. In consequence, the time-flow approach leads to formal integral solutions for the power spectrum $P_{ab}(\mathbf{k}, \eta)$ and the bispectrum $B_{abc}(\mathbf{k}, \mathbf{q}, \mathbf{p}, \eta)$, which can then be evaluated successively by means of perturbation theory. The time-flow approach has the particular advantage that it can be straightforwardly applied to cosmological models other than EdS and ΛCDM, such as those containing massive neutrinos or scalar-tensor modifications of gravity. Applications of the time-flow approach can bee found in [301, 303, 347–350]. Beyond that, this approach can be considered as a generalization of the *renormalization group perturbation theory (RGPT)* [150] which constitutes an attempt to regulate the UV divergence of the one-loop density power spectrum in SPT by use of renormalization group methods.

In [151–153], different framework has been developed by implementing a *path-integral for-*

mulation of the Vlasov equation (2.18) in terms of the distribution function $f(\boldsymbol{x}, \boldsymbol{p}, \tau)$ in (2.17). A similar technique, which we here refer to as *large-N theory*, with N being a fictitious parameter, has been applied to the fluid equations in [154]. These two methods rely on taking functional derivatives of an appropriately constructed path integral, the generating functional, to derive correlation functions like the power spectrum. While the straightforward perturbative evaluation of the generating functional reproduces the predictions of SPT, applying large-N expansion techniques and truncating at a fixed order in $1/N$ leads to an approximate perturbative solution for the power spectrum. This coincides with the corresponding SPT predictions up to a fixed order in the initial power spectrum. Beyond this order, it includes additional non-perturbative contributions from infinite partial resummations of the perturbative SPT expansion.

Furthermore, let us mention the *Lagrangian resummation theory* [114, 115], which has been followed by a number of subsequent extensions [118, 120–122, 124, 126, 351]. The Lagrangian resummation theory approach reproduces the density power spectrum of SPT at the linear perturbative order, but additionally yields a non-perturbative prediction for the power spectrum corresponding to a resummation of an infinite set of terms in the perturbative SPT expansion. Thereby, the first term of the resummed power spectrum is identical to the respective tree-level prediction of RPT in the large-momentum limit.

In order to compare the accuracy of the different resummation schemes discussed above, we show in Figure 5.2 and Figure 5.3 their perturbative predictions for the power spectrum of density perturbations, $P(k, z = 0) \equiv P_{11}(k, \eta(z = 0))$, at present time, or equivalently redshift $z = 0$ (see (1.1)), for a ΛCDM universe in comparison to results of tree-level SPT and N-body simulations performed in [138].[2] Thereby, each power spectrum contribution has been divided by the 'no-wiggle' Eisenstein-Hu fit $P_{\mathrm{nw},0}(k)$ of the density power spectrum (see [352]) for illustrating the accuracy of the perturbative predictions around the baryon acoustic oscillations.

In detail, Figure 5.2 shows the perturbative contributions to the density power spectrum at tree-level, one-loop and two-loop order in RPT and closure theory, respectively. In both approaches, the higher loop corrections improve upon the tree-level contribution. For RPT, the one-loop results performs rather well for momenta $k \lesssim 0.15\,h/\mathrm{Mpc}$, whereas the two-loop contribution, similar as in SPT, systematically overpredicts the density power spectrum compared to the results from numerical simulations. In contrast to RPT, closure theory appears to improve by going from one-loop to two-loop order. It extends the range of agreement with

---

[2]The cosmological parameters which have been used to perform the numerical simulations for the flat ΛCDM model are the density parameters $\Omega_{m,0} = 0.25$, $\Omega_{b,0}\,h^2 = 0.0224$, the dimensionless Hubble parameter $h = 0.72$, the power spectrum renormalization $\sigma_8 = 0.8$ and the primordial spectral index $n_s = 0.97$ [138].
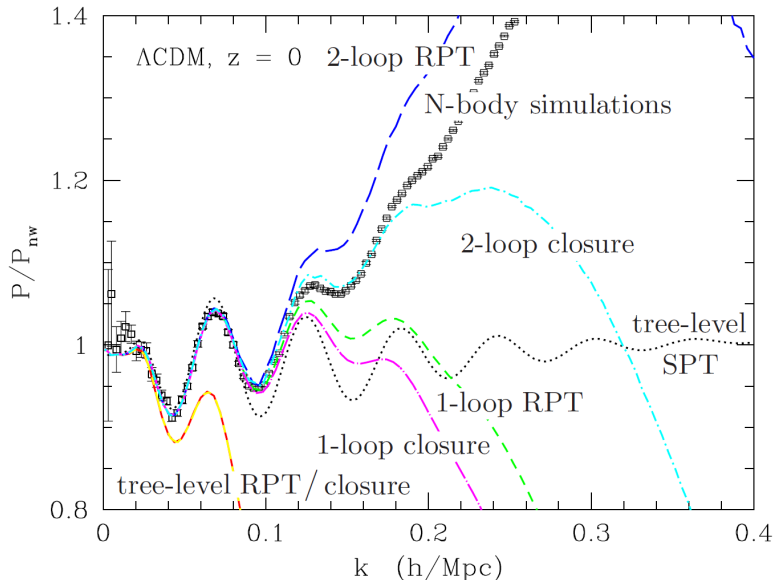
Fig. 5.2.: Comparison of perturbative contributions to the power spectrum of density perturbations, $P(k, z = 0) \equiv P_{11}(k, \eta(z = 0))$, at present time (or equivalently at redshift $z = 0$) and for a ΛCDM universe at tree-level, one- and two-loop order in RPT and closure theory, respectively (adapted and reprinted from [120]). Each power spectrum contribution has been divided by the 'no-wiggle' Eisenstein-Hu fit $P_{\mathrm{nw},0}(k)$ of the initial density power spectrum [352] for highlighting the accuracy of the perturbative predictions around the baryon acoustic oscillations. Here, the black squares and the black dotted line indicate the results for the density power spectrum from numerical simulations and tree-level SPT for reference. The red solid line represents the corresponding predictions of tree-level RPT, the green dashed line of one-loop RPT and the blue long-dashed line of two-loop RPT, whereas the yellow short-long-dashed line shows the predictions of tree-level closure theory, the magenta dot-long-dashed line of one-loop closure theory and the cyan dot-dashed line of two-loop closure theory.

the N-body simulation data significantly at two-loop order.

Moreover, in Figure 5.3, the one-loop contributions to the density power spectrum in SPT as well as the remaining resummation schemes introduced before, namely the time-flow approach, RGPT, large-N theory and Lagrangian resummation theory, are presented. Therein, the one-loop SPT contribution, always over-predicting the power spectrum compared to numerical simulations, clearly reveals the overshooting phenomenon of SPT. Besides, the one-loop prediction of large-N theory roughly follows that of SPT before turning over at high momenta.
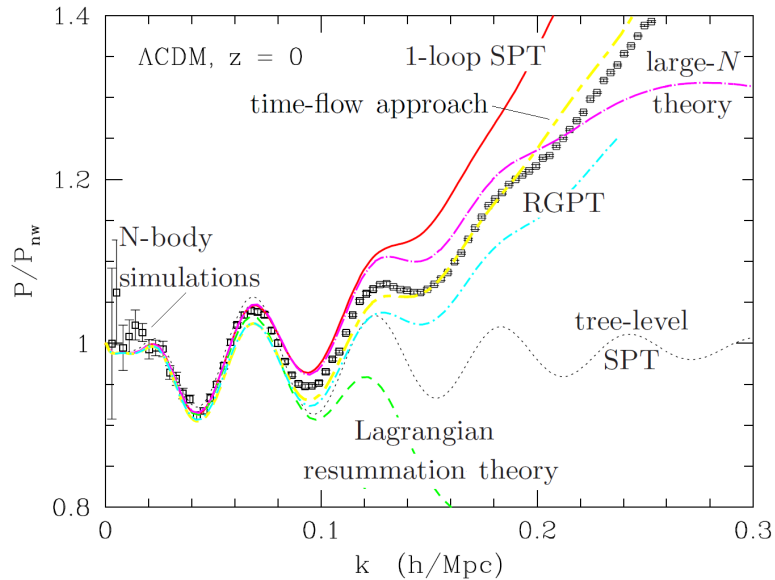
Fig. 5.3.: Comparison of the one-loop predictions for the power spectrum of density perturbations, $P(k, z = 0) \equiv P_{11}(k, \eta(z = 0))$, at present time (i.e., at redshift $z = 0$) and for a ΛCDM universe, in SPT, the time-flow approach, RGPT, large-N theory and Lagrangian resummation theory, respectively (adapted and reprinted from [120]). As in Figure 5.2, each power spectrum contribution has been divided by the 'no-wiggle' Eisenstein-Hu fit $P_{\mathrm{nw}}(k, z = 0)$ of the initial density power spectrum (see [352]), whereas the black squares and the black dotted line represent the results for density power spectrum from numerical simulations and tree-level SPT for comparison. In this figure, the red solid line shows the one-loop contribution to the density power spectrum in SPT, the yellow short-long-dashed line the respective one in the time-flow approach and the cyan dot-dashed line the one in RGPT, whereas the magenta dot-long-dashed line represents the one-loop power spectrum correction in large-N theory and the green dashed lined the one in Lagrangian resummation theory.

Lagrangian resummation theory, on the other hand, is much too strongly damped beyond the first oscillation. Apart from this, the time-flow approach as well as RGPT follow the general behavior of the numerical simulations, but without fitting any of its characteristics precisely.

In summary, Figure 5.2 and Figure 5.3 reveal that in comparison to the results from numerical simulations, the power spectrum of density perturbations is well modeled by the theoretical predictions of the discussed resummation schemes (as well as SPT) in comparison up to $k \simeq 0.1\,h/\mathrm{Mpc}$ at redshift $z = 0$ for a ΛCDM universe [138]. Note that for higher redshifts, the performance of the perturbative methods improves, as expected. Although

the resummation techniques lead to a slight improvement of power spectrum predictions in the weakly non-linear regime compared to SPT, non of these methods provides sufficiently accurate predictions beyond it.

5.2.2. Current focus of analytic studies

Currently, the main focus of analytic studies in the field of LSS formation can be broadly classified in two categories [89, 100]. First, the impact of *soft, long-wavelength (IR)* perturbations on modes around the BAO scale (see (5.1)) has been studied from different points of view, e.g., by exploiting symmetry arguments such as (extended) Galilean invariance and the equivalence principle [165–177], or using the *eikonal approximation* [101, 159, 160]. We discuss the latter in detail in Section 5.4 and apply explicitly in Section 6.1.1.

Second, a lot of effort has been devoted to understanding the influence of *hard, short-wavelength (UV)* perturbations. Due to the non-linear dynamics of dark matter clustering on short momentum scales, their treatment is more complicated. Thereby, the effective field theory approach (see for instance [63, 178, 208]) has emerged as a useful tool to parameterize the imprint of UV modes on long-distance observables. Furthermore, motivated by various results from numerical simulations [209, 210], complementary approaches have been developed which aim at addressing the intrinsic limitations of SPT from first principles, such as [102, 215, 216] (see also [211–214] in this context).

For future progress in cosmological perturbation theory, it is still of major importance to assess and analyze the impact of UV modes on small momentum scales in further detail. We present an effort in this direction in Chapter 7. Therein, we develop methods to deduce a *non-perturbative* equation for the power spectrum in the soft limit which in turn allows us to draw conclusions about the UV divergence in perturbation theory. In general, the efforts of studying the UV effects should be regarded as part of a grander program with the ultimate goal to develop efficient analytic methods to accurately predict the large-scale structure observables in the cosmologically interesting intermediate regime.

After this overview of the various existing analytic approaches in the field of large-scale structure formation, we present a selection of analytic methods in further detail in the next sections. Apart from the pioneering work of RPT discussed in what follows, we focus on those methods which we need for further perturbative investigations in Chapter 6. We consider the eikonal approximation and the time-flow approach in Section 5.4 and Section 5.5, respectively.

5.3. Renormalized perturbation theory

To overcome the shortcomings of SPT, discussed in Section 5.1, and to improve upon its perturbative predictions in the weakly non-linear regime, a lot of effort has been devoted to the development of alternative approaches in cosmological perturbation theory in the last decade. The first significant progress in this direction was made by the introduction of the renormalized perturbation theory (RPT) in [142–144], which transfers techniques developed in quantum field theory as well as in the theory of turbulence in the context of hydrodynamics (see e.g., [147]) to the field of large-scale structure formation.

The development of RPT was driven by the observation that large perturbative contributions arising from soft-mode effects can be resummed in perturbation theory. This result leads to a reorganization of the perturbative expansion compared to SPT. Thereby, the linear propagator $g_{ab}(\eta, \eta_0)$ and the vertex function $\gamma_{abc}(\boldsymbol{k}, \boldsymbol{q}, \boldsymbol{p})$, constituting together with initial power spectrum the fundamental building blocks of the diagrammatic formulation in SPT, are replaced by a generalized *non-linear* propagator $G_{ab}(k, \eta, \eta_0)$ and a non-linear vertex function $\Gamma_{abc}(\boldsymbol{k}, \boldsymbol{q}, \boldsymbol{p}, \eta, \eta', \eta'')$ in RPT. Based on this, the RPT approach implements, to an even higher degree than SPT, standard tools of quantum field theory. Besides the diagrammatic representation of the basic building blocks, it expresses the non-linear propagator $G_{ab}(k, \eta, \eta_0)$ in form of a Dyson equation for the renormalized Green's function [353]. As mentioned before, in the limit of large momentum, it is then possible to resum infinite classes of subdiagrams in the perturbative expansion yielding an exponential suppression of large soft-mode effects in terms of the non-linear scale k_{NL}. If the non-linear vertex function is in turn approximated by its tree-level form (being essentially $\gamma_{abc}(\boldsymbol{k}, \boldsymbol{q}, \boldsymbol{p})$), the power spectrum can be written as as expansion in the non-linear propagator. Then, the resulting perturbative series for the power spectrum does not constitute an expansion in power of the initial density contrast $\delta_0(\boldsymbol{k})$ any more, but rather corresponds to an 'expansion in orders of the complexity of the interaction' [147].

While in the initially developed RPT approach in [142–144], it is only made use of the non-linear two-point propagator $G_{ab}(k, \eta, \eta_0)$ to rewrite the resummation series of the power spectrum, in [339, 340], the concept of multi-point propagators $G^{(n)}_{ab_1 \ldots b_n}(\boldsymbol{q}_1, \ldots, \boldsymbol{q}_n, \eta, \eta_0)$ with $k = |\boldsymbol{q}_1 + \ldots + \boldsymbol{q}_n|$ has been introduced as an alternative scheme to evaluate the perturbative expansion of the power spectrum in RPT. Moreover, the concept of multi-point propagators has led to effective implementations of RPT, namely MPTbreeze [145] and RegPT [146], which significantly simplify the computationally demanding evaluation procedure of the power spectrum in RPT.

In the following, we review the fundamental aspects of the perturbative RPT approach and give explicit expressions of the most important quantities it introduces, such as the non-linear propagator, and the results, as for instance for the power spectrum, derived thereof.

5.3.1. Non-linear propagator

A possible way to account for the non-linearities in the perturbative treatment of large-scale structure formation consists in interpreting them as modifications to the linear propagator $g_{ab}(\eta, \eta_0)$ (see (3.68)). This idea, which leads to a renormalization of the propagator and allows in turn a partial resummation of the perturbative series for correlation functions, is the key aspect at the heart of RPT [142–144].

In the framework of RPT, the linear propagator $g_{ab}(\eta, \eta_0)$ is consequently generalized to a fully non-linear one, denoted by $G_{ab}(k, \eta, \eta_0)$, which effectively describes the time evolution in the presence of mode-coupling. This non-linear propagator is formally defined as [142]

$$G_{ab}(k, \eta, \eta_0)\, \delta^{\mathrm{D}}(\boldsymbol{k} - \boldsymbol{k}') \equiv \left\langle \frac{\delta \psi_a(\boldsymbol{k}, \eta)}{\delta \psi_b(\boldsymbol{k}', \eta_0)} \right\rangle , \tag{5.3}$$

where $\delta \psi_a(\boldsymbol{k}, \eta)$ denote variations with respect to the doublet fields. Note that in contrast to the linear propagator $g_{ab}(\eta, \eta_0)$, the non-linear propagator $G_{ab}(k, \eta, \eta_0)$ is momentum dependent, even in the case of an EdS cosmological model. Hence, the Dirac delta distribution in the definition above is necessary to ensure translation invariance, that is, $\boldsymbol{k}' = \boldsymbol{k}$.

To be precise, $G_{ab}(k, \eta, \eta_0)$ is not a true propagator since it does *not* lead to a relation $\psi_a(\boldsymbol{k}, \eta) = G_{ab}(k, \eta, \eta_0)\, \psi_b(\boldsymbol{k}, \eta_0)$, analogous to (3.56) for the linear propagator, for the non-linear case. (For Gaussian initial conditions, it leads instead to a relation of the form (5.5)). It rather has to be considered as a generalization of the linear propagator in the sense that it can be diagrammatically represented with one incoming and one outgoing arrow, analogously to the linear propagator in Figure 3.1. Explicit diagrams including the non-linear propagator $G_{ab}(k, \eta, \eta_0)$ can be found in [142].

By using the perturbative solution for the doublet fields $\psi_a(\boldsymbol{k}, \eta)$ in (3.72) with (3.73), we can recast the definition of the non-linear propagator in (5.3) as a correction to the linear propagator in terms of a series expansion,

$$G_{ab}(k, \eta, \eta_0) = g_{ab}(\eta, \eta_0) + \sum_{n=2}^{\infty} \left\langle \frac{\delta \psi_a^{(n)}(\boldsymbol{k}, \eta)}{\delta \psi_b(\boldsymbol{k}, \eta_0)} \right\rangle . \tag{5.4}$$

Here, we have explicitly separated the linear from the non-linear contributions. Notice that for Gaussian initial conditions, the non-linear contributions are only composed by the odd terms of the perturbative expansion. The series expansion of the non-linear propagator in the equation

above can be represented diagrammatically by interpreting the linear propagator $g_{ab}(\eta, \eta_0)$ as the tree-level contribution and consequently the higher-order contributions as loop corrections to the non-linear propagator $G_{ab}(k, \eta, \eta_0)$. Thereby, the non-linear contribution at order n constitutes the nth-order loop correction. Explicit diagrams for the non-linear propagator up to the two-loop level can be found in [142].

As we can see from the series expansion in (5.4), the non-linear propagator represents the ensemble-averaged response of the fields $\psi_a^{(n)}(\boldsymbol{k}, \eta)$ at the time η to variations in the initial conditions $\psi_b(\boldsymbol{k}, \eta_0)$ set up at some initial time η_0. In other words, it quantifies how much information of the initial distribution of a $\boldsymbol{k}$-mode remains in the final state at the same $\boldsymbol{k}$ in terms of an ensemble average [142]. In this sense, the non-linear propagator can be thought of as measuring the 'memory of initial conditions' [143]. For Gaussian initial conditions, the non-linear propagator fulfills the relation

$$\left\langle \psi_a(\boldsymbol{k}, \eta)\, \psi_b(\boldsymbol{k}', \eta_0) \right\rangle = G_{ac}(k, \eta, \eta_0) \left\langle \psi_c(\boldsymbol{k}, \eta_0)\, \psi_b(\boldsymbol{k}', \eta_0) \right\rangle, . \tag{5.5}$$

Thus, In case of Gaussian initial conditions, we can interpret it as a measure of the cross-correlation between the initial and the final state of the doublet fields or indeed as a genuine propagator (Greens function) in terms of two-point cross-correlation functions.

By using the diagrammatic representation of perturbation theory, it is possible to reformulate the perturbative expansion (5.4) as a formal integral solution for the non-linear propagator. This integral solution has the form of a Dyson equation [353] with the non-linear propagator $G_{ab}(k, \eta, \eta_0)$ corresponding to the renormalized Green's function [142],

$$G_{ab}(k, \eta, \eta_0) = g_{ab}(\eta, \eta_0) + \int_{\eta_0}^{\eta} d\eta' \int_{\eta_0}^{\eta'} d\eta''\, g_{ac}(\eta, \eta')\, \Sigma_{cd}(k, \eta', \eta'')\, G_{db}(k, \eta'', \eta_0) \tag{5.6}$$

with time ordering $\eta \geq \eta' \geq \eta'' \geq 0$ to ensure causality. Here, $\Sigma_{ab}(k, \eta, \eta')$ is defined as the sum of the perturbative contributions to the non-linear propagator consisting of 'principle path irreducible diagrams', i.e., the diagrams which cannot be disconnected by removing a linear propagator from the principal path. Thereby, the principal path constitutes the chain of linear propagators that runs through the diagram without intersecting the initial conditions.

Rewriting the non-linear propagator $G_{ab}(k, \eta, \eta_0)$ as a Dyson equation can be seen as a first step leading to a resummation of the perturbative expansion for the non-linear propagator in (5.4). However, in order to derive an explicit expression for the resummed propagator in the framework of RPT, a considerable conceptual and computational effort is required. This can be avoided by resorting to the so-called eikonal approximation. As we review in the next section, the eikonal approximation provides a transparent and straightforward way to

derive the resummed non-linear RPT propagator (see Section 6.1.1). Beyond that, it allows for a generalization of this results and thus also indicates its limitations. We give a detailed derivation of the resummed propagator in Section 6.1.1 and concentrate here on the discussion of its characteristic properties.

Resummation in the limit of large momentum

If we consider very large distance scales, i.e., small momenta k, the dynamics of gravitational instability are dominated by the linear evolution. Hence, the non-linear contributions to $G_{ab}(k, \eta, \eta_0)$ in the perturbative series (5.4) vanish for $k \to 0$ so that [144]

$$G_{ab}(k \to 0, \eta, \eta_0) = g_{ab}(\eta, \eta_0) \,. \tag{5.7}$$

On the other hand, if we approach small distance scales, corresponding to large momenta k, where the dynamics are dominated by the non-linear evolution, the mode-coupling interactions gradually 'erase' the initial distribution. Hence, we expect the non-linear propagator to decay for $k \to \infty$, that is,

$$G_{ab}(k \to \infty, \eta, \eta_0) = 0 \,. \tag{5.8}$$

Indeed, if we assume Gaussian initial conditions (see (3.70)) and consider the limit of large momentum k, the series expansion of the non-linear propagator in (5.4) can be resummed. The non-linear propagator $G_{ab}(k, \eta, \eta_0)$ then follows a Gaussian decay with respect to k in the limit of large momentum [143]

$$G_{ab}(k, \eta, \eta_0) = g_{ab}(\eta, \eta_0) \, \exp\left[-\frac{1}{2}k^2 \sigma_d^2 \left(e^\eta - e^{\eta_0}\right)^2\right] \,, \tag{5.9}$$

where the dimensionful quantity σ_d^2 is the so-called variance of the initial 'displacement field', given by [142, 143]

$$\sigma_d^2 = \frac{4\pi}{3} \int dq \, P_0(q) \,. \tag{5.10}$$

In general, the variance of the displacement fields is defined as

$$\sigma_{ab}^2(\eta) \equiv \frac{1}{k^2} \int d^3q \, \frac{(\boldsymbol{k} \cdot \boldsymbol{q})^2}{q^4} \, P_{ab}(q, \eta) = \frac{4\pi}{3} \int dq \, P_{ab}(q, \eta) \,. \tag{5.11}$$

At the initial time η_0 and for the correlation of density perturbations with $a = b = 1$, the previous equation includes the initial density power spectrum. By assuming growing-mode Gaussian initial conditions (see (3.70) and (4.15)), it then reduces to $\sigma_d^2 \equiv \sigma_{11}^2(\eta_0)$.

Recalling the form of the linear power spectrum of density perturbations $P_{11}^L(k, \eta)$ for growing-mode initial conditions, (4.17), we find that the variance σ_d^2 is directly related to

the non-linear scale k_{NL} in (5.2). In fact, the non-linear scale k_{NL} represents the characteristic decay scale of the non-linear RPT propagator in (5.9), indicating the breakdown of perturbation theory. However, the form of the propagator in (5.9) suggests that the impact of modes from the highly non-linear regime $k \gg k_{\mathrm{NL}}$ on the dynamics of the long-wavelength modes is exponentially small. Thus, as a result of the resummation of the non-linear propagator according to (5.9) in RPT, the long-distance scales are effectively 'shielded' from the short-distance scales. This property draws a distinction between the perturbative frameworks of RPT and SPT since the latter suffers from the lack of being highly sensitive to the influence of the UV modes (see Section 5.1).

The relation for the non-linear propagator $G_{ab}(k, \eta, \eta_0)$ in (5.9) has been compared with respective predictions from numerical simulations in [339]. Therein, it has been found that the functional behavior of the non-linear propagator in the limit of large momentum k is indeed very well described by a Gaussian decay with respect to k.

5.3.2. Power Spectrum

The non-linear power spectrum $P_{ab}(k, \eta)$, which is expressed in SPT by a characteristic loop expansion of the form (4.12) with (4.13), can be effectively reformulated in RPT. In particular, if the non-linear vertex function is approximated by its tree-level form, the power spectrum can be recast as an expansion in the non-linear propagator $G_{ab}(k, \eta, \eta_0)$ of the form [142, 144, 339],

$$P_{ab}(k, \eta) = G_{ac}(k, \eta, \eta_0) \, P_{cd,0}(k) \, G_{bd}(k, \eta, \eta_0) + P_{ab}^{\mathrm{MC}}(k, \eta) \,, \qquad (5.12)$$

where $P_{ab,0}(k) = u_a u_b P_0(k)$ for Gaussian-distributed growing-mode initial conditions, (4.3) and (4.15). Note that the non-linear propagator does only depend on the magnitude of the momentum $\boldsymbol{k}$, as we show explicitly later on (see (5.17)). Here, the first contribution sums up the diagrams to all loop orders that contain only one initial power spectrum $P_0(k)$ at the 'principal cross section'. We have introduced the latter in Section 4.4.1 and indicated it in Figure 4.5 by the dotted line. In Figure 4.5, examples of diagrams with only one initial power spectrum at the principal cross section are those for the SPT tree-level power spectrum $P_{ab}^L(k, \eta)$ and the one-loop contribution $P_{ab}^{(13)}(k, \eta)$. In contrast to this, the diagram for the SPT one-loop contribution $P_{ab}^{(22)}(k, \eta)$ involves two initial power spectra at the principal cross section. Diagrams of this type form a special class since they cannot be split in two parts by cutting one linear propagator. They are characterized by an irreducible structure enclosing the principal cross section that ends with two vertices. We denote the sum of all these irreducible structures by the quantity $\Psi_{cd}(k, \eta, \eta')$. The sum of all diagrams, containing more than one initial power spectrum $P_0(k)$ at the principal cross section and thus including

such an irreducible structure, comprises the second contribution $P_{ab}^{\mathrm{MC}}(k, \eta)$ of the previous equation. Its explicit form reads [142]

$$P_{ab}^{\mathrm{MC}}(k, \eta) = \int\limits_{\eta_0}^{\eta} d\eta' \int\limits_{\eta_0}^{\eta} d\eta'' \, G_{ac}(k, \eta, \eta') \, \Psi_{cd}(k, \eta', \eta'') \, G_{bd}(k, \eta, \eta'') \,. \qquad (5.13)$$

If we assume Gaussian-distributed growing-mode initial conditions so that $P_{ab}^0(k) = u_a u_b P_0(k)$ and introduce a simplified notation with regard to the non-linear propagator of density perturbations, $G_{1b} u_b = G_{11} + G_{12} \equiv G$, the RPT power spectrum in (5.12) for density fluctuations reduces to the exact and simple form [144]

$$P_{11}(k, \eta) = G^2(k, \eta, \eta_0) \, P_0(k) + P_{11}^{\mathrm{MC}}(k, \eta) \,. \qquad (5.14)$$

A completely equivalent equation holds for the power spectrum of the velocity fields $P_{22}(k, \eta)$. By rewriting the density power spectrum in this form, we can easily deduce the meaning of the two different contributions to the power spectrum that we have formally introduced in (5.12). The first term in (5.12) and (5.14), respectively, includes all contributions of the perturbative expansion (in SPT) being proportional to the initial power spectrum $P_0(k)$ at the *same* scale k. Due to this, it contains the most direct information about the initial power spectrum. One can probe $P_0(k)$ by varying k, as long as the first term in (5.14) (and equivalently in (5.12)) is dominant, i.e., for small values of k where the non-linear propagator has not yet significantly decayed (see (5.9)). Due to the decay of the non-linear propagator, the first term represents how much of the initial conditions remains at a given scale k and a certain point in time η. As the non-linear propagator decays, a given mode looses memory about its initial value. Then, an important fraction to the power spectrum is contributed by non-linear effects through the second term in (5.14). This second term $P_{11}^{\mathrm{MC}}(k, \eta)$ in (5.14), which is given in its general form in (5.12) and (5.13), constitutes the so-called mode-coupling term. At the scale k, it comprises all non-linear contributions to the power spectrum which have been generated by mode-coupling on smaller momentum scales. Hence, this term depends on the initial (linear) power $P_0(q)$ spectrum from a wide range of scales q, *other than* k, weighted by rather complicated convolution kernels.

In [339, 340], it has been shown that these kernels can be expressed in terms of so-called multi-point propagators, which we denote here by $G_{ab_1...b_n}^{(n)}$. These constitute a natural extension of the non-linear RPT propagator $G_{ab}(k, \eta, \eta_0)$ in (5.3) and are defined as [339]

$$G_{ab_1...b_n}^{(n)}(\boldsymbol{q}_1, \ldots, \boldsymbol{q}_n, \eta, \eta_0) \, \delta^{\mathrm{D}}(\boldsymbol{k} - \boldsymbol{q}_{1...n}) \equiv \frac{1}{n!} \left\langle \frac{\delta^n \psi_a(\boldsymbol{k}, \eta)}{\delta\psi_{b_1}(\boldsymbol{q}_1, \eta_0) \cdots \delta\psi_{b_n}(\boldsymbol{q}_n, \eta_0)} \right\rangle \qquad (5.15)$$

with $\boldsymbol{q}_{1...n} \equiv \boldsymbol{q}_1 + \ldots + \boldsymbol{q}_n$. Notice that $G_{ab_1...b_n}^{(n)}(\boldsymbol{q}_1, \ldots, \boldsymbol{q}_n, \eta, \eta_0)$ corresponds to the $(n+1)$-point propagator, though it depends, due to translation invariance ensured by the Dirac delta

distribution, only on n wavenumbers in Fourier space. Besides, it possesses the property [337]

$$G_{ab_1\ldots b_n}^{(n)}(-\boldsymbol{q}_1,\ldots,-\boldsymbol{q}_n,\eta,\eta_0) = G_{ab_1\ldots b_n}^{(n)}(\boldsymbol{q}_1,\ldots,\boldsymbol{q}_n,\eta,\eta_0)\,. \tag{5.16}$$

For $n=1$, the definition (5.15) reduces to the familiar non-linear two-point propagator in RPT in (5.3),

$$G_{ab}^{(1)}(k,\eta,\eta_0) \equiv G_{ab}(k,\eta,\eta_0)\,, \tag{5.17}$$

depending as a consequence of the property (5.16) only on the magnitude of the momentum $\boldsymbol{k}$. From the formal definition in (5.15), the multi-point propagators $G_{ab_1\ldots b_n}^{(n)}$ can be computed order-by-order in a field expansion. Thus, they can be represented diagrammatically. Thereby, $G_{ab_1\ldots b_n}^{(n)}$ corresponds to the sum of all diagrams with n incoming lines and one outgoing line (see [339]).

$$G_{ab_1\ldots b_n}^{(n)}(\boldsymbol{q}_1,\ldots,\boldsymbol{q}_n,\eta,\eta_0) = G_{ab_1\ldots b_n,\text{tree}}^{(n)}(\boldsymbol{q}_1,\ldots,\boldsymbol{q}_n,\eta,\eta_0)\,\exp\left[-\frac{1}{2}k^2\sigma_d^2\left(e^\eta - e^{\eta_0}\right)^2\right]\,, \tag{5.18}$$

generating an exponential suppression with respect to σ_d^2 and thus the non-linear scale k_{NL} (see (5.10) and (5.2)). Note that the multi-point propagators at tree-level can be identified with the SPT kernels defined in (3.73),

$$G_{ab_1\ldots b_n,\text{tree}}^{(n)}(\boldsymbol{q}_1,\ldots,\boldsymbol{q}_n,\eta,\eta_0) = \bar{\mathcal{F}}_{aa_1a_2\ldots a_n}^{(n)}(\boldsymbol{q}_1,\ldots,\boldsymbol{q}_n,\eta)\,, \tag{5.19}$$

which are for Gaussian-distributed growing-mode initial conditions related to the usual kernels $\mathcal{F}_a^{(n)}(\boldsymbol{q}_1,\ldots,\boldsymbol{q}_n,\eta)$ in SPT (see (3.75)).

The implementation of the concept of the multi-point propagators according to (5.15) then allows to rewrite the RPT relation for the non-linear power spectrum in (5.12) as follows [337],

$$\begin{aligned}P_{ab}(k,\eta) = \sum_{n=1}^\infty n! \int d^3q_1\ldots d^3q_n\,\delta^{\text{D}}(\boldsymbol{k}-\boldsymbol{q}_{1\ldots n})\\\times G_{aa_1\ldots a_n}^{(n)}(\boldsymbol{q}_1,\ldots,\boldsymbol{q}_n,\eta,\eta_0)\,P_{a_1b_1,0}(q_1)\cdots P_{a_nb_n,0}(q_n)\,G_{bb_1\ldots b_n}^{(n)}(-\boldsymbol{q}_1,\ldots,-\boldsymbol{q}_n,\eta,\eta_0)\end{aligned} \tag{5.20}$$

with (5.16). If we compare this expression with the RPT relation for the power spectrum in (5.12), we see that the contribution $n=1$ coincides with the first term in (5.12). Thus, we can identify the contributions for $n \geq 2$ in the previous equation with the second term in the RPT power spectrum relation, i.e., the mode-coupling term $P_{ab}^{\text{MC}}(k,\eta)$. Similar to the perturbative expansion of the power spectrum in terms of loop orders in SPT (see (4.12)), we can then perform a loop expansion of the mode-coupling term,

$$P_{ab}^{\text{MC}}(k,\eta) = \sum_{\ell=1}^\infty P_{ab}^{\text{MC},(\ell)}(k,\eta)\,, \tag{5.21}$$

where $\ell = n - 1$ for $n \geq 2$ so that $P_{ab}^{\mathrm{MC},(\ell)}(k, \eta)$ denotes the ℓ-loop contribution to the mode-coupling term. Due to the exponential suppression of the n-point propagators $G_{ab_1\ldots b_n}^{(n)}$ for large external momentum k according to (5.18), we expect the individual power spectrum contributions and thus their overall sum in (5.20) to converge in the UV limit. As a consequence, we also presume the RPT loop expansion of the mode-coupling term $P_{ab}^{\mathrm{MC}}(k, \eta)$ in (5.21) to have better convergence properties than the loop expansion (4.12) in SPT.

On the one hand, the resummation method of RPT indeed improves upon the SPT approach in the sense that all loop contributions of (5.21) to the resummed power spectrum in (5.20) are positive and well-defined in the non-linear regime by dominating at some characteristic scale each and being subdominant otherwise. In this regard, the RPT approach constitutes in fact an improvement over SPT, where the loop expansion, depending on the initial conditions, does not necessarily converge (see Figure 5.1). Moreover, the resummation technique of RPT leads to more accurate predictions than SPT for the power spectrum at the onset of non-linearity [138, 144].

On the other hand, the RPT approach has a number of computational disadvantages and conceptual drawbacks. Concerning the former, it is, for instance, necessary to include perturbative corrections beyond one-loop order to obtain an accurate predictions for the power spectrum in the mildly non-linear regime [294]. This is additionally complicates by the fact that the evaluating the power spectrum $P_{ab}(k, \eta)$ in (5.20) is a cumbersome and computationally demanding procedure (see e.g., [339]). Due to this, the multi-point propagator concept has been used to formulate effective implementations of RPT, called MPTbreeze [145] and RegPT [146], which significantly simplify the evaluation procedure of the RPT power spectrum. These effective propositions incorporate calculations of the power spectrum in RPT up to two-loop order and are accompanied by publicly released codes (see [145, 146]).

Apart from the computational effort, RPT possesses a number of conceptual shortcomings as well. Although the resummation scheme of RPT leads to an improved convergence of the power spectrum at intermediate scales compared to SPT, it resums an only a specific subset of the SPT diagrams. Due to this, one may doubt whether this technique can give rise to a systematic improvement of the predictions for the power spectrum on large momentum scales (for similar conclusions see [101, 354]). In detail, the method of RPT relies on the assumption that the exponential suppression associated to the non-linear scale (see (5.18) and (5.20)) constitutes the leading soft-mode effect in the power spectrum. However, it has been proven that the leading contributions from soft modes cancel at arbitrary loop order in perturbation theory [237, 306], as we discussed in Section 5.1.3, whereas this cancellation is not explicit in the RPT approach (see also [101]). Moreover, it has been shown by use of the eikonal approximation [159, 160] that the exponential suppression indeed occurs for the non-linear

propagator, but is absent in the power spectrum. In consequence, this suggests that the effects associated to the non-linear scale in the resummed RPT power spectrum are spurious.

In order to address the conceptual issues of RPT in further detail as well as to study soft-mode effects greater generality, we introduce the eikonal approximation in what follows.

5.4. Eikonal approximation

Compared to the techniques developed in the framework of RPT [142–144], there exists a direct and more efficient approach to (re-)derive the resummation of the non-linear propagator $G_{ab}(k, \eta, \eta_0)$ in the limit of large momentum k in (5.9). As mentioned in [355] and explicitly demonstrated in [157, 237, 340], it is possible to resum the same class of contributions to the non-linear propagator in the large-k limit by using a single or finite number of random variables, whose statistical properties can be determined from the initial conditions, to describe the effect of long-wavelength (soft) fluctuations on the dynamics of the short-wavelength (hard) modes. Later on, in [159, 160], this method has then been successfully applied to recover the resummed non-linear RPT propagator as well as to extend the RPT approach to arbitrary cosmological models. There, it has been named the 'eikonal approximation', borrowing the terminology of quantum field theory where related techniques are used. In quantum field theory, the eikonal approximation is, for instance, applied to exponentiate the effect of soft photon modes on the propagator of electrons [356, 357], in a manner similar to the way we will implement it. While the eikonal approximation is used in various areas of physics, it has been originally developed as an approximation in the equations of wave propagation which leads to the laws of geometric optics [358].[3]

The essence of the eikonal approximation is that it allows to account for the impact of long-wavelength modes on the development of the small-scale perturbations in a non-perturbative way, based on a separation of these scales. Indeed, if the long wavelengths are much longer than the short ones, their effect can be interpreted as a redefinition of the background for the small scales. We take this point up again and proceed in a similar direction in Chapter 6 and Chapter 7 (see in particular Section 6.1.1). In the eikonal approximation, the separation of scales is used to introduce a redefined set of fluid equations for the hard modes embedded in an external random medium incorporating the impact of the soft modes. The eikonal approximation is based on the same motivation as RPT which consists in addressing the convergence problems of SPT related to the enhancement of the vertex function through the coupling between soft and hard modes. However, in contrast to RPT, the eikonal approximation does

---

[3]The word 'eikonal' can be retraced to the ancient Greek word '$\varepsilon\iota\kappa\acute{\omega}\nu$', meaning icon or image [359].

not only provide a partial resummation of the effects of soft modes, but has the purpose to deal with all soft corrections to the hard-mode observables [159]. Hence, applications of the eikonal approximation in [159] have comprised both the recovering of the large-momentum resummation of the non-linear two-point propagator in RPT as well as the derivation of the respective resummation properties of the multi-point propagators [339, 340], introduced in the previous section, which can been see as the building blocks for constructing next-to-leading order perturbative predictions. Moreover, in [101, 160], the eikonal approximation has been used to investigate the impact of long-wavelength modes on correlation functions, such as the power spectrum or the bispectrum, on short distance scales. Therein, it has been shown that equal-time correlation functions do not depend on the impact of soft modes on these scales. Moreover, it constitutes an extension of the findings in [237] where the absence of soft-mode effects has been demonstrated for the power spectrum only, though for all loop orders. In [306], this has been interpreted as consequence of Galilean invariance (see also [167])

Furthermore, in contrast to most other approaches in cosmological perturbation theory, especially also RPT, the eikonal approximation is not restricted to the treatment of a single pressureless CDM fluid. Hence, it can also be applied to treat systems of multiple (pressureless) fluids with non-adiabatic, isodensity soft modes, including for instance CDM and baryons (see also [360]). In such a case, the eikonal approximation provides an effective formalism to derive the resummed non-linear propagators in the presence of isodensity soft modes. This has been done in [159, 160]. Another perturbative formalism that is not limited to the single-fluid case is, the time-flow formalism, introduced in [156] and applied to case of massive neutrinos in [303]. We give an overview of the time-flow approach in Section 5.5.

In the following, we review the basic aspects of the eikonal approximation. Thereby, we decompose the fluid equations by introducing a separation of long and short distance scales. This decomposition allows us to encode the impact of the soft modes in the fluid equations in a resummed eikonal propagator. Subsequently, we use the latter to show how the non-linear RPT propagator in the limit of large-momentum can be recovered with the eikonal approximation.

5.4.1. Decomposition of the fluid equations

In [340], it has been shown that the RPT expression for the non-linear propagator $G_{ab}(k, \eta, \eta_0)$ in the limit of large momentum k in (5.9) contain non-linear terms that couple different modes, they directly allow to study the effect of long-wavelength (soft) modes $\boldsymbol{q}$ on the dynamics of a given short-wavelength (hard) mode $\boldsymbol{k}$ in the limit where $k \gg q$. This is done in the eikonal approximation [160, 340]. In this limit, spatial variations of the long-wavelength modes are

small with respect to the modes $\boldsymbol{k}$. Hence, the long-wavelength modes can be treated as an external random background. If we neglect the mode couplings on short momentum scales, the non-linear fluid equations can be rewritten as linear equations embedded in an external medium.

In the fluid equations (3.54), the non-linear mode-coupling terms are characterized by the vertex function $\gamma_{abc}(\boldsymbol{k}, \boldsymbol{p}_1, \boldsymbol{p}_2)$, defined in (3.53). Here, the internal mode-coupling of the vertex function are denoted by $\boldsymbol{p}_1$ and $\boldsymbol{p}_2$, such that $\boldsymbol{k} = \boldsymbol{p}_1 + \boldsymbol{p}_2$, to avoid confusion with the soft mode $\boldsymbol{q}$. We can split the non-linear mode-coupling terms in two different contributions by drawing a distinction between couplings where the internal modes have comparable amplitudes, $p_1 \simeq p_2$, and couplings where they possess very different amplitudes, $p_1 \ll p_2$ or $p_1 \gg p_2$. If we indicate the soft modes in the latter case by $\boldsymbol{q}$ and assume them to be much smaller than the momentum $\boldsymbol{k}$ itself, we can decompose the fluid equations in (3.54) as [340]

$$\partial_\eta \psi_a(\boldsymbol{k}, \eta) + \Omega_{ab}(\eta)\, \psi_b(\boldsymbol{k}, \eta) - \Xi_{ab}(\boldsymbol{k}, \eta)\, \psi_b(\boldsymbol{k}, \eta)$$
$$\simeq [\gamma_{abc}(\boldsymbol{k}, \boldsymbol{p}_1, \boldsymbol{p}_2)\, \psi_b(\boldsymbol{p}_1, \eta)\psi_c(\boldsymbol{p}_2, \eta)]_S \, , \tag{5.22}$$

where we can interpret $\Xi_{ab}(\boldsymbol{k}, \eta)$ as a corrective term to the linear evolution of the mode $\boldsymbol{k}$. It is given by

$$\Xi_{ab}(\boldsymbol{k}, \eta) \equiv 2 \int^{q \ll k} d^3q\, \gamma_{abc}(\boldsymbol{k}, \boldsymbol{k} - \boldsymbol{q}, \boldsymbol{q})\, \psi_c(\boldsymbol{q}, \eta)\, . \tag{5.23}$$

In the previous definition of the matrix function $\Xi_{ab}(\boldsymbol{k}, \eta)$, we have explicitly written down the internal momentum integration to emphasize that the domain of integration is restricted to soft momenta $q \ll k$. Conversely, the non-linear mode-coupling contribution on the right-hand side of (5.22), containing the vertex function $\gamma_{abc}(\boldsymbol{k}, \boldsymbol{p}_1, \boldsymbol{p}_2)$, excludes the soft domain by comprising only hard modes or modes of comparable size. This domain of short-wavelength modes is indicated by the subscript 'S' in (5.22).

In this limit of separation of scales, $q \ll k$, the matrix function $\Xi_{ab}(\boldsymbol{k}, \eta)$ in (5.23) constitutes a random variable. It depends on the initial conditions, imposed through the doublet field $\psi_c(\boldsymbol{q}, \eta)$, but is (assumed to be) independent of the evolution of the soft mode $\boldsymbol{q}$. Consequently, the decomposed fluid equations (5.22) can be interpreted as the equations of motions of cosmological modes in a random medium with long-wavelength modes. Thus, they allow us to compute how the presence of long-wavelength modes influences the growth of structures (see also our considerations in Chapter 6 and Chapter 7).

According to the definition of the vertex function in (3.53) and the mode-coupling functions therein (see (3.23)), the leading-order expression of the vertex $\gamma_{abc}(\boldsymbol{k}, \boldsymbol{k} - \boldsymbol{q}, \boldsymbol{q})$ in (5.23) for $q \ll k$ reads

$$\gamma_{abc}(\boldsymbol{k}, \boldsymbol{k} - \boldsymbol{q}, \boldsymbol{q}) \simeq \frac{1}{2} \frac{\boldsymbol{k} \cdot \boldsymbol{q}}{q^2}\, \delta_{ab}\, \delta_{c2} \tag{5.24}$$

with δ_{ab} corresponding to the Kronecker delta. By inserting this relation in the definition of the matrix function $\Xi_{ab}(\boldsymbol{k}, \eta)$ in (5.23), the latter becomes proportional to the identity matrix,

$$\Xi_{ab}(\boldsymbol{k}, \eta) \simeq \Xi(\boldsymbol{k}, \eta)\, \delta_{ab}\,, \tag{5.25}$$

where we introduced the function

$$\Xi(\boldsymbol{k}, \eta) \equiv \int^{q \ll k} d^3 q\, \frac{\boldsymbol{k} \cdot \boldsymbol{q}}{q^2}\, \psi_2(\boldsymbol{q}, \eta)\,. \tag{5.26}$$

Due to the form of the vertex function (5.24), $\Xi(\boldsymbol{k}, \eta)$ only contains the velocity divergence field $\psi_2(\boldsymbol{q}, \eta) \equiv \Theta(\boldsymbol{q}, \eta)$, as defined in (3.51), but not the density field $\delta(\boldsymbol{q}, \eta)$. Since the doublet field $\psi_a(\boldsymbol{x}, \eta)$ is a real variable and its Fourier transform $\psi_a(\boldsymbol{k}, \eta)$ in turn a complex quantity, i.e., $\psi_a(\boldsymbol{k}, \eta) = \psi_a^*(-\boldsymbol{k}, \eta)$ with '$*$' being the complex conjugate [40], the function $\Xi(\boldsymbol{k}, \eta)$ is purely imaginary.

In the decomposed fluid equations in (5.22), we have absorbed the non-linear coupling to the soft modes in the linear term $\Xi_{ab}(\boldsymbol{k}, \eta)\, \Psi_b(\boldsymbol{k}, \eta)$. Thus, the impact of the soft modes is completely encoded in the linearized (homogeneous) evolution equation, neglecting the non-linear mode-coupling terms $[\ldots]_S$ on the right-hand side of (5.22). The eikonal approximation then consists in deriving a solution for this linearized evolution equations by neglecting the terms $[\ldots]_S$ in the hard domain. Due to this, we can proceed analogously as for solving the linear fluid equations in (3.55) in terms of the linear propagator $g_{ab}(\eta, \eta')$ (see our derivations in Section 3.3.2 and Section 3.3.3). This means a new propagator $\xi_{ab}(\boldsymbol{k}, \eta, \eta')$ is introduced which satisfies the equation (see (3.58))

$$\big[\delta_{ab}\, [\partial_\eta - \Xi(\boldsymbol{k}, \eta)] + \Omega_{ab}(\eta)\big] \xi_{bc}(\boldsymbol{k}, \eta, \eta') = 0\,, \tag{5.27}$$

so that we can determine the formal solution of the decomposed fluid equations in (5.22) in terms of this propagator as (see (3.67))

$$\begin{aligned}
\psi_a(\boldsymbol{k}, \eta) &= \xi_{ab}(\boldsymbol{k}, \eta, \eta_0)\, \psi_b(\boldsymbol{k}, \eta_0) \\
&\quad + \int_{\eta_0}^{\eta} d\eta'\, \xi_{ab}(\boldsymbol{k}, \eta, \eta')\, \big[\gamma_{bcd}(\boldsymbol{k}, \boldsymbol{p}_1, \boldsymbol{p}_2)\psi_c(\boldsymbol{p}_1, \eta')\psi_d(\boldsymbol{p}_2, \eta')\big]_S\,,
\end{aligned} \tag{5.28}$$

where the last line of the equation above includes the contributions of hard-mode domain. The propagator $\xi_{ab}(\boldsymbol{k}, \eta, \eta')$ can be explicitly determined from the relation (5.27). By accounting for causal boundary conditions,

$$\xi_{ab}(\boldsymbol{k}, \eta, \eta) = \delta_{ab}\,, \tag{5.29}$$

in analogy to (3.59), we can express it in terms of the linear propagator $g_{ab}(\eta, \eta')$ (see (3.56)) as

$$\xi_{ab}(\boldsymbol{k}, \eta, \eta') = g_{ab}(\eta, \eta') \exp\left[\int_{\eta'}^{\eta} d\eta'' \, \Xi(\boldsymbol{k}, \eta'')\right] . \tag{5.30}$$

Thus, similarly as in RPT (see (5.9)), the eikonal approximation leads to the emergence of a resummed propagator. As we can see from the definition of $\Xi(\boldsymbol{k}, \eta)$ in (5.26), the argument of the exponential function in the equation above corresponds to the time integral of the velocity divergence $\psi_2(\boldsymbol{q}, \eta) \equiv \Theta(\boldsymbol{q}, \eta)$ projected along the direction of the momentum $\boldsymbol{k}$, that is, the displacement component along $\boldsymbol{k}$. Note that in RPT, the derivation of the non-linear propagator $G_{ab}(k, \eta, \eta_0)$ in the limit of large momentum k in (5.9) relies on the assumption that the soft modes are in the linear and growing-mode regime, $\psi_a(\boldsymbol{q}, \eta) \simeq \psi_a^L(\boldsymbol{q}, \eta)$ with $\psi_a^L(\boldsymbol{q}, \eta) \simeq e^{(\eta-\eta_0)} u_a \, \delta_0(\boldsymbol{q})$ (see (3.74) and (3.76)) [143]. In contrast to this, the equation for the propagator $\xi_{ab}(\boldsymbol{k}, \eta, \eta')$ in (5.30) does not require to make any assumptions on the form of the soft mode $\Theta(\boldsymbol{q}, \eta)$. In particular, it is valid irrespective of the initial conditions imposed on the soft mode.

Besides, there is another aspect of (5.30) which is worth mentioning. In (5.30), the dependence of the propagator $\xi_{ab}(\boldsymbol{k}, \eta, \eta')$ on the soft modes is encoded in the function $\Xi(\boldsymbol{k}, \eta)$ of (5.26), which is purely imaginary. Thus, if we contract this propagator with a hard mode $\psi_a(\boldsymbol{k}, \eta)$, as for instance in (5.28), the impact of the soft modes only gives rise to a change of the phase of the hard mode, but not of its amplitude. Consequently, it does not cause a modification of the equal-time correlation functions (see also [101, 160]). However, the soft modes have an effect on the amplitudes of the propagators. Indeed, the change of the phase leads to a damping of correlation functions including modes at unequal times. This effect is the key point of the regularization scheme implemented in perturbative approaches such as RPT.

5.4.2. Propagator resummation

To gain a detailed understanding of these considerations, let us explore how one can recover the expression for the non-linear RPT propagator $G_{ab}(k, \eta, \eta_0)$ in (5.9) using the formal solution (5.28) and the resummed propagator (5.30) in the eikonal approximation. If we define the resummed propagator $\xi_{ab}(\boldsymbol{k}, \eta, \eta_0)$ formally with respect to an initial field $\Psi_b(\boldsymbol{k}', \eta_0)$ in analogy to (5.3), we can derive its form from the formal solution (5.28). After taking the ensemble average, we derive the relation

$$G_{ab}(k, \eta, \eta_0) = \left\langle \xi_{ab}(\boldsymbol{k}, \eta, \eta_0) \right\rangle_{\Xi} . \tag{5.31}$$

Hence, the ensemble average of the resummed eikonal propagator $\xi_{ab}(\boldsymbol{k}, \eta, \eta_0)$ over the possible realizations of $\Xi(\boldsymbol{k})$ equals the non-linear propagator $G_{ab}(k, \eta, \eta_0)$ in RPT. According to the explicit expression for the propagator $\xi_{ab}(\boldsymbol{k}, \eta, \eta_0)$ in (5.30), its ensemble average reads

$$\left\langle \xi_{ab}(\boldsymbol{k}, \eta, \eta_0) \right\rangle_\Xi = g_{ab}(\eta, \eta_0) \left\langle \exp\left[\int_{\eta_0}^{\eta} d\eta'\, \Xi(\boldsymbol{k}, \eta') \right] \right\rangle. \tag{5.32}$$

As discussed before, the matrix function $\Xi_{ab}(\boldsymbol{k}, \eta)$ in (5.25) and thus also the function $\Xi(\boldsymbol{k}, \eta)$ arising from it constitute random variables. Hence, we can evaluate the ensemble average of the exponential function above, including $\Xi(\boldsymbol{k}, \eta)$, by use of the cumulant expansion theorem for random variables [361]. Applying the cumulant expansion theorem yields

$$\left\langle \exp\left[\int_{\eta_0}^{\eta} d\eta'\, \Xi(\boldsymbol{k}, \eta') \right] \right\rangle = \exp\left[\sum_{p=2}^{\infty} \frac{c_p(\boldsymbol{k}, \eta, \eta_0)}{p!} \right], \tag{5.33}$$

where $c_p(\boldsymbol{k}, \eta, \eta_0)$ denotes the pth-order cumulant of the random field $\int_{\eta_0}^{\eta} d\eta'\, \Xi(\boldsymbol{k}, \eta')$. It is given by

$$c_p(\boldsymbol{k}, \eta, \eta_0) = \int_{\eta_0}^{\eta} d\eta_1 \ldots d\eta_p \left\langle \Xi(\boldsymbol{k}, \eta_1) \cdots \Xi(\boldsymbol{k}, \eta_p) \right\rangle_c. \tag{5.34}$$

To ensure that the non-linear propagator $G_{ab}(k, \eta, \eta_0)$ in (5.31) and thus the ensemble average $\left\langle \xi_{ab}(\boldsymbol{k}, \eta, \eta_0) \right\rangle_\Xi$ in (5.32) is real (non-imaginary), the relation (5.33) requires that the cumulants $c_p(\boldsymbol{k}, \eta, \eta_0)$ have to be real as well. From the previous equation and by taking into account that the function $\Xi(\boldsymbol{k}, \eta)$ is imaginary, we see that the sum over the cumulants in (5.33) is restricted to even values of p. Moreover, for Gaussian initial conditions, the cumulants with $p > 2$ in (5.34) vanish in consequence of the Wick theorem (4.6), as discussed in Section 4.3. Hence, the only remaining contribution to the sum in (5.33) is the second-order cumulant $c_2(k, \eta, \eta_0)$. Note that due to the form of the function $\Xi(\boldsymbol{k}, \eta)$ (see (5.26)) entering in (5.34), the second-order cumulant does not depend on the momentum $\boldsymbol{k}$, but only on its absolute value k. If we then approximate the soft mode incorporated in the function $\Xi(\boldsymbol{k}, \eta)$ by its linear contribution, $\psi_2(\boldsymbol{q}, \eta) \simeq \psi_2^L(\boldsymbol{q}, \eta)$ with $\psi_2^L(\boldsymbol{q}, \eta) = g_{2a}(\eta, \eta_{\text{in}})\, \psi_a(\boldsymbol{q}, \eta_{\text{in}})$ (see (3.56)), the function $\Xi(\boldsymbol{k}, \eta)$ in (5.26) becomes

$$\Xi(\boldsymbol{k}, \eta) = g_{2a}(\eta, \eta_0) \int^{q \ll k} d^3 q\, \frac{\boldsymbol{k} \cdot \boldsymbol{q}}{q^2}\, \psi_a(\boldsymbol{q}, \eta_0). \tag{5.35}$$

By inserting this expression in definition of the cumulants in (5.34), we can determine the second-order cumulant $c_2(k, \eta, \eta_0)$ in terms of the initial power spectrum $P_{ab}^0(k)$ defined (4.2).

5. Overview of Perturbative Approaches

As a result, we obtain the relation [101]

$$
\begin{aligned}
c_2(k, \eta, \eta_0) &= \int_{\eta_0}^{\eta} d\eta' \, d\eta'' \, \langle \Xi(\boldsymbol{k}, \eta') \, \Xi(\boldsymbol{k}, \eta'') \rangle_c \\
&\simeq - \int_{\eta_0}^{\eta} d\eta' d\eta'' \, g_{2a}(\eta', \eta_{\rm in}) \, g_{2b}(\eta'', \eta_{\rm in}) \int^{q \ll k} d^3q \, \frac{(\boldsymbol{k} \cdot \boldsymbol{q})^2}{q^4} \, P_{ab,0}(q) \, .
\end{aligned}
\tag{5.36}
$$

Next, we assume Gaussian-distributed growing-mode initial conditions so that the initial power spectrum equals $P_{ab,0}(k) = u_a u_b P_0(k)$ (see (4.3) with (3.71)). If we in addition specify the underlying cosmological model, what has not been necessary so far, to be an EdS cosmology and consider only the growing mode of the linear propagator in EdS, i.e., $g_{ab}(\eta, \eta_{\rm in}) = e^{(\eta - \eta_{\rm in})} u_a u_b$ (see (3.68)), the previous relation simplifies to

$$
c_2(k, \eta, \eta_0) = -k^2 \sigma_d^2 \left(e^{\eta - \eta_{\rm in}} - e^{\eta_0 - \eta_{\rm in}} \right)^2 \, .
\tag{5.37}
$$

Here, we have encoded the dependence on the initial power spectrum in the variance of the initial displacement field σ_d^2, introduced in (5.10).

$$
\sigma_d^2 = \frac{4\pi}{3} \int^{q \ll k} dq \, P_0(q) \, ,
\tag{5.38}
$$

which at this stage depends on the domain of integration and hence on k. However, by taking the value of σ_d^2 in the large-k limit and setting $\eta_{\rm in} \equiv 0$ for convenience, we recover the result for the non-linear RPT propagator $G_{ab}(k, \eta, \eta_0)$ in the limit of large momentum in (5.9). Besides, the eikonal approximation gives a possible physical interpretation of the propagator $G_{ab}(k, \eta, \eta_0)$ in the large-k limit. In fact, one can imagine the hard modes to be scattered by the background of soft modes, leading to a decorrelation of the hard modes and thus to an exponential decay of the non-linear propagator over time [101]. The fact that the large-momentum expression for the non-linear RPT propagator in (5.9) can be rederived in the eikonal approximation shows that the latter can be indeed used to resum the leading-order soft mode effects.

To go beyond that, another advantage of the eikonal approximation is that it allows not only to compute the impact of the soft modes on the propagator but also on equal- and unequal-time correlation functions, as we discussed before. In particular, it reveals that a suppression of the propagator arises due to effects of the soft modes. However, the equal-time correlators, such as the power spectrum or the bispectrum, remain unchanged [101, 159]. This means in particular with regard to the power spectrum that the complete resummation of the leading effect of the soft modes does not result in an expression of the from (5.14) as in RPT.

The reason for this is that in RPT, only a *partial* resummation of the effects of the soft modes is performed, whereas the eikonal approximations provides a consistent framework to resum the impact of *all* soft corrections.

Moreover, the cancellation of the soft-mode effects in the power spectrum, derived from the eikonal approximation, suggests resumming the impact of soft modes does not lead to an improvement of the convergence properties of SPT. On top of that, it even indicates that the enhancement of the non-linear corrections to the power spectrum in SPT, due to the impact of the soft modes, is spurious. In particular, in [101], it has been shown that at any loop order in SPT, the effects of soft modes produce at most a logarithmic enhancement of the non-linear corrections to the power spectrum in comparison to the linear contribution.

All perturbative approaches in the literature providing a resummation scheme for the soft modes only resum certain subsets of diagrams that arise in the perturbative expansion in SPT. As we have explicitly seen in the case of RPT, these subsets do not necessarily reproduce the cancellation of the soft-mode effects for the equal-time correlators proven by the eikonal approximation. Although these resummation schemes may accomplish to resum the necessary subdiagrams to provide relative accurate results on intermediate scales (see e.g., [337]) and are also useful to describe unequal-time correlation functions, it is questionable if these lead to a systematic improvement in the determination of equal-time correlation functions for large momenta. For a detailed discussion in this direction, we refer to [101].

To go beyond that, we proceed in Chapter 6 and Chapter 7 to non-perturbative methods to investigate soft mode effects in further detail. In particular, these non-perturbative derivations allow us to draw conclusions about different perturbative approaches. Apart from SPT, we consider the so-called 'time-flow approach' in this context. Since the time-flow approach implements a different method for solving the fluid equations perturbatively, compared to SPT and RPT, we review its crucial aspects in the next section.

5.5. Time-flow approach

In the following, we give an overview of another approach to describe the non-linear large-scale structure formation in the Universe by means of perturbation theory. We refer to this perturbative scheme, which has been introduced in [156] and found applications in [301, 303, 347–350], as the time-flow approach. However, its is also referred to as time-renormalization group (TRG) approach since it can be interpreted as particular formulation of the Wilsonian renormalization group (RG), applied in quantum field theory and statistical physics [342–346], with the time constituting the flow parameter in this context (see [148, 304]).

The time-flow approach differs from the perturbative approaches considered in detail before,

namely SPT, RPT and the eikonal approximation, by its strategy to derive a perturbative solutions for the correlation functions, such as the power spectrum or the bispectrum. While the previously discussed approaches intend to solve the non-linear fluid equations (3.54) perturbatively with respect to the doublet fields $\psi_a(\boldsymbol{k}, \eta)$, defined in (3.51), the time-flow approach extend the fluid equations to an hierarchical system of (integro-)differential evolution equations directly in terms of the correlations functions, such as the power spectrum and the bispectrum.

By applying an appropriate approximation to close the infinite hierarchical system, the integration of the differential evolution equations then allows to determine the correlation functions for all combinations of density and velocity perturbations at any point of time and any momentum scale. Thus, one of the advantages of the time-flow approach is that it provides expressions for the correlation functions in a compact diagrammatic formulation. Thereby, the method applied in the time-flow approach to close the infinite hierarchy of differential equations resembles the one for solving the BBGKY hierarchy [362].[4]

If the infinite hierarchy of evolution equations in the time-flow approach is, for instance, truncated at the level of the trispectrum, the solutions of the equations for the correlation functions correspond to the summation of an infinite class of perturbative corrections. In this sense, the time-flow formalism is comparable to resummation schemes such as RPT [142–144] or [148, 304]. However, as opposed to the latter, it possesses a clear and systematic way to impose the approximation on which it relies. This fact or clearness consists in the same time a limitation of the time-flow approach. In fact, one always needs to implement a (not physically motivated) approximation at a certain level of the infinite hierarchy of evolution equations to obtain a closed, solvable system of equations. Based on [156], the 'closure approximation', which we apply in the following, relies on neglecting the trispectrum. However, as we demonstrate explicitly in Section 6.2.2, this closure approximations deviates from the SPT predictions for the bispectrum already at next-to-leading order. Due to this, it is not clear whether it constitutes a reasonable approximation.

To go beyond that, the next step consists in including the tree-level trispectrum in the evolution equation for the bispectrum (see [349]). Although, in comparison to numerical simulations, the predictions for the bispectrum including the linear trispectrum contributions improve in the mildly non-linear regime (up to $k \simeq 0.25 \, h/\mathrm{Mpc}$), their performance becomes worse than without the trispectrum contribution beyond the non-linear regime and the perturbative description fails [349]. In addition, it has been shown in [348] that the power spectrum,

---

[4] The so-called Bogoliubov–Born–Green–Kirkwood–Yvon (BBGKY) hierarchy represents a hierarchically coupled set of differential equations that describes the dynamics of a system with a large number of interacting particles (for details see e.g., [92]).

which arises in dependence of the bispectrum in the time-flow approach, strongly depends on the initial conditions chosen for the bispectrum. Due to these issues, the advantage of the time-flow approach is more a conceptual one. In fact, the formulation of the time-flow approach is particularly suited to treat general cosmological models, other then the usually considered EdS and ΛCDM cosmology.

Most perturbative approaches, in particular SPT and RPT, are formulated for an EdS background cosmology and further extended to more general cosmologies, such as the ΛCDM model, by keeping the EdS expression for the background-dependent matrix $\Omega_{ab}(\eta)$ (see (3.62) with (3.64)) and taking only the time dependence $\eta = \ln D_1(\tau)$ via the linear growth factor $D_1(\tau)$) in (3.9) correctly into account. As we discussed in Section (3.3.3), this generalization procedure is exact at linear order, but introduces inaccuracies at higher orders, though these are actually very small (see Section 3.2.4). In the perturbative approaches which implement this generalization, the validity of this approximation cannot be assessed independently. Moreover, they can also not be trivially extended to cosmological models involving a scale-dependent linear growth factor, as it is for instance the case if contributions of massive neutrinos are included in the fluid equations [363–365].

In contrast to this, the formulation of the time-flow approach does not require an a priori specification of the background cosmology encoded in the matrix Ω_{ab} (and thus in the linear propagator of (3.56)) to derive the governing equations for the correlation functions. Hence, the advantage of the time-flow approach is that it provides a formalism which can be straightforwardly applied to cosmological models more general than EdS and ΛCDM cosmologies, e.g., those containing massive neutrinos [301–303] or scalar-tensor modifications of gravity [366]. However, to derive tight upper bounds on the neutrino mass scale, perturbative approaches providing accurate predictions for the non-linear corrections (from the neutrino fluid component) to the power spectrum are needed. For a treatment of the non-linear power spectrum corrections from massive neutrinos within the framework of the time-flow approach, see e.g., [303].

In the following, we introduce the time-flow approach by concentrating on flat cosmological models, as for instance EdS or ΛCDM cosmologies. In this case, the background-encoding matrix in the fluid equations and hence the linear propagator in (3.56) are momentum independent, $\Omega_{ab}(\eta)$ and $g_{ab}(\eta, \eta')$. However, since the explicit form of $\Omega_{ab}(\eta)$ and $g_{ab}(\eta, \eta')$ is not needed to derive the time-flow relations for the correlation functions, a generalization to more complicated cosmologies can be straightforwardly obtained by replacing $\Omega_{ab}(\eta)$ and $g_{ab}(\eta, \eta')$ by the corresponding scale-dependent quantities. The general scale-dependent form of the matrix $\Omega_{ab}(\boldsymbol{k}, \eta)$ and the respective linear propagator $g_{ab}(\boldsymbol{k}, \eta, \eta')$ is explicitly given in [156].

5.5.1. Infinite hierarchy of differential evolution equations

While in SPT one aims to solve the evolution equations of the fields $\psi_a(\boldsymbol{k}, \eta)$ themselves (see Section 3.3.5), in the time-flow approach one formulates the evolution equations directly in terms of the final quantities of interest, namely the correlation functions such as the power spectrum $P_{ab}(k, \eta)$ and the bispectrum $B_{abc}(\boldsymbol{k}, \boldsymbol{q}, \boldsymbol{p}, \eta)$.

For this purpose, one multiplies the non-linear fluid equations (3.54) by an increasing number of additional fluctuation fields and takes the statistical average afterwards. The η-evolution of the correlation functions can then be written as

$$\partial_\eta \langle \psi_a \psi_b \rangle = -\Omega_{ac} \langle \psi_c \psi_b \rangle - \Omega_{bc} \langle \psi_a \psi_c \rangle$$
$$+ \gamma_{acd} \langle \psi_c \psi_d \psi_b \rangle + \gamma_{bcd} \langle \psi_a \psi_c \psi_d \rangle \,,$$

$$\partial_\eta \langle \psi_a \psi_b \psi_c \rangle = -\Omega_{ad} \langle \psi_d \psi_b \psi_c \rangle - \Omega_{bd} \langle \psi_a \psi_d \psi_c \rangle - \Omega_{cd} \langle \psi_a \psi_b \psi_d \rangle \qquad (5.39)$$
$$+ \gamma_{ade} \langle \psi_d \psi_e \psi_b \psi_c \rangle + \gamma_{bde} \langle \psi_a \psi_d \psi_e \psi_c \rangle + \gamma_{cde} \langle \psi_a \psi_b \psi_d \psi_e \rangle \,,$$

$$\partial_\eta \langle \psi_a \psi_b \psi_c \psi_d \rangle = \dots \,.$$

We refer to this infinite hierarchy of evolution equations as *flow equations*. For better readability, we have omitted the momentum and time dependence of the correlation functions here. All fields are evaluated at the same time η. Note that in contrast to the flow equations in [156], the equations (5.39) do not contain explicit factors e^η. This is due to the fact that the convention we use for defining the fields $\psi_a(\boldsymbol{k}, \eta)$ (see (3.51)) differs from the one in [156] by a factor $e^{-\eta}$.

The procedure above generates an infinite hierarchy of evolution equations corresponding to an infinite system of coupled differential equations. To determine the evolution of a correlation function of order $\mathcal{N}$ from this hierarchy, the correlation function of the next higher order $\mathcal{N}+1$ needs to be known. Hence, it is required to truncate the infinite hierarchy at a certain order of correlation functions to obtain a closed set of equations. Consequently, the usefulness of the time-flow approach relies on finding a suitable closure approximation.

5.5.2. Closure approximation

In order to close the infinite hierarchy of evolution equations (5.39), we first decompose the two-, three- and four-point correlation functions in their connected parts by using (4.7). According to (4.8), the decomposition of the four-point correlation function, for instance,

yields

$$\langle\psi_a\psi_b\psi_c\psi_d\rangle = \langle\psi_a\psi_b\psi_c\psi_d\rangle_c + \langle\psi_a\psi_b\rangle_c\langle\psi_c\psi_d\rangle_c + \langle\psi_a\psi_c\rangle_c\langle\psi_b\psi_d\rangle_c + \langle\psi_a\psi_d\rangle_c\langle\psi_b\psi_c\rangle_c. \quad (5.40)$$

Next, we express the connected correlators via the definition (4.9) in terms of the power spectrum $P_{ab}(k,\eta)$, the bispectrum $B_{abc}(\boldsymbol{k},\boldsymbol{q},\boldsymbol{p},\eta)$ and the trispectrum $Q_{abc}(\boldsymbol{k},\boldsymbol{q},\boldsymbol{p},\boldsymbol{r},\eta)$. This allows us finally to rewrite the (unconnected) two-, three- and four-point correlations functions as (see (4.10))

$$
\begin{aligned}
\langle\psi_a(\boldsymbol{k},\eta)\psi_b(\boldsymbol{q},\eta)\rangle &= \delta^{\mathrm{D}}(\boldsymbol{k}+\boldsymbol{q})P_{ab}(k,\eta), \\
\langle\psi_a(\boldsymbol{k},\eta)\psi_b(\boldsymbol{q},\eta)\psi_c(\boldsymbol{p},\eta)\rangle &= \delta^{\mathrm{D}}(\boldsymbol{k}+\boldsymbol{q}+\boldsymbol{p})\,B_{abc}(\boldsymbol{k},\boldsymbol{q},\boldsymbol{p},\eta), \\
\langle\psi_a(\boldsymbol{k},\eta)\psi_b(\boldsymbol{q},\eta)\psi_c(\boldsymbol{p},\eta)\psi_d(\boldsymbol{w},\eta)\rangle &= \delta^{\mathrm{D}}(\boldsymbol{k}+\boldsymbol{q})\delta^{\mathrm{D}}(\boldsymbol{p}+\boldsymbol{w})\,P_{ab}(k,\eta)\,P_{cd}(p,\eta) \\
&\quad + \delta^{\mathrm{D}}(\boldsymbol{k}+\boldsymbol{p})\delta^{\mathrm{D}}(\boldsymbol{q}+\boldsymbol{w})\,P_{ac}(k,\eta)\,P_{bd}(q,\eta) \\
&\quad + \delta^{\mathrm{D}}(\boldsymbol{k}+\boldsymbol{w})\delta^{\mathrm{D}}(\boldsymbol{q}+\boldsymbol{p})\,P_{ad}(k,\eta)\,P_{bc}(q,\eta) \\
&\quad + \delta^{\mathrm{D}}(\boldsymbol{k}+\boldsymbol{q}+\boldsymbol{p}+\boldsymbol{w})\,Q_{abcd}(\boldsymbol{k},\boldsymbol{q},\boldsymbol{p},\boldsymbol{w},\eta)\,.
\end{aligned}
\quad (5.41)
$$

Following [156], we can close the infinite set of evolution equations at this level by neglecting the trispectrum, namely setting

$$Q_{abcd}(\boldsymbol{k},\boldsymbol{q},\boldsymbol{p},\boldsymbol{w},\eta) \equiv 0\,. \quad (5.42)$$

This closure approximation allows us to express the four-point correlation function in terms of power spectra. Consequently, the first two equations of the hierarchy (5.39) form a simplified system which is completely determined only by the corresponding power spectra and bispectra.

Note that the closure approximation (5.42), which allows us to split the four-point correlation function in terms of two-point ones, yields the same result as applying the Wick theorem for Gaussian random fields in (4.6). However, it does *not* imply that we assume the fields $\psi_a(\boldsymbol{k},\eta)$ to be Gaussian. This can be directly seen from the fact that the three-point function in (5.41) (or equivalently the bispectrum $B_{abc}(\boldsymbol{k},\boldsymbol{q},\boldsymbol{p},\eta)$) does not vanish as it would be the case for Gaussian fields due to the Wick theorem (4.6), but is fully taken into account instead.

If we apply the closure approximation (5.42) to the correlation functions (5.41) and insert these into the flow equations in (5.39) afterwards, we truncate the infinite hierarchy so that the first two flow equations now constitute a *closed* system in terms of the power spectrum and the bispectrum. By restoring the momentum dependencies and writing down the integration

over internal momenta explicitly, the closed system is formed by the relations

$$
\begin{aligned}
\partial_\eta \, P_{ab}(k, \eta) = & - \Omega_{ac}(\eta) P_{cb}(k, \eta) - \Omega_{bc}(\eta) P_{ac}(k, \eta) \\
& + \int d^3 q \, \Big[\, \gamma_{acd}(-\boldsymbol{k}, -\boldsymbol{q}, \boldsymbol{q} - \boldsymbol{k}) \, B_{bcd}(\boldsymbol{k}, -\boldsymbol{q}, \boldsymbol{q} - \boldsymbol{k}, \eta) \\
& \qquad\quad + \gamma_{bcd}(-\boldsymbol{k}, -\boldsymbol{q}, \boldsymbol{q} - \boldsymbol{k}) \, B_{acd}(\boldsymbol{k}, -\boldsymbol{q}, \boldsymbol{q} - \boldsymbol{k}, \eta) \, \Big] \,,
\end{aligned}
\tag{5.43}
$$

$$
\begin{aligned}
\partial_\eta \, B_{abc}(\boldsymbol{k}, -\boldsymbol{q}, \boldsymbol{q} - \boldsymbol{k}, \eta) = & - \Omega_{ad}(\eta) \, B_{dbc}(\boldsymbol{k}, -\boldsymbol{q}, \boldsymbol{q} - \boldsymbol{k}, \eta) - \Omega_{bd}(\eta) \, B_{adc}(\boldsymbol{k}, -\boldsymbol{q}, \boldsymbol{q} - \boldsymbol{k}, \eta) \\
& - \Omega_{cd}(\eta) \, B_{abd}(\boldsymbol{k}, -\boldsymbol{q}, \boldsymbol{q} - \boldsymbol{k}, \eta) \\
& + 2 \, \Big[\, \gamma_{ade}(-\boldsymbol{k}, -\boldsymbol{q}, \boldsymbol{q} - \boldsymbol{k}) \, P_{db}(q, \eta) \, P_{ec}(|\boldsymbol{q} - \boldsymbol{k}|, \eta) \\
& \qquad\quad + \gamma_{bde}(-\boldsymbol{q}, \boldsymbol{q} - \boldsymbol{k}, -\boldsymbol{k}) \, P_{dc}(|\boldsymbol{q} - \boldsymbol{k}|, \eta) \, P_{ea}(k, \eta) \\
& \qquad\quad + \gamma_{cde}(\boldsymbol{q} - \boldsymbol{k}, -\boldsymbol{k}, -\boldsymbol{q}) \, P_{da}(k, \eta) \, P_{eb}(q, \eta) \, \Big] \,.
\end{aligned}
\tag{5.44}
$$

Here, we have reintroduced the dependence of the power spectrum and bispectrum on the momenta $\boldsymbol{k}$ and $\boldsymbol{q}$ such that momentum conservation according to (5.41) is fulfilled. Note that our convention for the momentum dependence of the vertex function γ_{abc} (see (3.53)) differs from the one used in the original work [156]. Besides, notice that the only momentum integration in the equations above is the one which is indicated in (5.43).

Moreover, it is worth mentioning that the closure approximation (5.42) does only affect the hierarchy of flow equations in (5.39) at the level of the second evolution equation for the bispectrum and at the subsequent higher orders. As a consequence, the differential evolution equation for the power spectrum $P_{ab}(k, \eta)$ in (5.43) is an exact solution for the power spectrum. However, since it depends on the bispectrum $B_{abc}(\boldsymbol{k}, -\boldsymbol{q}, \boldsymbol{q} - \boldsymbol{k})$, it is influenced by the closure approximation as soon as we insert a relation for the bispectrum based on the differential equation (5.44). Thus, we can benefit from the exactness of the solution for the power spectrum only in the case where we additionally find a non-perturbative solution for the bispectrum, as we show in Chapter 7.

5.5.3. Analytical solutions

Analogously to the formal integral solution of the non-linear fluid equations we derived in terms of the doublet field $\psi_a(\boldsymbol{k}, \eta)$ in (3.67), we can formally solve the closed system of differential equations in (5.43) and (5.44) in terms of the power spectrum $P_{ab}(\boldsymbol{k}, \eta)$ and the bispectrum $B_{abc}(\boldsymbol{k}, -\boldsymbol{q}, \boldsymbol{q} - \boldsymbol{k}, \eta)$ by integrating over the time variable η. If we use the properties (3.58) and (3.59) of the linear propagator to simplify (5.43) and (5.44) after time

integration, the formal integral solution of the closed system reads

$$P_{ab}(k, \eta) = g_{ac}(\eta, \eta_0)\, g_{bd}(\eta, \eta_0)\, P_{cd}^0(k)$$
$$+ \int_{\eta_0}^{\eta} d\eta' \int d^3 q\, g_{ae}(\eta, \eta')\, g_{bf}(\eta, \eta')$$
$$\times \Big[\; \gamma_{ecd}(-\boldsymbol{k}, -\boldsymbol{q}, \boldsymbol{q} - \boldsymbol{k})\, B_{fcd}(\boldsymbol{k}, -\boldsymbol{q}, \boldsymbol{q} - \boldsymbol{k}, \eta')$$
$$+ \gamma_{fcd}(-\boldsymbol{k}, -\boldsymbol{q}, \boldsymbol{q} - \boldsymbol{k})\, B_{ecd}(\boldsymbol{k}, -\boldsymbol{q}, \boldsymbol{q} - \boldsymbol{k}, \eta') \;\Big],$$
(5.45)

$$B_{abc}(\boldsymbol{k}, -\boldsymbol{q}, \boldsymbol{q} - \boldsymbol{k}, \eta) = g_{ad}(\eta, \eta_0)\, g_{be}(\eta, \eta_0)\, g_{cf}(\eta, \eta_0)\, B_{def,0}(\boldsymbol{k}, -\boldsymbol{q}, \boldsymbol{q} - \boldsymbol{k})$$
$$+ 2 \int_{\eta_0}^{\eta} d\eta'\, g_{ad}(\eta, \eta')\, g_{be}(\eta, \eta')\, g_{cf}(\eta, \eta')$$
$$\times \Big[\; \gamma_{dgh}(-\boldsymbol{k}, -\boldsymbol{q}, \boldsymbol{q} - \boldsymbol{k})\, P_{eg}(q, \eta')\, P_{fh}(|\boldsymbol{q} - \boldsymbol{k}|, \eta')$$
$$+ \gamma_{egh}(-\boldsymbol{q}, \boldsymbol{q} - \boldsymbol{k}, -\boldsymbol{k})\, P_{fg}(|\boldsymbol{q} - \boldsymbol{k}|, \eta')\, P_{dh}(q, \eta')$$
$$+ \gamma_{fgh}(\boldsymbol{q} - \boldsymbol{k}, -\boldsymbol{k}, -\boldsymbol{q})\, P_{dg}(k, \eta')\, P_{eh}(q, \eta') \;\Big],$$
(5.46)

where $P_{ab,0}(k) \equiv P_{ab}(k, \eta_0)$ and $B_{def,0}(\boldsymbol{k}, -\boldsymbol{q}, \boldsymbol{q} - \boldsymbol{k}) \equiv B_{def}(\boldsymbol{k}, -\boldsymbol{q}, \boldsymbol{q} - \boldsymbol{k}, \eta_0)$ denote the power spectrum and the bispectrum evaluated at the initial time η_0 (see also (4.2)). Notice that as a consequence of the exactness of the differential evolution equation for the power spectrum in (5.43), the analytic solution for $P_{ab}(k, \eta)$ in (5.45) is also not affected by the closure approximation. However, the solution for the bispectrum in (5.46) relies on the closure approximation.

In order to understand which classes of perturbative corrections are maintained and which are neglected by performing the closure approximation (5.42), we expand the formal integral solutions for the power spectrum and the bispectrum in (5.45) and (5.46) in power of the interaction vertex γ_{abc}. By setting the vertices on the right-hand side of (5.45) to zero, we obtain the linear solution (of the order $\mathcal{O}(\gamma^0)$) for the power spectrum in the time-flow approach,

$$P_{ab}^L(k, \eta) = g_{ac}(\eta, \eta_0)\, g_{bd}(\eta, \eta_0)\, P_{cd,0}(k).$$
(5.47)

If we compare this relation for the linear power spectrum with the one we derived in SPT in (4.16), taking into account the definition of the initial power spectrum $P_{cd,0}(k)$ for Gaussian-distributed initial conditions in (4.3), it is obvious that at lowest order in perturbation theory the power spectrum in the time-flow approach and in SPT coincide. Its diagrammatic representation is shown in Figure 4.5.

Next, let us determine the linear-order relation for the bispectrum in the time-flow approach from it formal integral solution in (5.46). By assuming Gaussian initial conditions further on,

we notice that the initial bispectrum in (5.46) under this assumption vanishes due to the Wick theorem in (4.6), $B_{def,0}(\boldsymbol{k}, -\boldsymbol{q}, \boldsymbol{q} - \boldsymbol{k}) = 0$. For Gaussian initial conditions, we thus obtain the lowest perturbative order for the bispectrum in the time-flow approach, i.e., the $\mathcal{O}(\gamma^1)$-contribution, by using the linear power spectrum in (5.47) to approximate the power spectra on the right-hand side of the formal integral solution for the bispectrum in (5.46). The resulting $\mathcal{O}(\gamma^1)$-contribution in terms of the linear power spectrum yields the linear bispectrum relation in the time-flow approach. From the structure of this contribution outlined in (5.46), we deduce by comparison with the tree-level bispectrum for Gaussian (growing-mode) initial conditions in SPT, given in (4.28) with the kernels defined in (3.76) and (3.78), that also the linear bispectrum in the time-flow approach is identical to the one in SPT. Thus, it is graphically represented by the first diagram on the left-hand side in Figure 4.6.

Continuing this iteration procedure, we insert the linear bispectrum relation of the order $\mathcal{O}(\gamma^1)$ into the bispectra on the right-hand side of the formal solution for the power spectrum in (5.45). These $\mathcal{O}(\gamma^2)$-contributions to the power spectrum determine the one-loop power spectrum correction in the time-flow approach. They receive contributions from the (linear) power spectra in the $\mathcal{O}(\gamma^1)$-contribution to the bispectrum in (5.46). If we only compare the momentum dependence of the power spectra arising from (5.46) and of the (initial) power spectra contributing to the one-loop power spectrum in SPT (see (4.19)-(4.21)), we see that the structure of momentum dependence is equivalent. This is a hint that also the one-loop contributions to the power spectrum in the time-flow approach and in SPT coincide. Indeed, by using the decomposition rule for the linear propagator in (3.60) the SPT one-loop power spectrum contribution in (4.19)-(4.21) with the kernels in (3.78) and (3.76) can be transformed in the corresponding time-flow expression for Gaussian growing-mode initial conditions [156]. In conclusion, up to one-loop order the power spectrum in SPT and in the time-flow approach coincide. Consequently, the one-loop power spectrum contribution derived from the time-flow approach can be separated three one-loop diagrams presented in Figure 4.5.

Iterating the procedure once more, the first differences between the perturbative predictions of the time-flow approach and SPT arise. By substituting the power spectra on the right-hand side of the formal integral solution for the bispectrum in (5.46) with the one-loop time-flow power spectrum contribution of the order $\mathcal{O}(\gamma^2)$, we obtain the $\mathcal{O}(\gamma^3)$-contribution to the bispectrum, that is, the one-loop correction to the bispectrum, in the time-flow approach. However, compared to SPT, there are other one-loop corrections to the bispectrum of the order $\mathcal{O}(\gamma^3)$ which are not generated by this iteration procedure. These omitted corrections to the one-loop bispectrum correspond exactly to the contributions which are neglected by setting the trispectrum in the closure approximation to zero (see (5.41) and (5.42)). Hence,

imposing the closure approximation at the level of the trispectrum leads to differences between the time-flow approach and SPT at first at one-loop order for the bispectrum and thus at two-loop order for the power spectrum. We investigate these deviations of the perturbative predictions between the time-flow formalism and SPT for the case of the one-loop bispectrum in further detail in Section 6.2.

In a field theoretical language, as a consequence of applying the closure approximation (5.42), the vertex renormalization is neglected in the time-flow approach, whereas the renormalization of the power spectrum is taken into account. This finding generalizes to any order in perturbation theory. It can be directly understood by considering the formal integral solutions for the power spectrum in (5.45). Therein, the non-linear power spectrum formally corresponds to a one-loop expression where the linear power spectrum contributions are replaced by non-linear ones, while the vertices are left untouched. Furthermore, the non-linear bispectrum in (5.46) is formally a tree-level expression since it involves no momentum integration.

As the time-flow approach resums the perturbative corrections where the interaction vertex is kept at its tree-level form, it performs a resummation of the same class of perturbations as the renormalization group (RG) approach of [148]. Therein, renormalization group equations are solved under the approximation of keeping the tree-level expression for the vertex. Indeed, the perturbative predictions of the time-flow approach and the results presented in [148] agree very well [156]. However, there are some differences between the time-flow formalism and the RG approach in [148] which are worth mentioning.

First, in the RG approach in [148] as well as in RPT (see Section 5.3), the computation of the power spectrum is performed in two steps. However, each step involves further approximations apart from keeping the vertex at tree-level. Thereby, the first step consists in computing the non-linear propagator. In the limit of large external momentum, the non-linear propagator is given by a simple analytic expression at any order in perturbation theory (see (5.9)). However, it turns out that the use of the resummed non-linear propagator in the large-momentum limit yields inaccurate results so that it is necessary to take subleading corrections into account [144]. In the second step, the resummed propagator is used to compute the power spectrum (see (5.12)). The calculation of the power spectrum is then performed by applying additional approximations either to the relevant RG equations [148] or at finite loop order in RPT [144]. In contrast to this two-step computation procedure for the power spectrum in the RG approach in [148] and in RPT, the remarkable feature of the time-flow approach is that it is not necessary to calculate the propagator first to arrive at an expression for the power spectrum, and equivalently the bispectrum as well as higher-order correlation functions. The reason for this is that the time-flow formalism treats the information on the time evolution, which is contained in the non-linear propagator in the

RG approach of [148] and in RPT, exactly by the structure of the differential time-evolution equations, the flow equations, in (5.39). After the closure approximation at the level of the trispectrum (see (5.42)) is applied, the closed system of flow equations is solved without any further approximation.

Building up on this, the next level of imposing the closure approximation then consists in keeping the contributions of the trispectrum $Q_{abcd}(\boldsymbol{k}, \boldsymbol{q}, \boldsymbol{p}, \boldsymbol{w}, \eta)$, but truncating the infinite hierarchy of flow equations at the level of the connected five-point correlation function. This truncation procedure can be continued up to arbitrary order in the correlation functions. Due to this, the time-flow approach provides a transparent and systematic way of imposing the approximations necessary to determine the correlation functions by means of perturbation theory. However, since the closure approximation does not constitute a physically motivated approximation, the perturbative predictions of the time-flow approach have to be investigated with respect to their reasonability and accuracy, as we do explicitly in Section 6.2.2.

The second important difference between the time-flow approach and other perturbative approaches, such as SPT, RPT or the afore mentioned RG approach (see also [304]), consists in the treatment of the dependence on the background cosmology, encoded in the fluid equations. The time-flow approach does not require a specification of the cosmological model to predict relations for the correlation functions. Thus, it is applicable for arbitrary cosmological models, in particular other ones than EdS or ΛCDM, e.g., models containing massive neutrinos or modifications of gravity [301–303, 366]. Unlike this, the other perturbative approaches considered so far are only exact in the EdS case where the matrix $\Omega_{ab}(\eta)$, appearing in the fluid equations (3.54), equals (3.64). Other cosmological models, such as the phenomenologically interesting cases of ΛCDM and (non-clustering) quintessence, are in these approaches accounted for by keeping the EdS expression for the $\Omega_{ab}(\eta)$ and adapting only the time dependence via the proper linear growth factor $D_1(\tau)$ in (3.9).

Since the time-flow approach does not rely on this approximation for treating the background dependence, one can use it to estimate the error made by applying this approximation. We expect the error of this background approximation to increase for lower redshifts. However, the comparison with the time-flow approach reveals that the error of the background approximation in the BAO regime (5.1) is below the $\mathcal{O}(10^{-3})$-level at redshift $z = 1$. and not even of the order $\mathcal{O}(10^{-2})$ at present time, i.e., at redshift $z = 0$ [156]. Consequently, we conclude that the approximate treatment of the background dependence of the fluid equations, which is implemented in most perturbative approaches other than the time-flow approach, but in particular in SPT and RPT, constitute indeed a well motivated approximation. Hence, this conclusion derived from the time-flow approach can be understood as an independent probe of this approximations. Thereby, the findings of [156] confirm the extremely reliable

accuracy of this approximation, as pointed out in Section 3.2.4.

In the following chapter, we use the perturbative frameworks of SPT, the time-flow approach and the eikonal approximation – as well as a non-perturbative background method – to study large-scale structure correlation functions in the soft limit. This allows us to set up so-called consistency conditions for the correlation functions, for example for the bispectrum.

Chapter 6

Bispectrum Consistency Conditions

Contents

Our intention in this chapter is to study large-scale structure correlation functions, such as the bispectrum, in the limit where one wavenumber becomes small, that is, in the squeezed or *soft limit*. In the soft limit, $(\mathcal{N}+1)$-point and $\mathcal{N}$-point correlators of density and velocity perturbations can be linked to so-called 'consistency conditions'. These have recently received significant attention [167–171, 173–176, 228–234]. In the following, we derive and discuss consistency conditions for correlation functions both at equal and at unequal times.

For *unequal-time* correlators, the main appeal of the consistency conditions lies in the fact that they can be deduced solely from symmetry arguments. The only assumption on which the unequal-time consistency relations are based is single-field inflation providing the initial conditions for the seeds of structure, as discussed in Section 4.1, together with the diffeomorphism invariance (general covariance) of general relativity. Due to the universality of these underlying assumptions, the unequal-time consistency relations yield fairly generic, non-perturbative predictions about the dynamics of the system on short distance scales, which can serve as a probe of the basic aspects of theory [165–171, 228, 235]. This becomes a powerful tool, in particular with regard to upcoming large-scale structure surveys, since it would allow

to test the assumption of single-field inflation, providing the initial seed fluctuations, as well as the equivalence principle in gravitational theories.[1]

The consistency conditions are most meaningful at unequal times. However, for the observationally most interesting *equal-time* correlation functions these consistency conditions become degenerate, i.e., they vanish at leading order in the soft momentum (the long-wavelength mode) q. The reason for this is that, when dealing with the density and velocity fields (as opposite to the potential), the leading-order term scales like q^{-1}. In order to deduce information about equal-time correlators, one thus has to investigate next-to-leading order effects. At next-to leading order, the equal-time correlation functions depend on the interplay between soft and hard modes so that dynamical information, as opposed to gauge artifacts in general relativity, starts to become relevant [165, 166, 224]. Hence, it is important to investigate the existence and validity of equal-time consistency conditions even when the short-wavelength modes are deep in the non-linear regime. In fact, (angular-averaged) equal-time consistency conditions that are allegedly non-perturbative relations have been advocated in the recent literature [173, 174].

For assessing these equal-time consistency conditions, we use two different approaches, namely the time-flow formalism, that we introduced in Section 5.5, as well as a background method, which was first discussed in [165, 166] and is referred to as so-called 'separate universe' approach in the context of N-body simulations [238–241]. In this background method, one can absorb the influence of a soft, long-wavelength perturbation within a flat FRW metric, by implementation of a map, into a locally curved FRW background. It is exactly this equivalence between a soft perturbation in a flat universe and a locally curved background which has inspired angular-averaged equal-time consistency relations in [173, 174]. In the following, we investigate the accuracy and validity of these consistency conditions within and beyond perturbation theory.

6.1. Correlation functions at unequal times in the soft limit

In this section, we (re-)derive the large-scale structure consistency conditions for density and velocity correlation functions at *unequal* times in the soft limit. We work in the Eulerian representation of cosmological perturbation theory and use the compact notation of Section 3.3.1 in terms of the doublet field $\psi_a(\boldsymbol{k}, \eta)$ (see (3.51)), which simultaneously includes the density contrast and the velocity divergence. We neglect deviations from the perfect-fluid approximation, which would in principle be required to account for the imprint of hard modes on the long

---

[1]Soft limits of inflationary correlation functions have also been extensively studied in the literature, see for instance [33, 217–227].

distance scales [63, 178], so that the non-linear fluid equations for the doublet field $\psi_a(\boldsymbol{k}, \eta)$ are given by (3.54). Moreover, we assume a flat, matter-dominated EdS cosmology if not mentioned otherwise.

One crucial aspect in the derivation of consistency conditions at unequal times is the factorization of soft and hard modes. Due to this, we can resum the soft effects into a so-called eikonal phase. Thereby, we make use of the eikonal approximation [159, 160, 237], which we introduced in Section 5.4. This allow us not only to (re-)derive the unequal-time consistency conditions of density perturbations in a straightforward way, but in addition, by relying on the doublet field notation, to naturally extend the consistency conditions at unequal times to the velocity perturbation fields.

6.1.1. Eikonal approximation

The derivation of consistency conditions for large-scale structure correlation functions in the soft limit is relatively straightforward for unequal times. The reason for this is that soft and hard modes evolve independently at leading order in the soft momentum q. Consequently, the soft effect can be resummed yielding an eikonal phase [159, 160, 237] (see also [101, 125] in this context). Hence, we can directly build upon our considerations of the eikonal approximation in Section 5.4 and make use of the relations (5.28) and (5.30) with (5.26) to express the fluctuations of the hard modes $\boldsymbol{k}$, with $k \gg q$, as

$$\psi_a(\boldsymbol{k}, \eta) \simeq \exp\left[\int^{\eta} d\eta' \int^{\Lambda_L} d^3p \, \frac{\boldsymbol{k} \cdot \boldsymbol{p}}{p^2} \, \psi_2^L(\boldsymbol{p}, \eta') \right] \times \psi_a^S(\boldsymbol{k}, \eta) \,, \tag{6.1}$$

where we have denoted the internal momentum by $\boldsymbol{p}$. We introduced a cutoff Λ_L to emphasize that the momentum integral is performed over soft momenta (see (5.26)). Moreover, $\psi_a^S(\boldsymbol{k}, \eta)$ denotes the fluctuations on short scales, including interactions of the short-short type, whereas $\psi_2^L(\boldsymbol{p}, \eta) \equiv \Theta^L(\boldsymbol{p}, \eta)$ are linear long-wavelength perturbations of the velocity field. Note that according to the definition of the velocity perturbation field in (3.48), the (growing-mode) solutions for the density and velocity perturbations at leading order are equal (see also (3.11) and (3.12)), $\Theta^L(\boldsymbol{p}, \eta) = \delta^L(\boldsymbol{p}, \eta)$. Thus, the impact of the long-wavelength modes in (6.1) arises in form of an exponential function involving the linear density field. Moreover, notice that the effect of soft physics completely factorizes at this order.

Proceeding from this, the expression (6.1) allows to derive the large-scale structure consistency conditions at unequal times in a straightforward manner. By using it, we can directly determine the form of unequal-time correlation functions in the soft limit $q \to 0$, as for instance

$$\left\langle \psi_a^L(\boldsymbol{q}, \eta_q)\, \psi_{b_1}(\boldsymbol{k}_1, \eta_1) \cdots \psi_{b_\mathcal{N}}(\boldsymbol{k}_\mathcal{N}, \eta_\mathcal{N}) \right\rangle'$$

$$\xrightarrow{q \to 0} \left\langle \psi_a^L(\boldsymbol{q}, \eta_q)\, \exp\left[\sum_i \int^{\eta_i} d\eta_i' \int^{\Lambda_L} d^3p\, \frac{\boldsymbol{k} \cdot \boldsymbol{p}}{p^2}\, \delta^L(\boldsymbol{p}, \eta_i')\right]\right\rangle' \times \left\langle \psi_{b_1}^S(\boldsymbol{k}_1, \eta_1) \cdots \psi_{b_\mathcal{N}}^S(\boldsymbol{k}_\mathcal{N}, \eta_\mathcal{N}) \right\rangle',$$

$$(6.2)$$

and

$$\left\langle \psi_{b_1}(\boldsymbol{k}_1, \eta_1) \cdots \psi_{b_\mathcal{N}}(\boldsymbol{k}_\mathcal{N}, \eta_\mathcal{N}) \right\rangle'$$

$$\xrightarrow{q \to 0} \left\langle \exp\left[\sum_i \int^{\eta_i} d\eta_i' \int^{\Lambda_L} d^3p\, \frac{\boldsymbol{k} \cdot \boldsymbol{p}}{p^2}\, \delta^L(\boldsymbol{p}, \eta_i')\right]\right\rangle' \times \left\langle \psi_{b_1}^S(\boldsymbol{k}_1, \eta_1) \cdots \psi_{b_\mathcal{N}}^S(\boldsymbol{k}_\mathcal{N}, \eta_\mathcal{N}) \right\rangle',$$

$$(6.3)$$

where the prime $\langle \dots \rangle'$ indicates that the momentum conserving Dirac delta distribution has been removed. By assuming Gaussian-distributed growing-mode initial conditions (see (3.70)-(3.71)) and subsequently evaluating the correlation functions, we obtain

$$\frac{\left\langle \psi_a^L(\boldsymbol{q}, \eta_q)\, \exp\left[\sum_i \int^{\eta_i} d\eta_i' \int^{\Lambda_L} d^3p\, \frac{\boldsymbol{k}_i \cdot \boldsymbol{p}}{p^2}\, \delta^L(\boldsymbol{p}, \eta_i')\right]\right\rangle'}{\left\langle \exp\left[\sum_i \int^{\eta_i} d\eta_i' \int^{\Lambda_L} d^3p\, \frac{\boldsymbol{k}_i \cdot \boldsymbol{p}}{p^2}\, \delta^L(\boldsymbol{p}, \eta_i')\right]\right\rangle'} = -u_a P^L(q, \eta_q) \sum_i \frac{D_1(\eta_i)}{D_1(\eta_q)} \frac{\boldsymbol{k}_i \cdot \boldsymbol{q}}{q^2}. \quad (6.4)$$

Here, the linear power spectrum $P^L(q, \eta)$ is defined as in (4.17) and its time-dependence is expressed in terms of the linear growth factor $D_1(\eta)$, given in (3.49).

If we finally relate the equations (6.2) and (6.3) via (6.4), we can determine the consistency conditions for unequal-time correlation functions in the soft limit,

$$\left\langle \psi_a^L(\boldsymbol{q}, \eta_q)\, \psi_{b_1}(\boldsymbol{k}_1, \eta_1) \cdots \psi_{b_\mathcal{N}}(\boldsymbol{k}_\mathcal{N}, \eta_\mathcal{N}) \right\rangle' \xrightarrow{q \to 0} -u_a P^L(q, \eta_q) \sum_i \frac{D_1(\eta_i)}{D_1(\eta_q)} \frac{\boldsymbol{k}_i \cdot \boldsymbol{q}}{q^2}$$

$$\times \left\langle \psi_{b_1}(\boldsymbol{k}_1, \eta_1) \cdots \psi_{b_\mathcal{N}}(\boldsymbol{k}_\mathcal{N}, \eta_\mathcal{N}) \right\rangle'. \quad (6.5)$$

This result reproduces the unequal-time consistency conditions for the density perturbation fields which have been recently derived in the literature, see e.g., [167, 169–171, 228–230]. At the same time, it constitutes a generalization of the results in the literature by including not only the density perturbations but also the velocity fluctuations. Besides, the derivation by use of the eikonal approximation we presented here has the advantage of leading to the unequal-time consistency conditions in a straightforward and transparent way. For this reason, it can be easily generalized to account for different background cosmologies.

Notice that the determination of the unequal-time consistency conditions in (6.5) did not require more than the leading-order factorization of long-wavelength modes in the squeezed limit. However, if we evaluate the right-hand side of (6.5) at $\eta_q = \eta_i$ for all $i \in \{1, \dots \mathcal{N}\}$, it vanishes at leading order in q due to momentum conservation. This is nothing but a reflection

of the equivalence principle (see e.g., [171]). Consequently, a calculation at next-to-leading order is necessary to study the existence and the validity of consistency conditions for equal-time correlations functions in the soft limit.

6.2. Correlation functions at equal times in the soft limit

In the following, we direct our attention to correlation functions at *equal* times in the soft limit. Thereby, our aim is to explore the circumstances under which equal-time consistency conditions may exist beyond a perturbative treatment of the hard modes, i.e., when the coupling between long- and short-wavelength fluctuations becomes important.

In order to access the validity of consistency relations between correlation functions at equal times, we compute the soft limit of the equal-time connected three-point correlation function, the bispectrum, up to next-to-leading order with different perturbative and non-perturbative methods. In this way, we can use the soft limit of the bispectrum to compare the predictions of the individual methods.

6.2.1. Soft limit of the bispectrum in SPT

To explore the existence of a soft-limit connection between the bispectrum and the power spectrum beyond leading order, let us, as a first example, compute the soft limit of the bispectrum up to one-loop order in dependence of the linear power spectrum in SPT (see Section 4.4).

Although, depending on the form of the initial power spectrum, the loop integrals of the bispectrum (and also of the power spectrum) can be divergent in the UV limit of large loop momentum, the SPT predictions for the bispectrum consistency relations should agree with the exact, non-perturbative solution within their realm of validity. In other words, by judiciously choosing the initial conditions for the power spectrum in SPT, the arising loop integrals are always dominated by modes well within the perturbative regime so that SPT converges quickly. Thus, the comparison of the one-loop bispectrum in the soft limit in SPT with other perturbative and non-perturbative methods has to be interpreted in the sense of a mathematical statement at the level of the integrands. Note, however, that in order to account properly for the imprint of the short-distance UV physics, methods other than SPT are required. One approach in this direction is the effective field theory framework of LSS. Therein, the loop integrals of SPT are regularized by introducing counter-terms that cancel the possible non-physical UV divergences [49, 63, 89, 178–208] An appropriate regularization becomes even more relevant when considering correlation functions of the velocity divergence field, which constitutes a composite operator [63, 181, 208].

6. Bispectrum Consistency Conditions

Leading order

Proceeding from these considerations, let us explicitly derive the soft limit of the bispectrum at leading order in SPT and determine an angular-averaged consistency relation from it. For the moment, we base our calculation on the assumptions of an EdS background cosmology and Gaussian-distributed growing-mode initial conditions. We discussed the implications of these assumptions in detail in Section 3.3.3. In the calculation, we use the definition of the power spectrum and the bispectrum in (4.1) and (4.10). For reasons of clarity and comprehensibility, we only consider the bispectrum of density perturbations, i.e., $B_{111}(\boldsymbol{k}, -\boldsymbol{q}, \boldsymbol{q} - \boldsymbol{k}, \eta)$ at first. Here, we have chosen the momenta such that momentum conservation, required by the Dirac delta distribution in the definition of the bispectrum (4.10), is fulfilled.

From the perturbative expansion of the bispectrum in terms of loop orders in Section 4.4, we have deduced that the bispectrum at leading order (at loop order $\ell = 0$) in SPT is given by the relation (4.27) with (4.28). In case of growing-mode initial conditions, the kernels have the simple form (3.76) and (3.78). Consequently, the leading-order bispectrum of density perturbations reduces to (see [40])

$$
\begin{aligned}
B_{111}^L(\boldsymbol{k}, -\boldsymbol{q}, \boldsymbol{q} - \boldsymbol{k}, \eta) = {}& 2\, F_2^s(\boldsymbol{k}, -\boldsymbol{q})\, P^L(k, \eta)\, P^L(q, \eta) \\
& + 2\, F_2^s(\boldsymbol{k}, \boldsymbol{q} - \boldsymbol{k})\, P^L(k, \eta)\, P^L(|\boldsymbol{q} - \boldsymbol{k}|, \eta) \\
& + 2\, F_2^s(-\boldsymbol{q}, \boldsymbol{q} - \boldsymbol{k})\, P^L(q, \eta)\, P^L(|\boldsymbol{q} - \boldsymbol{k}|, \eta)\,,
\end{aligned}
\tag{6.6}
$$

where the symmetrized kernels are explicitly given in (3.37). Moreover, we have absorbed the time dependence of the linear bispectrum into the linear power spectrum of density fluctuations, $P^L(k, \eta) \equiv P_{11}^L(k, \eta)$, defined in (4.17).

To determine the soft limit of the linear bispectrum in (6.6), we assume that one of its momenta, say $\boldsymbol{q}$, is soft. This implies for the absolute values of the momenta that $q \ll k$. Consequently, we can expand all quantities in (6.6) which depend on the difference between the soft and the hard mode, $|\boldsymbol{q} - \boldsymbol{k}|$, in a perturbative series about the soft mode q. For this purpose, we express the linear bispectrum as a function of the magnitudes k, q and the parameter

$$
\mu \equiv \cos\theta_{kq} = \frac{\boldsymbol{k} \cdot \boldsymbol{q}}{kq}\,,
\tag{6.7}
$$

characterizing the angle between the momenta $\boldsymbol{k}$ and $\boldsymbol{q}$. In the series expansion, that we perform afterwards, up to the first order in the soft mode q, we do not only have to include the kernels entering in the linear bispectrum (6.6), but the linear power spectra as well,

$$
P^L(|\boldsymbol{q} - \boldsymbol{k}|, \eta) \simeq P^L(k, \eta) - q\, \mu\, \partial_k P^L(k, \eta) + \mathcal{O}(q^2)\,.
\tag{6.8}
$$

Since the series expansion of the kernel $F_2^s(\boldsymbol{k}, \boldsymbol{q} - \boldsymbol{k})$ yields a term linear in q, it adds up with the power spectra in the second line of (6.6) to a contribution that vanishes in the squeezed

limit $q \to 0$. This is different for the other two kernels in (6.6). The series expansion of these kernels about q generates not only a term linear in q, but also a constant term and a term proportional to $1/q$. Multiplying the series expansion of the kernels and the one of the power spectrum in (6.21), these terms proportional to $1/q$ that cancel the linear q-dependence of the derivative term with respect to the power spectrum, $\partial_k P^L(k, \eta)$. As a result, the series expansion of the bispectrum does generate not only constant terms, but also a characteristic derivative term with respect to the linear power spectrum, which is not even canceled when finally taking the soft limit $q \to 0$.

The resulting equation we obtain from taking $q \to 0$ yields the linear bispectrum in the soft limit, $B_{111}^L(\boldsymbol{k}, -\boldsymbol{q}, \boldsymbol{q} - \boldsymbol{k}, \eta)_{q \to 0}$. However, this relation still depends on the angle between the soft and the hard mode via the parameter μ. To remove the angular dependence, we take the angular average, $(\ldots)^{\mathrm{av}} \equiv \int d\Omega / (4\pi) \ldots$, where the solid angle is $d\Omega = 2\pi \, d\mu$ in our case. In the end, this yields a relation between the angular-averaged leading-order bispectrum in the soft limit and the linear power spectrum,

$$B_{111}^L(\boldsymbol{k}, -\boldsymbol{q}, \boldsymbol{q} - \boldsymbol{k}, \eta)^{\mathrm{av}} \xrightarrow{q \to 0} P^L(q, \eta) \left(\frac{47}{21} - \frac{1}{3} \, k \, \partial_k \right) P^L(k, \eta) \,, \tag{6.9}$$

and thus an angular-averaged *consistency relation* for the linear bispectrum in the soft limit. In the context of SPT, this bispectrum consistency relation was first derived (in real space) in [166].

Next-to-leading order

Next, our intention is to derive an angular-averaged soft-limit consistency relation for the bispectrum of density perturbations at next-to-leading order, i.e., $B_{111}^{1-\mathrm{loop}}(\boldsymbol{k}, -\boldsymbol{q}, \boldsymbol{q} - \boldsymbol{k}, \eta)_{q \to 0}^{\mathrm{av}}$. In SPT, the one-loop correction to the bispectrum of density perturbations arises as the sum of four contributions (see (4.30)),

$$\begin{aligned} B_{111}^{1-\mathrm{loop}}(\boldsymbol{k}, -\boldsymbol{q}, \boldsymbol{q} - \boldsymbol{k}, \eta) = {} & B_{111}^{(222)}(\boldsymbol{k}, -\boldsymbol{q}, \boldsymbol{q} - \boldsymbol{k}, \eta) + B_{111}^{(321, \mathrm{I})}(\boldsymbol{k}, -\boldsymbol{q}, \boldsymbol{q} - \boldsymbol{k}, \eta) \\ & + B_{111}^{(321, \mathrm{II})}(\boldsymbol{k}, -\boldsymbol{q}, \boldsymbol{q} - \boldsymbol{k}, \eta) + B_{111}^{(411)}(\boldsymbol{k}, -\boldsymbol{q}, \boldsymbol{q} - \boldsymbol{k}, \eta) \,, \end{aligned} \tag{6.10}$$

which are graphically represented by four independent diagrams involving different correlations of density fields (see Figure 4.6). According to (4.31)-(4.34), the mathematical expressions for these one-loop contributions read

$$\begin{aligned} B_{111}^{(222)}(\boldsymbol{k}, -\boldsymbol{q}, \boldsymbol{q} - \boldsymbol{k}, \eta) \equiv {} & 8 \int d^3 l \, F_2^s(-\boldsymbol{l}, \boldsymbol{l} + \boldsymbol{k}) \, F_2^s(\boldsymbol{l} + \boldsymbol{k}, \boldsymbol{q} - \boldsymbol{k} - \boldsymbol{l}) \, F_2^s(\boldsymbol{l}, \boldsymbol{q} - \boldsymbol{k} - \boldsymbol{l}) \\ & \times P^L(l) P^L(|\boldsymbol{l} + \boldsymbol{k}|) P^L(|\boldsymbol{l} - \boldsymbol{q} - \boldsymbol{k}|) \,, \end{aligned} \tag{6.11}$$

$$
\begin{aligned}
B_{111}^{(321,\mathrm{I})}(\boldsymbol{k},-\boldsymbol{q},\boldsymbol{q}-\boldsymbol{k},\eta) \;\equiv\;& 6\,P^L(k) \\
&\times \int d^3l\, F_2^s(\boldsymbol{l},-\boldsymbol{q}-\boldsymbol{l})\, F_3^s(-\boldsymbol{l},\boldsymbol{l}+\boldsymbol{q},-\boldsymbol{k})\, P^L(l) P^L(|\boldsymbol{l}+\boldsymbol{q}|) \\
&+ 5 \text{ permutations},
\end{aligned} \tag{6.12}
$$

$$
\begin{aligned}
B_{111}^{(321,\mathrm{II})}(\boldsymbol{k},-\boldsymbol{q},\boldsymbol{q}-\boldsymbol{k},\eta) \;\equiv\;& 6\,F_2^s(\boldsymbol{k},\boldsymbol{q}-\boldsymbol{k})\,P^L(k) P^L(|\boldsymbol{q}-\boldsymbol{k}|) \int d^3l\, F_3^s(\boldsymbol{q}-\boldsymbol{k},\boldsymbol{l},-\boldsymbol{l})\, P^L(l) \\
&+ 5 \text{ permutations} \\
\;\equiv\;& F_2^s(\boldsymbol{k},\boldsymbol{q}-\boldsymbol{k})\,P^L(k)\,P_{11}^{(13)}(\boldsymbol{q}-\boldsymbol{k},\eta) \\
&+ 5 \text{ permutations},
\end{aligned} \tag{6.13}
$$

$$
\begin{aligned}
B_{111}^{(411)}(\boldsymbol{k},-\boldsymbol{q},\boldsymbol{q}-\boldsymbol{k},\eta) \;\equiv\;& 12\,P^L(k) P^L(q) \int d^3l\, F_4^s(\boldsymbol{l},-\boldsymbol{l},-\boldsymbol{k},\boldsymbol{q})\, P^L(l) \\
&+ 2 \text{ cyclic permutations}.
\end{aligned} \tag{6.14}
$$

Here, the symmetrized kernels can be computed by using the recursion relation (3.33) (or equivalently from (3.78) with (3.79)) and symmetrizing with respect to their momenta (see (3.36)) afterwards. The permutations have to be taken with respect to the external momenta. As in the case of the linear bispectrum in (6.6), we have incorporated the time dependence of the one-loop bispectrum in the linear power spectra.

In order to determine an angular-averaged consistency relation for the one-loop bispectrum (6.10), we have to proceed in the same way as we did in the case of the linear bispectrum. In turns out, however, that the resulting expression is too cumbersome to allow for a meaningful analytic comparison with other methods. For practical reasons, we thus restrict our considerations to the limit where the loop momentum l is much larger than the external momenta k and q, i.e., $l \gg k, q$. Note that this is exactly the UV limit of loop integrals in SPT which requires a judicious choice of initial conditions to avoid divergences, as we discussed before. To derive the UV limit of the loop integrals which appear in the next-to-leading order bispectrum, we first rewrite the one-loop contributions (6.10)-(6.14) in terms of the absolute values of the external momenta and the loop momentum k, q and l, the parameter μ as well as the angles spanned between the external momenta $\boldsymbol{k}$, $\boldsymbol{q}$ and the loop momentum $\boldsymbol{l}$. Then, we take the large l-limit and remove the angular dependence with respect to the loop momentum by averaging over the respective angles afterwards. The resulting expressions for the one-loop bispectrum contributions are given in Appendix A.1.

Based on the one-loop bispectrum contributions involving the UV limit of the loop integrals, which possess a structure that allows for comparison with other methods, we can now deduce an angular-averaged consistency relation for the one-loop bispectrum in the soft limit. For

this purpose, we perform a series expansion of the expressions (A.2)-(A.5) about the soft mode q, take the squeezed limit $q \to 0$ and finally perform the angular average with respect to μ. As a result, we obtain four angular-averaged expressions for the one-loop contributions in the soft limit (see (A.7)-(A.8)),[2]

$$B_{111}^{(222)}(\boldsymbol{k}, -\boldsymbol{q}, \boldsymbol{q} - \boldsymbol{k}, \eta)^{\text{av}} \xrightarrow{q \to 0} 0,$$

$$B_{111}^{(321,I)}(\boldsymbol{k}, -\boldsymbol{q}, \boldsymbol{q} - \boldsymbol{k}, \eta)^{\text{av}} \xrightarrow{q \to 0} P^L(q, \eta) (2\pi)^3 \frac{k^4}{\pi^2} \gamma^{\text{SPT}} \int dl \, l^2 \left(\frac{P^L(l, \eta)^2}{l^4} \right),$$

$$B_{111}^{(321,II)}(\boldsymbol{k}, -\boldsymbol{q}, \boldsymbol{q} - \boldsymbol{k}, \eta)^{\text{av}} \xrightarrow{q \to 0} P^L(q, \eta) (2\pi)^3 \frac{k^2}{\pi^2} \left(\alpha_1^{\text{SPT}} k \, \partial_k + \beta_1^{\text{SPT}} \right) P^L(k, \eta) \int dl \, l^2 \left(\frac{P^L(l, \eta)}{l^2} \right),$$

$$B_{111}^{(411)}(\boldsymbol{k}, -\boldsymbol{q}, \boldsymbol{q} - \boldsymbol{k}, \eta)^{\text{av}} \xrightarrow{q \to 0} P^L(q, \eta) (2\pi)^3 \frac{k^2}{\pi^2} \left(\alpha_2^{\text{SPT}} k \, \partial_k + \beta_2^{\text{SPT}} \right) P^L(k, \eta) \int dl \, l^2 \left(\frac{P^L(l, \eta)}{l^2} \right),$$

$$(6.15)$$

where we have defined the coefficients

$$\gamma^{\text{SPT}} = \frac{515}{5292}, \qquad \alpha_1^{\text{SPT}} = \alpha_2^{\text{SPT}} = \frac{61}{3780}, \qquad \beta_1^{\text{SPT}} = -\frac{671}{8820}, \qquad \beta_2^{\text{SPT}} = -\frac{155}{756}. \quad (6.16)$$

According to (6.10), the sum of these contributions gives the angular-averaged soft-limit consistency relation for the next-to-leading order bispectrum in SPT (see (A.9)-(A.10)),

$$B_{111}^{\text{1-loop}}(\boldsymbol{k}, -\boldsymbol{q}, \boldsymbol{q} - \boldsymbol{k}, \eta)^{\text{av}} \xrightarrow{q \to 0} P^L(q, \eta) (2\pi)^3 \frac{k^2}{\pi^2} \left[\left(\alpha^{\text{SPT}} k \, \partial_k + \beta^{\text{SPT}} \right) P^L(k, \eta) \int dl \, l^2 \left(\frac{P^L(l, \eta)}{l^2} \right) \right.$$
$$\left. + \gamma^{\text{SPT}} k^2 \int dl \, l^2 \left(\frac{P^L(l, \eta)^2}{l^4} \right) \right],$$

$$(6.17)$$

where we defined $\alpha^{\text{SPT}} \equiv \alpha_1^{\text{SPT}} + \alpha_2^{\text{SPT}}$ and $\beta^{\text{SPT}} \equiv \beta_1^{\text{SPT}} + \beta_2^{\text{SPT}}$. Hence, the three characteristic coefficients parameterizing the bispectrum consistency relation at one-loop order in SPT are

$$\alpha^{\text{SPT}} = \frac{61}{1890} \simeq 0.032, \qquad \beta^{\text{SPT}} = -\frac{3719}{13230} \simeq -0.281, \qquad \gamma^{\text{SPT}} = \frac{515}{5292} \simeq 0.097. \quad (6.18)$$

In the following, we use the values of these coefficients as a benchmark for comparing predictions of different methods for the soft limit of the bispectrum at next-to-leading order. This will allow us to evaluate the validity of each attempt to extend the equal-time bispectrum consistency relation (6.9) beyond linear order.

---

[2]Note that in this work, the Fourier conventions we use, as given in (1.6), differ from those applied in [1]. In comparison to [1], the results presented here contain an additional factor $(2\pi)^3$.

6. Bispectrum Consistency Conditions

For later use, let us in addition calculate the next-to-leading order contribution to the power spectrum of density as well as velocity fluctuations, $P_{ab}^{1-\text{loop}}(k, \eta)$, in SPT in the limit of large loop momentum. The one-loop contribution to the power spectrum, given in (4.19)-(4.21), consists of two terms which are graphically represented by the diagrams in Figure 4.5. To compute the UV limit of the loop integrals entering in these terms, we assume the loop momentum l to be much larger than the external momentum k, i.e., $l \gg k$, remove the angular dependence of the two momenta by angular averaging and finally take the limit of large loop momentum. The resulting expression for the one-loop power spectrum in the limit of large loop momentum reads

$$P_{ab}^{1-\text{loop}}(k, \eta) = \begin{pmatrix} \frac{9}{196} & \frac{19}{588} \\ \frac{19}{588} & \frac{61}{980} \end{pmatrix} (2\pi)^3 \frac{k^4}{\pi^2} \int dl \, l^2 \left(\frac{P^L(l, \eta)^2}{l^4} \right)$$
$$- \begin{pmatrix} \frac{61}{630} & \frac{25}{126} \\ \frac{25}{126} & \frac{3}{10} \end{pmatrix} (2\pi)^3 \frac{k^2 P^L(k, \eta)}{\pi^2} \int dl \, l^2 \left(\frac{P^L(l, \eta)}{l^2} \right). \quad (6.19)$$

We can use this expression as a direct probe to explore the existence and the validity of equal-time bispectrum consistency relations at next-to-leading order. For a first study in this direction, let us consider the time-flow approach in what follows.

6.2.2. Soft limit of the bispectrum in the time-flow approach

In this section, we use the time-flow formalism, which was developed in [156], to set up bispectrum consistency relations in the soft limit. The time-flow approach, which we have introduced in Section 5.5, relies on the flow equations composing an infinite hierarchy of evolution equations (see (5.39)). In order to close the infinite set of equations and to derive perturbative statements, the time-flow approach generally requires a truncation of the hierarchy at a certain level, that is, a 'closure approximation'. In the literature, this closure approximation usually consists in neglecting the connected part of the four-point correlation function, the trispectrum, as denoted in (5.42). Although it is generally possible to derive soft-limit consistency relations from the time-flow approach, the 'closure' approximation plays an important role for assessing the validity of such a consistency relation, as we show in the following.

Bispectrum consistency conditions

If we close the infinite hierarchy of flow equations (5.39) by neglecting the trispectrum, as in (5.42), the closed system of evolution equations can be formally solved. The formal solution for the bispectrum $B_{abc}(\boldsymbol{k}, -\boldsymbol{q}, \boldsymbol{q} - \boldsymbol{k}, \eta)$ is then given by (5.46).

Provided the closure approximation holds, we can use this formal solution for the bispectrum as a starting point to derive an angular-averaged bispectrum consistency relation in the soft limit. In contrast to the derivation in SPT, where we have restricted our considerations to the bispectrum of density fluctuations, $B_{111}(\mathbf{k}, -\mathbf{q}, \mathbf{q} - \mathbf{k}, \eta)$, we do not specify the fluctuation fields composing the bispectrum here and treat the bispectrum in its general form, $B_{abc}(\mathbf{k}, -\mathbf{q}, \mathbf{q} - \mathbf{k}, \eta)$. In addition, while we have derived the bispectrum consistency relations in SPT under the assumption of an EdS universe, the time-flow approach allows in principle for a determination of consistency conditions without specifying the background cosmology and thus for general classes of cosmological models (for details of treating different cosmologies in the time-flow approach see [156]). Taking these points into account, the derivation of consistency relations from the time-flow approach provides a generalization of the computation we performed in the last section in the context of SPT.

The only assumption we rely on for the derivation of the bispectrum consistency relations in the following is the one of Gaussian initial conditions. Due to the Wick theorem, which we discussed in Section 4.3.1, this implies that the initial bispectrum vanishes, $B_{abc}(\mathbf{k}, -\mathbf{q}, \mathbf{q} - \mathbf{k}, \eta_0) = 0$. Consequently, the formal integral solution of the flow equation for the bispectrum, (5.46), simplifies to

$$
\begin{aligned}
B_{abc}(\mathbf{k}, -\mathbf{q}, \mathbf{q} - \mathbf{k}, \eta) = 2 \int_{\eta_0}^{\eta} d\eta' \, g_{ad}(\eta, \eta') \, g_{be}(\eta, \eta') \, g_{cf}(\eta, \eta') \\
\times \Big[\, \gamma_{dgh}(-\mathbf{k}, -\mathbf{q}, \mathbf{q} - \mathbf{k}) \, P_{eg}(q, \eta') \, P_{fh}(|\mathbf{q} - \mathbf{k}|, \eta') \\
+ \gamma_{egh}(-\mathbf{q}, \mathbf{q} - \mathbf{k}, -\mathbf{k}) \, P_{fg}(|\mathbf{q} - \mathbf{k}|\eta') \, P_{dh}(q, \eta') \\
+ \gamma_{fgh}(\mathbf{q} - \mathbf{k}, -\mathbf{k}, -\mathbf{q}) \, P_{dg}(k, \eta') \, P_{eh}(q, \eta') \, \Big].
\end{aligned}
\tag{6.20}
$$

Notice that if we assume an EdS background cosmology and growing-mode initial conditions for computing the linear bispectrum from this equation, we can replace the power spectra by the linear power spectra according to (4.16), $P_{ab}^L(k, \eta) = u_a u_b P^L(k)$ with $u_a \equiv (1, 1)$. In this case, it becomes directly obvious from the recursion relations (3.78) with (3.76) in the diagrammatic formulation of SPT that we can rewrite the bispectrum relation above in terms the kernels $\mathcal{F}_a^{(2)}(\mathbf{q}_1, \mathbf{q}_2, \eta)$ and $\mathcal{F}_a^{(2)}(\mathbf{q}_1, \eta)$ with $\mathbf{q}_1, \mathbf{q}_2 \in \{\mathbf{k}, -\mathbf{q}, \mathbf{q} - \mathbf{k}\}$. For the assumption of an EdS cosmology and growing-mode initial conditions, these kernels are explicitly given in (3.79). As a consequence, we reobtain exactly the linear SPT bispectrum, in the diagrammatic formulation and for density perturbations only (see (4.28) and (6.6)), from the time-flow approach by imposing these assumptions. However, note that the results from SPT and from the time-flow approach only agree for the bispectrum at leading order and for the power spectrum up the next-to-leading order, as discussed in Section 5.5.3. We address this

point in more detail below.

Let us now determine an angular-averaged soft-limit consistency relation from the bispectrum relation in (6.20). We proceed analogously as in the derivation in SPT we performed in the last section. This means that we have to expand all quantities in (6.20) which depend on the difference between the soft and the hard mode, $|\boldsymbol{q} - \boldsymbol{k}|$ with $q \ll k$, in a perturbative series up to first order in q.

Equivalently to the second term of the linear SPT bispectrum in (6.6), which vanishes in the soft limit due to the linear q-dependence of the series expansion of the respective kernel (see the discussion below (6.6)), we can already neglect the second term of the bispectrum (6.20) at this stage since the series expansion of the vertex function $\gamma_{egh}(-\boldsymbol{q}, \boldsymbol{q} - \boldsymbol{k}, -\boldsymbol{k})$ with $e, g, h \in \{1, 2\}$ only generates terms linear in q. The definition of the vertex functions γ_{abc} is given in (3.53). If we then insert the series expansion of the power spectrum (see (6.21)),

$$P_{ab}(|\boldsymbol{q} - \boldsymbol{k}|, \eta) \simeq P_{ab}(k, \eta) - q\,\mu\,\partial_k P_{ab}(k, \eta) + \mathcal{O}(q^2) \tag{6.21}$$

into the bispectrum relation (6.20) (with μ defined in (6.7)), we can summarize the resulting expression as

$$B_{abc}(\boldsymbol{k}, -\boldsymbol{q}, \boldsymbol{q} - \boldsymbol{k}, \eta) = 2 \int_{\eta_0}^{\eta} d\eta'\, g_{ad}(\eta, \eta')\, g_{be}(\eta, \eta')\, g_{cf}(\eta, \eta')\, P_{eh}(q, \eta')$$

$$\times \left[\gamma_{dhg}(-\boldsymbol{k}, \boldsymbol{q} - \boldsymbol{k}, -\boldsymbol{q}) \Big(P_{fg}(k, \eta') - \mu\, q\, \partial_k P_{fg}(k, \eta') \Big) + \gamma_{fgh}(\boldsymbol{q} - \boldsymbol{k}, -\boldsymbol{k}, -\boldsymbol{q})\, P_{dg}(k, \eta') \right]. \tag{6.22}$$

After performing a series expansion of the remaining γ-vertices about the soft mode q (see (3.53)) and taking the squeezed limit $q \to 0$ afterwards, the expression within the bracket in (6.22) can be rewritten in the form

$$\Bigg[\delta_{h1} \Big(M_{dg}^A P_{gf}(k, \eta') + P_{dg}(k, \eta')\, M_{gf}^A \Big)$$
$$+ \delta_{h2} \Big(M_{dg}^B P_{gf}(k, \eta') + P_{dg}(k, \eta')\, M_{gf}^B - \frac{1}{2}\big(1 + \mu^2\, k\, \partial_k\big) P_{df}(k, \eta') \Big) \Bigg], \tag{6.23}$$

where we have defined the matrices

$$M^A = \begin{pmatrix} 0 & \frac{1}{2} \\ 0 & 0 \end{pmatrix}, \qquad M^B = \begin{pmatrix} \frac{1}{2} & 0 \\ 0 & \mu^2 \end{pmatrix}. \tag{6.24}$$

Next, we perform the angular average to remove the dependence on μ. Moreover, we make the reasonable approximation to replace the power spectrum of the soft, long-wavelength mode, $P_{ab}(q, \eta)$, by its linear contribution $P_{ab}^L(q, \eta)$. According to (4.16), this approximation reduces under the assumption of growing-mode initial conditions to

$$P_{ab}(q, \eta) \simeq u_a u_b\, P^L(q, \eta). \tag{6.25}$$

By inserting this linear approximation for the power spectrum in the angular-averaged soft-limit bispectrum relation resulting from (6.22) with (6.24), we finally obtain the following consistency relation based on the time-flow approach

$$
B_{abc}(\boldsymbol{k}, -\boldsymbol{q}, \boldsymbol{q} - \boldsymbol{k}, \eta)^{\mathrm{av}} \xrightarrow{q \to 0} u_b \, P^L(q, \eta) \int_{\eta_0}^{\eta} d\eta' \, g_{ad}(\eta, \eta') \, g_{cf}(\eta, \eta') \, e^{-2(\eta - \eta')}
$$
$$
\times \left[M_{dg}^{\mathrm{av}} \, P_{gf}(k, \eta') + P_{dg}(k, \eta') \, M_{gf}^{\mathrm{av}} - \left(1 + \frac{1}{3} k \, \partial_k \right) P_{df}(k, \eta') \right].
$$
(6.26)

Here, the exponential factor in the first line of the equation above arises from moving the linear power spectrum $P^L(q, \eta) = e^{2(\eta - \eta_0)} P_0(k)$, as defined in (4.17), outside of the integral (see (6.22)). By performing the angular average, we can summarize the contributions of the matrices M^A and M^B in (6.24) by the matrix

$$
M^{\mathrm{av}} = 2 \left[M^A + M^B \right]^{\mathrm{av}} = \begin{pmatrix} 1 & 1 \\ 0 & \frac{2}{3} \end{pmatrix}.
$$
(6.27)

At this point, we would like to emphasize the generality of the bispectrum consistency relation (6.26) derived from the time-flow approach. Up to here, we neither specified the background cosmological model, the kind of fluctuation fields composing the bispectrum nor did we perform any perturbative loop expansion of correlation functions.

Leading order

In order to compare the predictions of the bispectrum consistency relations based on the time-flow approach, (6.26), with the ones obtained in SPT (see (6.9) and (6.17)), let us assume an EdS background cosmology in what follows. In the EdS case, the explicit form of the linear propagator $g_{ab}(\eta, \eta')$ is given by (3.68)-(3.69). Moreover, we rely on the assumption of growing-mode initial conditions so that the linear power spectrum $P_{ab}^L(k, \eta)$ arises as (4.16).

To determine the leading order of the angular-averaged soft-limit consistency relation for the bispectrum in (6.9) in the EdS case, we replace the power spectra with respect to the hard mode k by their linear contribution, $P_{ab}(k, \eta) \simeq P_{ab}^L(k, \eta)$, in analogy to (6.25). Since then the time dependence of the linear propagator and the power spectra is known, it is possible to perform the integration over time in (6.9). Thereby, we choose the initial time to be $\eta_0 = 0$. The resulting consistency relation for the bispectrum at leading order,

$$
B_{abc}^L(\boldsymbol{k}, -\boldsymbol{q}, \boldsymbol{q} - \boldsymbol{k}, \eta)^{\mathrm{av}} \xrightarrow{q \to 0} P^L(q, \eta) \, u_b \left[\frac{1}{21} \begin{pmatrix} 47 & 39 \\ 39 & 31 \end{pmatrix}_{ac} - \frac{1}{3} u_a u_c \, k \, \partial_k \right] P^L(k, \eta) , \quad (6.28)
$$

coincides with the SPT prediction for the component describing the linear bispectrum of density perturbations, $B_{111}^L(\boldsymbol{k}, -\boldsymbol{q}, \boldsymbol{q} - \boldsymbol{k}, \eta)_{q \to 0}^{\mathrm{av}}$, in (6.9) and thus also reproduces the result

in the literature [166]. However, at the same time, the bispectrum consistency relation (6.28) derived from the time-flow approach constitutes a generalization of [166]. It is restricted not only to the bispectrum of density perturbations, but also comprises the bispectra including velocity fluctuation fields. Note that in addition, the linearized form of the bispectrum relation in (6.26) is valid for general background cosmologies. To evaluate this relation for cosmological models other than EdS, it is only required to choose the corresponding linear propagator (for details see [156]).

While the angular-averaged consistency relation for the linear bispectrum in the soft limit, as given in (6.28), constitutes a generalization of the result in the literature [166], which is restricted to the bispectrum of density perturbations, our actual motivation is to derive soft-limit relations that are valid non-perturbatively. The bispectrum consistency relation (6.26), however, is derived from the time-flow approach and thus relies on the closure approximation. While neglecting the trispectrum is a suitable closure approximation at linear order, this is not clear to be a reasonable approach holding beyond leading order or even at the non-perturbative level. In fact, the trispectrum obeys an evolution equation that cannot be consistently set to zero at all times, although this is usually done for closing the hierarchical system of flow equations (see [156]). Due to this, it is important to analyze the extent of non-linear information captured by the bispectrum consistency relation based in the time-flow approach in (6.26).

Next-to-leading order

To address this issue, we compute the angular-averaged soft-limit consistency relation for the next-to-leading order bispectrum from the time-flow approach and compare it to the corresponding relation in SPT (see (6.17)). We continue working under the assumptions of an EdS universe and growing-mode initial conditions. As discussed in Section 5.5.3, in this case the one-loop power spectrum in SPT and the time-flow approach are equivalent. This means that we can use the one-loop SPT power spectrum in the limit of large loop momentum, given in (6.19), to approximate the power spectra with respect to the hard mode k contained in the bispectrum consistency relation (6.26), $P_{ab}(k, \eta) \simeq P_{ab}^{1-\mathrm{loop}}(k, \eta)$, in order to evaluate the consistency relation for the bispectrum at next-to-leading order. Afterwards, we read off the characteristic coefficients parameterizing the bispectrum at one-loop order in the time-flow approach from the resulting expression, analogously as in (6.17),

$$\alpha^{\mathrm{TF}} = \frac{103}{6930} \simeq 0.015 \,, \qquad \beta^{\mathrm{TF}} = -\frac{233}{1890} \simeq -0.123 \,, \qquad \gamma^{\mathrm{TF}} = \frac{271}{19404} \simeq 0.014 \,. \qquad (6.29)$$

By comparing the characteristic parameters obtained in the time-flow approach to those in SPT that are denoted in (6.18), we find that their values differ significantly from each other.

Since neglecting the trispectrum as a closure approximation has been the only assumption on which the derivation of the bispectrum consistency relation (6.26) relies, the difference of the coefficients leads to the clear conclusion that the trispectrum cannot be ignored for deriving a consistency relation for the bispectrum beyond linear order in perturbation theory. Hence, we have explicitly demonstrated that, for an EdS cosmology, the angular-averaged consistency relations for the bispectrum in the soft limit based on the time-flow approach are only fulfilled at linear order, but fail to capture the non-linear information at next-to-leading order.

Note that the procedure we applied in the time-flow approach to derive an angular-averaged soft-limit consistency relation for the bispectrum can be easily generalized to determine a consistency relation for connected $\mathcal{N}$-point correlation functions, as defined in (4.9), which include a large number of fields. This requires to truncate the hierarchy of flow equations at the level of the connected part of $\mathcal{N}'$-point correlator with $\mathcal{N} \leq \mathcal{N}'$. Although this can be successfully done in perturbation theory, the corresponding closure approximation would still fail to fully capture the non-perturbative physics.

Apart from this, an attempt at including the information from the trispectrum to improve the predictions for the power spectrum in the time-flow approach appeared in [349]. The results therein suggest that the trispectrum contributions to the power spectrum is non-negligible already in the mildly non-linear regime. Despite this, one could have hoped that the trispectrum was less relevant for the bispectrum in the soft limit so that the equal-time bispectrum consistency relations based on the time-flow approach may be approximately accurate. Unfortunately, the large deviations between the predictions for the one-loop bispectrum in the soft limit derived in SPT and from the time-flow approach indicate that this is not the case. Including the trispectrum and truncating the infinite hierarchy of flow equations at a higher-order level, would in principle allow to reproduce the one-loop SPT result for the bispectrum in the soft limit with the time-flow approach. However, as argued before, the latter would then nevertheless fail at some given loop order depending on the truncation. Thus, a truly non-perturbative result for an equal-time consistency condition using the time-flow formalism seems out of reach.

Although the perturbative relations between equal-time correlation functions in the soft limit based on the time-flow approach do not hold up the same status as the unequal-time consistency relations derived in Section 6.1, they may still be useful in special circumstances where the short modes are kept in the mildly non-linear regime. The perturbative relations of the time-flow approach are, for instance, well suited to study baryon acoustic oscillations in a background cosmology which requires numerical input, such as models including massive neutrinos or quintessence. Since the time-flow approach, unlike SPT, only deals with equal-time correlation functions such that soft effects cancel out from the outset, the perturbative

time-flow relations for equal-correlations functions in the soft limit may improve numerical stability and simplify the computational treatment of the fluctuations.

6.3. Background method for a spherically symmetric soft mode

We now present an alternative, non-perturbative approach to derive angular-averaged equal-time consistency relations in the soft limit. This approach is inspired by the proposal for equal-time consistency conditions in [173] and [174], and based on ideas introduced in [165, 166].

In [165, 166], a background method is studied which implements a map between the dynamics on short distance scales within a flat FRW universe in the presence of a soft, long-wavelength perturbation and a locally curved FRW cosmology. Thereby, the soft mode is absorbed into the locally curved background. In the context of N-body simulations, this method is referred to as the so-called 'separate universe' approach [238–241] and used to compute the power spectrum response function, which we introduce in Section 7.4.3.

6.3.1. Perturbed FRW metric in the Newtonian gauge

In order to establish the background method which provides a mapping from a flat FRW background cosmology in the presence of a long-wavelength perturbation to a locally curved FRW cosmology, let us consider the metric of a perturbed FRW universe in the so-called Newtonian gauge as a basis of the following calculations.

In the general relativistic framework of cosmological perturbation theory, one studies linear perturbations to the metric of a spatially flat FRW background cosmology. These metric perturbations are related to perturbations of the stress energy tensor via the Einstein equations and thus to the matter density perturbations. The symmetries of the flat FRW cosmology allow to decompose the metric perturbations into independently evolving scalar, vector and tensor components. Since the growth of structures is predominantly affected by the scalar metric perturbations, we focus on these scalar modes here. It is beyond the scope of this thesis to discuss the relativistic the theory of cosmological perturbations. Instead, we refer to [272, 284] for details.

Due to the gauge invariance of general relativity, certain combinations of metric perturbations and in particular physical observables are invariant under a change of coordinates by gauge transformations. In case of scalar metric perturbations, one uses this gauge freedom of general relativity to eliminate two scalar degrees of freedom of the perturbed FRW metric. A particularly simple gauge to use for the scalar metric perturbations is the so-called Newtonian gauge, introduced in [272], where the perturbations to the flat FRW cosmology are

characterized by two scalar potentials, $\Psi(\boldsymbol{x}, t)$ and $\Phi(\boldsymbol{x}, t)$,

$$ds^2 = -\big[1 + 2\,\Phi(\boldsymbol{x}, t)\big]dt^2 + a^2(t)\big[1 - 2\,\Psi(\boldsymbol{x}, t)\big]d\boldsymbol{x}^2\,. \tag{6.30}$$

Note that we here use $\boldsymbol{x}$ and t to denote the physical coordinates.

The name 'Newtonian gauge' originates from the fact that in the non-relativistic Newtonian limit, the potential $\Phi(\boldsymbol{x}, t)$ in the perturbed Einstein equations can be interpreted as the gravitational potential of classical Newtonian gravity [27]. We defined the Newtonian gravitational potential in (2.14). In the Newtonian limit, where the expansion of the Universe can be neglected, the potential $\Phi(\boldsymbol{x}, t)$ fulfills the (perturbed) Poisson equation [92, 272] for non-relativistic matter (see (2.21) and (2.22)),

$$\nabla^2 \Phi(\boldsymbol{x}, t) = 4\pi G a^2 \left(\rho - \bar{\rho}\right) = \frac{3}{2}\Omega_m\, a^2 H^2\, \delta\,. \tag{6.31}$$

The second scalar potential $\Psi(\boldsymbol{x}, t)$ is often referred to as curvature perturbation. In case of a universe with vanishing anisotropic stress, that is, if the stress-energy tensor is invariant under spatial rotations, the two scalar potentials are equal

$$\Psi(\boldsymbol{x}, t) = \Phi(\boldsymbol{x}, t)\,. \tag{6.32}$$

6.3.2. Newtonian mapping

Based on the perturbed FRW metric in Newtonian gauge in (6.30), our aim is to set up the background method in the following. Thereby, the calculations we perform are closely related to the analysis in [165, 166], where further details can be found. However, we present here a straightforward and shortened derivation of the relevant transformations in the background method which does, in contrast [165, 166], not rely on introducing so-called Fermi coordinates [367–369], but directly matches a flat FRW cosmology in the presence of a soft mode to a locally curved universe.

As a starting point for the derivation of the background method, let us consider a flat FRW background cosmology in global coordinates which includes a linear long-wavelength perturbation denoted by $\Phi^L(\boldsymbol{x}, t)$. Since we intend to study the properties of large-scale structure correlation functions mainly in the regime where the soft, long-wavelength mode is linear, we assume that there is no anisotropic stress at the linear level. According to (6.32), this implies that the two scalar potentials are equivalent so that the perturbed FRW metric in Newtonian gauge reads (see (6.30))

$$ds^2 = -\big[1 + 2\Phi^L(\boldsymbol{x}, t)\big]dt^2 + a^2(t)\big[1 - 2\Phi^L(\boldsymbol{x}, t)\big]d\boldsymbol{x}^2\,. \tag{6.33}$$

6. Bispectrum Consistency Conditions

As discussed in Section 2.1.2, large-scale structure formation on sub-horizon scales, on which $(aH)/k \ll 1$, can be described in the Newtonian limit of cosmological perturbation theory. Due to this, we assume that the soft mode $\Phi^L(\boldsymbol{x}, t)$ is sufficiently far inside the horizon so that the Newtonian approximation holds for it as well. In the Newtonian limit, $\Phi^L(\boldsymbol{x}, t)$ fulfills the Poisson equation (6.31) and is thus related to the linear density contrast δ^L. If we assume here, in contrast to Section 7.2 where we discuss the case of a directional long-wavelength perturbation, that the soft mode is spherically symmetric, we can determine its explicit form from (6.31),

$$\Phi^L(\boldsymbol{x}, t) \simeq \frac{1}{4}\Omega_m\, a^2 H^2 \delta^L\, \boldsymbol{x}^2 \ll 1\,. \tag{6.34}$$

Notice that in the derivation of this relation we have neglected the spatial dependence of the linear density contrast by assuming $\delta^L(\boldsymbol{x}, t) \ll 1$. Moreover, we have not included the constant and gradient contributions to the perturbation $\Phi^L(\boldsymbol{x}, t)$ here. This is because these pieces can be removed by performing a coordinate transformation to a free-falling frame, as shown in [169, 170]. In fact, such a transformation also leads to the unequal-time consistency relations we (re-)derived in Section 6.1. However, we only deal with the quadratic part of the potential, $\Phi^L(\boldsymbol{x}, t) \propto \boldsymbol{x}^2$ here, since we are in the *physical* squeezed limit of the correlations functions (see [165]).

Our next step consists in determining the coordinate transformation which provides the essence of the background method by mapping the flat FRW metric (6.33) with a soft and spherically symmetric perturbation of the form (6.34) to an unperturbed, locally curved FRW cosmology. To derive the form of this map, we make the following ansatz for the coordinate transformation

$$t = t_K + f(t_K, \boldsymbol{x}_K)\,, \qquad \boldsymbol{x} = \boldsymbol{x}_K\left[1 + g(t_K, \boldsymbol{x}_K)\right]\,, \tag{6.35}$$

where we have denoted the coordinates of the locally curved FRW cosmology by t_K and $\boldsymbol{x}_K$ and introduced the coordinate-dependent functions $f(t_K, \boldsymbol{x}_K)$ and $g(t_K, \boldsymbol{x}_K)$. The latter have to be determined such that they provide a transformation to a locally curved FRW cosmology with a metric (in isotropic coordinates) given by

$$ds^2 = -dt_K^2 + a_K^2(t_K)\frac{d\boldsymbol{x}_K^2}{\left(1 + \frac{1}{4}K\boldsymbol{x}_K^2\right)^2} \tag{6.36}$$

with K indicating the local curvature. Since we intend to study a *locally* curved background cosmology, we only have to assume that the change of coordinates defined in (6.35) is locally valid at small distances. Consequently, we can treat the functions $f(t_K, \boldsymbol{x}_K)$ and $g(t_K, \boldsymbol{x}_K)$ as small corrections and perform a series expansion about them in order to transform the perturbed, flat FRW metric (6.33) into the locally curved one in the previous equation.

If we use the change of coordinates (6.35) to transform the metric in (6.33) into the one given in (6.36), we deduce by comparison of the time-time components of the two metrics that

$$\dot{f} = -\Phi^L \,, \tag{6.37}$$

where the dot denotes the derivative with respect to the time variable t here, $\dot{f} \equiv \partial f / \partial t$. Moreover, since the time-space parts in both metrics vanish, we obtain in addition the relation

$$a^2 \, \dot{g} \, \boldsymbol{x} = \nabla f \tag{6.38}$$

with the gradient taken with respect to $\boldsymbol{x}$, $\nabla \equiv \nabla_{\boldsymbol{x}}$. Notice that based on the assumption $\Phi^L \ll 1$ (see (6.34)), the last two equations are valid provided $\delta^L \ll 1$ and $H^2 \boldsymbol{x}^2 \ll 1$, such that $f \propto \boldsymbol{x}^2$ and $g \propto \boldsymbol{x}^0$. If these constraints are not fulfilled, spatial gradients of the linear density contrast arise in the coordinate transformation and the analysis has to be modified. However, the restriction to this particular subclass of soft and spherically symmetric perturbations is suitable and sufficient for our purpose to study the soft limit of correlation functions.

Moreover, the change from global to local time coordinates according to (6.35) leads to a transformation of the time-dependent scale factor $a(t)$ as well. It arises as

$$a(t) = a(t_K) \, (1 + H \, f) \tag{6.39}$$

and contributes to the curvature K in the locally curved FRW cosmology. By transforming the space-space components of the metrics (6.33) and (6.36) into each other, we furthermore find the relations

$$a_K(t_K) \equiv \ a(t_K) \, (1 + g) \,, \qquad K \, \boldsymbol{x}_K^2 \equiv \ 4\Phi^L + 4H \int dt \, \Phi^L \,. \tag{6.40}$$

These provide the final constituents to transform the perturbed, flat FRW metric (6.33) into the unperturbed, locally curved one of (6.36). By using the expressions (6.34), (6.38) and (6.40) which arise in this transformation, we can furthermore deduce that the Hubble parameter in the locally curved FRW cosmology reads

$$H_K \equiv \frac{\dot{a}_K}{a_K} \simeq H + \dot{g} = H - \frac{1}{2a^2} \int dt \, \Omega_m \, a^2 H^2 \, \delta^L \,. \tag{6.41}$$

In order to be able to compare the predictions of these results for soft-limit consistency conditions to those derived in the framework of SPT and the time-flow approach in the Sections 6.2.1 and 6.2.2, we restrict ourselves henceforth to an EdS cosmology describing a flat universe containing matter only. Thus, we set $\Omega_m = 1$ in the following (see Section 3.1.1). Moreover, we

can use the fact that the Hubble parameter and the growing mode of the linear density contrast in the EdS case scale like $H \propto a^{-3/2}$ and $\delta^L \propto a$ (see (3.16) and (3.11) with (3.17)), to determine the explicit form of the Hubble parameter H_K, the scale factor a_K and the curvature K in the locally curved universe. Note that the integrand in the relation (6.41) for the Hubble parameter H_K is approximately constant in time. For the calculation of the scale factor a_K as given in (6.40), we first need to compute the coordinate-dependent function g from (6.38) and thus also the function f by use of (6.37) and (6.34). In the EdS case, these are given by

$$f = -\frac{1}{6}\,H_0\,a^{1/2}\,\delta^L\,\boldsymbol{x}^2\,, \qquad g = -\frac{1}{3}\delta^L\,. \tag{6.42}$$

Based on this, we obtain for the Hubble parameter, the scale factor and the curvature in the locally curved EdS universe the following expressions,

$$H_K \;\simeq\; H\left(1-\frac{1}{3}\delta^L\right)\,, \tag{6.43}$$

$$a_K \;\simeq\; a\left(1-\frac{1}{3}\delta^L\right)\,, \tag{6.44}$$

$$K \;\simeq\; \frac{5}{3}H^2 a^2 \delta^L\,. \tag{6.45}$$

Next, let us discuss the implications of these results. If we, for instance, express the matter density parameter (2.8) of the locally curved cosmology as $\Omega_{m,K} = (a_K^3\,H^2)/(a^3 H_K^2)$ by taking into account that the mean density in a matter-dominated (EdS) universe scales like $\bar{\rho} \propto a^{-3}$, we can rewrite the first Friedmann equation in (2.9) for the locally curved system as

$$H_K^2 = H^2 \frac{a^3}{a_K^3} - \frac{K}{a_K^2}\,. \tag{6.46}$$

We find that the results (6.43)-(6.45) fulfill this equation. In total, we deduce that the relations we derived for the locally curved cosmology are consistent with the corresponding Friedmann equations.

Besides, it is worth pointing out that the mean density in the locally curved universe, i.e., $\bar{\rho}_K$, is bigger than in a flat one,

$$\bar{\rho}_K = \bar{\rho}\,\frac{a^3}{a_K^3} \simeq \bar{\rho}\left(1+\delta^L\right)\,, \tag{6.47}$$

where we used (6.44). However, this is not the case for the physical Hubble H_K, as given in (6.43), since the curvature over-compensates the density increase.

6.3.3. Non-perturbative bispectrum consistency condition

Based on the mapping from a flat FRW cosmological model in the presence of long-wavelength perturbation to a locally curved FRW cosmology that we discussed in the last section and that

led to the relations (6.44)-(6.45) in the particular case of an EdS universe, our aim is now to study the imprint of the soft, long-wavelength perturbation on the dynamics of the hard, short-scale modes. The transformation to the locally curved EdS universe will affect the dynamics of the hard modes on the one hand through the change in the spatial coordinates (6.35) by an additional 'contraction' $(1 + g)$, with g given in (6.42), and on the other hand through the modified expansion rate according to (6.44).

For instance, transforming the density contrast of the hard mode in real space, $\delta_K(\boldsymbol{x}_K, a_K)$, to the locally curved EdS universe consequently yields

$$\delta_K(\boldsymbol{x}_K, a_K) = \delta(\boldsymbol{x}, a)\left(1 - \delta^L\right). \tag{6.48}$$

Note that we have expressed the dependence of the density contrast on the time in terms of the scale factor here. In turn, the relation above allows us to derive the corresponding two-point correlation function of the density contrast in real space. This two-point correlation function, which constitutes the real-space equivalent of the power spectrum (see (4.1)), is defined as [40]

$$\xi_{ab}(r, a) \equiv \left\langle \psi_a(\boldsymbol{x}, a)\, \psi_b(\boldsymbol{x} + \boldsymbol{r}, a) \right\rangle. \tag{6.49}$$

Due to statistical homogeneity and isotropy, discussed in Section 4.2, it does not depend on the two different locations $\boldsymbol{x}$ and $\boldsymbol{x} + \boldsymbol{r}$ (in comoving coordinates), but on their separation r only. According to the transformation of the real-space density contrast of the hard mode in (6.48), the respective two-point correlation function of the density contrast, that is,

$$\xi(r, a) \equiv \xi_{11}(r, a) = \left\langle \delta(\boldsymbol{x}, a)\, \delta(\boldsymbol{x} + \boldsymbol{r}, a) \right\rangle, \tag{6.50}$$

according to (6.49), in the presence of a long-wavelength perturbation arises as

$$\begin{aligned}
\xi_{\delta^L}(r, a) &= \left[1 + \delta^L\left(2 + \frac{1}{3}r\partial_r\right)\right]\xi_K(r, a_K)\\
&= \left[1 + \delta^L\left(2 + \frac{1}{3}r\partial_r - \frac{1}{3}\partial_\eta\right)\right]\xi_K(r, a),
\end{aligned} \tag{6.51}$$

where $\xi_K(r, a)$ refers to the two-point correlator of the density contrast in the locally curved system. In the derivation of this equation, we have applied once more the transformation of the spatial coordinates in (6.35), such that $r_K = r(1 - g)$ with $g = -\delta^L/3$ in the EdS case (see (6.42)), and the change of the scale factor as given in (6.40).

Furthermore, the mapping to a locally curved universe entails a different growth of structures since the latter is affected by the curvature. In other words, the linear growth factor in the locally curved system, $D_1(K, a_K)$, has a different form as in the pure flat EdS case where

it simply equals $D_1(K = 0, a) = a$ (see (3.17)). Indeed, we obtain that the linear growth factor in the locally curved EdS cosmology equals

$$
\begin{aligned}
D_1(K, a_K) &\simeq D_1(0, a) + K \frac{d}{dK} D_1(K, a_K)\Big|_{K=0} \\
&= \left(1 + \frac{13}{21}\delta^L\right) D_1(0, a).
\end{aligned}
\tag{6.52}
$$

Equivalently to the linear power spectrum (see (4.16)), the real-space two-point correlation function scales at the linear level like the square of the linear growth factor. Consequently, the different growth of structure in the original (flat) and the locally curved system is taken into account at linear order by the replacement

$$
\xi_K^L(r, a_K) \to \left(1 + 2 \times \frac{13}{21}\delta^L\right) \xi^L(r, a),
\tag{6.53}
$$

where $\xi^L(r, a)$ corresponds to the two-point correlation function in the flat background cosmology without the soft mode.

By combining the prefactors of the expressions (6.51) and (6.53) and correlating the resulting two-point correlation function with δ^L, we can directly determine the real-space three-point correlation function $\langle \xi_{\delta^L}(r, a) \delta^L \rangle$. If we perform the Fourier transform of this quantity afterwards, we obtain the three-point correlation function in Fourier space in the presence of a soft mode. This is exactly the soft limit of the bispectrum at linear order. The resulting expression we derive in this way from the background method,

$$
B_{111}^L(\boldsymbol{k}, -\boldsymbol{q}, \boldsymbol{q} - \boldsymbol{k}, \eta)^{\mathrm{av}} \xrightarrow{q \to 0} P^L(q, \eta) \left(\frac{47}{21} - \frac{1}{3} k\, \partial_k\right) P^L(k, \eta),
\tag{6.54}
$$

coincides completely with the leading-order angular-averaged consistency relations which we calculated in SPT and from the time-flow approach (see (6.9) and (6.28)).

In contrast to SPT and the time-flow formalism being perturbative approaches, the background method we developed in this section is a non-perturbative approach. This means that absorbing a soft perturbation into a locally curved background cosmological constitutes a correct and consistent method also at the non-linear level, as advocated in [165]. Note that this procedure has also been applied, e.g., in [224], to derive a physical squeezed limit for correlation functions in the inflationary case. By following similar steps as in [224], we can thus use the background method to derive a generic, non-perturbative consistency relation for the bispectrum in the soft limit.

In our previous considerations, the only step where we referred to perturbation theory consisted in considering the scaling of the two-point correlation at linear order in (6.53).

Thus, we can simply derive a non-perturbative relation for the bispectrum in the soft limit by using the expression for the two-point correlation function in the equation before (see (6.51)), as well as the relation (6.45) between the local curvature K and the linear density contrast in the EdS case. If we introduce the notation

$$P(k, \eta) \equiv P_{11}(k, \eta) \tag{6.55}$$

for the density-density power spectrum, the background method yields the following non-perturbative consistency relation for the soft limit of the bispectrum of density perturbation in an EdS cosmology,

$$B_{111}(\boldsymbol{k}, -\boldsymbol{q}, \boldsymbol{q} - \boldsymbol{k}, \eta)^{\mathrm{av}} \xrightarrow{q \to 0} P^L(q, \eta) \left[\left(1 - \frac{1}{3} k \, \partial_k - \frac{1}{3} \partial_\eta \right) P(k, \eta) + \frac{5}{3} \frac{\partial}{\partial \kappa} P_K(k, \eta) \Big|_{K=0} \right], \tag{6.56}$$

where $P_K(k, \eta)$ denotes the power spectrum of the density contrast in the presence of (local) curvature. Furthermore, we have defined the curvature parameter

$$\kappa = \frac{K}{a^2 H^2} = \frac{5}{3} \delta^L \tag{6.57}$$

with K given in (6.45). Thereby, the term $\left(1 - \frac{1}{3} k \partial_k \right)$ arising in the non-perturbative bispectrum consistency relation is a combination of two effects, namely, the difference in the density contrast between the flat and the locally curved cosmology plus the shift induced by the displacement term (or equivalently the eikonal phase). Moreover, the contribution $\frac{1}{3} \partial_\eta$ follows from the change in the scale factor.

Although the expression in (6.56) constitutes a generic result for the bispectrum in the soft limit, it does not represent a consistency relation which one would confront against observations, since it depends on the power spectrum $P_K(k, \eta)$ parameterizing the hypothetical case of a curved universe. In addition, the impact of the curvature on the fluctuations and hence on the power spectrum, $\partial P_K(k, \eta) / \partial K$, cannot be readily determined in terms of curvature-dependent quantities at $K = 0$, as for instance done in (6.52), without resorting to numerical simulations of perturbative methods. For instance, one may use N-body simulations in the framework of the so-called 'separate universe' approach [238–241] to determine the derivative with respect to curvature. We take this point up again in Section 7.4. On the other hand, an attempt to replace the variation with respect to curvature by curvature-independent quantities without resorting to numerical simulations or perturbation theory has been presented in [173, 174]. We study this (allegedly non-perturbative) proposal, in particular with regard to its validity beyond perturbation theory, in what follows.

6.4. VKPR proposal of 'equal-time consistency relations'

A proposal by Valageas, as well as by Kehagias, Perrier and Riotto (VKPR) to extend the soft-limit consistency relation for the bispectrum at linear order, that was first derived (in real) space in [166] and that we recovered in SPT, the time-flow approach and the background method (see (6.9), (6.28) and (6.54)), into the non-linear regime appeared in [173] and [174]. These works coined the term (angular-averaged) 'equal-time consistency conditions' for large-scale structure.

In practice, the VKPR proposal consists in replacing each linear growth function for the short modes by the one for a locally curved EdS universe given in (6.52). Thus, in comparison to (6.51), the two-point correlation function in real space in the presence of the soft, long-wavelength mode reads

$$\xi_{\delta^L}^{\text{VKPR}}(r, \eta) = \left[1 + \delta^L \left(2 + \frac{1}{3}r\partial_r + \frac{13}{21}\partial_\eta\right)\right] \xi(r, \eta). \tag{6.58}$$

Note that this relation does not show an explicit dependence on the two-point correlator $\xi_K(r, a)$ of a locally curved system. After correlating $\xi_{\delta^L}^{\text{VKPR}}(r, \eta)$ with the soft mode δ^L and transforming to Fourier space, the resulting consistency relation for the bispectrum in the soft limit is

$$B_{111}^{\text{VKPR}}(\boldsymbol{k}, -\boldsymbol{q}, \boldsymbol{q} - \boldsymbol{k}, \eta)^{\text{av}} \xrightarrow{q \to 0} P^L(q, \eta) \left[2 - \frac{1}{3}(3 + k\,\partial_k) + \frac{13}{21}\partial_\eta\right] P(k, \eta). \tag{6.59}$$

Consequently and in contrast to (6.56), this bispectrum consistency relation does not involve a power spectrum $P_K(k, \eta)$ in the presence of (local curvature).

On the other hand, by comparing the non-perturbative bispectrum consistency condition in (6.56) with the one based on the VKPR proposal in the previous equation, one can rephrase the VKPR proposal as

$$\text{VKPR}: \qquad \frac{\partial}{\partial \kappa} P_K(k, \eta)\bigg|_{K=0} = \frac{4}{7}\partial_\eta P_{K=0}(k, \eta). \tag{6.60}$$

Thus, one can regard it as an attempt to replace the variation of the power spectrum $P_K(k, \eta)$ with respect to curvature by a time derivative of the power spectrum $P_{K=0}(k, \eta)$ in the absence of curvature, i.e., $K = 0$.

6.4.1. VKPR bispectrum consistency relation

In the following, our aim is to assess the validity of the VKPR bispectrum consistency relation (6.59) within and beyond perturbation theory. Let us start by comparing its predictions with the perturbative results we derived for the soft limit of the bispectrum at leading and next-to-leading order in SPT.

Leading order

In order to check the validity of the VKPR bispectrum consistency relation (6.59) at leading order, we replace the density power spectrum of the hard modes, i.e., $P(k, \eta)$, by the respective linear power spectrum. The linear power spectrum of density perturbations is explicitly written down in (4.17). Since its scaling with time is known, $P^L(k, \eta) \propto e^{2\eta}$, we can perform the derivative with respect to η in (6.59). Recall that in the EdS case $\eta = \ln a(\tau)$ (see (3.63)) so that the logarithmic derivative can be understood as a counter. The resulting expression for the bispectrum consistency relation (6.59) at linear order is equivalent to the leading-order prediction for the soft-limit bispectrum in SPT in (6.9), and hence also coincides with the respective linear-order results derived from the time-flow approach in (6.28) and the background method in (6.54). Thus, we can conclude that the VKPR proposal correctly reproduces the bispectrum consistency relation at linear order.

Next-to-leading order

However, the VKPR consistency condition (6.59) is advocated in [173] and [174] as being valid even in the non-linear regime. Hence, it is even more interesting to investigate the validity of this relation beyond linear order. Consequently, our next step consists in confronting the predictions of the VKPR consistency condition at next-to-leading order against the corresponding results in SPT. In order to do so, we insert the one-loop SPT power spectrum (6.19) on the right-hand side of the VKPR relation (6.59). After bringing the resulting expression into a form analogous to (6.17), we can compare the one-loop coefficients that emerge from the VKPR proposal,

$$\alpha^{\text{VKPR}} = \frac{61}{1890} \simeq 0.032 \,, \qquad \beta^{\text{VKPR}} = -\frac{3599}{13230} \simeq -0.272 \,, \qquad \gamma^{\text{VKPR}} = \frac{135}{1372} \simeq 0.098 \,, \tag{6.61}$$

to those in SPT, given in (6.18). We find that the VKPR coefficients overall differ from those in SPT. Nonetheless, we observe that $\alpha^{\text{VKPR}} = \alpha^{\text{SPT}}$. Note that this must, however, be the case since this coefficients originates from the eikonal phase in (6.1), which we argued is universal (see Section 6.1.1).

6.4.2. Validity of the VKPR proposal

From our previous considerations in the context of the background method, in particular in Section 6.3.3 where we discussed the transformations of correlation functions to account for the impact of a soft mode, it is clear that the subtle step on which the VKPR consistency

6. Bispectrum Consistency Conditions

condition is based is the replacement

$$\xi_K^{\text{VKPR}}(r, a_K) = \left(1 + \frac{13}{21}\delta^L\,\partial_\eta\right)\xi(r, a)\,.\tag{6.62}$$

In detail, this substitution aims at generalizing the linear-order relation (6.53) to the non-linear level. However, as we have explicitly shown by the comparison of the one-loop VKPR and SPT coefficients, it is not valid beyond leading order even for an EdS cosmological model. The reason for this is that the replacement (6.62) does not capture the full impact of the soft perturbation, which is relevant for a consistent description of the dynamics of the hard modes.

We can already identify the seed of the failure to capture the full relevant dynamics directly in the perturbative expansion of the density field, even before performing the correlation with the soft mode. As discussed in [165], we can use the framework of SPT to expand the density contrast $\delta(\mathbf{k}, \eta)$, according to (3.30) with (3.31), in a perturbative series up to a given order, determine its soft limit and perform a Fourier transform to real space. After correlating the series expansion of the density contrast to obtain the real-space two-point correlation function and subsequently the bispectrum in the presence of a soft mode, we can then compare the resulting expressions order-by-order with the VKPR relations in (6.58) and (6.59). Based on SPT and following [166], we can write the perturbative expansion of the density contrast in real space in the presence of a soft mode, $\delta_{\delta L}^S(\mathbf{x}, \eta)$, up to the next-to-leading (second) order as

$$\delta_{\delta L}^S(\mathbf{x}, \eta) = \delta^{(1),S}(\mathbf{x} + \mathbf{d}(\mathbf{x}, \eta), \eta) + \frac{34}{21}\delta^{(1),L}(\mathbf{x}, \eta)\,\delta^{(1),S}(\mathbf{x}, \eta) + \frac{4}{7}K_{ij}^L(\mathbf{x}, \eta)\,K_{ij}^S(\mathbf{x}, \eta) + \dots\,,\tag{6.63}$$

where the ellipses represent the higher-order contributions of the perturbative expansion. Furthermore, we have introduced here the so-called displacement and anisotropy terms as (see [166])

$$\begin{aligned}
\mathbf{d}(\mathbf{x}, \eta) &\equiv -\int d^3q\, e^{i\mathbf{q}\cdot\mathbf{x}}\,\frac{i\mathbf{q}}{q^2}\,\delta^{(1)}(\mathbf{q}, \eta)\,,\\
K_{ij}(\mathbf{x}, \eta) &\equiv \int d^3q\, e^{i\mathbf{q}\cdot\mathbf{x}}\left(\frac{q_i q_j}{q^2} - \frac{1}{3}\delta_{ij}\right)\delta^{(1)}(\mathbf{q}, \eta)\,.
\end{aligned}\tag{6.64}$$

Note that we have resummed the effects of the displacement to all orders. This follows from the eikonal approximations in (6.1) or can also be shown directly in Lagrangian space [208].

Proceeding from the expansion of the density contrast $\delta_{\delta L}^S(\mathbf{x}, \eta)$ in (6.63), it is straightforward to check the validity of the VKPR relations for the two-point correlation in real space in (6.58) and the corresponding bispectrum in the soft limit in (6.59). First, we perform the correlation of the density contrast (6.63) at two different locations $\mathbf{x}$ and $\mathbf{x} + \mathbf{r}$ to obtain the real-space two-point correlation function $\xi_{\delta L}(r, \eta)$ according to its definition in (6.50). Then,

by correlating $\xi_{\delta L}(r, \eta)$ with the long-wavelength perturbation δ^L, we obtain the three-point correlation function

$$\langle \xi_{\delta L}(r, \eta)\, \delta^L \rangle = \langle \delta^S_{\delta L}(\boldsymbol{x} + \boldsymbol{r}, \eta)\, \delta^S_{\delta L}(\boldsymbol{x}, \eta)\, \delta^L \rangle, \tag{6.65}$$

which directly leads to the soft-limit bispectrum relation in Fourier space after angular averaging. Determining the two-point correlation function in the equation above, we find that the piece from the displacement reproduces the factor of $\frac{1}{3} r\, \partial_r \xi(r)$ in (6.58). Furthermore, it is crucial in this derivation that the anisotropy term does not contribute upon angular averaging, since $\langle \delta^L(\boldsymbol{x}, \eta)\, K^L_{ij}(\boldsymbol{x}, \eta) \rangle^{\mathrm{av}} \to 0$. Thus, the angular average removes the anisotropic contributions and accounts in this way for the effect of spherically symmetric perturbations.

At next-to-leading order in SPT, the validity of the VKPR proposal requires that the expansion of the density contrast $\delta^S_{\delta L}(\boldsymbol{x}, \eta)$ may be written as

$$\delta^S_{\delta L}(\boldsymbol{x}, \eta) \supset \delta^{(2),S}(\boldsymbol{x} + \boldsymbol{d}(\boldsymbol{x}, \eta), \eta) + \frac{47}{21} \delta^{(1),L}(\boldsymbol{x}, \eta)\, \delta^{(2),S}(\boldsymbol{x}, \eta) + \frac{4}{7} K^L_{ij}(\boldsymbol{x}, \eta)\, A^S_{ij}(\boldsymbol{x}, \eta) + \dots \tag{6.66}$$

with the ellipses including higher-order contributions. The factor $47/21$ would arise as a consequence of the scaling $\delta^{(2)} \propto D_1(\eta)^2$, as dictated by the VKPR expression in [173, 174]. In the equation above, we have also collected the anisotropy piece into the term containing $A^S_{ij}(\boldsymbol{x}, \eta)$, which vanishes by averaging over angles. Regarding the assumption of spherical symmetry, one may be worried that the anisotropy terms could survive after angular averaging. In fact, even though we take the soft limit $q \to 0$, the angular dependence coming from the soft mode remains because of the $1/q^2$ enhancement from the eikonal phase, as for instance $(\boldsymbol{k} \cdot \boldsymbol{q})^2/q^2$. However, due to the factorization, at equal times the anisotropy terms vanish upon angular averaging. In other words, we do not encounter singularities of the form $1/q^4$ at equal times since the contributions from the eikonal phase cancel each other and the remaining terms are analytic in q. This can be explicitly checked up to next-to-next-to-leading order (NNLO) in perturbation theory.

As expected from the explicit one-loop check of the VKPR bispectrum consistency relation (see (6.59) and (6.61)), the next-to-leading order relation for the density contrast in (6.66) is not fulfilled in this form. In detail, after performing the angular average, we find an additional piece (see (6.76)) which causes the small discrepancy between the β- and γ-coefficients of the one-loop bispectrum in the soft limit derived in SPT and from the VKPR proposal (see (6.18) and (6.61)). Although being formally not valid at one-loop order, the arising errors in the coefficients β^{VKPR} and γ^{VKPR} are small. If we take the expansion of the density contrast up to fourth order, i.e., up to $\delta^{(4)}(\boldsymbol{x}, \eta)$, into account, the calculation reveals that the claim for the form of the density perturbations based on the VKPR proposal is quantitatively very close, but not exactly equal, to the result we obtain in SPT.[3]

---

[3]Notice, however, although the errors in the coefficients β^{VKPR} and γ^{VKPR} are small, these coefficients are

6.5. Generalization of the background method

Proceeding from these considerations, our aim is to elaborate the reason behind the discrepancy of the VKPR proposal. To identify plausible causes, we start our investigations by considering the velocity perturbations. Based on this, we subsequently generalize the background method, introduced in Section 6.3 to properly incorporate the effect of curvature not only in the density but also in the velocity fluctuations on short distance scales. Thereby, we demonstrate that the velocity perturbations react differently, by a factor of one, to the presence of local curvature.

6.5.1. Impact of the velocity

Let us deduce the response of the velocity fields to the presence of a long-wavelength mode and compare it to the case of the density contrast. As discussed in Section 3.1.1, the linear growth factor describes the evolution of the growing mode of the density contrast in time. Consequently, the change in the growth factor by transforming to a locally curved EdS cosmology in (6.52) only affects the density contrast, but not the velocity field. In this expression, the dependence of the growth factor on the curvature originates from two different sources,

$$\frac{dD_1(K, a_K)}{d\delta^L} = \frac{\partial D_1}{\partial K}\frac{dK}{d\delta^L} + \frac{\partial D_1}{\partial a_K}\frac{da_K}{d\delta^L}\,. \tag{6.67}$$

The first term, which describes how the growth factor as a function of a (or equivalently η) is modified by the curvature K, contributes with a factor $20/21$. On the other hand, the second term, that accounts for the change of the scale factor in the presence of curvature, gives a contribution including a factor $-1/3$ when the growing mode is compared at the same proper time. In total, the linear growth factor of the density contrast increases by a factor $(1 + 13/21\,\delta^L)$ in the locally curved EdS cosmology (see (6.52)) [165, 166]. By using the inverse of the transformation for the density contrast in (6.48), we can conclude that the growth of the density contrast is enhanced by a factor $(1 + 34/21\,\delta^L)$ in the presence of a soft mode.

Next, we perform an analogous calculation for the divergence of the velocity $\Theta(\boldsymbol{x}, a)$, which is defined in (3.48). We find that the velocity field responds differently to the effect of local curvature as the density contrast does. In detail, we obtain that the contribution $\partial D_{1,\Theta}/\partial K$ is twice as large as the respective contribution in (6.67). Notice that this is also required

---

still multiplied by integrals which, depending on the initial conditions, can be large (or even divergent and thus need to be regularized). This means that the discrepancy can be ultimately large (or divergent) for initial conditions where the integrals are dominated by the hard part of the spectrum.

for the continuity equation to be valid. Hence, the growth of the velocity divergence in a locally curved EdS universe increases by an overall factor $(1 + 33/21\,\delta^L)$. To obtain the final expression for the change of velocity field Θ in the presence of a soft mode, we need in addition to include the effect of the coordinate transformation (6.35). Since the physical velocity $\boldsymbol{v}$ is the same in both systems, the transformation of the velocity divergence in real space to the locally curved EdS cosmology reads (see (6.48))

$$\Theta_K(\boldsymbol{x}_K, a_K) = \Theta(\boldsymbol{x}, a)\,(1 + \delta^L/3)\,. \tag{6.68}$$

Taking this relation into account, we deduce that the velocity in the presence of a long-wavelength perturbation grows faster by a total factor of $(1 + 26/21\,\delta^L)$. Note that this result is consistent with what one can derive in an explicit calculation in SPT. In addition, it is also confirmed by our findings for the soft-limit bispectrum consistency relation at linear order in the time-flow approach, given in (6.28), since $2 \times 26/21 - 1 = 31/21$ reproduces the correct contribution to the velocity-velocity components (where $a = c = 2$).

The result that the growth of the velocity perturbations in the presence of a soft mode is enhanced by an overall factor $(1 + 26/21\,\delta^L)$ has important consequences. Namely, it implies that, by using the transformations discussed above, the bispectrum consistency relation based on the VKPR proposal in (6.59) may be (naively) generalized to a form (6.28) which also includes the velocity components. By translating the steps in [173, 174] that lead to the bispectrum consistency relation (6.59) to the case of velocity perturbations, one would then write the velocity divergence in real space in the presence of a soft mode as

$$\Theta_{\delta^L}^S(\boldsymbol{x}, \eta) \supset \Theta^{(n),S}(\boldsymbol{x} + \boldsymbol{d}(\boldsymbol{x}, \eta), \eta) + \delta^{(1),L}(\boldsymbol{x}, \eta)\left(-\frac{1}{3} + \frac{33}{21}\partial_\eta\right)\Theta^{(n),S}(\boldsymbol{x}, \eta) + \dots \tag{6.69}$$

with $n \geq 1$ and $\delta^{(1),L}(\boldsymbol{x}, \eta) = \Theta^{(1),L}(\boldsymbol{x}, \eta)$. Here, the ellipses would include either terms that vanish upon angular averaging or are of higher order in perturbation theory. However, as we show in what follows, this expression extending the VKPR proposal to the velocity field dramatically fails beyond leading order. This has to be interpreted as a clear sign that the impact of a long-wavelength perturbation on the velocity fields has to be carefully accounted for and requires a systematical implementation to correctly reproduce the predictions of perturbative methods such as SPT.

6.5.2. Fluid perturbations in a curved background

Although the response of density and velocity fields to the presence of a long-wavelength perturbation is different, one replaces $\delta^{(1)}$ by $\Theta^{(1)}$ in the usual SPT computations. In order to account for the different impact of local curvature on each component consistently, one would

have to deduce the dependence of the non-linear power spectrum on the two growing and decaying modes associated to the doublet field of density and velocity perturbations, $\psi_a(\boldsymbol{k}, \eta)$ in (3.51), separately. However, there is no easy way to do so. By disregarding the different effect of curvature on the density and velocity fields, one would then expect to find a significant departure from the VKPR bispectrum consistency relation (6.59) for the density contrast and its equivalent for the velocity fields beyond linear order. On the one hand, these expectations turn out to be fulfilled for the case of the velocity field. On the other hand, however, we find that the VKPR bispectrum relation for the density field qualitatively reproduces the perturbative predictions in SPT up to a small discrepancy.

To gain some intuition behind the smallness of the discrepancy, let us next investigate the dynamics of fluid fluctuations in curved background cosmology by means of perturbation theory in more detail. For this purpose, we consider the non-linear fluid equations (3.54) for the short modes in a (locally) curved EdS cosmology. Since the dependence of the fluid equations is entirely encoded in the matrix $\Omega_{ab}(\eta)$, defined in (3.52) and in the EdS case given in (3.64), transforming to a locally curved universe in the fluid description simply amounts to a change of Ω_{ab}. At leading order in the curvature K (see (6.45)), the corresponding modification of the matrix Ω_{ab} for an EdS cosmology, (3.64), in the presence of (local) curvature reads

$$\Omega_{ab,K} \simeq \Omega_{ab,K=0} + K\frac{\partial}{\partial K}\Omega_{ab,K}\bigg|_{K=0} = \Omega_{ab}^{\text{EdS}} + \kappa \begin{pmatrix} 0 & 0 \\ -3/2 & -1/2 \end{pmatrix}. \tag{6.70}$$

Note that although the curvature K, according to (6.45), is time independent for an EdS cosmology, the corresponding curvature parameter κ, defined in (6.57), depends on time and scales like $\kappa \propto a$ in the EdS case.

Due to the fact that the matrix $\Omega_{ab,K}$ enters in the solution of the fluid equations through the linear propagator (see (3.56)), the additional curvature contribution in (6.70) leads to a modification of the linear propagator in the perturbative analysis. However, at leading order in the curvature $K \propto \delta^L$ (see (6.45)) and thus in the soft mode δ^L, it sufficient to treat the effect of the curvature as an additional interaction. Consequently, the first-order solution of the doublet field for the short modes, $\psi_{a,K}^{(1)}(\boldsymbol{k}, \eta)$, at linear order in K can be written as

$$\psi_{a,K}^{(1)}(\boldsymbol{k}, \eta) \simeq \psi_{a,K=0}^{(1)}(\boldsymbol{k}, \eta) + K\left.\frac{\partial}{\partial K}\psi_{a,K}^{(1)}(\boldsymbol{k}, \eta)\right|_{K=0}$$
$$= \left[\begin{pmatrix} 1 \\ 1 \end{pmatrix} + \frac{4\kappa}{7}\begin{pmatrix} 1 \\ 2 \end{pmatrix}\right] e^{\eta-\eta_0}\, \delta^{(1)}(\boldsymbol{k}, \eta_0)\,, \tag{6.71}$$

where have used that $\psi_{a,K=0}^{(1)}(\boldsymbol{k}, \eta) = e^{\eta-\eta_0}\, u_a\, \delta_0(\boldsymbol{k})$ for growing-mode initial conditions, as defined in (3.74) with (3.76). Note that as discussed in the previous section, the impact of the curvature on the velocity field is twice as large as on the density field.

For the higher-order solutions of the doublet field at linear order in K,

$$\psi_{a,K}^{(n)}(\boldsymbol{k},\eta) \simeq \psi_{a,K=0}^{(n)}(\boldsymbol{k},\eta) + K \left. \frac{\partial}{\partial K} \psi_{a,K}^{(n)}(\boldsymbol{k},\eta) \right|_{K=0} \tag{6.72}$$

with $n > 1$, the second term includes in general two different contributions,

$$\begin{aligned} K \left. \frac{\partial}{\partial K} \psi_{a,K}^{(n)}(\boldsymbol{k},\eta) \right|_{K=0} = \; & K \int_{\eta_0}^{\eta} d\eta'\, g_{ab}(\eta,\eta') \left[\frac{\partial}{\partial K}\, \Omega_{bc}(\eta')\, \psi_c^{(n)}(\boldsymbol{k},\eta') \right. \\ & \left. + \; \gamma_{bcd}(\boldsymbol{k},\boldsymbol{q}_1,\boldsymbol{q}_2)\, \frac{\partial}{\partial K} \sum_{m=1}^{n-1} \psi_{c,K}^{(m)}(\boldsymbol{q}_1,\eta')\, \psi_{d,K}^{(n-m)}(\boldsymbol{q}_2,\eta') \right]. \end{aligned} \tag{6.73}$$

While the first contribution corresponds to the additional interaction induced by the presence of curvature, just as the second term in the leading-order expression (6.71), the second contribution arises due to the curvature-dependent lower-order solutions entering in the SPT recursion relation (3.77). If we, for instance, compute the next-to-leading (second) order solution of the doublet field in the presence of curvature,

$$\psi_{a,K}^{(2)}(\boldsymbol{k},\eta) \simeq \psi_{a,K=0}^{(2)}(\boldsymbol{k},\eta) + K \left. \frac{\partial}{\partial K} \psi_{a,K}^{(2)}(\boldsymbol{k},\eta) \right|_{K=0}. \tag{6.74}$$

the two contributions to the linear curvature term are given by

$$\begin{aligned} K \left. \frac{\partial}{\partial K} \psi_{a,K}^{(2)}(\boldsymbol{k},\eta) \right|_{K=0} = \; & \frac{4\kappa}{7} \begin{pmatrix} 2 & 0 \\ 0 & 3 \end{pmatrix}_{ab} \psi_{b,K=0}^{(2)}(\boldsymbol{k},\eta) \\ & + \frac{\kappa}{147} \begin{pmatrix} 1 \\ 3 \end{pmatrix} \int d^3 q_1 \int d^3 q_2 \; \delta^{\mathrm{D}}(\boldsymbol{k}-\boldsymbol{q}_1-\boldsymbol{q}_2) \\ & \times \frac{(\boldsymbol{q}_1 \cdot \boldsymbol{q}_2)^2 - q_1^2 q_2^2}{q_1^2 q_2^2} \; e^{2(\eta-\eta_0)}\, \delta^{(1)}(\boldsymbol{q}_1,\eta_0)\, \delta^{(1)}(\boldsymbol{q}_2,\eta_0). \end{aligned} \tag{6.75}$$

From this, we can deduce that already at next-to-leading order of the solution for the doublet field, the linear curvature contribution $K\, \partial \psi_{a,K}^{(2)}(\boldsymbol{k},\eta)/\partial K$ is not any more proportionally related to the doublet field $\psi_{a,K=0}^{(2)}(\boldsymbol{k},\eta)$ itself. Moreover, the overall difference with the expression in (6.59) for the density contrast (first entry) is rather small. At the same time, we see that the extension for the velocities in (6.69) fails (compare with second entry).

In conclusion, we find that it is not possible to naturally reformulate the curvature dependence of the density and velocity fields in terms of a time derivative with respect to η. Thus, the assumption on which the VKPR proposal in [173, 174] is based does not hold in general and in particular not non-perturbatively. However, we also find that the suggestion of the VKPR proposal to parameterize the curvature dependence by a time derivative gives a reasonable *empirical* perturbative approximation. Hence, we can generalize the results for the

6. Bispectrum Consistency Conditions

doublet fields for the short modes at leading and next-to-leading order in (6.71) and (6.74) with (6.76) to the nth-order in perturbation theory by the approximation

$$K \left. \frac{\partial}{\partial K} \psi_{a,K}^{(n)}(\boldsymbol{k}_K, \eta) \right|_{K=0} \simeq \frac{4\kappa}{7} \begin{pmatrix} \partial_\eta & 0 \\ 0 & \partial_\eta + 1 \end{pmatrix}_{ab} \psi_{b,K=0}^{(n)}(\boldsymbol{k}_K, \eta), \tag{6.76}$$

which translates into the relation

$$\left. \frac{\partial}{\partial \delta^L} \psi_{a,\delta^L}^{(n)}(\boldsymbol{k}, \eta) \right|_{\delta^L=0} \simeq \frac{1}{21} \begin{pmatrix} 21 + 13\,\partial_\eta & 0 \\ 0 & 13 + 13\,\partial_\eta \end{pmatrix}_{ab} \psi_{b,K=0}^{(n)}(\boldsymbol{k}_K, \eta). \tag{6.77}$$

The approximation (6.76) can be understood as follows. If we do not base our considerations on the form of the non-linear fluid equations for an EdS background cosmology, but start from their general form with the velocity dependence $\Theta(\boldsymbol{k}, \eta)$ and the matrix $\Omega_{ab}(\eta)$ being dependent on the growth rate $f(\eta)$ (see (3.48) and (3.52)) as well as the time variable $\eta \equiv \ln D_1(\tau)$ of (3.49). By mapping to a locally curved universe, η and $f(\eta)$ transform into

$$\eta \to \ln D_{1,K}(\eta), \qquad f(\eta) \to \frac{\partial \ln D_{1,K}(\eta)}{\partial \ln a} \tag{6.78}$$

with $D_{1,K}(\eta)$ being the linear growth factor in the presence of curvature for the EdS case. As a consequence, we obtain a new system of fluid equations containing the matrix

$$\Omega_{ab,f} = \begin{pmatrix} 0 & -1 \\ -\frac{3}{2} \frac{\Omega_m}{f^2} & \frac{3}{2} \frac{\Omega_m}{f^2} - 1 \end{pmatrix} \simeq \Omega_{ab}^{\text{EdS}} + \frac{3\kappa}{14} \begin{pmatrix} 0 & 0 \\ 1 & -1 \end{pmatrix}. \tag{6.79}$$

Here, we used the fact that for an EdS cosmology in the presence of curvature the matter density parameter and the growth rate are given by $\Omega_m \simeq 1 + \kappa$ and $f \simeq 1 + \frac{4}{7}\kappa$ up to linear order in κ, respectively. Thus, we can absorb the information regarding the background cosmology into the time evolution up to an interaction term proportional to the curvature parameter κ (see (6.79)).

If we, however, neglect this κ-dependent interaction term in the matrix $\Omega_{f,ab}$ in (6.79) and solve the fluid equations by means of perturbation theory, we can derive that the nth-order solution of the doublet field $\psi_{a,K}^{(n)}(\boldsymbol{k}_K, \eta)$ for the soft mode in the presence of curvature fulfills the relation (6.76) (and thus the VKPR relation for the density power spectrum in (6.60)). In other words, in to obtain (6.76), one has to absorb the dependence of the fluid equations on the curved background cosmology not in the matrix $\Omega_{f,ab}$, but merely into the linear growth factor $D_{1,K}(\eta)$. In this case, the derivatives with respect to the curvature K can be reformulated as derivatives with respect to the time variable η.

Consequently, assessing the accuracy of the VKPR relation in (6.60) amounts to estimating the error induced by this approximation. On the one hand, the accuracy of the VKPR proposal

can be related to the variation (see (6.57))

$$\frac{\partial}{\partial \delta^L} \left(\frac{3}{2} \frac{\Omega_m}{f^2} \right) \simeq -\frac{5}{14}, \tag{6.80}$$

in the presence of a long-wavelength perturbation which has been absorbed into the background. Notice, however, that the explicit perturbative computations, e.g., the one-loop check of the density bispectrum in the soft limit (compare (6.61) with (6.18)), reveal a much better precision of the VKPR proposal. In fact, this is related to the appearance of extra cancellations. We find that the linear κ-dependent contribution to the matrix $\Omega_{f,ab}$ in (6.79) almost annihilates the growing-mode solution at any given order in SPT, which is dominated by $\delta^{(n)} \simeq \Theta^{(n)}$ (i.e., $\psi^{(n)} \propto (1,1)$). This explains the smallness of the discrepancy between the predictions obtained in SPT and by use of the approximation (6.76), and thus the *unreasonable effectiveness* of the VKPR proposal in perturbative computations.

As shown in [173], it is possible to derive exact relations in a simplified $(1+1)$-dimensional toy model, whose background equations resemble an EdS cosmology. In this case, the response to a soft mode is given by $\psi_{a,\delta^L} \simeq [1 + \delta^L(1 + \partial_\eta)] \psi_a$.

Apart from this, attempts of testing the VKPR proposal against numerical simulations have appeared in [231, 238]. The small deviations between the VKPR proposal and the numerical results found therein are consistent with our findings. We take this interesting point up again in Section 7.4.3. There, we make use of the so-called response function of the density power spectrum to confront the VKPR proposal against N-body simulation data.

Proceeding from the derivation of a non-perturbative relation for the bispectrum in the soft limit, we take another step in this direction in what follows. To be precise, our intention in the next chapter is to derive a non-perturbative equation for the power spectrum in the soft limit. Before doing so, we motivate why it is interesting and important to derive and investigate such a non-perturbative power spectrum equation.

Chapter 7

Non-Perturbative Power Spectrum Equation

Contents

Based on the insights on analytic methods in the theory of large-scale structure formation we gained in Chapter 5, we can summarize that current attempts to improve perturbation theory approaches can be broadly classified into two categories (see Section 5.2.2). On the one hand, studies have been undertaken to investigate the effects of long-wavelength (IR) fluctuations on modes around the scale of the baryon acoustic oscillations in [1, 101, 143, 159, 176, 182, 189, 208]. On the other hand, there have been efforts directed towards an understanding of the impact of short-wavelength (UV) perturbations. Thereby, the treatment of UV modes is complicated by the fact that the dynamics of gravitational instability is non-linear on short distance scales.

Since SPT fails to capture the correct dynamics on short distance scales due to the emergence of UV dependencies, other tools have been developed to study the imprint of UV modes on long-distance variables. The most prominent example among these is maybe the effective field theory of LSS [49, 63, 89, 178–208]. Besides, other attempts in this direction appeared. These are based on a different implementation of perturbation theory (see e.g., [212]) or,

motivated by numerical simulations [209, 210], perform a reorganization of the perturbative expansion [102, 213, 214].

In contrast to the approaches above, which rely on means of perturbation theory, our aim in this chapter is to study the long-wavelength, soft limit of the power spectrum *non-perturbatively*. By making use of the background method, introduced in the previous chapter to derive a (non-perturbative) bispectrum consistency relation (see (6.56)), and performing an operator product expansion (OPE), we derive a non-perturbative equation for the power spectrum of long-wavelength modes in what follows. This equation encodes the coupling to the UV modes in two time-dependent coefficients. Hence, these allow us to investigate the actual impact of the UV fluctuations on the power spectrum on large distance scales. Moreover, we can use them to assess the UV dependence of the leading-order – renormalized – EFT coefficients [63, 178, 208, 370]. Since the two coefficients of the non-perturbative power spectrum relation may be obtained from small-volume N-body simulations of an 'anisotropic separate universe' with spatial curvature, it is in principle possible to additionally use our non-perturbative approach to precisely infer the relevance of the leading-order EFT coefficients.

As a first step, let us next set up all the necessary ingredients to derive the non-perturbative equation for the power spectrum on large distance scales. This includes, among others, establishing the OPE in order to determine the two coefficients encoding the coupling to the UV modes in the non-perturbative power spectrum relation.

7.1. Derivation of a non-perturbative power spectrum equation

As deduced in Section 3.3.1, we can express the non-linear evolution equations of large-scale structure in a compact matrix form by using the doublet field $\psi_a(\boldsymbol{k}, \eta)$ of density and velocity perturbations in (3.51) so that we obtain the fluid equations, defined in (3.54). If we rewrite the left-hand side of the fluid equations (3.54) in terms of the momentum $\boldsymbol{q}$ and ensure momentum conservation in the vertex function γ_{abc} of (3.53) on the right-hand side, we can recast (3.54) in

$$\partial_\eta \psi_a(\boldsymbol{q}, \eta) + \Omega_{ab}(\eta)\, \psi_b(\boldsymbol{q}, \eta) = \gamma_{abc}(\boldsymbol{q}, \boldsymbol{q}/2 - \boldsymbol{k}, \boldsymbol{q}/2 + \boldsymbol{k})\, \psi_b(\boldsymbol{q}/2 - \boldsymbol{k}, \eta)\, \psi_c(\boldsymbol{q}/2 + \boldsymbol{k}, \eta). \quad (7.1)$$

As introduced in (3.52), the matrix $\Omega_{ab}(\eta)$ encodes the dependence of the fluid equations on the underlying cosmological model. In what follows, we account for the dependence on the background cosmology by applying the approximation discussed in Section (3.3.3). This means that we approximate the matrix $\Omega_{ab}(\eta)$ by its form in the EdS case, (3.64), but properly treat the model-dependent linear growth $D_1(\tau)$ (see (3.9)) in the time variable $\eta = \ln D_1(\tau)$. Furthermore, in the fluid equations (7.1), we use the conventions to sum repeated indices

and integrate over internal momenta associated to the vertex function γ_{abc}, as introduced in Section 3.3.1.

In the effective field theory approach of LSS [63, 178, 208], the fluid equations are modified by additional terms to account for smoothed regions. The relevance of these additional terms can then be determined by the mismatch of the solutions to the fluid equations (7.1) in comparison to data from observations or numerical simulations. In principle, one reason for this mismatch is that we neglect the contribution of the vorticity, i.e., the curl modes of the velocity field as defined in (3.20). As we discussed in Section 2.4, the latter can be ignored in the soft limit $q \to 0$ (see also [40]), but matter on short distance scales where $k \gg q$. However, neglecting the vorticity does not have an influence on our main finding. We take this issue up again in Section 7.4.

If one solves the non-linear fluid equations (7.1) perturbatively within the framework of the effective field theory, the resulting EFT coefficients of the perturbative solutions also include counter-terms. These counter-terms are required to cancel possible divergences in the loop integrals arising for different initial conditions [63, 208], for instance, by introducing a cutoff. Even after the cutoff dependence is removed by the counter-terms, the EFT coefficients do not necessarily vanish. In fact, the remaining renormalized contribution, being non-divergent and thus physical, accounts for the finite-size corrections of the fluid equations (7.1).

Starting from the fluid equations (7.1), we can in principle obtain the dynamics of the power spectrum $P_{ab}(q, \eta)$ by applying the time-flow approach which we have introduced in Section 5.5 and already used before in Section 6.2.2. This implies to multiply both sides of the fluid equations by an additional fluctuation field $\psi_a(\boldsymbol{q}, \eta)$ and take the statistical average afterwards. As we can explicitly see in (5.39), the resulting equation for the power spectrum depends on the bispectrum. This, in turn, is dependent on the four-point correlation function, the trispectrum. Like this, the time-flow approach generates an infinite hierarchy of evolution equations between $\mathcal{N}$- and $\mathcal{N}+1$-point functions, the so-called flow equations, and thus relies on a suitable closure approximation, e.g., (5.42), to obtain a closed analytic form for the power spectrum.

In contrast to this, our aim is to derive a closed, non-perturbative expression for the power spectrum which only depends on the latter itself and derivatives thereof. Even though we expect that it is not possible to derive such a relation in full generality, we are able to deduce such a non-perturbative expression in certain limits. Based one our results in the previous chapter, it seems natural to seek for a non-perturbative power spectrum equation in the case where one momentum, say $\boldsymbol{q}$, becomes small. In other words, we intend to derive a non-perturbative expression for the power spectrum in the soft limit $q \to 0$.

7. Non-Perturbative Power Spectrum Equation

For the derivation we can use a relation for the doublet fields $\psi_a(\boldsymbol{k}, \eta)$ that resembles the operator product expansion in quantum field theory. We discuss this in detail in the next section.

7.1.1. Operator product expansion

In order to derive a non-perturbative equation for the power spectrum, we can resort to methods of quantum field theory by performing an operator product expansion for two fluctuation fields at nearby points. For details on operator product expansions in quantum field theory see e.g., [371–374]. Notice that an explicit example of a product expansion is given by the non-perturbative soft-limit bispectrum consistency condition which we derived in the last section in (6.56).

For performing an OPE in the context of large-scale structure formation, we can regard the as the relevant degree of freedom from which a solution for the perturbation fields $\psi_a(\boldsymbol{x}, \eta)$ (in real space) follows (see also Section 6.3.1). For instance, the forces induced by its spatial gradient $-\nabla\Phi(\boldsymbol{x}, \eta)$ allow us to deduce the displacement fields as a function of time. Based on this, an OPE in the theory of structure formations refers to an expansion of a product of doublet fields $\psi_a(\boldsymbol{x}, \eta)$ and $\psi_b(\boldsymbol{y}, \eta)$ at nearby points $\boldsymbol{x}$ and $\boldsymbol{y}$ as a function of composite operators $\mathcal{O}\big[\Phi, \partial\Phi, \cdots\big]$ which are built in terms of $\Phi(\boldsymbol{x}, \eta)$ and its derivatives. Formulated in terms of an equation, this means

$$\psi_a(\boldsymbol{x}, \eta)\,\psi_b(\boldsymbol{y}, \eta) \xrightarrow{\boldsymbol{x} \to \boldsymbol{y}} \sum_{\mathcal{O}} f_{ab}^{\mathcal{O}}(|\boldsymbol{x} - \boldsymbol{y}|, \eta)\, \mathcal{O}\big[\Phi, \partial\Phi, \cdots\big]\big(\tfrac{1}{2}(\boldsymbol{x} + \boldsymbol{y}), \eta\big) \tag{7.2}$$

with space- and time-dependent coefficient functions $f_{ab}^{\mathcal{O}}(|\boldsymbol{x} - \boldsymbol{y}|, \eta)$. Consequently, the corresponding OPE for the doublet fields in Fourier space reads

$$\psi_a(\boldsymbol{q}/2 - \boldsymbol{k}, \eta)\,\psi_b(\boldsymbol{q}/2 + \boldsymbol{k}, \eta) \xrightarrow{k \gg q} \sum_{\mathcal{O}} f_{ab}^{\mathcal{O}}(k, \eta)\, \mathcal{O}\big[\Phi, \partial\Phi, \cdots\big](\boldsymbol{q}, \eta)\,. \tag{7.3}$$

Note that applying an OPE in our setting has some caveats. First of all, there exist only a few exemplary cases that obey an OPE beyond perturbation theory (for an overview see e.g., [375]). Furthermore, in the theory of large-scale structure formation, the statistical properties of the initial state constitute an additional complication, since the existence of different possible realizations generates stochastic terms which are not necessarily proportional to products of long-wavelength fields. In the language of quantum field theory, these stochastic terms correspond to the so-called 'contact terms' [376]. For our purposes, however, it is appropriate to neglect these terms since they are known to enter in the evolution equations for the power spectrum only at higher order, more precisely at q^4 [92]. Nevertheless, the relevance of these terms when approaching the non-linear scale has been recently emphasized

in [196, 198]. Finally, we have to be aware that the operators on the right-hand side of the OPE in (7.3) can themselves include products of the doublet fields at the same point, which in turn need to be regularized [208]. However, since these extra terms are suppressed by additional powers of P^L, their effect is only sub-leading and thus negligible here.

Next, let us determine explicitly the operators $\mathcal{O}\big[\Phi, \partial\Phi, \cdots\big](\boldsymbol{q}, \eta)$ of the OPE in (7.3). In order to do so, it is sufficient to only keep terms linear in Φ due to the smallness of the density perturbations as well as the gradients in the soft limit $q \to 0$. Moreover, we can make use of statistical isotropy, parity and the equivalence principle to deduce the form of the operators. The equivalence principle restricts the first term of the series expansion to include – at least – two derivatives with respect to the gravitational potential. The operators we need then possess the form

$$
\begin{aligned}
\mathcal{O}_0(\boldsymbol{q}, \eta) &= q^2 \Phi(\boldsymbol{q}, \eta) \propto \delta(\boldsymbol{q}, \eta)\,, \\
\mathcal{O}_i(\boldsymbol{q}, \eta) &= q^2 q^i \Phi(\boldsymbol{q}, \eta) \propto q^i \delta(\boldsymbol{q}, \eta)\,, \\
\mathcal{O}_{ij}^{\mathrm{TF}}(\boldsymbol{q}, \eta) &= (q^i q^j)_{\mathrm{TF}}\ \Phi(\boldsymbol{q}, \eta)\,, \\
\mathcal{O}_{ijl}^{\mathrm{TF}}(\boldsymbol{q}, \eta) &= (q^i q^j q^l)_{\mathrm{TF}}\ \Phi(\boldsymbol{q}, \eta)
\end{aligned}
\tag{7.4}
$$

with $i, j, l \in \{1, 2, 3\}$ and 'TF' standing for trace-free. The traces renormalize the coefficients of the tensor operators with fewer indices. To keep the simplicity of the notation, we do not include them here.

Similarly to the operator relations in (7.4), we can additionally split the coefficient functions of the hard modes, $f_{ab}^{\mathcal{O}}(k, \eta)$, in (7.3) into scalar functions. Beside the lowest-order coefficient function $f_{ab}^{\mathcal{O}_0}(k, \eta)$, we thus obtain coefficients of the form

$$
\begin{aligned}
f_{ab;i}^{\mathcal{O}_i}(k, \eta) &= \frac{k^i}{k} f_{ab}^{\mathcal{O}_i}(k, \eta)\,, \\
f_{ab;ij}^{\mathcal{O}_{ij}^{\mathrm{TF}}}(k, \eta) &= \frac{(k^i k^j)_{\mathrm{TF}}}{k^2}\ f_{ab}^{\mathcal{O}_{ij}^{\mathrm{TF}}}(k, \eta)\,, \\
f_{ab;ijl}^{\mathcal{O}_{ijl}^{\mathrm{TF}}}(k, \eta) &= \frac{(k^i k^j k^l)_{\mathrm{TF}}}{k^3} f_{ab}^{\mathcal{O}_{ijl}^{\mathrm{TF}}}(k, \eta)\,.
\end{aligned}
\tag{7.5}
$$

After inserting these coefficient functions and the operators of (7.4) in the OPE in (7.3) and performing the contractions of the indices i, j, l, the resulting expression reads

$$
\psi_a(\boldsymbol{q}/2 - \boldsymbol{k}, \eta)\, \psi_b(\boldsymbol{q}/2 + \boldsymbol{k}, \eta) \xrightarrow{k \gg q} \left(f_{ab}(k, \mu, \eta) + g_{ab}(k, \mu, \eta)\, \frac{q}{k} \right) \psi^L(\boldsymbol{q}, \eta) + \dots\,,
\tag{7.6}
$$

where $\psi^L(\boldsymbol{q}, \eta)$ constitutes the linearized long-wavelength perturbation in the soft limit $q \to 0$. To be precise, the function $f_{ab}(k, \mu, \eta)$ and $g_{ab}(k, \mu, \eta)$ (not to be confused with the linear propagator defined via (3.56)) represent polynomials up to third order in μ. Higher-order polynomials in μ arise, if we perform a series expansion to higher orders in q. However, since

the functions $f_{ab}(k,\mu,\eta)$ and $g_{ab}(k,\mu,\eta)$ only comprise terms up to order μ^3, we can rewrite them in terms of Legendre polynomials $Q_\ell(\mu)$ up to third order in ℓ,

$$
\begin{aligned}
f_{ab}(k,\mu,\eta) &= f_{ab}^{(0)}(k,\eta) + f_{ab}^{(2)}(k,\eta)\,Q_2(\mu)\,,\\
g_{ab}(k,\mu,\eta) &= f_{ab}^{(1)}(k,\eta)\,Q_1(\mu) + f_{ab}^{(3)}(k,\eta)\,Q_3(\mu)
\end{aligned}
\tag{7.7}
$$

with [377]

$$
Q_0(\mu) = 1\,, \qquad Q_1(\mu) = \mu\,, \qquad Q_2(\mu) = \frac{1}{2}\left(3\mu^2 - 1\right)\,, \qquad Q_3(\mu) = \frac{1}{2}\left(5\mu^3 - 3\mu\right)\,. \tag{7.8}
$$

Note that the relation (7.6) with the coefficient functions (7.7) is only accurate at leading order in q we consider here.

As a consequence, we can conclude that the expression (7.6), originating from the OPE in (7.3), confirms our preconceived idea that the fluid dynamics on short distance scales is influenced by long-wavelength modes in a very specific way. This finding is also reflected by the non-perturbative soft-limit bispectrum consistency condition in dependence on the power spectrum of a hypothetically curved universe, derived in the previous chapter (see (6.56)).

Similarly to the soft-limit bispectrum consistency condition (6.56), we can deduce a relation for the bispectrum in the soft limit based on the OPE. In order to do so, we correlate the product of doublet fields in (7.6) with an additional soft-mode perturbation $\psi_a^L(\boldsymbol{q},\eta)$ and account for momentum conservation according to the definition of the bispectrum in (4.10). Thus, the bispectrum in the soft limit is given by

$$
B_{abc}(-\boldsymbol{q}, \boldsymbol{q}/2 - \boldsymbol{k}, \boldsymbol{q}/2 + \boldsymbol{k}, \eta) \xrightarrow{q\to 0} u_a\left(f_{bc}(k,\mu,\eta) + g_{bc}(k,\mu,\eta)\,\frac{q}{k}\right)P^L(q,\eta) + \ldots\,, \tag{7.9}
$$

where $u_a = (1,1)$ (see (4.15)) so that $B_{1ab} = B_{2ab}$. Recall that the linear solution $\psi_a^L(\boldsymbol{q},\eta)$ for the doublet field, given in (3.56) with (3.70), implies for the linear power spectrum that $P^L(q,\eta) = P_{11}^L(q,\eta) = P_{22}^L(q,\eta)$ (see (4.16) and (4.17)). Notice that even before angular averaging, the bispectrum in the soft limit based on the OPE does not reveal terms proportional to $1/q$ even before angular averaging, in contrast to the perturbative derivations of the bispectrum consistency relations in Section 6.2. As we discuss explicitly in the next section, we can use the consistency condition to determine the coefficients of the bispectrum relation from the OPE in (7.9) in terms of the power spectrum on short distance scales.

Building up on the relation (7.9) for the bispectrum in the soft limit, we can next set up an non-perturbative equation for the power spectrum based on the fluid equations (7.1).

7.1.2. Fluid equations in the soft limit

For the derivation of the power spectrum equation in the soft limit, we do not want to rely on any perturbative methods. However, in the first step, we can proceed accordingly to

the time-flow approach (see Section 5.5.1) since at this stage perturbation theory is not yet applied. Thus, in order to obtain an evolution equation for the power spectrum $P_{ab}(q, \eta)$, we correlate the fluid equations (7.1) with an additional fluctuation field. This yields the first flow equation for the two-point correlation function in (5.39). Next, express the two- and three-point correlation function arising in the first flow equation in terms of the power spectrum and the bispectrum by using their definitions in (4.1) and (4.10) and applying momentum conservation. Thus, we obtain the following differential evolution equation for the soft-mode power spectrum $P_{ab}(q, \eta)$,

$$
\partial_\eta P_{ab}(q, \eta) = - \Omega_{ac}(\eta) P_{cb}(q, \eta) - \Omega_{bc}(\eta) P_{ac}(q, \eta)
$$
$$
+ \int d^3k \left[\, \gamma_{acd}(\boldsymbol{q}, \boldsymbol{q}/2 - \boldsymbol{k}, \boldsymbol{q}/2 + \boldsymbol{k}) B_{bcd}(-\boldsymbol{q}, \boldsymbol{q}/2 - \boldsymbol{k}, \boldsymbol{q}/2 + \boldsymbol{k}, \eta) \right.
$$
$$
\left. + \gamma_{bcd}(\boldsymbol{q}, \boldsymbol{q}/2 - \boldsymbol{k}, \boldsymbol{q}/2 + \boldsymbol{k}) B_{acd}(-\boldsymbol{q}, \boldsymbol{q}/2 - \boldsymbol{k}, \boldsymbol{q}/2 + \boldsymbol{k}, \eta) \, \right].
$$
(7.10)

Note that we have explicitly written down the momentum integration here for the sake of clarity. In addition, notice that the differential evolution equation above coincides (apart from the choice of momenta) with the one obtained in the framework of the time-flow approach in (5.43). The reason for this is that the closure approximation (5.42) which is applied in the time-flow formalism to close the infinite hierarchy of flow equations (5.39) does not affect the first flow equation for the power spectrum, but only the higher-order flow equations starting at the level of the bispectrum. In other words, in contrast to these higher-order flow equations, the flow equation for the power spectrum is exact and thus non-perturbatively valid.

To derive a non-perturbative relation for the power spectrum in the soft limit, our next step is to insert the soft-limit bispectrum relation, which we derived based on the OPE in (7.9), in the differential evolution equation in (7.10) and investigate which contributions are relevant in the soft limit $q \to 0$.

In order to do so, let us first elucidate why it is justified to employ – right from the beginning – the soft limit of the bispectrum in the equation for the power spectrum in (7.10). Using the bispectrum expression for small modes q in (7.9) in (7.10) implies that contributions of the integral from loop momenta $k \lesssim q$ can be neglected. Indeed, in the case of a physical power spectrum $P_0(k) \propto k^{n_s}$ (see (4.5)) with spectral index $n_s \simeq 1$ and for small external momentum q, the ultra soft momenta $k \lesssim q$ contribute like $\int^q d^3k \, P_0(k) \sim q^{n_s+3} \sim q^4$ to the loop integral in (7.10). At the same time, the hard momenta $k > q$ yield contributions scaling like $\sim q^2 \sigma_d^2$ (see (5.10)), with σ_d^2 being in turn dominated by modes $k \gg q$ beyond the maximum of the power spectrum. Consequently, in the soft limit $q \to 0$, the contributions of the integral from the loop momenta $k \lesssim q$ are subdominant. This justifies to consider the bispectrum in the soft limit in the equation for the power spectrum in (7.10) directly from

the onset.

To identify the relevant contributions in the soft limit which arise from inserting the soft-limit bispectrum relation (7.10) in the differential evolution equation for the power spectrum in (7.9), we split the power spectrum in three parts,

$$P_{ab}(q,\eta) = P_{ab}^{\mathrm{hom}}(q,\eta) + P_{ab}^{\alpha}(q,\eta) + P_{ab}^{\beta}(q,\eta)\,. \tag{7.11}$$

Thereby, the first term $P_{ab}^{\mathrm{hom}}(q,\eta)$ corresponds to the homogeneous solution of the differential equation. The homogeneous solution is obtained when neglecting the contributions in (7.10) which include the vertex function γ_{abc},

$$\partial_\eta P_{ab}^{\mathrm{hom}}(q,\eta) = -\Omega_{ac}(\eta)\, P_{cb}^{\mathrm{hom}}(q,\eta) - \Omega_{bc}(\eta)\, P_{ac}^{\mathrm{hom}}(q,\eta)\,. \tag{7.12}$$

In the soft limit, it is then simply given by the linear power spectrum (see also the discussion in Section 5.5.3),

$$P_{ab}^{\mathrm{hom}}(q,\eta) = P_{ab}^{L}(q,\eta) = u_a u_b P^L(k)\,, \tag{7.13}$$

where we assumed Gaussian-distributed growing-mode initial conditions in the last equality (see (4.16) and (4.17)).

Furthermore, the other two terms in (7.11), $P_{ab}^{\alpha}(q,\eta)$ and $P_{ab}^{\beta}(q,\eta)$, constitute the non-linear contributions to the power spectrum which are sourced either by the mode-coupling function α or β entering in the vertex γ_{abc} (see (3.23) and (3.53)).

In the following, let us first investigate the contributions to the differential equation for the power spectrum in (7.10) that are associated to the vertex elements involving the mode-coupling function β. In contrast to the contributions from the mode-coupling function α, the former can be determined in a straightforward manner.

Non-linear β-contributions

According to the definition of the vertex function γ_{abc} in (3.53), we obtain the non-linear contributions to the differential equation for the power spectrum (7.10) which involve the mode-coupling function β by setting $c = d = 2$ in (3.53). Thereby, we do not have to specify the indices a and b. Consequently, for $a, b, \in \{1, 2\}$, the β-contributions from the two vertices in (7.10) are of the form

$$\int d^3k\, u_a\, \beta(\boldsymbol{q}/2 - \boldsymbol{k}, \boldsymbol{q}/2 + \boldsymbol{k})\, B_{b22}(-\boldsymbol{q}, \boldsymbol{q}/2 - \boldsymbol{k}, \boldsymbol{q}/2 + \boldsymbol{k}, \eta)\,. \tag{7.14}$$

This is quite fortunate since the mode-coupling function $\beta(\boldsymbol{q}/2 - \boldsymbol{k}, \boldsymbol{q}/2 + \boldsymbol{k})$, expanded in a series up to the second-order in the soft momentum q, scales like (see (3.23))

$$\beta(\boldsymbol{q}/2 - \boldsymbol{k}, \boldsymbol{q}/2 + \boldsymbol{k}) \simeq -\frac{q^2}{2k^2} \tag{7.15}$$

so that the β-contribution in (7.14) becomes

$$-\frac{q^2}{2}\int\frac{d^3k}{k^2}\,u_a B_{b22}(-\boldsymbol{q},\boldsymbol{q}/2-\boldsymbol{k},\boldsymbol{q}/2+\boldsymbol{k},\eta)\,. \tag{7.16}$$

If we next insert the soft-limit bispectrum relation derived from the OPE in (7.9) into the equation above and restrict our considerations to the leading order in q, we can neglect the contribution of the bispectrum term including the function $g_{bc}(k,\mu,\eta)$ to the integral in (7.9). Hence, the resulting expression reads

$$-\frac{q^2}{2}P^L(q,\eta)\,u_a u_b\int\frac{d^3k}{k^2}\,f_{22}(k,\mu,\eta)\,. \tag{7.17}$$

Then, we express the remaining function $f_{22}(k,\mu,\eta)$ in terms of Legendre polynomials according to (7.7) and perform the angular integration over $d\Omega=2\pi\,d\mu$. The first term of the function $f_{22}(k,\mu,\eta)$, i.e., $f_{22}^{(0)}(k,\eta)$, does not depend on the angular parameter μ so that the angular integration simply yields a factor 4π. On the other hand, the second term $f_{22}^{(2)}(k,\eta)\,Q_2(\mu)$ vanishes upon angular integration due to the form of the second-order Legendre polynomial, given in (7.8). Thus, we can express the β-contributions of the two vertices in (7.10) at leading order in q as

$$-\frac{q^2}{2}P^L(q,\eta)\,u_a u_b\,C_{22}^{(0)}(\eta)\,, \tag{7.18}$$

where we have introduced the time-dependent coefficient

$$C_{22}^{(0)}(\eta)\equiv 4\pi\int dk\,f_{22}^{(0)}(k,\eta)\,. \tag{7.19}$$

As a result, we find that the non-linear contributions of the β-terms to the differential evolution equation for the power spectrum in (7.10) at leading order in q are given by

$$\partial_\eta P_{ab}^\beta(q,\eta)+\Omega_{ac}(\eta)\,P_{cb}^\beta(q,\eta)+\Omega_{bc}(\eta)\,P_{ac}^\beta(q,\eta)=-\frac{q^2}{2}P^L(q,\eta)\begin{pmatrix}0&1\\1&2\end{pmatrix}_{ab}C_{22}^{(0)}(\eta)\,. \tag{7.20}$$

In principle, we can directly extract the time-dependent coefficient $C_{22}^{(0)}(\eta)$, or equivalently the function $f_{22}^{(0)}(k,\eta)$ in (7.19), entering in the power spectrum equation above by confronting the soft-limit bispectrum relation based on the OPE in (7.9) against observational data or numerical simulations. This is similar to determining the local non-Gaussianity parameter $f_{\rm NL}^{\rm loc}$ in the squeezed limit of the respective CMB bispectrum.

In the derivation of the β-contributions to the differential equation (7.20), the form of the mode-coupling function β allowed us to integrate out the angular dependence of the terms arising from the soft-limit bispectrum relation based on the OPE in (7.9). This means that ultimately only the angular-averaged soft-limit bispectrum enters in (7.20).

7. Non-Perturbative Power Spectrum Equation

Consequently, we can determine the coefficient $C_{22}^{(0)}(\eta)$ further by using a non-perturbative angular-averaged soft-limit bispectrum consistency relation including both the density and velocity perturbation field. We can deduce such a relation in a straightforward way by following the derivation of the non-perturbative angular-averaged consistency condition for the bispectrum of density perturbations in (6.56) and taking the impact of the velocity fields, as discussed in Section 6.5, into account. The resulting relation reads

$$B_{abc}(\mathbf{k}, -\mathbf{q}, \mathbf{q} - \mathbf{k}, \eta)^{\mathrm{av}} \xrightarrow{q \to 0} P^L(q, \eta) \, u_b \left[\left(N_{ac} - \frac{1}{3} k \, \partial_k - \frac{1}{3} \partial_\eta \right) P_{ac}(k, \eta) \right. \\ \left. + \frac{5}{3} \frac{\partial}{\partial \kappa} P_{ac,K}(k, \eta) \bigg|_{K=0} \right] \tag{7.21}$$

with $N_{11} = 1$, $N_{12} = N_{21} = -1/3$, $N_{22} = -5/3$. If we subsequently insert the equation above into the non-linear β-contribution (7.16) (by adapting the momentum dependence accordingly) and rewrite it in the form (7.17), we can express the coefficient $C_{22}^{(0)}(\eta)$ as

$$C_{22}^{(0)}(\eta) = -4 \, \sigma_{22}^2(\eta) + \partial_\eta \sigma_{22}^2(\eta) + 5 \frac{\partial}{\partial \kappa} \sigma_{22,K}^2(\eta) \bigg|_{K=0}. \tag{7.22}$$

Here, we have included the one-dimensional momentum integral of the power spectrum in the dimensionful variance of the displacement fields $\sigma_{ab}^2(\eta)$, which we defined in (5.11).

Following the Lagrangian-space EFT approach of [208], we could instead introduce the parameters $\epsilon_{ab}^{\psi<}(q, \eta) \equiv q^2 \int_0^q \frac{d^3k}{k^2} P_{ab}(k, \eta)$ and $\epsilon_{ab}^{\psi>}(q, \eta) \equiv q^2 \int_q^\infty \frac{d^3k}{k^2} P_{ab}(k, \eta)$. However, for reasons of clarity, we keep the explicit dependence of the β-contribution (7.17) on the soft-momentum factor q^2. Besides, the distinction between $\epsilon^{\psi<}$ and $\epsilon^{\psi>}$ is unnecessary in the soft limit $q \to 0$.

In order to specify the coefficient $C_{22}^{(0)}(\eta)$ in (7.22), we can go one step further. Since the expression (7.22) involves a curvature derivative, we can make use of the generalized VKPR proposal in (6.76), constituting a quantitatively reasonable empirical approximation, to reformulate this derivative with respect to curvature as a time derivative. Hence, we can finally transform the relation (7.22) into[1]

$$C_{22}^{(0)}(\eta) \simeq -\frac{8}{7} \sigma_{22}^2(\eta) + \frac{13}{7} \partial_\eta \, \sigma_{22}^2(\eta). \tag{7.23}$$

In Section (7.4), we use this result for the coefficient $C_{22}^{(0)}(\eta)$ to compare with numerical simulations. We omit the superscript of this coefficient in what follows so that

$$C_{22}(\eta) \equiv C_{22}^{(0)}(\eta). \tag{7.24}$$

---

[1] Notice that the expression for the coefficient $C_{22}^{(0)}(\eta)$ in (7.23) differs from the corresponding one in [2] since we have corrected a typographical error in the prefactor of the first term. This correction has no impact on the remaining results and our conclusions.

Non-linear α-contributions

From the form of the vertex function γ_{abc} in (3.53), we can extract the non-linear contributions of the mode-coupling function α to the differential evolution equation for the power spectrum in (7.10) if we set $c = 1, d = 2$ and $c = 2, d = 1$. Thus, for $a, b \in \{1, 2\}$, the form of the α-contributions in each of the two vertices in (7.10) equals

$$
\int d^3k \, \big[\, \gamma_{a12}(\boldsymbol{q}, \boldsymbol{q}/2 - \boldsymbol{k}, \boldsymbol{q}/2 + \boldsymbol{k}) \, B_{b12}(-\boldsymbol{q}, \boldsymbol{q}/2 - \boldsymbol{k}, \boldsymbol{q}/2 + \boldsymbol{k}, \eta) \\
+ \gamma_{a21}(\boldsymbol{q}, \boldsymbol{q}/2 - \boldsymbol{k}, \boldsymbol{q}/2 + \boldsymbol{k}) \, B_{b21}(-\boldsymbol{q}, \boldsymbol{q}/2 - \boldsymbol{k}, \boldsymbol{q}/2 + \boldsymbol{k}, \eta) \, \big] \, .
\tag{7.25}
$$

We can combine the second term in the integrand with the first one by reformulating the momentum dependence of the former. Thereby, we make use of the fact that the integrand remains invariant if we change the sign of both momenta $\boldsymbol{k}$ and $\boldsymbol{q}$. Additionally, we take into account that the soft-limit bispectrum relation deduced from the OPE in (7.9) does not depend on the sign of the soft mode $\boldsymbol{q}$, but only on its magnitude q. As a result, we can rewrite the previous equation such that the α-contributions in each vertex are of the form (see (7.14))

$$
\int d^3k \, u_a \, \alpha(\boldsymbol{q}/2 - \boldsymbol{k}, \boldsymbol{q}/2 + \boldsymbol{k}) \, B_{b12}(-\boldsymbol{q}, \boldsymbol{q}/2 - \boldsymbol{k}, \boldsymbol{q}/2 + \boldsymbol{k}, \eta) \, .
\tag{7.26}
$$

Next, we perform a series expansion of the mode-coupling function α, defined in (3.23), up the second order in the soft momentum q,

$$
\alpha(\boldsymbol{q}/2 - \boldsymbol{k}, \boldsymbol{q}/2 + \boldsymbol{k}) = \frac{q^2}{2k^2} - \frac{\boldsymbol{q} \cdot \boldsymbol{k}}{k^2} - \frac{(\boldsymbol{q} \cdot \boldsymbol{k})^2}{k^4} \, .
\tag{7.27}
$$

Afterwards, we insert this series expansion together with the soft-limit OPE bispectrum relation in (7.9) into the expression for the α-contribution in (7.26). By decomposing the soft-limit bispectrum in terms of Legendre polynomials $Q_\ell(\mu)$, analogously as in (7.7), we can subsequently specify the different term contributing to (7.26) in more detail. Since each of the three terms in the series expansion of the mode-coupling function α in (7.26) involves a different dependence on the angular parameter μ, defined in (6.7), they generate in combination with the Legendre polynomials three different terms from the α-contribution (7.26). Since the first term in the series expansion (7.27) does not incorporate any dependence on the angular parameter μ, it basically amounts to an angular average of the bispectrum in the soft limit, analogous to the β-contributions in (7.14)-(7.17). Hence, we can write the first term in the α-contribution (7.26) in terms of the time-dependent coefficient (see (7.19))

$$
C_{12}^{(0)}(\eta) \equiv -\frac{4\pi}{3} \int dk \, f_{12}^{(0)}(k, \eta) \, .
\tag{7.28}
$$

7. Non-Perturbative Power Spectrum Equation

Moreover, as the second term in the series expansion of the mode-coupling function α in (7.27) scales like μ, only the first-order Legendre polynomial $Q_1(\mu)$ (see (7.8)) leads to a non-vanishing contribution after angular integrating. Hence, according to (7.7), the resulting time-dependent coefficient,

$$C_{12}^{(1)}(\eta) \equiv \frac{8\pi}{3} \int dk \, f_{12}^{(1)}(k,\eta) \,, \tag{7.29}$$

includes the function $f_{12}^{(1)}(k,\eta)$. Finally, the μ^2-dependence of the last term in the series expansion (7.27) entails that the only remaining contribution upon angular averaging arises from the bispectrum term including the second-order Legendre polynomial $Q_2(\mu)$. Thus, we can express the third term, which involves the function $f_{12}^{(2)}(k,\eta)$, through the coefficient

$$C_{12}^{(2)}(\eta) \equiv \frac{16\pi}{15} \int dk \, f_{12}^{(2)}(k,\eta) \,. \tag{7.30}$$

If we summarize the three time-dependent coefficients in (7.28)-(7.30) as

$$C_{12}(\eta) \equiv C_{12}^{(0)}(\eta) + C_{12}^{(1)}(\eta) + C_{12}^{(2)}(\eta) \,, \tag{7.31}$$

our result for the non-linear contributions of the α-terms to the differential power spectrum equation in (7.10) at leading order in the soft momentum q reads (see (7.20))

$$\partial_\eta P_{ab}^\alpha(q,\eta) + \Omega_{ac}(\eta)\, P_{cb}^\alpha(q,\eta) + \Omega_{bc}(\eta)\, P_{ac}^\alpha(q,\eta) = -\frac{q^2}{2} P^L(q,\eta) \begin{pmatrix} 2 & 1 \\ 1 & 0 \end{pmatrix}_{ab} C_{12}(\eta) \,. \tag{7.32}$$

Finally, by adding the three parts (7.11) contributing to the differential power spectrum equation in (7.10), namely the linear homogeneous contribution (7.13) also as the non-linear contributions from the mode-coupling functions β and α in (7.20) with (7.24) and (7.32), we can rewrite the differential equation for the power spectrum in (7.10) at leading order in the soft mode q as

$$\begin{aligned} \partial_\eta P_{ab}(q,\eta) = &- \Omega_{ac}(\eta)\, P_{cb}(q,\eta) - \Omega_{bc}(\eta)\, P_{ac}(q,\eta) \\ &- \frac{q^2}{2} P^L(q,\eta) \left[\begin{pmatrix} 0 & 1 \\ 1 & 2 \end{pmatrix}_{ab} C_{22}(\eta) + \begin{pmatrix} 2 & 1 \\ 1 & 0 \end{pmatrix}_{ab} C_{12}(\eta) \right] \,. \end{aligned} \tag{7.33}$$

At this point, we have arrived at the desired non-perturbative equation for the power spectrum in the soft limit. It is solely written in terms of the power spectrum $P_{ab}(q,\eta)$ itself and a set of coefficients, $C_{22}(\eta)$ and $C_{12}(\eta)$, depending on fluctuations on short distance scales. Notice that the expansion in terms of small momenta q in the power spectrum equation is only viable if the momentum integrals contained in the coefficients $C_{22}(\eta)$ and $C_{12}(\eta)$ are dominated by

the hard modes $k \gg q$. We illustrated at the beginning of this section that this is indeed the case.

In order to use this expression to evaluate the power spectrum $P_{ab}(q, \eta)$, it is necessary to further determine the coefficients $C_{22}(\eta)$ and $C_{12}(\eta)$. As discussed for the coefficient $C_{22}(\eta)$, that arises from the non-linear β-contributions in (7.31), this can be achieved by using non-perturbative consistency conditions for the bispectrum in the soft limit (see e.g., (7.21)). With regard to the coefficient $C_{12}(\eta)$ in (7.31) parameterizing the non-linear contributions of the mode-coupling function α, we can in principle follow a similar path as for the β-contributions by resorting to a non-perturbative consistency condition for the bispectrum in the soft limit. However, in the case of the β-contributions, the independence of the mode-coupling function β of the angle between the momenta $\boldsymbol{q}$ and $\boldsymbol{k}$ for $q \ll k$ (see (7.17)) simply reduced the three-dimensional momentum integral to an angular average of the bispectrum in the soft limit. Thus, we could make use of the angular-averaged consistency relation for the bispectrum which we derived from the background method for a spherically symmetric soft mode (see in particular Section 6.3).

It is not possible to use this angular-averaged soft-limit bispectrum relation for further specifying the coefficient $C_{12}(\eta)$ of the α-contributions in (7.31), at least not for $C_{12}^{(1)}(\eta)$ and $C_{12}^{(2)}(\eta)$. As the mode-coupling function α for small momenta $q \ll k$ depends on the angle between these momenta (see (7.27)), we need an *angular-dependent* consistency condition for the bispectrum in the soft limit in this case. In fact, it is possible to derive such a consistency condition by applying the background method not for a spherically symmetric, but for a *directional* soft mode and perform a Newtonian mapping to a locally curved anisotropic universe. As we can see explicitly in the following section, this is rather cumbersome.

7.2. Background method for a directional soft mode

Our considerations in the last section revealed that it is not possible to constrain the coefficient $C_{12}(\eta)$ in the non-perturbative differential equation for the power spectrum in the soft limit in (7.33) by an angular-averaged bispectrum consistency condition, as given in (7.21). In particular, determining the contributions to the coefficient $C_{12}(\eta)$, defined in (7.31), from the multipoles $\ell = \{1, 2\}$ requires the derivation of an angular-dependent non-perturbative consistency relation for the bispectrum in the soft limit. In order to derive such a relation, we resort to the background method, that we developed in Section 6.3 for a spherically symmetric soft, long-wavelength perturbation, and extend it to the case of a directional soft mode. Thereby, we implement a Newtonian mapping that transform a flat FRW cosmology in the presence of a directional soft mode into a locally curved anisotropic universe. For extracting

the coefficient $C_{12}(\eta)$ it turns out to be necessary to study this map up to the order $(\boldsymbol{q} \cdot \boldsymbol{x})^3$ in the soft mode.

In the following, we proceed in similar steps as in Section 6.3.1 for setting up the coordinate transformation mapping the directional soft mode to a locally curved anisotropic universe. Afterwards, we build upon the analysis in Section 6.3.3 in order to derive a non-perturbative consistency relation for the bispectrum in the soft limit from this coordinate transformation. We refer to the sections mentioned above for details. In addition, a related discussion within the framework of the 'separate universe' approach can be found in [241].

7.2.1. Newtonian mapping

To set up a mapping based on the background method which transforms a flat FRW background cosmology in the presence of a long-wavelength directional perturbation into a locally curved anisotropic universe, we start from the metric of a perturbed FRW cosmology in Newtonian gauge in terms of the global coordinates $(\boldsymbol{x}, t)$, given in (6.33). We assume the perturbation to be a directional long-wavelength, soft density fluctuation of the form

$$\delta^L(\boldsymbol{x}, t) \simeq \frac{1}{2}\delta^L(t)\, e^{i\,\boldsymbol{q}\cdot\boldsymbol{x}} + \dots . \tag{7.34}$$

By inserting this ansatz for the directional soft mode into the perturbed Poisson equation (6.31), we can subsequently determine the gravitational potential generated by the soft mode as (see (6.34))

$$\Phi^L(\boldsymbol{x}, t) \simeq \frac{3}{2}\frac{\Omega_m\, a^2 H^2}{q^2}\left[\frac{1}{2}\delta^L(t)\, e^{i\,\boldsymbol{q}\cdot\boldsymbol{x}} + \dots\right] . \tag{7.35}$$

For a discussion of the similar case of a plane-wave perturbation see [165].

In order to deduce the mapping needed to transform the flat FRW metric (6.33) with a directional soft perturbation of the form (7.35) to an unperturbed, locally anisotropic cosmology, our ansatz for the coordinate transformation is (compare with (6.35))

$$t = t_A + f(t_A, \boldsymbol{x}_A), \qquad \boldsymbol{x} = \boldsymbol{x}_A + \boldsymbol{g}(t_A, \boldsymbol{x}_A). \tag{7.36}$$

Here, we have added the subscript 'A' to indicate the coordinates in the locally curved anisotropic cosmology and introduced the functions $f(t_A, \boldsymbol{x}_A)$ and $\boldsymbol{g}(t_A, \boldsymbol{x}_A)$ depending on these local coordinates. Note that $\boldsymbol{g}(t_A, \boldsymbol{x}_A)$ is a vector-valued function.

Our intention is to determine the functions $f(t_A, \boldsymbol{x}_A)$ and $\boldsymbol{g}(t_A, \boldsymbol{x}_A)$ in the coordinate transformation (7.36) such that we can absorb the directional long-wavelength perturbation in (7.35) into a locally anisotropic (Bondi-type) metric. For this purpose, we perform a series expansion of perturbation (7.35) in $\boldsymbol{q}$. As a first application, let us determine the coordinate transformation (7.36) for the first non-trivial order of this expansion.

Parallel curvature and scale factor

We search for a coordinate transformation of the form (7.36) with coordinate-dependent functions $f(t_A, \boldsymbol{x}_A)$ and $\boldsymbol{g}(t_A, \boldsymbol{x}_A)$ mapping the perturbed flat FRW metric in (6.33) into a locally curved anisotropic metric of the form

$$
\begin{aligned}
ds^2 = &- dt_A^2 + a_\parallel^2(t_A)\, d\boldsymbol{x}_{A,\parallel}^2 + a_\perp^2(t_A)\, d\boldsymbol{x}_{A,\perp}^2 \\
&- \frac{1}{2} \left(K_\parallel(t_A)\, \boldsymbol{x}_{A,\parallel}^2(t_A) + K_\perp(t_A)\, \boldsymbol{x}_{A,\perp}^2 \right) a^2(t_A)\, d\boldsymbol{x}_A^2 ,
\end{aligned}
\tag{7.37}
$$

where we neglect corrections to the metric of order $\mathcal{O}(\boldsymbol{x}_A^3)$ for the moment. Moreover, the time-dependent quantities $a_\parallel$, $a_\perp$, $K_\parallel$ and $K_\perp$ represent the parallel and perpendicular scale factors and curvature parameters in the locally curved anisotropic universe. Thus, in the anisotropic universe described by the metric above, one observes two different expansion rates $a_\parallel, a_\perp$ and curvatures $K_\parallel, K_\perp$, parallel and perpendicular to the soft momentum $\boldsymbol{q}$. Here, the perpendicular and parallel directions are defined with respect to $\boldsymbol{q}$ as

$$
\boldsymbol{x}_{A,\parallel} = \frac{\boldsymbol{x} \cdot \boldsymbol{q}}{q^2}\, \boldsymbol{q} , \qquad \boldsymbol{x}_{A,\perp} = \boldsymbol{x} - \boldsymbol{x}_{A,\parallel} .
\tag{7.38}
$$

Notice that in the second term of the metric (7.37), involving the curvature parameters $K_\parallel$ and $K_\perp$, we do not distinguish between the respective scale factors $a_\parallel$ and $a_\perp$. As we show later on, this distinction is not necessary when considering the leading order in the density contrast δ^L only. For notational purposes, we drop the subscript 'A' in the following.

In analogy to the Newtonian mapping performed in Section 6.3, applying the change of coordinates (7.36) to transform the metric of the perturbed flat FRW background cosmology in (6.33) into the one describing a locally curved anisotropic cosmology in (7.37) allows us to derive constraints on the coordinate-dependent functions $f(t_A, \boldsymbol{x}_A)$ and $\boldsymbol{g}(t_A, \boldsymbol{x}_A)$. If we compare the time-time components of the two metrics (6.33) and (7.37), we find the same constraint as before (see (6.37)),

$$
\dot{f} = -\Phi^L .
\tag{7.39}
$$

The reason for this is simply that the coordinate transformations (6.35) and (7.36) possess the same general form for the transformation of the time variable. However, the structure of the spatial coordinate transformation in (7.36) differs from the one in (6.35). Hence, in contrast to (6.38), we find that the vanishing time-space parts in both metrics leads to the relation

$$
a^2 \dot{\boldsymbol{g}} = \nabla f .
\tag{7.40}
$$

As in (6.37) and (6.38), the derivatives in time and space in the equations (7.39) and (7.40) are taken with respect to the global coordinates $(t, \boldsymbol{x})$. By integrating the last two equations

7. Non-Perturbative Power Spectrum Equation

with respect to time t or equivalently the scale factor $a(t)$, we can determine the coordinate-dependent functions f and g in dependence of the long-wavelength perturbation Φ^L as

$$f = -\int \frac{da}{a} \frac{1}{H} \Phi^L, \qquad \boldsymbol{g} = \int \frac{da}{a} \frac{1}{a^2 H} \nabla f + \boldsymbol{c}. \tag{7.41}$$

While we can set the time-independent integration constant of the function f to zero (as in (6.42)), it is necessary to keep the vector-valued time-independent integration constant $\boldsymbol{c}$ associated to the function g. This becomes evident in the following calculations.

In order to evaluate the expressions for the functions f and g in the previous equation and derive concrete results, let us henceforth consider the case of a flat matter-dominated EdS background cosmology as a benchmark. In what follows, we thus set $\Omega_m = 1$ and assume the Hubble parameter and the linear density contrast in the growing mode to scale like $H \propto a^{-3/2}$ and $\delta^L \propto a$ (see (3.16) and (3.11) with (3.17)). Thus, for an EdS universe, the long-wavelength perturbation Φ^L is constant in time, $\Phi^L \propto a^0$, so that the explicit expressions for the functions f and g in (7.41) read

$$f = -\frac{2}{3} \frac{1}{H} \Phi^L, \qquad \boldsymbol{g} = -\frac{2}{3} \frac{1}{a^2 H^2} \nabla \Phi^L + \boldsymbol{c}. \tag{7.42}$$

Apart from the constraints in (7.39) and (7.40), which we derived by comparison of the time-time and (vanishing) time-space components of the metrics (6.33) and (7.37) under the coordinate transformation (7.36), we can obtain an additional relation between the space-space parts of the two metrics. We first apply the coordinate transformation (7.36) to the unperturbed metric (6.33) and use the general solution for the functions f and g in (7.41), yielding to write its space-space components as

$$ds^2 \supset \left(1 - 2\Phi^L - 2H \int \frac{da}{a} \frac{1}{H} \Phi^L \right) a^2 \, d\boldsymbol{x}^2 + (\nabla_i \, g_j + \nabla_j \, g_i) \, a^2 \, dx_i \, dx_j \tag{7.43}$$

with $i, j \in \{1, 2, 3\}$. Note that the terms within the first bracket are constant for an EdS cosmology since

$$2\Phi^L + 2H \int \frac{da}{a} \frac{1}{H} \Phi^L \simeq \frac{10}{3} \Phi^L. \tag{7.44}$$

Next, we perform a series expansion of the long-wavelength perturbation Φ^L, given in (7.35), with respect to $\boldsymbol{q} \cdot \boldsymbol{x}$,

$$\Phi^L(\boldsymbol{x}, t) \simeq \frac{3}{2} \frac{H^2 a^2}{q^2} \left[\frac{1}{2} \delta^L(t) \left(1 + i \, \boldsymbol{q} \cdot \boldsymbol{x} - \frac{1}{2}(\boldsymbol{q} \cdot \boldsymbol{x})^2 - \frac{i}{6}(\boldsymbol{q} \cdot \boldsymbol{x})^3 + \cdots \right) + \ldots \right]. \tag{7.45}$$

Likewise, we can expand the time-independent integration constant $\boldsymbol{c}$ of the function $\boldsymbol{g}$ in (7.42) as

$$\boldsymbol{c} = c_1 \, \boldsymbol{x} + c_2 \, (\boldsymbol{q} \cdot \boldsymbol{x}) \, \boldsymbol{x} + c_3 \, \boldsymbol{q} \, \boldsymbol{x}^2 + \mathcal{O}(\boldsymbol{x}^3) \, , \tag{7.46}$$

so that we generate an additional contribution to the metric (7.43) of the form

$$(\nabla_i \, c_j + \nabla_j \, c_i) \, dx_i dx_j = (c_1 + c_2 \, \boldsymbol{q} \cdot \boldsymbol{x}) \, d\boldsymbol{x}^2 + (c_2 + 2c_3) \, x_i q_j \, dx_i \, dx_j \, . \tag{7.47}$$

The expansion above allows us, through an appropriate choice of the involved constants, to remove the constant and linear contributions in the space-space part (7.43) of the perturbed metric. Thus, only one contribution to (7.43) remains, emerging from the time-dependent term of the function g (see (7.42)), which we can determine as

$$(\nabla_i \, g_j + \nabla_j \, g_i) \, dx_i \, dx_j \supset 2 \, \delta^L(t) \frac{(\boldsymbol{q} \cdot d\boldsymbol{x})^2}{q^2} \, . \tag{7.48}$$

If we finally add the different contributions that arise from applying the coordinate transformation (7.36) to the perturbed flat FRW metric (6.33), we find that the resulting metric in the anisotropic local coordinates $(t_A, \boldsymbol{x}_A)$ reads (restoring the labels)

$$ds^2 = -dt_A^2 + a^2 d\boldsymbol{x}_A^2 + 2 \, a^2 \delta^L(t) \frac{(\boldsymbol{q} \cdot d\boldsymbol{x}_A)^2}{q^2} - \frac{5}{2} a^2 H^2 \delta^L(t) \frac{(\boldsymbol{q} \cdot \boldsymbol{x}_A)^2}{q^2} d\boldsymbol{x}_A^2 \, . \tag{7.49}$$

At last, the comparison of the form of the locally curved anisotropic metric in the equation above with the one given in (7.37) shows that these can be transformed into each other by the identifications

$$a_\perp = a \, , \tag{7.50}$$

$$K_\perp = 0 \, , \tag{7.51}$$

$$a_\parallel = a \left(1 - \delta^L(t) \right) , \tag{7.52}$$

$$K_\parallel = 5H^2 a^2 \delta^L(t) \, . \tag{7.53}$$

Note that for being consistent, these expression have to reproduce the results for the scale factor a_K and the curvature K found in the case of a spherically symmetric perturbation, given in (6.44) and (6.45) (see also [165]), if we perform an angular averaging. However, it is slightly subtle to perform the angular average of the expressions in (7.50)-(7.53) since these are defined with respect to the soft momentum $\boldsymbol{q}$, constituting the actual quantity to be averaged over. Nonetheless, by realizing that performing the angular average with respect to $\boldsymbol{q}$ amounts in the replacement

$$\frac{q_i q_j}{q^2} \to \frac{1}{3} \delta_{ij} \tag{7.54}$$

with δ_{ij} denoting the Kronecker delta, we can conclude that the anisotropic locally curved metric (7.49) after angular averaging indeed reproduces the results for a_K and K in (6.44) and (6.45), respectively.

More anisotropy

Remember that our original motivation for extending the background method to the case of a directional soft mode was to derive an angular-dependent soft-limit bispectrum consistency relation to extract the coefficient $C_{12}(\eta)$ in the non-perturbative differential equation for the power spectrum in (7.33). In order to deduce the coefficient $C_{12}(\eta)$ from such a bispectrum consistency condition, involving curvature derivatives with respect to the power spectrum in locally curved anisotropic universe, it is necessary to extend our previous calculations and to include the next order in the soft mode q in the series expansions. Note that at this order in q, the anisotropies gain a fundamental role since the locally curved anisotropic background cosmology cannot simply be reduced to an isotropic locally curved FRW cosmology with tidal forces, as it is possible at leading order in q (see [241]).

Proceeding from these considerations, we extend the series expansions of the long-wavelength mode Φ^L in (7.45) and of the integration constant c, associated to the coordinate-dependent function g, in (7.46) about $q \cdot x$ to the next order. Afterwards, we can eliminate certain terms arising due to the series expansions in the space-space part of the locally curved anisotropic metric (7.43) by an appropriate choice of the expansion coefficients of the integration constant c. By doing so, we can transform terms of the form $x^2 dx^2$ into $(x \cdot dx)^2$. Afterwards, we combine the remaining terms with the other contributions to the metric generated by performing the coordinate transformation (7.36). Finally, this leads to the following locally curved anisotropic metric

$$ds^2 = - dt_A^2 + a^2 dx_A^2 + 2\,a^2 \delta^L(t) \frac{(q \cdot dx_A)^2}{q^2} - \frac{5}{2} a^2 H^2 \delta^L(t) \frac{(q \cdot x_A)^2}{q^2} dx_A^2$$
$$- \frac{5}{3} a^2 H^2 \delta^L(t) \frac{(q \cdot x_A)^3}{q^2} dx_A^2 + 2\,a^2 \delta^L(t) \frac{(q \cdot dx_A)^2}{q^2} (q \cdot x_A) \ . \tag{7.55}$$

In comparison to the metric in (7.49), the two additional higher-order terms with respect to the soft mode are given in the second line of this equation. We can subsequently transform the locally curved anisotropic metric above into a corresponding metric of the form

$$ds^2 = - dt_A^2 + a^2\,dx_{A,\perp}^2 + \left(1 + b_\parallel\,q\,x_{A,\parallel}\right) a_\parallel^2\,dx_{A,\parallel}^2$$
$$- \frac{1}{2}\left(K_\parallel + \mathcal{K}_\parallel\,q\,x_{A,\parallel}\right) a^2\,x_{A,\parallel}^2\,dx_K^2 \ , \tag{7.56}$$

by using the identifications for the parallel and perpendicular scale factors and curvature parameters, $a_\parallel$, $a_\perp$, $K_\parallel$ and $K_\perp$, in (7.50)-(7.53) and defining the parallel quantities

$$b_\parallel = 2\,\delta^L(t)\,, \tag{7.57}$$

$$\mathcal{K}_\parallel = \frac{10}{3}a^2 H^2 \delta^L(t) \tag{7.58}$$

with $\mathcal{K}_\parallel$ not to be confused with the parallel curvature $K_\parallel$, defined in (7.53). Moreover, note that we can make the replacement $b_\parallel a_\parallel^2 \to b_\parallel a^2$ when considering only the leading order in δ^L. However, if we average over the angles defined with respect to the soft momentum $\boldsymbol{q}$, the additional terms involving the quantities $b_\parallel$ and $\mathcal{K}_\parallel$ vanish.

7.2.2. Non-perturbative bispectrum consistency condition

Since the locally curved anisotropic background cosmology described by the metric (7.56) involves two time variables associated to the parallel and the perpendicular scale factor, $\eta_\parallel \equiv \ln a_\parallel$ and $\eta_\perp \equiv \ln a_\perp$ with $a_\perp = a$, as well as the curvature parameters $K_\parallel$ and $K_\perp$ with $K_\perp = 0$ (see (7.50)-(7.53)), the fluctuation fields $\psi_{a,A}$ and hence the corresponding correlation functions, such as the power spectrum, depend on these quantities. Furthermore, the power spectrum depends not only on the absolute value of the momentum $\boldsymbol{k}$, but separately also on the momenta $\boldsymbol{k}_\parallel$ and $\boldsymbol{k}_\perp$, denoting the projections relative to $\boldsymbol{q}$. Thus, in its most general form the power spectrum reads $P_{ab,A}(\boldsymbol{k}_\parallel, \boldsymbol{k}_\perp, \eta_\parallel, \eta_\perp, K_\parallel)$.

Following the steps outlined in Section 6.3.3, we can then derive a non-perturbative angular-dependent consistency condition for the bispectrum in the soft limit in dependence of the density-density power spectrum in the locally curved anisotropic background. As a result, we obtain for the bispectrum in the soft limit the (non-perturbative) relation (see (6.56))

$$B_{111}(\boldsymbol{k}, -\boldsymbol{q}, \boldsymbol{q} - \boldsymbol{k}, \eta) \xrightarrow{q \to 0} P^L(q, \eta) \Bigg[\left(1 - \boldsymbol{k}_\parallel \frac{\partial}{\partial \boldsymbol{k}_\parallel} - \frac{\partial}{\partial \eta_\parallel}\right) P_{11,A}(\boldsymbol{k}_\parallel, \boldsymbol{k}_\perp, \eta_\parallel, \eta_\perp, K_\parallel) $$
$$+ 5\frac{\partial}{\partial \kappa_\parallel} P_{11,A}(\boldsymbol{k}_\parallel, \boldsymbol{k}_\perp, \eta_\parallel, \eta_\perp, K_\parallel) \Bigg] + \dots, \tag{7.59}$$

where we have introduced

$$\kappa_\parallel = \frac{K_\parallel}{a^2 H^2}\,, \tag{7.60}$$

in analogy to the parameter κ in (6.57). Furthermore, after the derivatives of the bispectrum consistency relation in (7.59) have been performed, it is understood to be evaluated at $\eta_\parallel = \eta_\perp = \eta$, $\boldsymbol{k}_\parallel = \boldsymbol{k}_\perp = \boldsymbol{k}$ and $\kappa_\parallel = 0$. Besides, the ellipses in this equation represent higher-order contributions with respect to the soft mode q, incorporating derivatives, e.g., with respect to $\mathcal{K}_\perp$ in (7.55). To avoid a rather cumbersome expression, we do not write down these

higher-order contributions explicitly. However, they can be obtained in a straightforward manner from the locally curved anisotropic metric (7.56).

If we average the soft-limit bispectrum consistency condition in (7.59) over the angles related to the directional soft mode q according to (7.59), we regain exactly the relation for the bispectrum in the soft limit derived for the case of a spherically symmetric soft mode in an EdS background cosmology, given in (6.56) (see also [165, 166, 173, 174]). The corresponding bispectrum consistency relation including also the velocity perturbations can be found in (7.21). As we have shown in (7.22) with (5.11), this can be used to extract the multipole contribution $\ell = 0$ of the coefficient $C_{22}(\eta)$.

By performing an analogous computation as for $C_{22}(\eta)$, it is straightforward to determine the coefficient $C_{12}(\eta)$ in (7.31) from the non-perturbative angular-dependent bispectrum consistency relation in (7.59). Thereby, it is necessary to take the higher-order terms denoted by the ellipses in the bispectrum consistency relation (7.59) into account. These allow us, in particular, to extract the contributions $C_{ab}^{(\ell)}(\eta)$ for the multipoles $\ell = \{1, 2\}$ in (7.31). These can be expressed in terms of the variance of the displacements, defined in (5.11), in the locally curved anisotropic cosmology

$$\sigma^2_{ab,A}(\eta_{\parallel}, \eta_{\perp}, K_{\parallel}, \ldots) \equiv \frac{1}{3} \int \frac{d^3k}{k^2} \, P_{ab,A}(k_{\parallel}, k_{\perp}, \eta_{\parallel}, \eta_{\perp}, K_{\parallel}, \ldots) , \qquad (7.61)$$

which depends on a series of geometrical parameters arising from the inclusion of the higher-order bispectrum contributions. In analogy to (7.22), we can finally write the coefficient $C_{12}(\eta)$ in terms of derivatives with respect to these geometrical parameters. To evaluate $C_{12}(\eta)$, we consequently would have to set the geometrical derivatives in relation to quantities inferred from the flat EdS cosmology, either by deducing an empirical approximation similar to the generalized VKPR proposal for spherically symmetric soft modes (see (6.76)) or by performing numerical simulations in a locally curved anisotropic background cosmology. These would then be used as input in the non-perturbative differential equation for the power spectrum in the soft limit in (7.33). However, as we illustrate in the next section, the contributions of the coefficient $C_{12}(\eta)$ to the power spectrum equation (7.33) are only subleading. For this reason, we can neglect $C_{12}(\eta)$ In the end and solely focus on the impact of the remaining coefficient $C_{22}(\eta)$, given in (7.22). In contrast to $C_{12}(\eta)$, the latter can be extracted from the angular-averaged version of the bispectrum consistency relation (7.59), coinciding with (6.56).

7.3. Evaluation of the non-perturbative power spectrum equation

Apart from the parameterization of the non-linear α-contributions in terms of the coefficient $C_{12}(\eta)$ in Section 7.1.2, there exists another, perhaps more suggestive way, to quantify their impact in the non-perturbative differential equation for the power spectrum in (7.33). By a judicious shift in the integration variables, we can rewrite the non-linear α-contributions of (7.26) as

$$
\int d^3k \, u_a \, \alpha(\boldsymbol{q}/2 - \boldsymbol{k}, \boldsymbol{q}/2 + \boldsymbol{k}) \, B_{b12}(-\boldsymbol{q}, \boldsymbol{q}/2 - \boldsymbol{k}, \boldsymbol{q}/2 + \boldsymbol{k}, \eta)
$$
$$
= \int d^3k \, u_a \, \frac{\boldsymbol{q} \cdot \boldsymbol{k}}{2k^2} \left[B_{b12}(\boldsymbol{q}, -\boldsymbol{q}/2 - \boldsymbol{k}, -\boldsymbol{q}/2 + \boldsymbol{k}, \eta) - B_{b12}(-\boldsymbol{q}, \boldsymbol{q}/2 - \boldsymbol{k}, \boldsymbol{q}/2 + \boldsymbol{k}, \eta) \right].
$$
(7.62)

From this way of reformulating the α-contributions, we can directly see that these do not receive angular-averaged bispectrum contributions. In other words, if we replace the bispectra in the equation above by the OPE decomposition of the bispectrum in (7.9), only terms including the function $\tilde{f}_{12}^{(1)}(k, \eta)$ enter in the coefficient $C_{12}(\eta)$ and yield non-vanishing contributions to the α-terms. Here, we have used the tilde to distinguish from the direct OPE decomposition of the bispectrum in the soft limit, performed in Section 7.1 and leading to the coefficient $C_{12}(\eta)$ as given in (7.31).

Because of the explicit angular dependence of the α-contributions which is apparent in (7.62), one may suggest that they are of minor importance compared to the β-contributions so that their influence in the differential power spectrum equation in (7.33) corresponds only to a subleading effect. Indeed, by performing a perturbative cross check in SPT, we find that the α-contributions are roughly a factor 20 smaller than the leading contributions from the β-terms. In the non-perturbative regime, neglecting the α-contributions is in principle not justified and may still lead to sizeable errors. However, as we demonstrate in what follows, most of the modes contributing to the coefficient $C_{12}(\eta)$ come from near the non-linear scale. Thus, we expect only small deviations to occur due to neglecting the α-terms. In the analysis we perform next, we therefore ignore the α-terms by working under the hypothesis

$$
P_{ab}^{\alpha}(k, \eta) \ll P_{ab}^{\beta}(k, \eta).
$$
(7.63)

In Appendix A.2, we present a numerical estimate for the errors induced by neglecting the coefficient $C_{12}(\eta)$ that parameterizes the α-contributions. In fact, as we shall see in Section 7.4, this approximation fares well against numerical simulations.

Hence, by concentrating on the non-linear contributions of the β-terms, we can approximate

the fully non-linear power spectrum of (7.11) with (7.13) by

$$P_{ab}(q, \eta) \simeq P_{ab}^L(q, \eta) + P_{ab}^{\beta}(q, \eta) \,. \tag{7.64}$$

As a consequence, the non-perturbative equation for the power spectrum in (7.33) does only include the coefficient $C_{22}(\eta)$ arising from the β-contributions. By using the angular-averaged bispectrum consistency relation (7.21) and the generalized VKPR proposal (6.76) to express $C_{22}(\eta)$ as in (7.23), the non-perturbative equation for the power spectrum in the soft limit finally reads

$$\partial_\eta P_{ab}(q, \eta) = -\,\Omega_{ac}(\eta)\, P_{cb}(q, \eta) - \Omega_{bc}(\eta)\, P_{ac}(q, \eta)$$
$$+\, q^2 P^L(q, \eta) \begin{pmatrix} 0 & 1 \\ 1 & 2 \end{pmatrix}_{ab} \left(\frac{4}{7}\sigma_{22}^2(\eta) - \frac{13}{14}\partial_\eta\, \sigma_{22}^2(\eta) \right) \,. \tag{7.65}$$

Next, we parameterize the power spectrum in the soft limit as

$$P_{ab}(q, \eta) = \left[u_a u_b + q^2 c_{ab}(\eta) \right] P^L(q, \eta) \,. \tag{7.66}$$

If we subsequently insert this parameterization into the non-perturbative power spectrum equation in (7.65) and subtract the terms governing the evolution of the linear power spectrum, (7.12), we obtain a momentum-independent differential evolution equation for the coefficients $c_{ab}(\eta)$,

$$\partial_\eta c_{ab}(\eta) = -\,\Omega_{ac}(\eta)\, c_{cb}(\eta) - \Omega_{bc}(\eta)\, c_{ac}(\eta)$$
$$+ \begin{pmatrix} 0 & 1 \\ 1 & 2 \end{pmatrix}_{ab} \left(\frac{4}{7}\sigma_{22}^2(\eta) - \frac{13}{14}\partial_\eta\, \sigma_{22}^2(\eta) \right) \,. \tag{7.67}$$

This evolution equation for $c_{ab}(\eta)$ is the main relation on which our following numerical analysis relies.

7.4. Numerical analysis

In our numerical analysis, we treat the dependence of the evolution equation on the background cosmology, which is encoded in the matrix $\Omega_{ab}(\eta)$ (see (3.52)), by using the form of this matrix in the EdS case in (3.64) as input, $\Omega_{ab}(\eta) = \Omega_{ab}^{\mathrm{EdS}}$. To generalize to cosmological models other than EdS, we do not change the background-encoding matrix, but only adapt the time variable $\eta = \ln D_1(\tau)$ by taking the linear growth factor $D_1(\tau)$ in (3.9) correctly into account. This implies $D_1(\tau) = a(\tau)$ to hold only for an EdS cosmology (see (3.17)). In the

case of a ΛCDM universe, the linear growth factor is approximately given by (3.18). As discussed in the Sections 3.2.4 and 3.3.3, the error induced by this approximation is subdominant (see also [40]).

As a first example, let us evaluate the evolution equation (7.67) for the coefficients $c_{ab}(\eta)$ at leading order. Thereby, we use the fact that the variance (5.11) of the linear power spectrum (5.11) scales in time like

$$\sigma^2_{ab,L}(\eta) = \frac{4\pi}{3} \int dk \, P^L_{ab}(k, \eta) = e^{2(\eta - \eta_0)} \sigma^2_{ab,L}(\eta_0) \,, \tag{7.68}$$

when assuming growing-mode initial conditions for the linear power spectrum as in (4.16). This allows us to determine the time-derivative on the right-hand side of (7.65) and perform the integration over η afterwards. Hence, the resulting evolution coefficient at leading-order (LO) reads

$$c^{\mathrm{LO}}_{ab}(\eta) = -\frac{\sigma^2_{ab,L}(\eta)}{63} \begin{pmatrix} 38 & 76 \\ 76 & 114 \end{pmatrix}_{ab} \simeq -\sigma^2_{ab,L}(\eta) \begin{pmatrix} 0.60 & 1.21 \\ 1.21 & 1.81 \end{pmatrix}_{ab}. \tag{7.69}$$

In order to gain an insight on the accuracy of these predictions for the leading-order coefficients $c^{\mathrm{LO}}_{ab}(\eta)$, we compare them with the results arising from a direct computation in SPT. If we parameterize the power spectrum in the soft limit in SPT according to (7.66), we see that the first order of the non-linear contributions to the power spectrum, involving the coefficient $c_{ab}(\eta)$, corresponds to the one-loop order in SPT. Consequently, we have to confront the coefficient $c^{\mathrm{SPT}}_{ab}(\eta)$ extracted from the one-loop SPT power spectrum in the soft limit against the leading-order coefficient $c^{\mathrm{LO}}_{ab}(\eta)$ emerging from (7.67). Since it is equivalent to consider the one-loop power spectrum for soft external momenta q or hard loop momenta k with $k \gg q$, we can use the SPT power spectrum at one-loop order for large loop momenta, given in (6.19), to directly read off the coefficient $c^{\mathrm{SPT}}_{ab}(\eta)$ from the contribution proportional to the square of the external momentum,

$$c^{\mathrm{SPT}}_{ab}(\eta) = -\frac{\sigma^2_{ab,L}(\eta)}{105} \begin{pmatrix} 61 & 125 \\ 125 & 189 \end{pmatrix}_{ab} \simeq -\sigma^2_{ab,L}(\eta) \begin{pmatrix} 0.58 & 1.19 \\ 1.19 & 1.80 \end{pmatrix}_{ab}. \tag{7.70}$$

If we compare the coefficients $c^{\mathrm{LO}}_{ab}(\eta)$ in (7.69) and $c^{\mathrm{SPT}}_{ab}(\eta)$ in the expression above, we observe small deviations between the numerical values of the corresponding components. At this level, these small differences quantify the errors in the non-perturbative power spectrum equation (7.65) induced by neglecting the impact of the α-contributions (7.32) and by approximating the β-contributions (7.20) by the generalized VKPR proposal (6.76). As we illustrated in the previous chapter, the application of the VKPR proposal, being a reasonable empirical approximation, causes a small error within perturbation theory. Thus, for the non-linear

regime, we estimate the overall error generated by these approximations to be at most an effect of the order of $\sim 10\%$. This estimate is consistent with the conclusion we draw from determining the coefficients $c_{ab}(\eta)$ numerically.

7.4.1. Estimation of the error due to neglecting the α-terms

All numerical results we present in the following are based on predictions from N-body simulations that rely on a phase-space projection technique and have been performed in [378]. In detail, [378] provides N-body predictions for the power spectra $P_{ab}(k,\eta)$ of the density and velocity fields at present time, or equivalently at redshift $z = 0$, in a ΛCDM universe. In the N-body simulations, the cosmological parameters of the WMAP7 data release [379] have been used, i.e., the density parameters $\Omega_{m,0} = 0.276$, $\Omega_{\Lambda,0} = 0.724$ and $\Omega_{b,0} = 0.045$, a dimensionless Hubble parameter of $h = 0.703$, the power spectrum renormalization $\sigma_8 = 0.811$ as well as the primordial spectral index $n_s = 0.96$. For our numerical analysis, we have used the N-body predictions for the power spectra in [378] to numerically determine the variance of the displacement fields $\sigma_{ab}^2(\eta)$, defined in (5.11), by performing the momentum integral over the power spectra $P_{ab}(k,\eta)$.

For instance, we can use the N-body predictions for the velocity power spectrum $P_{22}(k,\eta)$ in the ΛCDM case to determine the corresponding variance $\sigma_{22}^2(\eta)$. Since $\sigma_{22}^2(\eta)$ is the only input needed to numerically evaluate the evolution equation for the coefficients $c_{ab}(\eta)$ in (7.67), we can consequently study these coefficients as a function of time η (see (3.49) with (3.18)) or equivalently of redshift z (see (1.1)). This is shown in Figure 7.1. By comparing in particular our numerical results for the coefficient $c_{11}(\eta)$, parameterizing the non-linear power spectrum of the density fields in the soft limit, with corresponding data from [199, 200], we find that the agreement within the error bars of the order of $\sim 10\%$ is remarkably good. Unfortunately, we currently do not have knowledge of data in the literature that could be used for comparison with our numerical results for the coefficients $c_{12}(\eta) = c_{21}(\eta)$ and $c_{22}(\eta)$.

7.4.2. Impact of hard modes beyond the non-linear scale

Additionally, there is another interesting aspect we can infer from Figure 7.1. In order to evaluate the coefficients $c_{ab}(\eta)$ numerically, we have determined the variance $\sigma_{22}^2(\eta)$ according to (5.11) by performing the momentum integral over the velocity power spectrum $P_{22}(k,\eta)$. We have set the upper integration limit to the scale $k_{\max} = 1\,h/\mathrm{Mpc}$ and $k_{\max} = 10\,h/\mathrm{Mpc}$, respectively. However, as we can see from Figure 7.1, the coefficients $c_{ab}(\eta)$ only depend very weakly on this choice of the cutoff scale $k_{\max}$.

To investigate this point in further detail, we adapt our definition of the variance of the
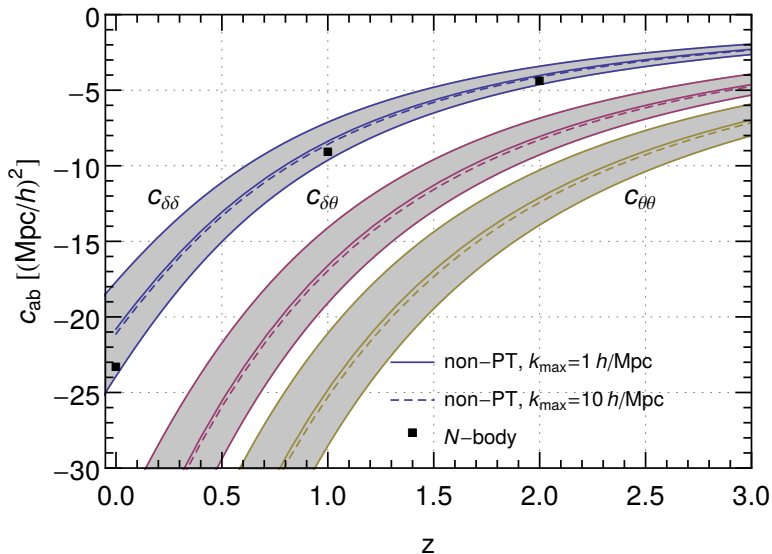
Fig. 7.1.: Numerical results for the coefficients $c_{ab}(z)$, parameterizing the non-linear power spectrum $P_{ab}(q, z)$ in the soft limit according to (7.66), as a function of redshift z and for a ΛCDM universe. The coefficients $c_{\delta\delta} \equiv c_{11}$, $c_{\delta\theta} \equiv c_{12} = c_{21}$ and $c_{\theta\theta} \equiv c_{22}$ are obtained from the relation (7.67) based on the non-perturbative equation for the power spectrum in the soft limit. Thereby, the only input needed to evaluate (7.67) consists of the variance of the displacement field $\sigma_{22}^2(z)$, defined in (5.11). Here, we have determined $\sigma_{22}^2(z)$ by using the power spectrum of the velocity divergence, $P_{\theta\theta}(q, z = 0) \equiv P_{22}(k, z = 0)$, from the numerical simulations in the ΛCDM case performed in [378] and performing the momentum integration up to a momentum k_{max} afterwards (see also (7.71)). The data points indicated by black squares correspond to numerical results for the coefficient $c_{11}(z)$ of the density power spectrum in the soft limit from [199, 200]. Moreover, the gray error bands indicate a 10%-deviation from the numerical results for the coefficients $c_{ab}(z)$ which constitutes a rough estimation of the error in the non-perturbative power spectrum equation (7.65), induced by ignoring the α-terms (7.32) and applying the VKPR approximation (6.76). By comparing the numerical results for the coefficient $c_{11}(z)$ with the data points from [199, 200], we see that the deviation is indeed at most a $\sim 10\%$ effect and becomes remarkably small at higher redshift z.

displacement fields $\sigma_{ab}^2(\eta)$ in (5.11) by reintroducing it as a cutoff-dependent quantity,

$$\sigma_{ab}^2(k_{\mathrm{max}}, \eta) \equiv \frac{4\pi}{3} \int\limits_0^{k_{\mathrm{max}}} dk\, P_{ab}(k, \eta) \,, \tag{7.71}$$
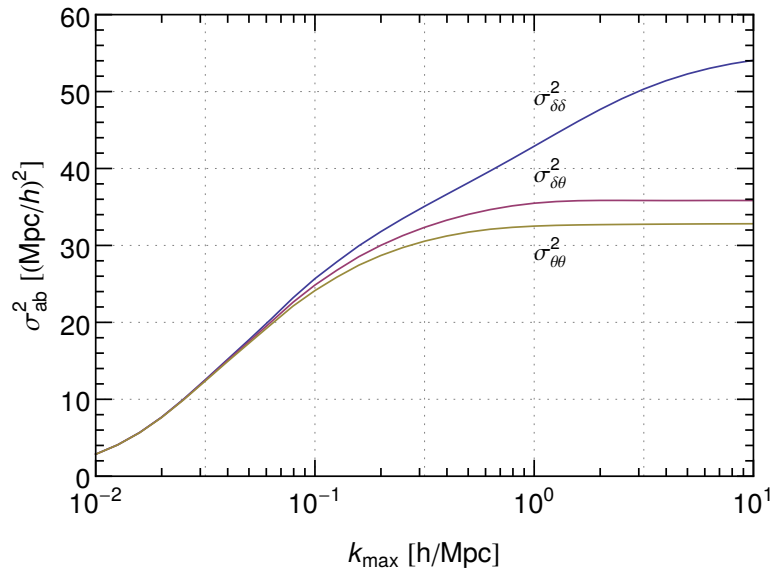
175

Fig. 7.2.: Dependence of the variance of the displacement fields $\sigma_{ab}^2(k_{\max})$, defined in (7.71), on the cutoff scale $k_{\max}$ at redshift $z = 0$ and for a ΛCDM universe. The variances $\sigma_{\delta\delta}^2 \equiv \sigma_{11}^2$, $\sigma_{\delta\theta}^2 \equiv \sigma_{12}^2$ and $\sigma_{\theta\theta}^2 \equiv \sigma_{22}^2$ are evaluated by using the numerical results for the power spectrum $P_{ab}(q, z = 0)$ based on the ΛCDM simulation data in [378]. While the variance of the density auto-correlation, $\sigma_{11}^2(k_{\max})$ depends significantly on the chosen cutoff scale, the variances associated to the density-velocity cross correlation and the velocity auto-correlation, $\sigma_{12}^2(k_{\max})$ and $\sigma_{22}^2(k_{\max})$, show a saturation behavior and thus only a weak dependence on modes $k_{\max}$ bigger than the non-linear scale $\Lambda_{\mathrm{NL}} \simeq 0.5 \, h/\mathrm{Mpc}$. Note that at earlier times where $z > 0$, the cutoff-dependence is even less relevant.

evaluated at present time $\eta(z = 0)$,

$$\sigma_{ab}^2(k_{\max}) \equiv \sigma_{ab}^2\big(k_{\max}, \eta(z = 0)\big) \,. \tag{7.72}$$

Here, we have refrained to propose an additional symbolic notation for the cutoff-dependent variance at present time, $\sigma_{ab}^2(k_{\max})$, that has to be distinguished from the time-dependent variance $\sigma_{ab}^2(\eta)$, defined in (5.11), for keeping the notation simple.

In Figure 7.2, we present the dependence of the variance $\sigma_{ab}^2(k_{\max})$ on the short-distance cutoff scale $k_{\max}$. Therein, the numerical results for $\sigma_{ab}^2(k_{\max})$ are evaluated at redshift $z = 0$ and for the ΛCDM cosmology as implemented in [378]. This figure illustrates that the variances arising from the cross-correlation of density and velocity fields as well as from the auto-

correlation of the latter, i.e., $\sigma_{12}^2(k_{\max})$ and $\sigma_{22}^2(k_{\max})$, do not vary significantly for $k_{\max} \gtrsim \Lambda_{\mathrm{NL}}$ with $\Lambda_{\mathrm{NL}} \simeq 0.5 \, h/\mathrm{Mpc}$ being the non-linear scale. In fact, $\sigma_{12}^2(k_{\max})$ and $\sigma_{22}^2(k_{\max})$ exhibit a saturation that sets in for $k_{\max} \gtrsim \Lambda_{\mathrm{NL}}$. In contrast to this, the variance of the density auto-correlation, $\sigma_{11}^2(k_{\max})$, does show a cutoff-dependent behavior beyond the non-linear scale Λ_{NL}.

7.4.3. Dependence on the background cosmology

In the non-perturbative power spectrum equation (7.10), the dependence on the cutoff scale $k_{\max}$ enters through the coefficients $C_{12}(\eta)$ and $C_{22}(\eta)$. These constitute – in their most general form – functions of the variances $\sigma_{12,A}^2(k_{\max}, \dots)$ and $\sigma_{22,A}^2(k_{\max}, \dots)$ in a (hypothetical) locally curved anisotropic background cosmology (see (7.61)). Here, we define the cutoff-dependent variance $\sigma_{ab,A}^2(k_{\max}, \dots)$ at zero redshift similarly as in (7.71). While we expect that the variance $\sigma_{ab,A}^2(k_{\max}, \dots)$ depends on the underlying cosmological model for $k_{\max} \ll \Lambda_{\mathrm{NL}}$, the situation is different if the cutoff scale $k_{\max}$ is much bigger than the non-linear scale Λ_{NL}. Since the curvature parameters and the other geometrical dependencies entering in the variance (7.61) are induced by the directional soft mode, they depend on the properties of the long-wavelength mode $\delta^L(\boldsymbol{q}, \eta) \ll 1$ with $q \ll \Lambda_{\mathrm{NL}}$. Thus, the details of the background cosmology, which are only relevant at long distances, should not significantly affect the qualitative behavior of the variance $\sigma_{ab,A}^2(k_{\max}, \dots)$ on short distance scales. In other words, we expect for $k_{\max} \gg \Lambda_{\mathrm{NL}}$ the relation

$$\sigma_{ab,A}^2(k_{\max}, \dots) \simeq \sigma_{ab}^2(k_{\max}) \tag{7.73}$$

to be valid. As a consequence, we can apply the conclusions we draw from Figure 7.1 and Figure 7.2 for the variance $\sigma_{ab,A}^2(k_{\max}, \dots)$ in the locally curved anisotropic universe. This implies in particular that $\sigma_{12,A}^2(k_{\max}, \dots)$ and $\sigma_{22,A}^2(k_{\max}, \dots)$ can only display a weak dependence on short-distance modes beyond the non-linear scale.

Let us next consider the case of a spherically symmetric perturbation, which is sufficient to determine the coefficient $C_{22}(\eta)$ in the non-perturbative power spectrum equation (7.10) in dependence of a locally curved background cosmology. Following the same arguments as used before to derive (7.73), we can approximate the variance in the locally curved background cosmology, induced by the spherically symmetric soft mode, for $k_{\max} \gg \Lambda_{\mathrm{NL}}$ as

$$\sigma_{ab,K}^2(k_{\max}) \simeq \sigma_{ab}^2(k_{\max}) \, . \tag{7.74}$$

Since the variance $\sigma_{22}^2(\eta)$ constitutes the crucial quantity to determine the coefficient $C_{22}(\eta)$ entering in the non-perturbative power spectrum equation (7.65), we can use the observed

saturation of $\sigma_{22}^2(\eta)$ beyond the non-linear scale to draw also conclusions about the cutoff-dependence of $C_{22}(\eta)$. In order to do so, we need to include one more step though. The reason for this is that the general form of the coefficient $C_{22}(\eta)$ in (7.22) includes, among others, a derivative with respect to curvature. However, for modes deep in the non-linear regime, i.e., for $k \gg \Lambda_{\mathrm{NL}}$, one can show that (see also (6.60))

$$\left. \frac{\partial}{\partial \kappa} P_{ab,K}(k,\eta) \right|_{K=0} < P_{ab}(k,\eta) \tag{7.75}$$

with κ defined in (6.57). This can be inferred from testing the background method, which absorbs a spherically symmetric soft mode into a locally curved background cosmology, with numerical simulations in the framework of the 'separate universe' approach [238–240, 380] (see also the discussion in Section 6.3). In [380], the 'separate universe' approach is used to calculate the derivative of the power spectrum with respect to curvature and to subsequently determine the response to the spherically symmetric long-wavelength perturbation numerically from N-body simulations. To be precise, the response function $G_1(k,\eta)$ of the density power spectrum $P(k,\eta) \equiv P_{11}(k,\eta)$ (see (6.55)), defined as [380]

$$G_1(k,\eta) \equiv -\frac{1}{3} \partial_\eta \ln P_{K=0}(k,\eta) + \frac{5}{3} \left. \frac{\partial}{\partial \kappa} \ln P_K(k,\eta) \right|_{K=0}, \tag{7.76}$$

is evaluated at different redshifts z and hence different times η. Note that the response function $G_1(k,\eta)$ incorporates exactly the combination of time and curvature derivatives which enters in the non-perturbative angular-averaged bispectrum consistency condition that we derived in (6.56) (see (7.21) as well). Thus, it is this combination of derivatives that determines the coefficient $C_{22}(\eta)$. Recall that in the final step of our derivation of $C_{22}(\eta)$ (see (7.23)), we applied the generalized VKPR proposal in (6.76) to approximate the derivative with respect to curvature by a time derivative. By using the results of the response function $G_1(k,\eta)$ from the numerical simulations of [380], we can judge the exactness of this approximation. For this purpose, we formulate the VKPR proposal (6.60) for the logarithm of the density power spectrum,

$$\left. \frac{\partial}{\partial \kappa} \ln P_K(k,\eta) \right|_{K=0} = \frac{4}{7} \partial_\eta \ln P_{K=0}(k,\eta). \tag{7.77}$$

Afterwards, we insert this expression into (7.76) and determine the response function based on the VKPR proposal. In Figure 7.3, we then compare the results for the power spectrum response function (7.76) based on the numerical simulations of [380] with the one arising from the VKPR proposal at redshift $z = 0$ (on the left) and $z = 2$ (on the right).[2] The results

---

[2]The cosmological parameters used for the N-body simulations in [380] are the density parameters $\Omega_{m,0} = 0.27$, $\Omega_{\Lambda,0} = 0.73$ and $\Omega_{b,0} = 0.023$, a dimensionless Hubble parameter of $h = 0.7$, the power spectrum renormalization $\sigma_8 = 0.8$ and the primordial spectral index $n_s = 0.95$.
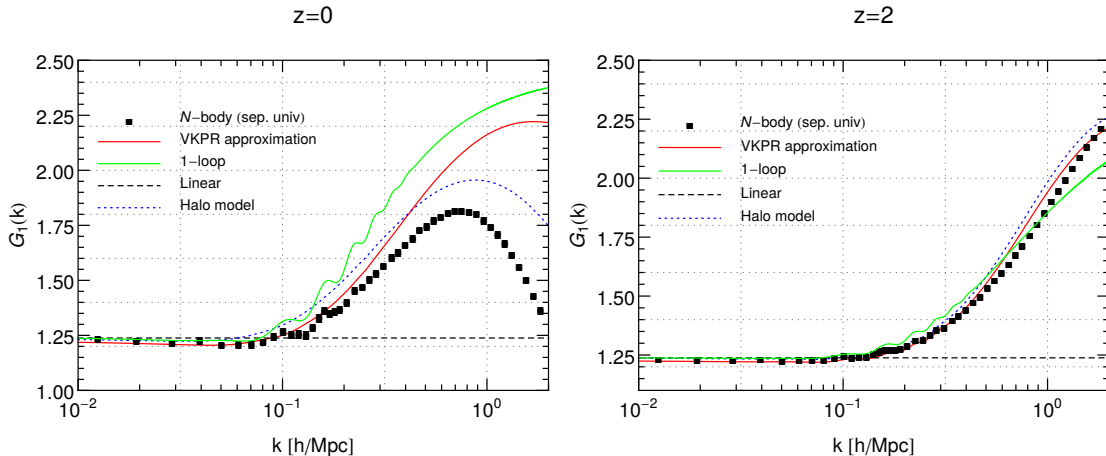
Fig. 7.3.: Momentum dependence of the density power spectrum response function $G_1(k, z)$, introduced in (7.76), to a spherically symmetric long-wavelength perturbation at redshift $z = 0$ (on the left) and $z = 2$ (on the right) for a ΛCDM universe. While the black squares represent the results for $G_1(k, z)$ from the N-body simulations for a ΛCDM universe performed in [380], the red solid line displays the predictions of the VKPR proposal (7.77) in [173, 174]. Besides, the numerical results for the power spectrum response function obtained from SPT computations in a curved background cosmology (see Section 6.5.2) and from the phenomenological 'halo model' [381–383] are indicated by the dashed black line and the dotted blue line, respectively. On the one hand, for both redshifts $z = 0$ and $z = 2$, we see a relatively good agreement of the VKPR proposal with the N-body simulation data at small wavenumbers k. On the other hand, at zero redshift, the VKPR proposal deviates from the numerical simulations at higher wavenumbers k near the non-linear scale $\Lambda_{\mathrm{NL}} \simeq 0.5 \, h/\mathrm{Mpc}$ with an error of the order of $\sim 10\%$. This disagreement increases significantly for momenta much bigger than the non-linear scale, $k \gg \Lambda_{\mathrm{NL}}$, such that the predictions of the VKPR proposal overestimate $G_1(k, z)$ compared to results based on the numerical simulations.

from the N-body simulations performed in [380] correspond to the black squares, whereas the predictions of the VKPR proposal are displayed by the red solid line. In addition, we show the power spectrum response function obtained from SPT computations in a curved background cosmology (dashed black line), implementing our results derived in Section 6.5.2, as well as from the phenomenological 'halo model' (dotted blue line).[3]

---

[3]The so-called 'halo model' [381–383] is a phenomenological model to describe the dynamics of gravitational clustering. In its simplest formulation, it relies on the approximation that all matter in the Universe is asso-

7. Non-Perturbative Power Spectrum Equation

Both at redshift $z = 0$ and $z = 2$, the N-body results and those relying on the VKPR approximation agree relatively well for small momenta k. However, at zero redshift, it is clearly visible that the VKPR proposal fails at higher momenta near the non-linear scale $\Lambda_{\mathrm{NL}} \simeq 0.5 \, h/\mathrm{Mpc}$ with an error of the order of $\sim 10\%$. If we consider even bigger momenta $k \gg \Lambda_{\mathrm{NL}}$, this disagreement increases significantly so that the VKPR predictions lie much above the results from the numerical simulations. Thus, the predictions of the VKPR proposal *overestimate* the power spectrum response function compared to the results obtained from the N-body simulations in [380]. Unfortunately, the numerical simulations in [380] only refer to the power spectrum of density perturbations, $P_{11}(k, \eta)$, and do not include the density-velocity or velocity-velocity power spectrum $P_{12}(k, \eta)$ and $P_{22}(k, \eta)$, respectively. However, we expect to deduce similar results for the latter.

Proceeding in this direction, we present in Figure 7.4 the time derivative of the variance, $\partial_\eta \sigma_{ab}^2(k_{\mathrm{max}}, \eta)$ (see (7.71)), based on the N-body simulation data for a ΛCDM universe in [378], as a function of the cutoff scale k_{max}. First of all, this figures illustrate once more the weak dependence of the variances $\sigma_{12}^2(k_{\mathrm{max}})$ and $\sigma_{22}^2(k_{\mathrm{max}})$ on modes k_{max} beyond the cutoff scales Λ_{NL}. Moreover, by comparing it with Figure 7.2, we see that the approximation $\partial_\eta \ln \sigma_{12(22)}^2(k_{\mathrm{max}}) \simeq 2$ is relatively accurate for $k_{\mathrm{max}} \gtrsim \Lambda_{\mathrm{NL}}$. If we transfer this finding to the power spectrum, i.e., $\partial_\eta \ln P_{12(22)}(k, \eta) \simeq 2$ with k much larger than Λ_{NL} (see (7.71)), and take into account that the predictions of the generalized VKPR proposal for $P_{12}(k, \eta)$ and $P_{22}(k, \eta)$ in the regime $k \gg \Lambda_{\mathrm{NL}}$ are an overestimation of the N-body results (see Figure 7.3), we conclude that the upper bound on the derivative of the power spectrum in (7.75) with respect to spatial curvature is fulfilled. This implies that the weak sensitivity to the hard modes beyond the non-linear scale also applies for the curvature derivatives of the variances $\sigma_{12,K}^2$ and $\sigma_{22,K}^2$. In particular, the latter enters through the coefficient $C_{22}(\eta)$, given in (7.22), in the non-perturbative power spectrum equation (7.65).

On physical grounds, we expect this saturation behavior beyond the non-linear scale to be a general feature that also occurs in the case of a locally curved anisotropic universe, for both the variances $\sigma_{12,A}^2$ and $\sigma_{22,A}^2$ as well as their variations with respect to the additional geometrical parameters introduced in (7.61). Since these quantities constitute the general contributions to the coefficients $C_{12}(\eta)$ and $C_{22}(\eta)$, we draw the conclusion that also $C_{12}(\eta)$ and $C_{22}(\eta)$

---

ciated to dark matter halos. The halo model yields a relatively accurate description for the power spectrum and bispectrum of density perturbations, with an precision of typically better than $\sim 10\%$ for $k < 1 \, h/\mathrm{Mpc}$ at redshift $z = 0$ [384]. The ideas of the halo model have been extended further into the direction of phenomenology by the implementation of the 'halofit' method [385, 386]. This method provides even more accurate predictions for the density power spectrum in form of a simulation-calibrated fitting formula, which is based on the halo model and contains numerous heuristic parameters matched to numerical simulations.
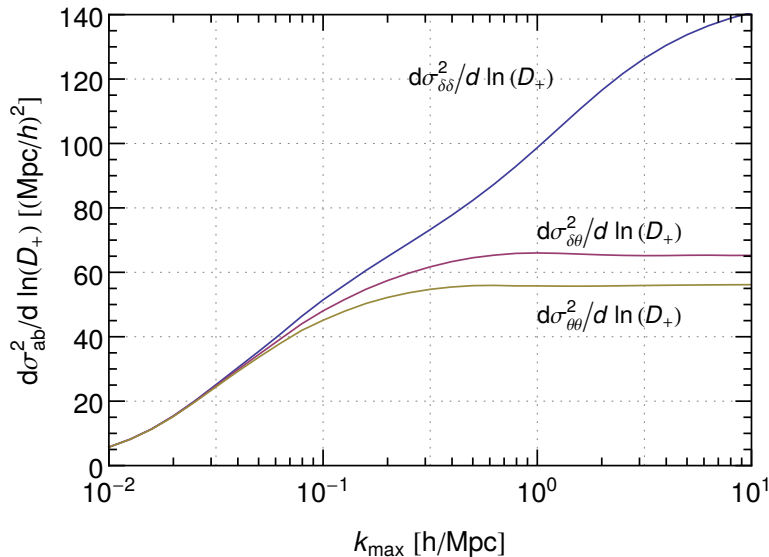
Fig. 7.4.: Time derivative of the variances of the displacement fields $\partial_\eta \sigma_{ab}^2(k_{\max}, \eta)$, introduced in (7.71), as a function of the cutoff scale $k_{\max}$ for a ΛCDM universe. Here, we use the notation $\sigma_{\delta\delta}^2 \equiv \sigma_{11}^2$, $\sigma_{\delta\theta}^2 \equiv \sigma_{12}^2$ and $\sigma_{\theta\theta}^2 \equiv \sigma_{22}^2$ for the variances of the displacement fields, defined in (7.71). The presented results are obtained by determining the variance of the displacement fields in (7.71) from the N-body simulation data for the power spectrum $P_{ab}(k, \eta)$ for a ΛCDM cosmology in [378]. By comparing with Figure 7.2, we deduce the approximation $\partial_\eta \ln \sigma_{12(22)}^2(k_{\max}) \simeq 2$, which is valid in the saturation range where $k_{\max} \gtrsim \Lambda_{\mathrm{NL}}$.

only depend weakly on short-distance modes beyond the non-linear scale. This finding has important consequences. As the coefficients $C_{12}(\eta)$ and $C_{22}(\eta)$ determine the non-perturbative equation for the power spectrum in the soft limit, given in (7.33) or in (7.65) if neglecting the subleading coefficient $C_{12}(\eta)$, the power spectrum $P_{ab}(q, \eta)$ in the soft limit receives most of its contributions from hard modes near the non-linear scale. This conclusion stands in contrast to the predictions for the power spectrum in SPT which show a UV-divergent behavior. In fact, studying the coefficients $c_{ab}(\eta)$, which parameterize the non-linear power spectrum (7.66) in dependence of the cutoff scale, confirms this conclusion, as we illustrate in what follows.

7.4.4. UV dependence of the SPT power spectrum

Let us explore the cutoff-scale dependence of the coefficients $c_{ab}(\eta)$ for the ΛCDM model considered in [378] in further detail. In the two upper panels of Figure 7.5, we show the coef-

ficients $c_{ab}(\eta)$ in dependence of the redshift z for two different cutoff scales $k_{\max} = 1\,h/\mathrm{Mpc}$ and $k_{\max} = 10\,h/\mathrm{Mpc}$, respectively. Thereby, we have obtained the results for the coefficients $c_{ab}(\eta)$ from the evolution equation (7.67) by either determining the variance $\sigma_{22}^2(\eta)$ perturbatively in SPT up to three-loop order (see also [102]) or non-perturbatively with the N-body simulation data of [378].

If we compare the values of the coefficients $c_{ab}(\eta)$ for the cutoff scale $k_{\max} = 1\,h/\mathrm{Mpc}$ (upper figure on the left) with the corresponding ones for $k_{\max} = 10\,h/\mathrm{Mpc}$ (upper figure on the right), we see that the perturbative SPT predictions depend strongly on the cutoff scale, in particular at two- and three-loop order, while the full solution is essentially robust. As opposed to this, the non-perturbative results for the coefficients $c_{ab}(\eta)$ extracted from the numerical simulations do not vary significantly when changing the cutoff scale by an order of magnitude. Hence, this implies that the main contribution to the coefficients $c_{ab}(\eta)$ arises from modes $k \lesssim 1\,h/\mathrm{Mpc}$. In turn, we arrive at the conclusion that the apparent strong(er) dependence of the perturbative calculations in SPT on the small-scale fluctuations, being clearly displayed by the two- and three-loop-order SPT results, is an artificial effect. Thus, the UV dependence observed in SPT computations is an artifact arising due to the inapplicability of perturbation theory beyond the non-linear scale.

This conclusion is confirmed by the comparison of the non-perturbative N-body results with the perturbative SPT predictions that we present in the lower panels of Figure 7.5. Therein, we display the variance $\sigma_{ab}^2(k_{\max})$, evaluated at redshift $z = 0$ in the discussed ΛCDM cosmology, as a function of the cutoff scale $k_{\max}$. We contrast the non-perturbative results for the variance $\sigma_{ab}^2(k_{\max})$ based on the N-body simulation data of [378] (solid lines) with the corresponding perturbative SPT predictions at one-loop order (dashed lines in the lower panel on the left) and at two-loop order (dotted lines in the lower panel on the right). Again, we notice that the perturbative SPT predictions or the variance $\sigma_{ab}^2(k_{\max})$ strongly depend on $k_{\max}$ beyond the non-linear scale $\Lambda_{\mathrm{NL}} \simeq 0.5\,h/\mathrm{Mpc}$. This becomes particularly obvious at the two-loop level for $\sigma_{11}^2(k_{\max})$ and $\sigma_{12}^2(k_{\max})$, but also to a lesser degree for $\sigma_{22}^2(k_{\max})$. Compared to the strong cutoff dependence of the perturbative predictions, we can consider the non-perturbative results for $\sigma_{ab}^2(k_{\max})$, especially for $\sigma_{12}^2(k_{\max})$ and $\sigma_{22}^2(k_{\max})$, to remain basically unaltered for $k_{\max}$ greater than the non-linear scale Λ_{NL}. Since the variance $\sigma_{22}^2(k_{\max})$ constitutes the crucial quantity that enters in the non-perturbative power spectrum equation (7.65), it is in particular the saturation beyond the non-linear scale observed for $\sigma_{22}^2(k_{\max})$ that has important consequences. It does not only allow us to conclude that the UV dependence of the SPT power spectrum constitutes an artifact, but it also has implications for the EFT of LSS. We discuss these in the following.
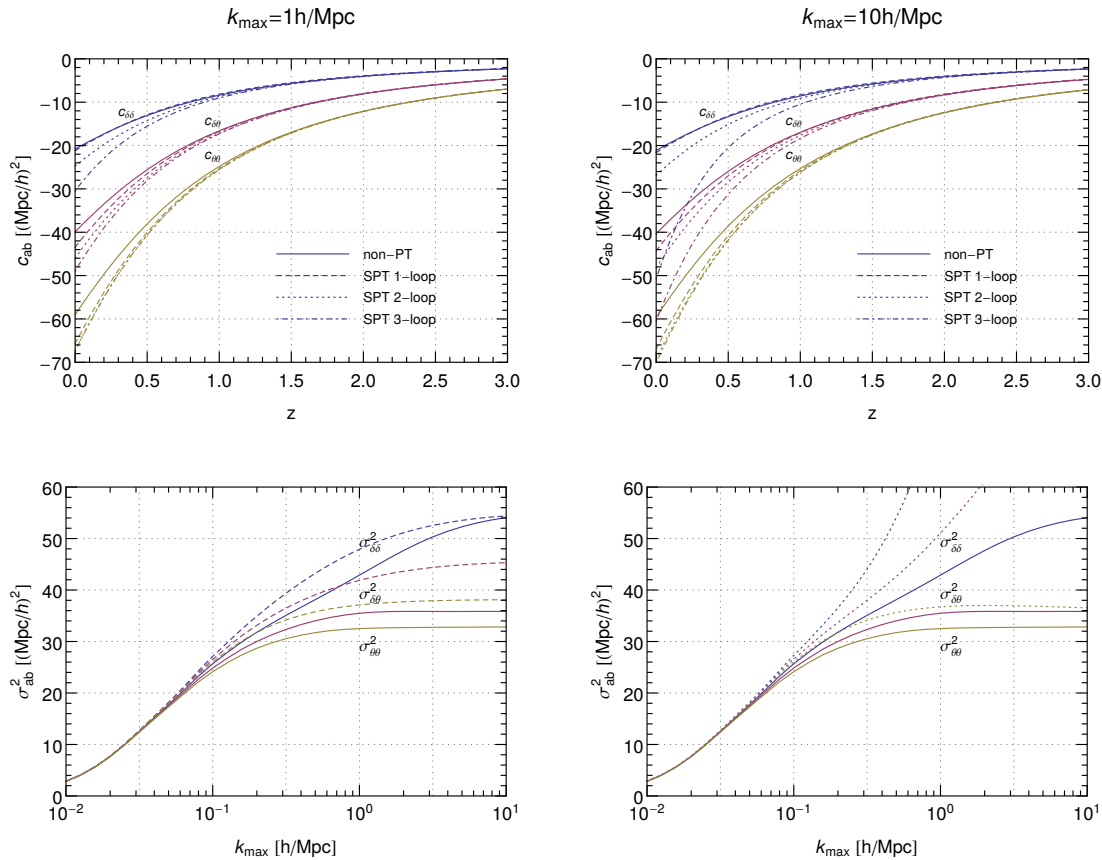
Fig. 7.5.: Comparison of the non-perturbative predictions with the perturbative SPT predictions for the cutoff-scale dependence of the coefficients $c_{ab}(z)$ in (7.66) and the variances of the displacement fields $\sigma_{ab}^2(k_{\max})$ at zero redshift (see (7.71)) and for a ΛCDM universe. For the non-perturbative evaluation of $\sigma_{ab}^2(k_{\max})$ and in turn $c_{ab}(z)$ in (7.67), we have used the N-body simulation data for a ΛCDM universe in [378] (solid lines). The corresponding perturbative evaluation has been performed in SPT at one-, two and three-loop order (dashed, dotted and dot-dashed lines), see also [102]. Here, the depicted non-perturbative results coincide with those in Figure 7.1 and Figure 7.2. In the upper two panels, we display the coefficients $c_{ab}(z)$ as a function of redshift z for the cutoff-scales $k_{\max} = 1\,h/\mathrm{Mpc}$ (on the left) and $k_{\max} = 10\,h/\mathrm{Mpc}$ (on the right). While this change of the cutoff scale only affects the non-perturbative results weakly (at the 2% level), the perturbative SPT predictions show a strong cutoff-scale dependence, in particular at two- and three-loop order. Moreover, in the lower panels, we show the variance $\sigma_{ab}^2(k_{\max})$ at redshift $z = 0$ in dependence of the cutoff scale $k_{\max}$. We also notice here that in contrast to the non-perturbative results, the SPT predictions at one-loop order (on the left) and especially at two-loop order (on the right) for $\sigma_{11(12)}^2(k_{\max})$ strongly depend on modes $k_{\max}$ beyond the non-linear scale Λ_{NL}.

7.4.5. Implications for the EFT of LSS

In the effective field theory approach of large-scale structure (EFT of LSS) [49, 63, 89, 178–208], one introduces an additional time-dependent (renormalized) parameter l_{ren}^2 at leading order in the soft wavenumber q. This parameter scales like $l_{\text{ren}}^2 \propto q^2 P^L(q, \eta)$ in the soft limit $q \to 0$. In the Eulerian framework of EFT, l_{ren}^2 can be interpreted as a 'sound speed' c_s^2 (see e.g., [63]), whereas it includes a series of response functions in the Lagrangian-space formulation LEFT, developed in [208]. As originally emphasized in [63, 178, 208], the effects of the EFT coefficient(s) can be read off from the discrepancy between observations (and/or pure numerical simulations), $P_{ab}^{\text{obs}}(q, \eta)$, and the theoretical solution of the flow equation (7.10) for the power spectrum, $P_{ab}^{\text{flow}}(q, \eta)$, without adding finite-size effects. In the context we consider here, we can alternatively use the non-perturbative power spectrum equation in (7.33), including both the coefficients $C_{12}(\eta)$ and $C_{22}(\eta)$ from the α- and β-contributions, to determine the theoretical solution $P_{ab}^{\text{flow}}(q, \eta)$ for the power spectrum.

Hence, by quantifying the mismatch of the power spectrum determined from observations and by solving the non-perturbative equation (7.33) as

$$\Delta P_{ab}(q, \eta, k_{\max}) \equiv P_{ab}^{\text{obs}}(q, \eta) - P_{ab}^{\text{flow}}(q, \eta, k_{\max}), \qquad (7.78)$$

we can define a (renormalized) parameter $l_{\text{ren}}^2(k_{\max})$ that incorporates the dependence on the short-distance modes at a given point of time η as

$$l_{\text{ren}}^2(k_{\max}) \equiv \frac{\Delta P(q, \eta, k_{\max})}{q^2 P^L(q, \eta)}, \qquad q \ll \Lambda_{\text{NL}} \ll k_{\max} \qquad (7.79)$$

with $\Delta P(q, \eta, k_{\max}) \equiv \Delta P_{11}(q, \eta, k_{\max})$. The actual cutoff-independent mismatch of the power spectra $\Delta P(q, \eta, k_{\max})$ and the corresponding parameter l_{ren}^2 is then determined by taking the cutoff to infinity or, in practice, much larger than the non-linear scale, $k_{\max} \gg \Lambda_{\text{NL}}$. While the dependence of the parameter $l_{\text{ren}}^2(k_{\max})$ on the cutoff scale $k_{\max}$ reflects the sensitivity of the power spectrum $P_{11}^{\text{flow}}(q, \eta, k_{\max})$ on the short-distance modes, the size of $l_{\text{ren}}^2(k_{\max})$ is however determined by the mismatch $\Delta P(q, \eta, k_{\max})$ between data from observations or numerical simulations and the theoretical solution to the non-perturbative equation for the power spectrum in the soft limit in (7.33).

In principle, the mismatch $\Delta P_{ab}(q, \eta, k_{\max})$ in (7.78) also measures the effect of neglecting the vorticity $\boldsymbol{w} \equiv \nabla \times \boldsymbol{u}$, as defined in (3.3), which has been neglected from the onset (see the discussion at the beginning of Section 3.2 for details). The vorticity enters in the fluid equations (7.1) through additional vertices, such as $\gamma_{\delta\theta\omega}$ with the indices referring to the density contrast δ, the velocity divergence θ and vorticity ω. These new vertices in turn lead to additional coefficients in the non-perturbative power spectrum equation (7.33) which are,

for instance, proportional to the variance of the vorticity auto-correlation $\sigma_{\omega\omega}^2(k_{\max})$. However, since the vorticity power spectrum $P_{\omega\omega}(k,\eta)$ is highly suppressed on small momentum scales and is at most of the same order as the velocity power spectrum on for large momenta (see [378]), we conclude that $\sigma_{\omega\omega}^2(k_{\max}) \ll \sigma_{22}^2(k_{\max})$. Thus, it is justified to neglect the impact of the vorticity in the non-perturbative equation for the power spectrum in (7.33).

As we argued in Section 7.4.3, the coefficients $C_{12}(\eta)$ and $C_{22}(\eta)$ depend only very weakly on the cutoff scale $k_{\max}$ beyond the non-linear scale Λ_{NL}. Since these coefficients determine the cutoff-dependence of the power spectrum $P_{ab}^{\mathrm{flow}}(q,\eta,k_{\max})$ through the non-perturbative equation (7.33), also $P_{ab}^{\mathrm{flow}}(q,\eta,k_{\max})$ depends only weakly on the cutoff scale for $k_{\max} \gg \Lambda_{\mathrm{NL}}$. This implies

$$P_{ab}^{\mathrm{flow}}(q,\eta,k_{\max}) \simeq P_{ab}^{\mathrm{flow}}(q,\eta,\Lambda_{\mathrm{NL}})\,, \qquad k_{\max} \gg \Lambda_{\mathrm{NL}}\,, \tag{7.80}$$

so that the EFT parameter $l_{\mathrm{ren}}^2(k_{\max})$, introduced in (7.79), can be expressed as

$$l_{\mathrm{ren}}^2(k_{\max} \gg \Lambda_{\mathrm{NL}}) \simeq \frac{\Delta P(q,\eta,\Lambda_{\mathrm{NL}})}{q^2 P^L(q)}\,, \qquad q \ll \Lambda_{\mathrm{NL}}\,. \tag{7.81}$$

Hence, at leading order in q, the renormalized coefficient(s) in the EFT framework [63, 178, 208] themselves possess only a weak dependence on modes beyond the non-linear scale. Consequently, they can be determined with information from modes up to or near the non-linear scale.

In fact, this result is not surprising. It reflects the statement that virialized scales decouple on large-scale dynamics, which was shown in [178] for the back-reaction on the evolution of the Universe. The reason for this is that short distance scales contribute through the expectation value of their quadrupole moment [208], that is suppressed relative to non-virialized scale (see [92]). Likewise, our analysis demonstrates that the same occurs for the response of this quadrupole to a long-wavelength perturbation entering at order q^2.[4] Our results are then compatible with numerical investigations of the impact of UV modes (see e.g., [209, 210]) as well as general expectations from analytic arguments (such as in [92, 96, 387]).

On the other hand, our findings are in contrast to the behavior of the solutions to the fluid equations (7.1) obtained in standard Eulerian (or Lagrangian) perturbation theory. In these frameworks, the power spectrum $P_{ab}^{\mathrm{flow}}(k,\eta)$ is determined as a perturbative expansion in terms of the linear power spectrum, involving possibly divergent loop integrals over all momentum scales. Within the effective field theory approach to LSS, the divergences are canceled

---

[4]Note that for virialized objects, the density contrast equals approximately $\delta_{\mathrm{vir}} \simeq 10^2$. However, if we use that the potential is roughly constant (of the order $\Phi \simeq 10^{-5}$) on all scales, this corresponds to $k_{\mathrm{vir}} \simeq 10\,\Lambda_{\mathrm{NL}}$. Furthermore, the power spectrum turns over near the horizon scale at matter-radiation equality $k \simeq k_{\mathrm{eq}} < \Lambda_{\mathrm{NL}}$. This introduces an additional suppressing factor. Thus, we see the turn-over of the power spectrum in Figure 7.2 to occur closer to the non-linear scale $\Lambda_{\mathrm{NL}} \simeq 0.5\,h/\mathrm{Mpc}$.

by counter-terms so that the physical renormalized coefficients remain. From our previous considerations, we deduce that any dependence of the leading-order EFT coefficient(s) in Eulerian (or Lagrangian) space on short-distance modes beyond the non-linear scales arises mainly from the counter-term(s). This finding also leads to the conclusion that the UV sensitivity in SPT is an artifact due to the inapplicability of perturbation theory beyond the non-linear scale, in contrast to the intrinsic UV dependence of the – physical – renormalized parameters, which encode finite-size effects.

To go beyond, let us discuss one further issue concerning the renormalized EFT parameter(s). Although our formulation of (7.79) suggest that $l_{\mathrm{ren}}^2(k_{\max})$ is constant for all values of q, this must not necessarily be the case. Instead, there may also be an inherited dependence of $l_{\mathrm{ren}}^2(k_{\max})$ on q that occurs due to the existence of non-analyticities, such as logarithms of the form $\propto q^2 (\ln q)^n$. Thus, the renormalized parameter(s) on different scales can differ by large logarithms so that they need to be resummed. This is achieved through the renormalization group flow. On the one hand, this does not affect our conclusions if we vary the momentum q towards the non-linear scale. The reason for this is that, for $q \simeq \Lambda_{\mathrm{NL}}$, the renormalized parameter(s) do not depend strongly on short-distance modes beyond the non-linear scale. On the other hand, there could still be an important renormalization group flow between modes with $q \ll \Lambda_{\mathrm{NL}}$ and the non-linear scale. Though we do not expect this scale dependence to have a large impact, it is nonetheless an important factor when hunting for a percent-level accuracy. In this regard, we also refer to [199, 200] for a related discussion.

The fact that the renormalized EFT parameter(s) at leading order in the soft mode q do not strongly depend on the UV modes does not mean that the effect of the additional EFT term $\propto l_{\mathrm{ren}}^2 q^2 P^L(q)$ with l_{ren}^2 given in (7.81), in the dynamics of the non-perturbative power spectrum equation (7.33) is necessarily small. As we can see from (7.81) with (7.78), its relevance rather relies on how well the theoretical solution for the power spectrum fares against observations or numerical simulations. Moreover, on physical grounds, we know that tidal effects are expected to contribute on large momentum scales [208, 370].

Due to the intricate series of approximations we applied to derive the non-perturbative equation for the soft-limit power spectrum in (7.65), it is not possible to directly extract the size of the renormalized EFT coefficient(s) in the soft limit. Nonetheless, we can conclude that their importance in correcting the underlying fluid equations (7.1) is at most of the same order as the error we estimated in Section 7.4.1, i.e., at the level of $\sim 10\%$.

Chapter 8

Conclusions and Outlook

In this thesis, we studied correlation functions of matter density and velocity perturbations, such as the power spectrum and the bispectrum, in the theory of large-scale structure formation. Thereby, we focused on the investigation of such correlation functions in the limit where one of their wavenumbers becomes small. In this squeezed or soft limit, $(\mathcal{N} + 1)$-point and $\mathcal{N}$-point correlators of density and velocity fields can be linked to so-called 'consistency conditions'. We deduced consistency conditions both for equal- and unequal-time correlation functions. Thereby, we worked in the Eulerian representation of cosmological perturbation theory and used the compact notation of the large-scale structure fluid equations in terms of a doublet field which simultaneously includes the density and velocity fluctuation fields (see [40, 236]). Afterwards, we explored the validity of these consistency conditions within and beyond perturbation theory.

Unequal-time consistency conditions for correlation functions in the soft limit

With regard to *unequal-time* correlation functions, the main appeal of the consistency conditions is that they can be derived solely from symmetry arguments and thus are universal. In fact, they are only based on the general assumption of a single-field inflation to impose the initial conditions for the seeds of structure, and the diffeomorphism invariance (general covariance) of general relativity. For that reason, the unequal-time consistency conditions lead to quite general, non-perturbative predictions about the dynamics on short distance scales [165–171, 228, 235]. Thus, they constitute a powerful tool to test the underlying assumptions and the basic aspects of the theory with upcoming large-scale structure surveys [53–60].

Here, we (re-)derived the consistency conditions for unequal-time correlation functions in the soft limit. One of the crucial aspects in the derivation was the factorization of soft and hard modes. Hence, we applied the eikonal approximation which naturally accounts for the resummation of the soft mode into a so-called eikonal phase [159, 160, 237]. By using the eikonal approximation, we did not only deduce the known consistency conditions for unequal-time correlation functions of density perturbations in a straightforward way (see e.g., [167, 169–171, 228–230]), but in addition extended them to unequal-time correlation functions including the velocity field. Moreover, the transparent derivation with the eikonal approximation has the advantage that it can be easily adapted to account for different cosmological models.

These consistency conditions become degenerate for the observationally most interesting case of equal-time correlation functions, that is, they vanish at leading order in the soft momentum q. To extract information about equal-time correlators, one consequently has to study next-to-leading order effects. Beyond linear order, equal-time correlation functions depend on the coupling between soft and hard modes so that dynamical information starts to become important. Hence, it is relevant to investigate under which circumstances consistency conditions for equal-time correlation functions in the soft limit exist beyond a perturbative treatment of the hard modes.

Equal-time consistency conditions for the bispectrum in the soft limit

In order to access the existence and validity of the consistency relations between correlation functions at *equal times*, we computed the soft limit of the angular-averaged equal-time connected three-point function, the bispectrum, up to next-to-leading order in SPT [40, 92–102] as a benchmark for the comparison of different methods. In detail, we scrutinized the predictions for the soft-limit of the bispectrum in two different approaches, namely in the perturbative time-flow approach [156] and in a non-perturbative background method where the soft mode is absorbed into a locally curved cosmology. The latter has been applied in [173, 174] for proposing allegedly non-perturbative equal-time consistency conditions.

Time-flow approach

The time-flow approach relies on applying a closure approximation to truncate a hierarchical system of differential evolution equations for equal-time correlators, the so-called flow equations. In general, deriving perturbative statements in the time-flow approach is only possible by imposing a suitable closure approximation.

Usually, the infinite hierarchy of flow equations is closed by neglecting the connected four-point correlation function, i.e., the trispectrum. However, the success of this closure approximation in computations involving the power spectrum is questionable (see [156, 348]). An attempt at including the information from the trispectrum to improve the predictions of the time-flow approach for the power spectrum appeared in [349]. The results therein point towards a non-negligible contribution to the power spectrum already in the mildly non-linear regime.

For the case of the soft-limit angular-averaged bispectrum consistency relations derived in the time-flow formalism, one could have hoped that the trispectrum was less relevant in the soft limit and that equal-time consistency conditions based on the time-flow approach may be approximately accurate. However, we showed that the trispectrum plays an important role in assessing the validity of the consistency relations for the bispectrum in the soft limit. We demonstrated explicitly that the time-flow approach reproduces the SPT predictions for the soft-limit angular-averaged bispectrum of density perturbations at linear order and thus coincides with the known result in the literature [166]. At this level, we could in fact use the time-flow approach to extend the known linear-order bispectrum consistency relations to correlation functions including the velocity fields and to general background cosmologies other than the simplest EdS one. Beyond the leading order, however, the time-flow approach fails to provide accurate predictions for the consistency relations of the angular-averaged bispectrum in the soft limit. Already at one-loop order, we found large deviations between the soft-limit bispectrum in SPT and from the time-flow approach.

If we include the trispectrum and truncate the infinite hierarchy of flow equations at a higher-order level of the correlations functions, we can in principle reproduce the one-loop SPT result for the bispectrum in the soft limit with the time-flow approach. Nevertheless, the time-flow approach will fail to provide accurate predictions for the bispectrum in the soft limit at some given loop order depending on the truncation. Thus, a truly non-perturbative result for an equal-time consistency condition seems out of reach in the time-flow formalism.

For this reason, the perturbative relations between equal-time correlation functions in the soft limit derived from the time-flow approach do not hold up the same status as the non-perturbative consistency conditions at unequal times. However, they may still be useful in special circumstances where the short-distance modes are kept in the mildly non-linear regime. For instance, the perturbative relations of the time-flow approach are well suited to study the baryon acoustic oscillations in a background cosmology that requires numerical input, such as cosmological models including massive neutrinos or quintessence. In contrast to SPT, the time-flow approach is formulated only in terms of equal-time correlation functions so that soft effects cancel out from the beginning. Thus, the perturbative time-flow relations for the

equal-time correlation functions in the squeezed limit may improve numerical stability and simplify the computational treatment of the fluctuations.

Non-perturbative background method

To assess the existence of equal-time soft-limit consistency conditions beyond the realm of perturbative methods, we subsequently presented an alternative, non-perturbative approach for deriving equal-time angular-averaged correlation functions in the soft limit. This approach was based on a background method, introduced in [165, 166], which implements a map between the dynamics on short distance scales within a flat FRW universe in the presence of a soft, long-wavelength perturbation and a locally curved background. In the context of N-body simulation, the background method was exploited in the so-called 'separate universe' approach [238–241]. It was argued in [165] that this physical equivalence between a perturbed FRW cosmology with a soft mode and a locally curved universe even applies if the short modes are deep in the non-linear regime. In turn, the proposal of allegedly non-perturbative 'angular-averaged equal-time consistency conditions' by Valageas, and also by Kehagias, Perrier and Riotto (VKPR) in [173, 174] appeared as an attempt to use this equivalence for extending the leading-order result of [166] into the non-linear regime.

Inspired by the VKPR proposal, our aim was to derive a non-perturbative consistency relation for the bispectrum in the soft limit from first principles using the background method. Thereby, we developed a straightforward and shortened derivation of the relevant transformations in the background method of [165, 166], which directly matches a flat FRW cosmology in the presence of a soft mode to a locally curved universe. Afterwards, we used these transformations to relate the bispectrum of density perturbations, $B_{111}(\boldsymbol{k}, -\boldsymbol{q}, \boldsymbol{q} - \boldsymbol{k}, \eta)$, in the soft limit $q \to 0$ to the variation of the density power spectrum on short distance scales, $P(k, \eta) \equiv P_{11}(k, \eta)$, in the presence of a local curvature K in an EdS cosmology. Consequently, we obtained the generic, non-perturbative angular-averaged bispectrum consistency condition (see (6.56))

$$B_{111}(\boldsymbol{k}, -\boldsymbol{q}, \boldsymbol{q} - \boldsymbol{k}, \eta)^{\text{av}} \xrightarrow{q \to 0} P^L(q, \eta) \left[\left(1 - \frac{1}{3} k \, \partial_k - \frac{1}{3} \partial_\eta \right) P(k, \eta) + \frac{5}{3} \left. \frac{\partial}{\partial \kappa} P_K(k, \eta) \right|_{K=0} \right],$$
(8.1)

where we denoted the full non-linear density power spectrum in the presence of local curvature as $P_K(k, \eta)$ and introduced the curvature parameter $\kappa = K/(a^2 H^2)$. The generalization for background cosmologies other than EdS is straightforward. Here, the term involving $\left(1 - \frac{1}{3} k \, \partial_k \right)$ results from the combination of two effects, namely, the difference in the density contrast between the two cosmologies plus the shift induced by the so-called displace-

ment term [208] (or equivalently the eikonal phase). Moreover, the contribution $\frac{1}{3}\partial_\eta$ arises from the transformation of the scale factor. Since the last term in the relation above involves the dependence on the power spectrum $P_K(k,\eta)$ in a hypothetically (locally) curved universe, this expression for the bispectrum in the soft limit, though universal, cannot be directly confronted against observations. However, one can, on the one hand, use numerical simulations to determine the derivative with respect to κ. This was done in [238–241] within the framework of the 'separate universe' approach. On the other hand, we demonstrated that one can use the VKPR proposal for this purpose.

Validity of the VKPR proposal

The VKPR proposal, introduced in [173, 174], can be rephrased as an attempt to replace the variation of the density power spectrum with respect to curvature with the corresponding one in the absence of curvature where $K = 0$ (see (6.60))

$$\text{VKPR}: \qquad \frac{\partial}{\partial\kappa}P_K(k,\eta)\bigg|_{K=0} = \frac{4}{7}\,\partial_\eta P_{K=0}(k,\eta)\,. \tag{8.2}$$

For assessing the accuracy of this VKPR relation, we reformulated the fluid equations with respect to a new time variable in terms of the linear growth factor in the presence of curvature, $D_{1,K}(\eta)$. Thus, we performed the transformation $\eta \to \ln D_{1,K}(\eta)$ to treat the fluid perturbations in a curved background. This allowed us to absorb the information on the background cosmology into the time evolution, up to a κ-dependent interaction (see (6.79)). As a result, we found that the VKPR relation in (6.60) is based on the approximation of neglecting this additional (time-dependent) interaction term. Due to this approximation, the VKPR proposal does not fully account for the effect of local curvature on the growth of structure and thus does not constitute a general, non-perturbatively valid relation. Through estimating the error induced by neglecting the curvature-dependent interaction term, we could assess the accuracy of the VKPR relation (6.60). We found the VKPR relation for the bispectrum of density perturbation is only exact at linear order in perturbation theory, but still quantitatively accurate (to the few-percent level) beyond leading order. We draw the same conclusion from investigating its predictions for the bispectrum of density perturbations at one-loop order. Hence, the VKPR proposal (6.60) can be regarded as a quantitatively reasonable empirical approximation within the realm of perturbation theory.

As opposed to this, transferring the VKPR proposal to the velocity fields fails significantly beyond leading order in perturbation theory. Consequently, we generalized the background method to properly account for the effect of local curvature both in the density and velocity perturbations on short distance scales. Based on this, we demonstrated that the velocity

fluctuations react differently by a factor of order one to the presence of curvature than the density perturbations. These findings allowed us finally to formulate a proper generalization of the VKPR proposal in terms of the doublet field $\psi_a(\boldsymbol{k}, \eta)$, including not only the density perturbations but also the velocity fluctuations (see (6.76))

$$\frac{\partial}{\partial \kappa} \psi_{a,K}(\boldsymbol{k}, \eta)\bigg|_{K=0} \simeq \frac{4}{7} \begin{pmatrix} \partial_\eta & 0 \\ 0 & \partial_\eta + 1 \end{pmatrix}_{ab} \psi_{b,K}(\boldsymbol{k}, \eta). \tag{8.3}$$

Finally, we investigated the reasons behind the accuracy of the VKPR proposal for the power spectrum of density perturbations in (6.60). At first, the accuracy of the VKPR proposal can be related to the variation (see (6.80))

$$\frac{\partial}{\partial \delta^L} \left(\frac{3}{2} \frac{\Omega_m}{f^2} \right) \simeq -\frac{5}{14}, \tag{8.4}$$

in the presence of a long-wavelength perturbation that has been absorbed into the background cosmology. Here, Ω_m and f are the matter density parameter and the linear growth rate in the presence of the soft mode. Note, however, that the precision of the VKPR proposal we observed in the perturbative computations is much better. In fact, it arises due to supplementary cancellations. At leading order in the curvature parameter κ, the additional term in the fluid equations accounting for the presence of curvature (see (6.79)) almost annihilates the growing-mode EdS solution at any given order n in SPT, which is dominated by $\delta^{(n)} \simeq \Theta^{(n)}$ (i.e., $\psi^{(n)} \propto (1, 1)$). While these cancellations explain the *unreasonable effectiveness* of the VKPR proposal (6.60) within the framework of perturbation theory, they do not necessarily imply a similar accuracy beyond it. Attempts at testing the VKPR proposal against N-simulations appeared in [231, 238]. The small deviations between the VKPR proposal and the numerical simulations are in agreement with our findings.

Non-perturbative power spectrum equation

After having derived a non-perturbative relation for the bispectrum in the soft limit (see (8.1)), we took a further step in this direction and derived a non-perturbative equation for the power spectrum in the soft limit. However, the road we pursued to deduce this power spectrum equation was slightly different.

First, we derived a non-perturbative relation for a product of doublet fields in the case where one momentum is taken to be soft, $q \to 0$, by performing an operator product expansion (OPE). By correlating this expression with an additional doublet field, we obtained an angular-dependent non-perturbative relation for the bispectrum in the soft limit. To parameterize its angular dependence, we then rewrote it in terms of Legendre polynomials. Next, we

multiplied the fluid equations with an additional fluctuation field and performed the statistical average to formulate a non-perturbative differential evolution equation for the soft-mode power spectrum $P_{ab}(q, \eta)$. This equation included two non-linear contributions, sourced either by the mode-coupling function α or β, respectively, in dependence of the angular-dependent bispectrum. On the basis of the overall momentum dependence of each of the non-linear contributions, we subsequently could infer the bispectrum contributions remaining after the loop integration. In turn, we expressed these in terms of two time-dependent coefficients, $C_{22}(\eta)$ and $C_{12}(\eta)$, arising from the β- and α-contributions, respectively. This allowed us finally to rewrite the non-perturbative differential evolution equation for the power spectrum in the soft limit solely in terms of the power spectrum $P_{ab}(q, \eta)$ itself and the coefficients $C_{22}(\eta)$ and $C_{12}(\eta)$ (see (7.33)),

$$
\begin{aligned}
\partial_\eta P_{ab}(q, \eta) = & -\Omega_{ac}(\eta)\, P_{cb}(q, \eta) - \Omega_{bc}(\eta)\, P_{ac}(q, \eta) \\
& -\frac{q^2}{2} P^L(q, \eta) \left[\begin{pmatrix} 0 & 1 \\ 1 & 2 \end{pmatrix}_{ab} C_{22}(\eta) + \begin{pmatrix} 2 & 1 \\ 1 & 0 \end{pmatrix}_{ab} C_{12}(\eta) \right] .
\end{aligned}
\tag{8.5}
$$

Let us emphasize here again that, due to the form of the vertex function in the fluid equations, the non-perturbative power spectrum equation above does not involve a coefficient $C_{11}(\eta)$. As a consequence, it does not receive a contribution from the density-density power spectrum on short distance scales.

For evaluating the power spectrum $P_{ab}(q, \eta)$ from this expression, we needed to further determine the coefficients $C_{22}(\eta)$ and $C_{12}(\eta)$, encoding in particular the dependence on the hard modes. This could be achieved by use of non-perturbative (angular-dependent) consistency conditions for the bispectrum in the soft limit. The coefficient $C_{22}(\eta)$, for instance, incorporated only a dependence on the angular-averaged bispectrum in the soft limit so that we could make use of the previously derived non-perturbative bispectrum consistency relation, (8.1), to determine it as (see (7.22) and (7.24))

$$
C_{22}(\eta) = -4\, \sigma_{22}^2 + \partial_\eta \sigma_{22}^2 + 5 \frac{\partial}{\partial \kappa} \sigma_{22,K}^2 \bigg|_{K=0}
\tag{8.6}
$$

with σ_{ab}^2 being the variance of the displacement fields, here expressed in dependence of a cutoff scale $k_{\max}$ (see (5.11) and (7.71)),

$$
\sigma_{ab}^2(k_{\max}, \eta) \equiv \frac{4\pi}{3} \int\limits_0^{k_{\max}} dk\, P_{ab}(k, \eta) .
\tag{8.7}
$$

Hence, this expression allowed us to connect the coefficient $C_{22}(\eta)$ to the power spectrum of hard modes, albeit to a certain extent in a locally curved background cosmology. However,

at this point, we made used of the generalized VKPR proposal (see (8.3)) to replace the derivative of the variance with respect to curvature with a time derivative.

In order to determine the coefficient $C_{12}(\eta)$, we needed to include information from an angular-dependent consistency relation for the bispectrum in the soft limit. We derived such a consistency condition by generalizing the background method from the case of a spherically symmetric soft mode to the one of a *directional* long-wavelength perturbation. Thereby, we implemented a map between the flat FRW cosmology in the presence of the directional soft mode and a locally curved anisotropic universe. Proceeding from this, we could determine an angular-dependent non-perturbative bispectrum consistency relation, which reproduces the expression in (8.1) by angular averaging. In turn, we could use the angular-dependent consistency condition to extract the coefficient $C_{12}(\eta)$ in dependence of the variance $\sigma^2_{ab,A}(k_{\max}, \ldots)$ on short distance scales (or the corresponding power spectrum of hard modes (see (8.7)) in a hypothetical locally curved anisotropic universe, and the derivatives thereof. Thereby, the variance $\sigma^2_{ab,A}(k_{\max}, \ldots)$ constitutes a function of a series of geometrical parameters arising from the form of the locally curved anisotropic metric. Because of the anisotropies, this metric includes, for instance, two different expansion rates, parallel and perpendicular to the directional soft mode $\boldsymbol{q}$, as a curvature parameter, $K_\parallel$, which only enters in the parallel direction.

Evaluating $C_{12}(\eta)$ thus requires either to deduce it by an empirical approximation extending the generalized VKPR proposal in (8.3) to the locally curved anisotropic case or by performing numerical simulations in a locally curved anisotropic background cosmology. However, since the coefficient $C_{12}(\eta)$ originated from higher-order terms with respect to the Legendre polynomials (in a suitable basis) and its contribution compared to the one involving the coefficient $C_{22}(\eta)$ was suppressed roughly by a factor 20 in perturbation theory, a reasonable approximation consisted in neglecting the coefficient $C_{12}(\eta)$. In other words, we truncated the non-perturbative power spectrum equation (8.5) in the numerical analysis by setting $C_{12}(\eta) = 0$.

Numerical analysis

Based on the numerical analysis we performed, we estimated the overall error in the non-perturbative power spectrum equation induced by neglecting the impact of the coefficient $C_{12}(\eta)$ and by approximating the curvature dependence of the coefficient $C_{22}(\eta)$ by the generalized VKPR proposal to be at most an effect of the order of $\sim 10\%$. We demonstrated explicitly that for a ΛCDM cosmology, the non-perturbative predictions for the power spectrum in the soft-limit, parameterized by the coefficients $c_{ab}(\eta)$ as (see (7.66))

$$P_{ab}(q,\eta) = \left[u_a u_b + q^2 c_{ab}(\eta) \right] P^L(q,\eta) \tag{8.8}$$

with $u_a = (1,1)$, agree remarkably well with the results from numerical simulations of [378] within the error bars of $\sim 10\%$ (see Figure 7.1). This level of precision is consistent with the numerical estimate of the impact of $C_{12}(\eta)$ in the non-perturbative power spectrum equation that we performed (see Figure A.1). Indeed, at present time (or equivalently at redshift $z = 0$), the prediction of the non-perturbative power spectrum equation under neglecting $C_{12}(\eta)$, that is $c_{11}\big(\eta(z = 0)\big) \simeq -21\,(\mathrm{Mpc}/h)^2$, lies within the error of the numerical value $c_{11}^{\mathrm{num}}\big(\eta(z = 0)\big) \simeq -23\,(\mathrm{Mpc}/h)^2$ [199, 200]. The accuracy of the order of $\sim 10\%$ for the non-perturbative predictions at redshift $z = 0$ improves to a percent-level precision at higher redshifts.

Our analysis of the coefficients $c_{ab}(\eta)$ parameterizing the non-linear power spectrum revealed in addition an important characteristic of the power spectrum in the soft limit. We showed for a ΛCDM cosmology that the coefficients $c_{ab}(\eta)$ in the non-perturbative case, determined by numerically evaluating the momentum integral contained in the variance $\sigma_{ab}^2(k_{\mathrm{max}}, \eta)$ in (8.7), only show a weak cutoff-scale dependence if k_{max} is chosen well within the non-liner regime (see Figure 7.1). To explore this feature in further detail, we investigated in turn the variance itself at redshift $z = 0$,

$$\sigma_{ab}^2(k_{\mathrm{max}}) \equiv \sigma_{ab}^2\big(k_{\mathrm{max}}, \eta(z = 0)\big) \tag{8.9}$$

for a ΛCDM cosmology as a function of the cutoff scale k_{max} (see Figure 7.2). As a result, we found that the variances $\sigma_{12}^2(k_{\mathrm{max}})$ and $\sigma_{22}^2(k_{\mathrm{max}})$, in contrast to $\sigma_{11}^2(k_{\mathrm{max}})$, notably show a clear saturation behavior for $k_{\mathrm{max}} \gg \Lambda_{\mathrm{NL}}$ with $\Lambda_{\mathrm{NL}} \simeq 0.5\,h/\mathrm{Mpc}$ being the non-linear scale. Note that it is exactly the variances $\sigma_{12}^2(k_{\mathrm{max}})$ and $\sigma_{22}^2(k_{\mathrm{max}})$ that enter through the coefficients $C_{12}(\eta)$ and $C_{22}(\eta)$ in the non-perturbative power spectrum equation in (8.5).

In their most general form, the coefficients $C_{12}(\eta)$ and $C_{22}(\eta)$ involve a dependence on the variance in a hypothetical locally curved (anisotropic) background cosmology. However, we argued that the dependence on the background cosmology through curvature or other geometrical (anisotropic) parameters, induced by a long-wavelength mode $q \ll \Lambda_{\mathrm{NL}}$, should not significantly affect the qualitative behavior of the variance on short distance scales where $k_{\mathrm{max}} \gg \Lambda_{\mathrm{NL}}$. Thus, in the case of the spherically symmetric soft mode, we expected the relation (see (7.74))

$$\sigma_{ab,K}^2(k_{\mathrm{max}}) \simeq \sigma_{ab}^2(k_{\mathrm{max}}) \tag{8.10}$$

to be valid for modes deep in the non-linear regime, i.e., for $k_{\mathrm{max}} \gg \Lambda_{\mathrm{NL}}$. We formulated an analogous approximation in the case of the directional soft mode, $\sigma_{ab,A}^2(k_{\mathrm{max}}, \ldots) \simeq \sigma_{ab}^2(k_{\mathrm{max}})$, for $k_{\mathrm{max}} \gg \Lambda_{\mathrm{NL}}$. From the equation above, we inferred that background-dependent variances $\sigma_{12,K}^2(k_{\mathrm{max}})$ and $\sigma_{22,K}^2(k_{\mathrm{max}})$ (as well as their anisotropic equivalents) display only a weak dependence on short-distance modes beyond the non-linear scale.

8. Conclusions and Outlook

To go beyond, we investigated whether this finding applies not only to the $\sigma^2_{12,K}(k_{\max})$ and $\sigma^2_{22,K}(k_{\max})$ themselves but also to their derivatives with respect to curvature. Thereby, we deduced that the derivative of the power spectrum on short distance scales with respect to spatial curvature fulfills the bound

$$\left.\frac{\partial}{\partial\kappa}P_{ab,K}(k,\eta)\right|_{K=0} < P_{ab}(k,\eta) \tag{8.11}$$

for modes deep in the non-linear regime, $k \gg \Lambda_{\mathrm{NL}}$. For deriving this bound, we first made use of the response function $G_1(k,\eta)$ for the density power spectrum $P(k,\eta) \equiv P_{11}(k,\eta)$ (see (7.76)),

$$G_1(k,\eta) \equiv -\frac{1}{3}\,\partial_\eta \ln P_{K=0}(k,\eta) + \frac{5}{3}\,\frac{\partial}{\partial\kappa}\ln P_K(k,\eta)\bigg|_{K=0}, \tag{8.12}$$

to confront the predictions of the VKPR proposal (6.60) against results from numerical simulations obtained within the 'separate universe' approach in [380] (see Figure 7.3). As a result, we found that the predictions of the VKPR proposal overestimate the response function of the density power spectrum $P_{11}(k,\eta)$ for modes much bigger than the non-linear scale, $k \gg \Lambda_{\mathrm{NL}}$. We expected the generalized VKPR proposal (see (8.3)) to lead to similar results for $P_{12}(k,\eta)$ and $P_{22}(k,\eta)$, respectively. Next, by comparison of Figure 7.4 with Figure 7.2, we deduced that the approximation $\partial_\eta \ln \sigma^2_{12(22)}(k_{\max}) \simeq 2$ is relatively accurate for $k_{\max} \gtrsim \Lambda_{\mathrm{NL}}$. Transferring this finding to the power spectra contained in $\sigma^2_{12(22)}(k_{\max})$ (see (8.7)) and taking into account the generalized VKPR proposal in (8.3) as an overestimation of the curvature derivative for $P_{12}(k,\eta)$ and $P_{22}(k,\eta)$, we deduced the upper bound on the derivative of the power spectrum in (8.11) with respect to spatial curvature is fulfilled. Consequently, we concluded that the weak sensitivity to the hard modes beyond the non-linear scale also applies for the curvature derivatives of the variances $\sigma^2_{12,K}(k_{\max})$ and $\sigma^2_{22,K}(k_{\max})$. We expect this saturation behavior beyond the non-linear scale to be a general feature occurring in the case of a locally curved anisotropic universe, for both the variances $\sigma^2_{12,A}(k_{\max})$ and $\sigma^2_{22,A}(k_{\max})$ as well as their variations with respect to the additional geometrical parameters.

Since these quantities constitute the general contributions to the coefficients $C_{12}(\eta)$ and $C_{22}(\eta)$, we concluded from the above reasoning that also $C_{12}(\eta)$ and $C_{22}(\eta)$ depend only weakly on short-distance modes beyond the non-linear scale. Since these coefficients determine the non-perturbative equation for the power spectrum in the soft limit (see (8.5)), we could finally draw the conclusion that the power spectrum $P_{ab}(q,\eta)$ in the soft limit involves only a weak dependence on hard modes deep in the non-linear regime, but receives most of its contributions from short-distance modes near the non-linear scale.

Implications for SPT and the EFT of LSS

The finding that the soft-limit power spectrum is only weakly dependent on short-distance modes beyond the non-linear scale stands in contrast to the predictions for the power spectrum in SPT that indicate a UV-divergent behavior. In fact, studying the coefficients $c_{ab}(\eta)$, which parameterize the non-linear power spectrum, as well as the variance $\sigma_{ab}^2(k_{\max})$, as a function of the cutoff scale $k_{\max}$, confirmed this finding (see Figure 7.5). Thereby, we evaluated $c_{ab}(\eta)$ and $\sigma_{ab}^2(k_{\max})$ either non-perturbatively, by using data from N-body simulations performed in [378], or perturbatively in SPT up the three-loop order (see also [102]). While we demonstrated that the non-perturbative numerical result does not vary significantly for $k_{\max}$ greater than the non-linear scale Λ_{NL}, the perturbative SPT predictions displayed a strong dependence on $k_{\max}$ beyond the non-linear scale Λ_{NL}, in particular at two- and three-loop order. Hence, we arrived at the conclusion that the apparent strong(er) dependence of the perturbative calculations in SPT on small-scale fluctuations is an artificial effect. The non-perturbative numerical result did not vary significantly for $k_{\max}$ greater than the non-linear scale Λ_{NL}. In other words, the UV dependence found in explicit computations in SPT is nothing but an artifact since the perturbative techniques on which SPT relies are inapplicable beyond the non-linear scale.

The results of our numerical analysis allow us not only to draw conclusions about the UV dependence of the SPT power spectrum, but has also important ramifications for the effective field theory (EFT) of LSS formation. In the framework of EFT, an additional parameter l_{ren}^2 is introduced, which scales like $l_{\mathrm{ren}}^2 \propto q^2 P^L(q,\eta)$ in the soft limit $q \to 0$. While l_{ren}^2 can be interpreted as 'sound speed' c_s^2 in the Eulerian framework of EFT [63], it includes a series of response functions in the Lagrangian-space formulation of EFT [208]. Here, we can infer the effects of the EFT coefficient(s) by quantifying the discrepancy of the power spectrum determined from observations (or pure numerical simulations) and by solving the non-perturbative power spectrum equation in (8.5)) for a given cutoff scale $k_{\max}$, that is, $\Delta P_{ab}(q,\eta,k_{\max})$. In principle, the mismatch $\Delta P_{ab}(q,\eta,k_{\max})$ also measures the effect of neglecting the vorticity of the velocity field in the fluid equations from the beginning. However, since the vorticity power spectrum is highly suppressed on long distance scales and is at most of the same order as the velocity power spectrum on short distance scales (see [378]), we argued that it is justified to neglect its impact in the non-perturbative power spectrum equation.

Based on the fact that the numerical analysis revealed only a very weak dependence of the coefficients $C_{12}(\eta)$ and $C_{22}(\eta)$ and thus of the non-perturbative power spectrum on the cutoff scale $k_{\max}$ beyond the non-linear scale Λ_{NL}, we could draw the same conclusion for the power spectrum discrepancy. Hence, we inferred the relation $\Delta P_{ab}(q,\eta,k_{\max}) \simeq \Delta P_{ab}(q,\eta,\Lambda_{\mathrm{NL}})$ to

8. Conclusions and Outlook

be valid for $k_{max} \gg \Lambda_{NL}$. Proceeding from this, we could introduce a (renormalized) EFT parameter $l^2_{ren}(k_{max})$ at a given point of time η as follows,

$$l^2_{ren}(k_{max} \gg \Lambda_{NL}) \simeq \frac{\Delta P(q, \eta, \Lambda_{NL})}{q^2 P^L(q)}, \qquad q \ll \Lambda_{NL}, \qquad (8.13)$$

where $\Delta P(q, \eta, \Lambda_{NL}) \equiv \Delta P_{11}(q, \eta, \Lambda_{NL})$. Hence, we arrived at the conclusion that the leading-order renormalized coefficient(s) in the EFT framework [63, 178, 208] themselves depend only weakly on modes beyond the non-linear scale. Consequently, they receive most of their contributions from modes up to or near the non-linear scale.

As opposed to SPT, the EFT of LSS introduces counter-terms to cancel the divergences in the perturbative expansion, e.g., by introducing a cutoff, so that the leftover renormalized contribution is physical. The previous considerations thus imply that any dependence of the leading-order EFT coefficient(s) in Eulerian (or Lagrangian) space on short-distance modes beyond the non-linear scale develops mainly from the counter-term(s). This finding also leads to the conclusion that the UV sensitivity in SPT arises as an artifact due to inapplicability of perturbative techniques beyond the non-linear scale.

As we discussed, our conclusion that the renormalized EFT coefficient(s) at leading order in the soft limit do not strongly depend on the UV modes does not imply that the effect of the additional EFT term $\propto l^2_{ren} q^2 P^L(q)$ in the dynamics of the non-perturbative power spectrum equation is necessarily small. In fact, its relevance relies on how well the theoretical solution for the power spectrum in the soft limit fares against observations or numerical simulations. However, due to the intricate series of approximations we applied to derive the non-perturbative equation for the soft limit power spectrum, it is not possible to directly extract the size of the renormalized EFT parameter(s) in the soft limit. Moreover, our analysis does not take into account the plausible scale dependence (through a renormalization group flow) of the renormalized EFT coefficient(s). We can, nonetheless, conclude that their importance in correcting the fluid equations is no more than of the same order as the deviations from numerical simulations we found, i.e., at most an effect of the order of $\sim 10\%$.

In general, the overall level of accuracy could be improved by fitting the time dependence of the power spectrum response function to a long-wavelength perturbation $G_1(k, \eta)$, integrated over wavenumbers k. It is this momentum integral of the response function that ultimately contributes to the coefficient $C_{22}(\eta)$ and thus determines the power spectrum through the non-perturbative equation. However, due to neglecting the second coefficient $C_{12}(\eta)$ in this equation, this was not justified at this stage. In fact, the generalized VKPR proposal turned out to be relatively accurate to compute the coefficient $C_{22}(\eta)$, with an error comparable to the one induced from ignoring the contribution associated to the coefficient $C_{12}(\eta)$. In order to include $C_{12}(\eta)$ in our computations, it is necessary to determine the momentum-integrated

power spectrum response function to a directional long-wavelength perturbation. This can be done by performing numerical simulations within an anisotropic 'separate universe' approach. In contrast to the direct extraction of the coefficients $c_{ab}(\eta)$ in the non-linear soft-limit power spectrum from N-body simulations where large simulation volumes are needed to beat the variance in the soft limit [199, 200]), computing the response function requires modest volumes [238–240, 380]. This suggests a hybrid analytic or a numerical approach to model the power spectrum. The numerical input would come from fitting the time dependence of the integrated response functions, unlike extracting the behavior of the power spectrum for small momenta q. In principle, this would allow us to precisely extract the size of the renormalized leading-order coefficients in the effective field theory approach. We leave this interesting aspect to be addressed in future work.

Appendix

A.1. The soft limit of the one-loop density bispectrum in SPT

In this appendix, we determine the soft limit of the angular-averaged bispectrum of density perturbations at one-loop order in SPT. Since the full soft-limit expression turns out to be too cumbersome to allow for a meaningful comparison with methods other than SPT, we derive the soft limit of the one-loop density bispectrum for the case where its loop momentum is much larger than its external momenta. In other words, we perform the derivation by restricting our considerations to the UV limit of the bispectrum loop integrals.

As we derived in Section 4.4.2, the one-loop contribution to the bispectrum of density perturbations in SPT, $B_{111}^{1-\text{loop}}(\boldsymbol{k}_1, \boldsymbol{k}_2, \boldsymbol{k}_3, \eta)$ denoting the external momenta here by $\boldsymbol{k}_1$, $\boldsymbol{k}_2$ and $\boldsymbol{k}_3$, arises as the sum of the four one-loop diagrams in Figure 4.6 and thus reads (see (4.30))

$$
\begin{aligned}
B_{111}^{1-\text{loop}}(\boldsymbol{k}_1, \boldsymbol{k}_2, \boldsymbol{k}_3, \eta) = {} & B_{111}^{(222)}(\boldsymbol{k}_1, \boldsymbol{k}_2, \boldsymbol{k}_3, \eta) + B_{111}^{(321,\text{I})}(\boldsymbol{k}_1, \boldsymbol{k}_2, \boldsymbol{k}_3, \eta) \\
& + B_{111}^{(321,\text{II})}(\boldsymbol{k}_1, \boldsymbol{k}_2, \boldsymbol{k}_3, \eta) + B_{111}^{(411)}(\boldsymbol{k}_1, \boldsymbol{k}_2, \boldsymbol{k}_3, \eta) \, .
\end{aligned}
\tag{A.1}
$$

The four individual one-loop contributions are explicitly given in (4.31)-(4.34).

For these one-loop bispectrum contributions, we determine the UV limit of the loop integrals with respect to the loop momentum $\boldsymbol{l}$. For this purpose, we first express the one-loop contributions in terms of the absolute values of the external momenta and the loop momentum, i.e., k_1, k_2, k_3 and l, integrate out their respective angles and take the UV limit $l \gg k_{1,2,3}$ afterwards. In the UV limit, the one-loop contributions of the density bispectrum are then of

A. Appendix

the form (see [187])[1]

$$
\begin{aligned}
B_{111}^{(222)}(k_1, k_2, k_3, \eta) \simeq {}& -\frac{(2\pi)^3}{4802\pi^2}\Big[30k_1^6 - 30k_1^4\big(k_2^2 + k_3^2\big) + k_1^2\big(-30k_2^4 + k_2^2 k_3^2 - 30k_3^4\big) \\
& + 30\big(k_2^2 - k_3^2\big)^2\big(k_2^2 + k_3^2\big)\Big] \int dl\, l^2 \left(\frac{P^L(l,\eta)^3}{l^6}\right),
\end{aligned}
\tag{A.2}
$$

$$
\begin{aligned}
B_{111}^{(321,\mathrm{I})}(k_1, k_2, k_3, \eta) \simeq {}& \frac{(2\pi)^3}{35280\pi^2 k_3^2}\Big[170k_1^6 + k_1^4\big(83k_2^2 + 190k_3^2\big) \\
& + 2k_1^2\big(67k_2^4 + 256k_2^2 k_3^2 - 445k_3^4\big) - \big(387k_2^2 - 530k_3^2\big)\big(k_2^2 - k_3^2\big)^2\Big] \\
& \times P^L(k_3, \eta) \int dl\, l^2 \left(\frac{P^L(l,\eta)^2}{l^4}\right) \\
& + \ 5 \text{ permutations}\,,
\end{aligned}
\tag{A.3}
$$

$$
\begin{aligned}
B_{111}^{(321,\mathrm{II})}(k_1, k_2, k_3, \eta) \simeq {}& -\frac{61}{105}\, F_2^s(\boldsymbol{k}_2, \boldsymbol{k}_3)\, P^L(k_2, \eta)\, P^L(k_3, \eta)\, k_3^2\, \frac{4\pi}{3} \int dl\, l^2 \left(\frac{P^L(l,\eta)}{l^2}\right) \\
& + \ 5 \text{ permutations}\,,
\end{aligned}
\tag{A.4}
$$

and

$$
\begin{aligned}
B_{111}^{(411)}(k_1, k_2, k_3, \eta) \simeq {}& -\frac{1}{226380}\frac{1}{k_2^2 k_3^2}\Big[12409k_1^6 + 20085k_1^4\big(k_2^2 + k_3^2\big) + k_1^2\big(-44518k_2^4 \\
& + 76684k_2^2 k_3^2 - 44518k_3^4\big) + 12024\big(k_2^2 - k_3^2\big)^2\big(k_2^2 + k_3^2\big)\Big] \\
& \times P^L(k_2, \eta)\, P^L(k_3, \eta)\, \frac{4\pi}{3} \int dl\, l^2 \left(\frac{P^L(l,\eta)^2}{l^2}\right) \\
& + \ 2 \text{ permutations}\,.
\end{aligned}
\tag{A.5}
$$

Here, $F_2^s(\boldsymbol{k}_2, \boldsymbol{k}_3)$ denotes the symmetrized second-order kernel in SPT, as defined in (3.36) with (3.33), and the permutations have to be taken with respect to the external momenta.

For deriving the soft limit of the angular-averaged one-loop density bispectrum, we next replace the external momenta k_1, k_2, and k_3 in (A.2)-(A.5) by k, q and $|\boldsymbol{q} - \boldsymbol{k}|$, involving the angular parameter μ of (6.7) and perform a series expansion about the soft mode q afterwards.

---

[1] Notice that in this work, we use different Fourier conventions than in [1] and [187]. Our Fourier conventions are given in (1.6). Besides, we have corrected typographical errors of [1] in (A.4) and (A.5). These corrections have no impact on the subsequent results and our conclusions.

Subsequently, we take the soft limit $q \to 0$ and perform the angular average with respect to μ. While

$$B_{111}^{(222)}(\boldsymbol{k}, -\boldsymbol{q}, \boldsymbol{q} - \boldsymbol{k}, \eta)^{\mathrm{av}} \xrightarrow{q \to 0} 0, \tag{A.6}$$

the other resulting angular-averaged expressions for one-loop bispectrum contributions in the soft limit read

$$B_{111}^{(321,I)}(\boldsymbol{k}, -\boldsymbol{q}, \boldsymbol{q} - \boldsymbol{k}, \eta)^{\mathrm{av}} \xrightarrow{q \to 0} P^L(q, \eta) \, (2\pi)^3 \frac{k^4}{\pi^2} \, \gamma^{\mathrm{SPT}} \int dl \, l^2 \left(\frac{P^L(l, \eta)^2}{l^4} \right),$$

$$B_{111}^{(321,II)}(\boldsymbol{k}, -\boldsymbol{q}, \boldsymbol{q} - \boldsymbol{k}, \eta)^{\mathrm{av}} \xrightarrow{q \to 0} P^L(q, \eta) \, (2\pi)^3 \frac{k^2}{\pi^2} \left(\alpha_1^{\mathrm{SPT}} k \, \partial_k + \beta_1^{\mathrm{SPT}} \right) P^L(k, \eta) \int dl \, l^2 \left(\frac{P^L(l, \eta)}{l^2} \right),$$

$$B_{111}^{(411)}(\boldsymbol{k}, -\boldsymbol{q}, \boldsymbol{q} - \boldsymbol{k}, \eta)^{\mathrm{av}} \xrightarrow{q \to 0} P^L(q, \eta) \, (2\pi)^3 \frac{k^2}{\pi^2} \left(\alpha_2^{\mathrm{SPT}} k \, \partial_k + \beta_2^{\mathrm{SPT}} \right) P^L(k, \eta) \int dl \, l^2 \left(\frac{P^L(l, \eta)}{l^2} \right),$$

$$\tag{A.7}$$

where we introduced the coefficients

$$\gamma^{\mathrm{SPT}} = \frac{515}{5292}, \qquad \alpha_1^{\mathrm{SPT}} = \alpha_2^{\mathrm{SPT}} = \frac{61}{3780}, \qquad \beta_1^{\mathrm{SPT}} = -\frac{671}{8820}, \qquad \beta_2^{\mathrm{SPT}} = -\frac{155}{756}. \tag{A.8}$$

Finally, the sum of these contributions (see (A.1)),

$$B_{111}^{\text{1-loop}}(\boldsymbol{k}, -\boldsymbol{q}, \boldsymbol{q} - \boldsymbol{k}, \eta)^{\mathrm{av}} \xrightarrow{q \to 0} P^L(q, \eta) \, (2\pi)^3 \frac{k^2}{\pi^2} \left[\left(\alpha^{\mathrm{SPT}} k \, \partial_k + \beta^{\mathrm{SPT}} \right) P^L(k, \eta) \int dl \, l^2 \left(\frac{P^L(l, \eta)}{l^2} \right) \right.$$
$$\left. + \gamma^{\mathrm{SPT}} k^2 \int dl \, l^2 \left(\frac{P^L(l, \eta)^2}{l^4} \right) \right] \tag{A.9}$$

with

$$\beta^{\mathrm{SPT}} \equiv \beta_1^{\mathrm{SPT}} + \beta_2^{\mathrm{SPT}} = -\frac{3719}{13230}, \qquad \alpha^{\mathrm{SPT}} \equiv \alpha_1^{\mathrm{SPT}} + \alpha_2^{\mathrm{SPT}} = \frac{61}{1890}, \tag{A.10}$$

yields the angular-averaged soft-limit bispectrum of density perturbations at one-loop order in SPT.

A.2. Estimating the impact of the coefficient C_{12}

In this appendix, we provide a numerical estimation of the impact of the coefficient $C_{12}(\eta)$ parameterizing the α-terms in (7.32) of Section 7.1.2. Since we have neglected the α-contributions $P_{ab}^{\alpha}(q, \eta)$ to the non-linear soft-limit power spectrum in the final non-perturbative equation (7.65) in Section 7.3, the numerical estimation also allows to estimate the errors induced by this approximation. These error estimations are important for being able to perform the numerical analysis of our analytical results in Section 7.4.

As discussed in Section 7.2, the coefficient $C_{12}(\eta)$ generally depends, through the variance of the density-velocity cross correlation in (7.61), on various geometrical parameters of the locally curved anisotropic background cosmology. In principle, this dependence can be extracted from suitable N-body simulations performed within anisotropic 'separate universe approach', similarly to [238–240, 380]. To our best knowledge, numerical simulations of these kind have not been performed yet. Thus, we estimate the error induced due to neglecting the coefficient $C_{12}(\eta)$ in the non-perturbative power spectrum equation (7.65) by another suitable numerical approach. Since we expect the final expression for $C_{12}(\eta)$ to show a functional dependence analogous to the one of the coefficient $C_{22}(\eta)$ in (7.23), we explore it by the ansatz

$$C_{12}(\eta) = d_1\, \sigma_{12}^2(\eta) + d_2\, \partial_\eta \sigma_{12}^2(\eta)\,, \tag{A.11}$$

where d_1 and d_2 constitute adjustable free parameters.

In order to estimate the plausible values of the parameters d_1 and d_2, we evaluate the ansatz for $C_{12}(\eta)$ in the previous equation within the perturbative approach of SPT. Thereby, we proceed as in our first example in the numerical analysis of Section 7.4, in which we evaluate the coefficients $c_{ab}(\eta)$ of the evolution equation (7.67) in SPT. If we include the ansatz for $C_{12}(\eta)$ in (A.11) in the non-perturbative equation for the power spectrum in the soft limit in (7.33), and parameterize its non-linear part by (7.66), the resulting evolution equation for the coefficients $c_{ab}(\eta)$ incorporating $C_{12}(\eta)$ reads (see (7.67))

$$
\begin{aligned}
\partial_\eta c_{ab}(\eta) = &-\Omega_{ac}(\eta)\, c_{cb}(\eta) - \Omega_{bc}(\eta)\, c_{ac}(\eta) \\
&+ \begin{pmatrix} 0 & 1 \\ 1 & 2 \end{pmatrix}_{ab} \left(\frac{4}{7}\, \sigma_{22}^2(\eta) - \frac{13}{14}\, \partial_\eta\, \sigma_{22}^2(\eta) \right) \\
&- \begin{pmatrix} 2 & 1 \\ 1 & 0 \end{pmatrix}_{ab} \left(\frac{d_1}{2} \sigma_{12}^2(\eta) + \frac{d_2}{2}\, \partial_\eta \sigma_{12}^2(\eta) \right)\,.
\end{aligned}
\tag{A.12}
$$

If we require that the left-hand side of the evolution equation above reproduces the results emerging from the one-loop power spectrum in the soft limit in SPT, i.e., $c_{ab}^{\mathrm{SPT}}(\eta)$ in (7.70),

and furthermore take into account that the variance $\sigma^2_{ab,L}(\eta)$ at leading order scales like $\sigma^2_{ab,L} = e^{2(\eta - \eta_0)}\,\sigma^2_{ab,L}(\eta_0)$, we obtain the constraint

$$-\frac{1}{2}\,(d_1 + 2\,d_2) = \frac{1}{35} \simeq 0.03\,. \tag{A.13}$$

Hence, in comparison to the terms associated to the coefficient $C_{12}(\eta)$ in the second line on the right-hand side of (A.12), yielding likewise $(4/7 - 2 \cdot 13/14) = -9/7 \simeq -1.29$, the contributions from the coefficient $C_{22}(\eta)$ are significantly suppressed. Since we extracted from the numerical results in Figure 7.4 that $\partial_\eta \ln \sigma^2_{12(22)}(k_{\max}) \simeq 2$ generally holds for $k_{\max} \gtrsim \Lambda_{\mathrm{NL}}$, we conclude that the overall small coefficient in (A.13) leads to a strong effective suppression of the impact of the coefficient $C_{12}(\eta)$, and of the related uncertainties. Moreover, notice that the constraint (A.13) precisely accounts for the %-level difference between the leading-order coefficients $c^{\mathrm{LO}}_{ab}(\eta)$ in (7.69), based on the non-perturbative evolution equation (7.67), and the coefficients $c^{\mathrm{SPT}}_{ab}(\eta)$ in (7.70), derived from the one-loop soft-limit power spectrum in SPT.

By varying the parameters d_1 and d_2 in (A.13), we can then estimate the error caused by neglecting the impact of the coefficient $C_{12}(\eta)$ in the non-perturbative equation for the power spectrum $P_{ab}(q,\eta)$ in (7.65) and thus in the evolution equation for the coefficients $c_{ab}(\eta)$ in (7.67). In Figure A.1, we show the resulting variations of $c_{ab}(\eta)$ as a function of redshift z, as given in (1.1), which is equivalent to the time variable η, for a ΛCDM universe (see (3.49) and (3.18)). To determine the variances in the displacement field $\sigma^2_{ab}(\eta)$, according to (5.11), and in turn the coefficients $c_{ab}(\eta)$ from (A.12), we have used the results of the numerical simulations in the ΛCDM case performed in [378]. This evaluation procedure is the same which has been applied in Figure 7.1. Furthermore, we have assumed for definiteness that $|d_1|, |d_2| \leq 3$. As we can see from Figure A.1, the coefficients $c_{ab}(\eta)$ depend only relatively mildly on the impact of $C_{12}(\eta)$. For instance, at redshift $z = 0\,(0.5)$, their variations $\Delta c_{ab}(\eta)$ are of the order

$$\Delta c_{11} \simeq 15\%\,(5\%)\,, \qquad \Delta c_{12} \simeq 5\%\,(1\%)\,, \qquad \Delta c_{22} \lesssim 1\%\,. \tag{A.14}$$

Here, the fact that the velocity-velocity components $\Delta c_{22}(\eta)$ are at least affected by the impact of $C_{12}(\eta)$ can be understood from the structure of the evolution equation (A.12). Note that the results for the coefficients $c_{ab}(\eta)$ in Figure 7.1, which are obtained from (7.65) neglecting $C_{12}(\eta)$, lie within the uncertainty bands shown in Figure A.1.

As a next step, we can require the evolution equation for the coefficients $c_{ab}(\eta)$ in (A.12), which includes the contributions from $C_{12}(\eta)$, to be (approximately) fulfilled at next-to-leading order in SPT. By adjusting the free parameters according to (A.13), we can reproduce the next-to-leading order corrections for the coefficients $c_{ab}(\eta)$ with a relative accuracy of at least $\sim 15\%$ for all auto- and cross-correlations of density and velocity fields, independent of the linear
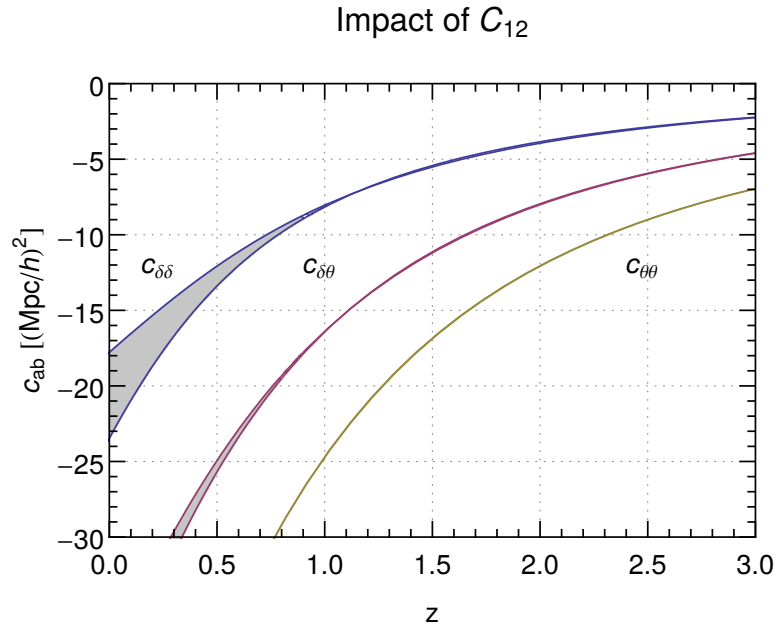
Impact of C_{12}

Fig. A.1.: Estimate for the impact of the coefficient $C_{12}(\eta)$, representing the neglected α-contributions in the non-perturbative power spectrum equation (7.33), on the coefficients $c_{ab}(z)$ in (7.66) as a function of redshift z for a ΛCDM universe. The coefficients $c_{\delta\delta} \equiv c_{11}$, $c_{\delta\theta} \equiv c_{12} = c_{21}$ and $c_{\theta\theta} \equiv c_{22}$ are obtained from the evolution equation (A.12), including $C_{12}(\eta)$, by determining the variances $\sigma_{ab}^2(\eta)$ in (5.11) from the ΛCDM N-body simulation data in [378] and taking into account the constraint on the free parameters d_1 and d_2 in (A.13). Thereby, we have assumed $|d_1|, |d_2| \leq 3$ for definiteness. By variation of the parameters d_1 and d_2 (grey regions), the numerical results for the coefficients $c_{ab}(\eta)$ show only a weak dependence on the value of $C_{12}(\eta)$.

input. Since the next-to-leading order correction is suppressed by a factor of a few compared to the leading-order contribution in the relevant regime, this level of accuracy is also compatible with our estimation of the error induced by neglecting the impact of the coefficient $C_{12}(\eta)$ and thus of the α-contributions, being of the order of $\sim 10\%$ (see Section 7.4.1).

Appendix B

Zusammenfassung

Summary

Large-scale structure surveys have the potential to become the leading probe for precision cosmology in the next decade. To extract valuable information on the cosmological evolution of the Universe from the observational data, it is of major importance to derive accurate theoretical predictions for the statistical large-scale structure observables, such as the power spectrum and the bispectrum of (dark) matter density perturbations. Hence, one of the greatest challenges of modern cosmology is to theoretically understand the non-linear dynamics of large-scale structure formation in the Universe from first principles. While analytic approaches to describe the large-scale structure formation are usually based on the framework of non-relativistic cosmological perturbation theory, we pursue another road in this thesis and develop methods to derive generic, non-perturbative statements about large-scale structure correlation functions. We study unequal- and equal-time correlation functions of density and velocity perturbations in the limit where one of their wavenumbers becomes small, that is, in the soft limit.

In the soft limit, it is possible to link $(\mathcal{N}+1)$-point and $\mathcal{N}$-point correlation functions to non-perturbative 'consistency conditions'. These provide in turn a powerful tool to test fundamental aspects of the underlying theory at hand. In this work, we first rederive the (resummed) consistency conditions at *unequal times* by using the so-called eikonal approximation. The main appeal of the unequal-time consistency conditions is that they are solely based on symmetry arguments and thus are universal. Proceeding from this, we direct our attention to consistency conditions at *equal times*, which, on the other hand, depend on the interplay between soft and hard modes. We explore the existence and validity of equal-

time consistency conditions within and beyond perturbation theory. For this purpose, we investigate the predictions for the soft limit of the bispectrum of density and velocity perturbations in two different approaches, namely in the perturbative time-flow approach and in a non-perturbative background method. This background method, which relies on absorbing a spherically symmetric soft mode into a locally curved background cosmology, has recently inspired a proposal for an (allegedly non-perturbative) angular-averaged equal-time consistency condition for the bispectrum of density perturbations (henceforth referred to as VKPR proposal). We demonstrate explicitly for an Einstein–de Sitter universe that the time-flow relations as well as the VKPR proposal are only fulfilled at leading order in perturbation theory, but are not exact beyond it. Since the VKPR proposal still leads to qualitatively accurate predictions for the bispectrum of density perturbations beyond the linear perturbative order, it can nevertheless be regarded as a reasonable *empirical* approximation in this case. However, transferring the VKPR proposal to the velocity perturbations significantly fails beyond linear order in perturbation theory. In consequence, we generalize the background method to properly account for the effect of local curvature both in the density and velocity perturbations on short distance scales. This allows us not only to identify the discrepancies of the VKPR proposal, but also to formulate a proper generalization of it which includes both the density and velocity perturbations. In addition, we use the background method to deduce a generic, non-perturbative angular-averaged bispectrum consistency condition, which depends on the density power spectrum of hard modes in the presence of local curvature.

Building upon this, we proceed by deriving a non-perturbative equation for the power spectrum in the soft limit. To this end, we perform an operator product expansion, on the one hand, and deduce a non-perturbative *angular-dependent* bispectrum consistency condition, on the other hand. We obtain the latter from extending the background method to the case of a directional soft mode, being absorbed into a locally curved anisotropic background cosmology. The resulting non-perturbative power spectrum equation encodes the coupling to ultraviolet (UV) modes in two time-dependent coefficients. These can most generally be inferred from response functions to geometrical parameters, such as spatial curvature, in the locally curved anisotropic background cosmology. However, we can determine one coefficient by use of the angular-averaged bispectrum consistency condition together with the generalized VKPR proposal, and we show that the impact of the other one is subleading. Neglecting the latter in consequence, we confront the non-perturbative power spectrum equation against numerical simulations and find indeed a very good agreement within the expected error bars. Moreover, we argue that both coefficients and thus the non-perturbative power spectrum in the soft limit depend only weakly on UV modes deep in the non-linear regime. This non-perturbative finding allows us in turn to derive important implications for pertur-

bative approaches to large-scale structure formation. First, it leads to the conclusion that the UV dependence of the power spectrum found in explicit computations within standard perturbation theory is an artifact. Second, it implies that in the Eulerian (Lagrangian) effective field theory (EFT) approach, where UV divergences are canceled by counter-terms, the renormalized leading-order coefficient(s) receive most contributions from modes close to the non-linear scale. The non-perturbative approach we developed can in principle be used to precisely infer the size of these renormalized leading-order EFT coefficient(s) by performing small-volume numerical simulations within an anisotropic 'separate universe' framework. Our results suggest that the importance of these coefficient(s) is a $\sim 10\%$ effect at most.

Zusammenfassung

Rotverschiebungssurveys zur Durchmusterung der großräumigen Struktur des Universums haben das Potential, innerhalb des nächsten Jahrzehnts die führende kosmologische Präzisionsmessung zu werden. Um aus den Beobachtungsdaten wertvolle Informationen über die kosmologische Entwicklung des Universums gewinnen zu können, ist es von größter Bedeutung präzise theoretische Vorhersagen für die statistischen Observablen der großräumigen Struktur des Universums, wie zum Beispiel das Leistungsspektrum und das Bispektrum der (Dunkle-) Materiedichtefluktuationen, zu machen. Eine der größten Herausforderungen der modernen Kosmologie ist es daher, die nicht-lineare Dynamik der kosmologischen Strukturbildung von Grund auf theoretisch zu verstehen. Während analytische Methoden zur Beschreibung der kosmologischen Strukturbildung in der Regel auf den Grundlagen der nicht-relativistischen kosmologischen Störungstheorie basieren, verfolgen wir in dieser Dissertation einen anderen Ansatz und entwickeln Methoden, um generelle, nicht-perturbative Aussagen über Korrelationsfunktionen der großräumigen Struktur des Universum herzuleiten. Hierfür untersuchen wir Korrelationen von Dichte- und Geschwindigkeitsfluktuationen ungleicher und gleicher Zeiten in dem Limes, in dem eine ihrer Wellenzahlen sehr klein wird, das heißt im sogenannten 'weichen' Limes.

In diesem weichen Limes ist es möglich, $(\mathcal{N} + 1)$-Punkts- und $\mathcal{N}$-Punktskorrelationsfunktionen zu nicht-perturbativen 'Konsistenzbedingungen' zu verknüpfen. Diese bilden ihrerseits ein mächtiges Handwerkszeug, um fundamentale Aspekte der zugrundliegenden physikalischen Theorie zu testen. Im Rahmen dieser Arbeit leiten wir zunächst die (resummierten) Konsistenzbedingungen für ungleiche Zeiten her, indem wir die sogenannte Eikonalnäherung verwenden. Der größte Reiz dieser Konsistenzbedingungen für ungleiche Zeiten besteht darin, dass sie auschließlich auf Symmetrieargumenten beruhen und daher universell sind. Danach wenden wir uns den Konsistenzbedingungen für gleiche Zeiten zu, die andererseits von der Wechselwirkung zwischen weichen und harten Moden abhängen. Wir erforschen die Existenz und Gültigkeit von Konsistenzbedingungen für gleichen Zeiten innerhalb der Störungstheorie sowie über sie hinausgehend. Zu diesem Zweck untersuchen wir die Vorhersagen zweier verschiedener Methoden für den weichen Limes des Bispektrums der Dichte- und Geschwindigkeitsfluktuationen, nämlich zum einen der perturbativen 'time-flow'-Methode und zum anderen einer nicht-perturbativen Hintergrundmethode. Diese Hintergrundmethode, die auf der Absorbierung einer sphärisch symmetrischen weichen Mode in eine lokal gekrümmte Hintergrundkosmologie basiert, hat kürzlich zu einem (vermeintlich nicht-perturbativen) Vorschlag einer winkelgemittelten Konsistenzbedingung gleicher Zeiten für das Bispektrum der Dichtefluktuationen (fortan als VKPR-Vorschlag bezeichnet) geführt. Wir weisen explizit für ein

Einstein-de-Sitter-Universum nach, dass die 'time-flow'-Relationen ebenso wie der VKPR-Vorschlag nur in Störungstheorie erster Ordnung, nicht aber darüber hinaus, exakt sind. Da der VKPR-Vorschlag jenseits der Störungstheorie erster Ordnung dennoch zu qualitativ korrekten Vorhersagen für das Bispektrum der Dichtefluktuationen führt, kann er jedoch als eine vernünftige *empirische* Näherung betrachtet werden. Wird der VKPR-Vorschlag allerdings auf die Geschwindigkeitsfluktuationen übertragen, ergeben sich signifikante Abweichungen jenseits der Störungstheorie erster Ordnung. Aufgrund dessen verallgemeinern wir die Hintergrundmethode, um den Effekt lokaler Krümmung auf die Dichte- und Geschwindigkeitsfluktuationen auf kurzen Distanzskalen physikalisch richtig zu beschreiben. Dadurch ist es uns möglich, nicht nur die Unstimmigkeiten des VKPR-Vorschlags auszumachen, sondern auch eine geeignete Verallgemeinerung des letzteren, die sowohl Dichte- als auch Geschwindigkeitsfluktuationen einbezieht, zu formulieren. Zusätzlich verwenden wir die Hintergrundmethode, um eine generelle, nicht-perturbative winkelgemittelte Bispektrumkonsistenzbedingung herzuleiten, die vom Dichteleistungsspektrum harter Moden in Gegenwart von lokaler Krümmung abhängt.

Wir fahren anschließend fort, indem wir eine nicht-perturbative Gleichung für das Leistungsspektrum im weichen Limes herleiten. Dafür führen wir einerseits eine Operator-Produkt-Entwicklung durch und ermitteln andererseits eine nicht-perturbative *winkelabhängige* Bispektrumkonsistenzbedingung. Wir erhalten diese, indem wir die Hintergrundmethode für den Fall einer gerichteten weichen Mode, die in eine lokal gekrümmte anisotrope Hintergrundkosmologie absorbiert wird, erweitern. Die resultierende nicht-perturbative Leistungsspektrumgleichung beinhaltet die Kopplung an ultraviolette (UV-)Moden durch zwei zeitabhängige Koeffizienten. Diese können am allgemeinsten durch Antwortfunktionen ('response functions') bezüglich geometrischer Parameter, wie etwa räumlicher Krümmung, in der lokal gekrümmten anisotropen Hintergrundkosmologie abgeleitet werden. Allerdings können wir einen Koeffizienten mithilfe der winkelgemittelten Bispektrumkonsistenzbedingung sowie des verallgemeinerten VKPR-Vorschlags bestimmen. Wir zeigen zudem, dass der andere Koeffizienten nur einen geringfügigen Einfluss hat. Daher vergleichen wir, unter Vernachlässigung des letzteren, die nicht-perturbative Leistungsspektrumgleichung mit numerischen Simulationen und stellen in der Tat eine sehr gute Übereinstimmung innerhalb der erwarteten Fehlergrenzen fest. Darüber hinaus erörtern wir, dass beide Koeffizienten und folglich das nicht-perturbative Leistungsspektrum im weichen Limes nur schwach von UV-Moden weit im nicht-linearen Bereich abhängen. Diese nicht-perturbative Erkenntnis ermöglicht es uns ihrerseits, wichtige Implikationen für perturbative Methoden der kosmologischen Strukturbildung abzuleiten. Zum einen führt sie zu der Schlussfolgerung, dass die UV-Abhängigkeit des Leistungsspektrums, die in expliziten Berechnungen innerhalb der perturbativen Standardmethode ('standard perturba-

tion theory') auftritt, ein Artefakt ist. Zum anderen impliziert sie, dass in der Eulerschen (Lagrangeschen) Methode der effektiven Feldtheorie (EFT), in der die UV-Divergenzen durch Gegenterme ('counter-terms') aufgehoben werden, die renormierten Koeffizient(en) führender Ordnung die größten Beiträge von Moden nahe des nicht-linearen Bereiches erhalten. Die von uns entwickelte nicht-perturbative Methode kann im Prinzip verwendet werden, um die Größe der renormierten EFT-Koeffizient(en) präzise mithilfe von numerischen Simulationen eines anisotropen unabhängigen Unversums ('separate universe') zu bestimmen. Unsere Ergebnissen nach entspricht die Relevanz dieser Koeffizient(en) allenfalls einem $\sim 10\%$-Effekt.

The results presented in this thesis are based on the following publications:

[1] I. Ben-Dayan, T. Konstandin, R. A. Porto, and L. Sagunski, "On Soft Limits of Large-Scale Structure Correlation Functions," *JCAP* **1502** no. 02, (2015) 026, `arXiv:1411.3225 [astro-ph.CO]`.

[2] M. Garny, T. Konstandin, R. A. Porto, and L. Sagunski, "On the Soft Limit of the Large Scale Structure Power Spectrum: UV Dependence," *JCAP* **1511** no. 11, (2015) 032, `arXiv:1508.06306 [astro-ph.CO]`.

Bibliography

[1] I. Ben-Dayan, T. Konstandin, R. A. Porto, and L. Sagunski, "On Soft Limits of Large-Scale Structure Correlation Functions," *JCAP* **1502** no. 02, (2015) 026, `arXiv:1411.3225 [astro-ph.CO]`.

[2] M. Garny, T. Konstandin, R. A. Porto, and L. Sagunski, "On the Soft Limit of the Large Scale Structure Power Spectrum: UV Dependence," *JCAP* **1511** no. 11, (2015) 032, `arXiv:1508.06306 [astro-ph.CO]`.

[3] K. Popper, *The Logic of Scientific Discovery*. Routledge Classics. Taylor & Francis, 2005.

[4] **Virgo, LIGO Scientific** Collaboration, B. P. Abbott *et al.*, "Observation of Gravitational Waves from a Binary Black Hole Merger," *Phys. Rev. Lett.* **116** no. 6, (2016) 061102, `arXiv:1602.03837 [gr-qc]`.

[5] A. Einstein, "Die Feldgleichungen der Gravitation," *Sitzungsberichte der Königlich Preußischen Akademie der Wissenschaften (Berlin), Seite 844-847.* (1915) .

[6] **Virgo, LIGO Scientific** Collaboration, B. P. Abbott *et al.*, "Tests of general relativity with GW150914," `arXiv:1602.03841 [gr-qc]`.

[7] E. Calabrese, N. Battaglia, and D. N. Spergel, "Testing Gravity with Gravitational Wave Source Counts," `arXiv:1602.03883 [gr-qc]`.

[8] E. Berti *et al.*, "Testing General Relativity with Present and Future Astrophysical Observations," *Class. Quant. Grav.* **32** (2015) 243001, `arXiv:1501.07274 [gr-qc]`.

[9] B. S. Sathyaprakash and B. F. Schutz, "Physics, Astrophysics and Cosmology with Gravitational Waves," *Living Rev. Rel.* **12** (2009) 2, `arXiv:0903.0338 [gr-qc]`.

Bibliography

[10] R. X. Adhikari, "Gravitational Radiation Detection with Laser Interferometry," *Rev. Mod. Phys.* **86** (2014) 121, `arXiv:1305.5188 [gr-qc]`.

[11] A. Guth, "A Golden Age of Cosmology." edge.org, 2001. `https://www.edge.org/conversation/alan_guth-a-golden-age-of-cosmology`. Accessed 2016-04-16.

[12] C. L. Bennett, A. Banday, K. M. Gorski, G. Hinshaw, P. Jackson, P. Keegstra, A. Kogut, G. F. Smoot, D. T. Wilkinson, and E. L. Wright, "Four year COBE DMR cosmic microwave background observations: Maps and basic results," *Astrophys. J.* **464** (1996) L1–L4, `arXiv:astro-ph/9601067 [astro-ph]`.

[13] **WMAP** Collaboration, G. Hinshaw *et al.*, "Nine-Year Wilkinson Microwave Anisotropy Probe (WMAP) Observations: Cosmological Parameter Results," *Astrophys. J. Suppl.* **208** (2013) 19, `arXiv:1212.5226 [astro-ph.CO]`.

[14] **BICEP2** Collaboration, P. A. R. Ade *et al.*, "Detection of *B*-Mode Polarization at Degree Angular Scales by BICEP2," *Phys. Rev. Lett.* **112** no. 24, (2014) 241101, `arXiv:1403.3985 [astro-ph.CO]`.

[15] **BICEP2, Planck** Collaboration, P. Ade *et al.*, "Joint Analysis of BICEP2/*KeckArray* and *Planck* Data," *Phys. Rev. Lett.* **114** (2015) 101301, `arXiv:1502.00612 [astro-ph.CO]`.

[16] **Planck** Collaboration, R. Adam *et al.*, "Planck 2015 results. I. Overview of products and scientific results," `arXiv:1502.01582 [astro-ph.CO]`.

[17] **Planck** Collaboration, P. A. R. Ade *et al.*, "Planck 2015 results. XIII. Cosmological parameters," `arXiv:1502.01589 [astro-ph.CO]`.

[18] **SDSS** Collaboration, M. Tegmark *et al.*, "The 3-D power spectrum of galaxies from the SDSS," *Astrophys. J.* **606** (2004) 702–740, `arXiv:astro-ph/0310725 [astro-ph]`.

[19] **SDSS** Collaboration, K. N. Abazajian *et al.*, "The Seventh Data Release of the Sloan Digital Sky Survey," *Astrophys. J. Suppl.* **182** (2009) 543–558, `arXiv:0812.0649 [astro-ph]`.

[20] **Supernova Cosmology Project** Collaboration, S. Perlmutter *et al.*, "Measurements of Omega and Lambda from 42 high redshift supernovae," *Astrophys. J.* **517** (1999) 565–586, `arXiv:astro-ph/9812133 [astro-ph]`.

[21] **Supernova Search Team** Collaboration, A. G. Riess *et al.*, "Observational evidence from supernovae for an accelerating universe and a cosmological constant," *Astron. J.* **116** (1998) 1009–1038, arXiv:astro-ph/9805201 [astro-ph].

[22] **Planck** Collaboration, P. A. R. Ade *et al.*, "Planck 2015 results. XX. Constraints on inflation," arXiv:1502.02114 [astro-ph.CO].

[23] **Planck** Collaboration, P. A. R. Ade *et al.*, "Planck 2015 results. XVII. Constraints on primordial non-Gaussianity," arXiv:1502.01592 [astro-ph.CO].

[24] A. H. Guth, "The Inflationary Universe: A Possible Solution to the Horizon and Flatness Problems," *Phys. Rev.* **D23** (1981) 347–356.

[25] A. D. Linde, "A New Inflationary Universe Scenario: A Possible Solution of the Horizon, Flatness, Homogeneity, Isotropy and Primordial Monopole Problems," *Phys. Lett.* **B108** (1982) 389–393.

[26] A. Albrecht and P. J. Steinhardt, "Cosmology for Grand Unified Theories with Radiatively Induced Symmetry Breaking," *Phys. Rev. Lett.* **48** (1982) 1220–1223.

[27] D. Baumann, "Inflation," in *Physics of the large and the small, TASI 09, proceedings of the Theoretical Advanced Study Institute in Elementary Particle Physics, Boulder, Colorado, USA, 1-26 June 2009*, pp. 523–686. 2011. arXiv:0907.5424 [hep-th].

[28] L. Senatore, "TASI 2012 Lectures on Inflation," in *Proceedings, Theoretical Advanced Study Institute in Elementary Particle Physics: Searching for New Physics at Small and Large Scales (TASI 2012)*, pp. 221–302. 2013.

[29] D. Baumann and L. McAllister, *Inflation and String Theory*. Cambridge University Press, 2015. arXiv:1404.2601 [hep-th].

[30] D. Baumann, D. Green, and R. A. Porto, "B-modes and the Nature of Inflation," *JCAP* **1501** no. 01, (2015) 016, arXiv:1407.2621 [hep-th].

[31] D. Baumann and D. Green, "Signatures of Supersymmetry from the Early Universe," *Phys. Rev.* **D85** (2012) 103520, arXiv:1109.0292 [hep-th].

[32] N. Arkani-Hamed and J. Maldacena, "Cosmological Collider Physics," arXiv:1503.08043 [hep-th].

[33] R. Flauger, D. Green, and R. A. Porto, "On squeezed limits in single-field inflation. Part I," *JCAP* **1308** (2013) 032, arXiv:1303.1430 [hep-th].

[34] R. A. Porto, "Gravitational waves and the (quantum) nature of the primordial seed,"
Int. J. Mod. Phys. **D23** no. 12, (2014) 1441005.

[35] D. Baumann, D. Green, H. Lee, and R. A. Porto, "Signs of Analyticity in Single-Field
Inflation," *Phys. Rev.* **D93** no. 2, (2016) 023523, `arXiv:1502.07304 [hep-th]`.

[36] M. Mirbabayi and M. Simonovic, "Effective Theory of Squeezed Correlation
Functions," *JCAP* **1603** no. 03, (2016) 056, `arXiv:1507.04755 [hep-th]`.

[37] M. Alvarez *et al.*, "Testing Inflation with Large Scale Structure: Connecting Hopes
with Reality," `arXiv:1412.4671 [astro-ph.CO]`.

[38] **2dFGRS** Collaboration, S. Cole *et al.*, "The 2dF Galaxy Redshift Survey:
Power-spectrum analysis of the final dataset and cosmological implications," *Mon.
Not. Roy. Astron. Soc.* **362** (2005) 505–534, `arXiv:astro-ph/0501174 [astro-ph]`.

[39] **Particle Data Group** Collaboration, S. Eidelman *et al.*, "Review of particle physics.
Particle Data Group," *Phys. Lett.* **B592** (2004) 1–1109.

[40] F. Bernardeau, S. Colombi, E. Gaztanaga, and R. Scoccimarro, "Large scale structure
of the universe and cosmological perturbation theory," *Phys. Rept.* **367** (2002) 1–248,
`arXiv:astro-ph/0112551 [astro-ph]`.

[41] C. L. Bennett, "Cosmology from start to finish," *Nature* **440** (2006) 1126–1131.

[42] B. A. Bassett and R. Hlozek, "Baryon Acoustic Oscillations," `arXiv:0910.5224
[astro-ph.CO]`.

[43] M. Colless *et al.*, "The 2dF Galaxy Redshift Survey: Final data release,"
`arXiv:astro-ph/0306581 [astro-ph]`.

[44] **BOSS** Collaboration, K. S. Dawson *et al.*, "The Baryon Oscillation Spectroscopic
Survey of SDSS-III," *Astron. J.* **145** (2013) 10, `arXiv:1208.0022 [astro-ph.CO]`.

[45] **BOSS** Collaboration, L. Anderson *et al.*, "The clustering of galaxies in the SDSS-III
Baryon Oscillation Spectroscopic Survey: baryon acoustic oscillations in the Data
Releases 10 and 11 Galaxy samples," *Mon. Not. Roy. Astron. Soc.* **441** no. 1, (2014)
24–62, `arXiv:1312.4877 [astro-ph.CO]`.

[46] **SDSS** Collaboration, D. J. Eisenstein *et al.*, "SDSS-III: Massive Spectroscopic
Surveys of the Distant Universe, the Milky Way Galaxy, and Extra-Solar Planetary
Systems," *Astron. J.* **142** (2011) 72, `arXiv:1101.1529 [astro-ph.IM]`.

[47] V. Springel *et al.*, "Simulating the joint evolution of quasars, galaxies and their large-scale distribution," *Nature* **435** (2005) 629–636, `arXiv:astro-ph/0504097 [astro-ph]`.

[48] M. Boylan-Kolchin, V. Springel, S. D. M. White, A. Jenkins, and G. Lemson, "Resolving Cosmic Structure Formation with the Millennium-II Simulation," *Mon. Not. Roy. Astron. Soc.* **398** (2009) 1150, `arXiv:0903.3041 [astro-ph.CO]`.

[49] R. Angulo, M. Fasiello, L. Senatore, and Z. Vlah, "On the Statistics of Biased Tracers in the Effective Field Theory of Large Scale Structures," *JCAP* **1509** no. 09, (2015) 029, `arXiv:1503.08826 [astro-ph.CO]`.

[50] V. Springel, C. S. Frenk, and S. D. M. White, "The large-scale structure of the Universe," *Nature* **440** (2006) 1137, `arXiv:astro-ph/0604561 [astro-ph]`.

[51] M. J. Geller and J. P. Huchra, "Mapping the universe," *Science* **246** (1989) 897–903.

[52] J. R. Gott, III, M. Juric, D. Schlegel, F. Hoyle, M. Vogeley, M. Tegmark, N. A. Bahcall, and J. Brinkmann, "A map of the universe," *Astrophys. J.* **624** (2005) 463, `arXiv:astro-ph/0310571 [astro-ph]`.

[53] **Dark Energy Survey** Collaboration, T. Abbott *et al.*, "The dark energy survey," `arXiv:astro-ph/0510346 [astro-ph]`.

[54] **DES** Collaboration, H. T. Diehl *et al.*, "The Dark Energy Survey and Operations: Year 1," *Proc. SPIE Int. Soc. Opt. Eng.* **9149** (2014) 91490V.

[55] K. S. Dawson *et al.*, "The SDSS-IV extended Baryon Oscillation Spectroscopic Survey: Overview and Early Data," *Astron. J.* **151** (2016) 44, `arXiv:1508.04473 [astro-ph.CO]`.

[56] **DESI** Collaboration, B. Flaugher and C. Bebek, "The Dark Energy Spectroscopic Instrument (DESI)," *Proc. SPIE Int. Soc. Opt. Eng.* **9147** (2014) 91470S.

[57] **LSST** Collaboration, Z. Ivezic, J. A. Tyson, R. Allsman, J. Andrew, and R. Angel, "LSST: from Science Drivers to Reference Design and Anticipated Data Products," `arXiv:0805.2366 [astro-ph]`.

[58] D. Spergel *et al.*, "Wide-Field InfrarRed Survey Telescope-Astrophysics Focused Telescope Assets WFIRST-AFTA 2015 Report," `arXiv:1503.03757 [astro-ph.IM]`.

Bibliography

[59] **EUCLID** Collaboration, R. Laureijs *et al.*, "Euclid Definition Study Report,"
`arXiv:1110.3193 [astro-ph.CO]`.

[60] **Euclid Theory Working Group** Collaboration, L. Amendola *et al.*, "Cosmology
and fundamental physics with the Euclid satellite," *Living Rev. Rel.* **16** (2013) 6,
`arXiv:1206.1225 [astro-ph.CO]`.

[61] A. Rassat, F. Lanusse, D. Kirk, O. Host, and S. Bridle, "Combining Probes," *IAU
Symp.* **306** (2015) 192–201.

[62] E. Di Dio, F. Montanari, J. Lesgourgues, and R. Durrer, "The CLASSgal code for
Relativistic Cosmological Large Scale Structure," *JCAP* **1311** (2013) 044,
`arXiv:1307.1459 [astro-ph.CO]`.

[63] J. J. M. Carrasco, M. P. Hertzberg, and L. Senatore, "The Effective Field Theory of
Cosmological Large Scale Structures," *JHEP* **09** (2012) 082, `arXiv:1206.2926
[astro-ph.CO]`.

[64] J. N. Fry, "Gravity, bias, and the galaxy three-point correlation function," *Phys. Rev.
Lett.* **73** (Jul, 1994) 215–219.

[65] L. Verde, L.-M. Wang, A. Heavens, and M. Kamionkowski, "Large scale structure, the
cosmic microwave background, and primordial non-gaussianity," *Mon. Not. Roy.
Astron. Soc.* **313** (2000) L141–L147, `arXiv:astro-ph/9906301 [astro-ph]`.

[66] R. Scoccimarro, E. Sefusatti, and M. Zaldarriaga, "Probing primordial
non-Gaussianity with large - scale structure," *Phys. Rev.* **D69** (2004) 103513,
`arXiv:astro-ph/0312286 [astro-ph]`.

[67] N. Bartolo, S. Matarrese, and A. Riotto, "Signatures of primordial non-Gaussianity in
the large-scale structure of the Universe," *JCAP* **0510** (2005) 010,
`arXiv:astro-ph/0501614 [astro-ph]`.

[68] D. Jeong and E. Komatsu, "Primordial non-Gaussianity, scale-dependent bias, and the
bispectrum of galaxies," *Astrophys. J.* **703** (2009) 1230–1248, `arXiv:0904.0497
[astro-ph.CO]`.

[69] T. Nishimichi, A. Taruya, K. Koyama, and C. Sabiu, "Scale Dependence of Halo
Bispectrum from Non-Gaussian Initial Conditions in Cosmological N-body
Simulations," *JCAP* **1007** (2010) 002, `arXiv:0911.4768 [astro-ph.CO]`.

[70] M. Liguori, E. Sefusatti, J. R. Fergusson, and E. P. S. Shellard, "Primordial non-Gaussianity and Bispectrum Measurements in the Cosmic Microwave Background and Large-Scale Structure," *Adv. Astron.* **2010** (2010) 980523, `arXiv:1001.4707 [astro-ph.CO]`.

[71] T. Baldauf, U. Seljak, and L. Senatore, "Primordial non-Gaussianity in the Bispectrum of the Halo Density Field," *JCAP* **1104** (2011) 006, `arXiv:1011.1513 [astro-ph.CO]`.

[72] A. Slosar, C. Hirata, U. Seljak, S. Ho, and N. Padmanabhan, "Constraints on local primordial non-Gaussianity from large scale structure," *JCAP* **0808** (2008) 031, `arXiv:0805.3580 [astro-ph]`.

[73] J.-Q. Xia, A. Bonaldi, C. Baccigalupi, G. De Zotti, S. Matarrese, L. Verde, and M. Viel, "Constraining Primordial Non-Gaussianity with High-Redshift Probes," *JCAP* **1008** (2010) 013, `arXiv:1007.1969 [astro-ph.CO]`.

[74] A. Mana, T. Giannantonio, J. Weller, B. Hoyle, G. Huetsi, and B. Sartoris, "Combining clustering and abundances of galaxy clusters to test cosmology and primordial non-Gaussianity," *Mon. Not. Roy. Astron. Soc.* **434** (2013) 684, `arXiv:1303.0287 [astro-ph.CO]`.

[75] A. J. Ross *et al.*, "The Clustering of Galaxies in SDSS-III DR9 Baryon Oscillation Spectroscopic Survey: Constraints on Primordial Non-Gaussianity," *Mon. Not. Roy. Astron. Soc.* **428** (2013) 1116–1127, `arXiv:1208.1491 [astro-ph.CO]`.

[76] T. Giannantonio, A. J. Ross, W. J. Percival, R. Crittenden, D. Bacher, M. Kilbinger, R. Nichol, and J. Weller, "Improved Primordial Non-Gaussianity Constraints from Measurements of Galaxy Clustering and the Integrated Sachs-Wolfe Effect," *Phys. Rev.* **D89** no. 2, (2014) 023511, `arXiv:1303.1349 [astro-ph.CO]`.

[77] T. Giannantonio and W. J. Percival, "Using correlations between CMB lensing and large-scale structure to measure primordial non-Gaussianity," *Mon. Not. Roy. Astron. Soc.* **441** (2014) L16–L20, `arXiv:1312.5154 [astro-ph.CO]`.

[78] W. Dehnen and J. Read, "N-body simulations of gravitational dynamics," *Eur. Phys. J. Plus* **126** (2011) 55, `arXiv:1105.1082 [astro-ph.IM]`.

[79] S. von Hoerner, "Die numerische Integration des n-Körper-Problemes für Sternhaufen. I," *Z. Astrophys.* **50** (1960) .

[80] V. Springel, N. Yoshida, and S. D. M. White, "GADGET: A Code for collisionless and gasdynamical cosmological simulations," *New Astron.* **6** (2001) 79, `arXiv:astro-ph/0003162 [astro-ph]`.

[81] V. Springel, "The Cosmological simulation code GADGET-2," *Mon. Not. Roy. Astron. Soc.* **364** (2005) 1105–1134, `arXiv:astro-ph/0505010 [astro-ph]`.

[82] R. Teyssier, S. Pires, S. Prunet, D. Aubert, C. Pichon, A. Amara, K. Benabed, S. Colombi, A. Refregier, and J.-L. Starck, "Full-Sky Weak Lensing Simulation with 70 Billion Particles," *Astron. Astrophys.* **497** (2009) 335, `arXiv:0807.3651 [astro-ph]`.

[83] J. Stadel, D. Potter, B. Moore, J. Diemand, P. Madau, M. Zemp, M. Kuhlen, and V. Quilis, "Quantifying the heart of darkness with GHALO - a multi-billion particle simulation of our galactic halo," *Mon. Not. Roy. Astron. Soc.* **398** (2009) L21–L25, `arXiv:0808.2981 [astro-ph]`.

[84] A. Klypin, G. Yepes, S. Gottlober, F. Prada, and S. Hess, "MultiDark simulations: the story of dark matter halo concentrations and density profiles," `arXiv:1411.4001 [astro-ph.CO]`.

[85] M. Vogelsberger, S. Genel, V. Springel, P. Torrey, D. Sijacki, D. Xu, G. F. Snyder, D. Nelson, and L. Hernquist, "Introducing the Illustris Project: Simulating the coevolution of dark and visible matter in the Universe," *Mon. Not. Roy. Astron. Soc.* **444** no. 2, (2014) 1518–1547, `arXiv:1405.2921 [astro-ph.CO]`.

[86] J. Schaye *et al.*, "The EAGLE project: Simulating the evolution and assembly of galaxies and their environments," *Mon. Not. Roy. Astron. Soc.* **446** (2015) 521–554, `arXiv:1407.7040 [astro-ph.GA]`.

[87] S. Tassev, M. Zaldarriaga, and D. Eisenstein, "Solving Large Scale Structure in Ten Easy Steps with COLA," *JCAP* **1306** (2013) 036, `arXiv:1301.0322 [astro-ph.CO]`.

[88] S. Tassev, D. J. Eisenstein, B. D. Wandelt, and M. Zaldarriaga, "sCOLA: The N-body COLA Method Extended to the Spatial Domain," `arXiv:1502.07751 [astro-ph.CO]`.

[89] R. A. Porto, "The Effective Field Theorist's Approach to Gravitational Dynamics," `arXiv:1601.04914 [hep-th]`.

[90] A. Schneider, R. Teyssier, D. Potter, J. Stadel, J. Onions, D. S. Reed, R. E. Smith, V. Springel, and F. R. Pearce, "Matter power spectrum and the challenge of percent accuracy," `arXiv:1503.05920 [astro-ph.CO]`.

[91] Ya. B. Zeldovich, "Gravitational instability: An Approximate theory for large density perturbations," *Astron. Astrophys.* **5** (1970) 84–89.

[92] P. Peebles, *The Large-scale Structure of the Universe.* Princeton Series in Physics. Princeton University Press, 1980.

[93] R. Juszkiewicz, "On the evolution of cosmological adiabatic perturbations in the weakly non-linear regime," *Monthly Notices of the Royal Astronomical Society* **197** no. 4, (1981) 931–940.

[94] E. T. Vishniac, "Why weakly non-linear effects are small in a zero-pressure cosmology," *Mon. Not. Roy. Astron. Soc.* **203** no. 2, (1983) 345–349.

[95] J. N. Fry, "The Galaxy correlation hierarchy in perturbation theory," *Astrophys. J.* **279** (1984) 499–510.

[96] M. H. Goroff, B. Grinstein, S. J. Rey, and M. B. Wise, "Coupling of Modes of Cosmological Mass Density Fluctuations," *Astrophys. J.* **311** (1986) 6–14.

[97] N. Makino, M. Sasaki, and Y. Suto, "Analytic approach to the perturbative expansion of nonlinear gravitational fluctuations in cosmological density and velocity fields," *Phys. Rev.* **D46** (1992) 585–602.

[98] B. Jain and E. Bertschinger, "Second order power spectrum and nonlinear evolution at high redshift," *Astrophys. J.* **431** (1994) 495, arXiv:astro-ph/9311070 [astro-ph].

[99] V. Sahni and P. Coles, "Approximation methods for nonlinear gravitational clustering," *Phys. Rept.* **262** (1995) 1–135, arXiv:astro-ph/9505005 [astro-ph].

[100] F. Bernardeau, "The evolution of the large-scale structure of the universe: beyond the linear regime," in *100e Ecole d'Eté de Physique: Post-Planck Cosmology Les Houches, France, July 8-August 2, 2013.* 2013. arXiv:1311.2724 [astro-ph.CO].

[101] D. Blas, M. Garny, and T. Konstandin, "On the non-linear scale of cosmological perturbation theory," *JCAP* **1309** (2013) 024, arXiv:1304.1546 [astro-ph.CO].

[102] D. Blas, M. Garny, and T. Konstandin, "Cosmological perturbation theory at three-loop order," *JCAP* **1401** no. 01, (2014) 010, arXiv:1309.3308 [astro-ph.CO].

[103] T. Buchert, "A class of solutions in Newtonian cosmology and the pancake theory," *Astron. Astrophys.* **223** (1989) 9–24.

[104] F. Moutarde, J.-M. Alimi, F. R. Bouchet, R. Pellat, and A. Ramani, "Precollapse scale invariance in gravitational instability," *Astrophysical Journal* **382** (Dec., 1991) 377–381.

[105] T. Buchert, "Lagrangian theory of gravitational instability of Friedman-Lemaitre cosmologies and the 'Zel'dovich approximation'," *Mon. Not. Roy. Astron. Soc.* **254** (1992) 729–737.

[106] T. Buchert, "Lagrangian theory of gravitational instability of Friedman-Lemaitre cosmologies: Generic third order model for nonlinear clustering," *Mon. Not. Roy. Astron. Soc.* **267** (1994) 811–820, `arXiv:astro-ph/9309055 [astro-ph]`.

[107] F. R. Bouchet, S. Colombi, E. Hivon, and R. Juszkiewicz, "Perturbative Lagrangian approach to gravitational instability," *Astron. Astrophys.* **296** (1995) 575, `arXiv:astro-ph/9406013 [astro-ph]`.

[108] P. Catelan, "Lagrangian dynamics in nonflat universes and nonlinear gravitational evolution," *Mon. Not. Roy. Astron. Soc.* **276** (1995) 115, `arXiv:astro-ph/9406016 [astro-ph]`.

[109] E. Hivon, F. R. Bouchet, S. Colombi, and R. Juszkiewicz, "Redshift distortions of clustering: A Lagrangian approach," *Astron. Astrophys.* **298** (1995) 643–660, `arXiv:astro-ph/9407049 [astro-ph]`.

[110] A. N. Taylor and A. J. S. Hamilton, "Nonlinear cosmological power spectra in real and redshift space," *Mon. Not. Roy. Astron. Soc.* **282** (1996) 767, `arXiv:astro-ph/9604020 [astro-ph]`.

[111] P. Catelan and T. Theuns, "Nonlinear evolution of the angular momentum of protostructures from tidal torques," *Mon. Not. Roy. Astron. Soc.* **282** (1996) 455, `arXiv:astro-ph/9604078 [astro-ph]`.

[112] J. Ehlers and T. Buchert, "Newtonian cosmology in Lagrangian formulation: Foundations and perturbation theory," *Gen. Rel. Grav.* **29** (1997) 733–764, `arXiv:astro-ph/9609036 [astro-ph]`.

[113] T. Tatekawa, "Lagrangian perturbation theory in Newtonian cosmology," *Recent Res. Devel. Phys.* **2** (2005) 1–26, `arXiv:astro-ph/0412025 [astro-ph]`.

[114] T. Matsubara, "Resumming Cosmological Perturbations via the Lagrangian Picture: One-loop Results in Real Space and in Redshift Space," *Phys. Rev.* **D77** (2008) 063530, `arXiv:0711.2521 [astro-ph]`.

[115] T. Matsubara, "Nonlinear perturbation theory with halo bias and redshift-space distortions via the Lagrangian picture," *Phys. Rev.* **D78** (2008) 083519, `arXiv:0807.1733 [astro-ph]`. [Erratum: Phys. Rev.D78,109901(2008)].

[116] T. Hiramatsu and A. Taruya, "Chasing the non-linear evolution of matter power spectrum with numerical resummation method: solution of closure equations," *Phys. Rev.* **D79** (2009) 103526, `arXiv:0902.3772 [astro-ph.CO]`.

[117] T. Matsubara, "Nonlinear Perturbation Theory Integrated with Nonlocal Bias, Redshift-space Distortions, and Primordial Non-Gaussianity," *Phys. Rev.* **D83** (2011) 083518, `arXiv:1102.4619 [astro-ph.CO]`.

[118] T. Okamura, A. Taruya, and T. Matsubara, "Next-to-leading resummation of cosmological perturbations via the Lagrangian picture: 2-loop correction in real and redshift spaces," *JCAP* **1108** (2011) 012, `arXiv:1105.1491 [astro-ph.CO]`.

[119] M. Sato and T. Matsubara, "Nonlinear Biasing and Redshift-Space Distortions in Lagrangian Resummation Theory and N-body Simulations," *Phys. Rev.* **D84** (2011) 043501, `arXiv:1105.5007 [astro-ph.CO]`.

[120] J. Carlson, B. Reid, and M. White, "Convolution Lagrangian perturbation theory for biased tracers," *Mon. Not. Roy. Astron. Soc.* **429** (2013) 1674, `arXiv:1209.0780 [astro-ph.CO]`.

[121] C. Rampf and T. Buchert, "Lagrangian perturbations and the matter bispectrum I: fourth-order model for non-linear clustering," *JCAP* **1206** (2012) 021, `arXiv:1203.4260 [astro-ph.CO]`.

[122] C. Rampf and Y. Y. Y. Wong, "Lagrangian perturbations and the matter bispectrum II: the resummed one-loop correction to the matter bispectrum," *JCAP* **1206** (2012) 018, `arXiv:1203.4261 [astro-ph.CO]`.

[123] C. Rampf, "The recursion relation in Lagrangian perturbation theory," *JCAP* **1212** (2012) 004, `arXiv:1205.5274 [astro-ph.CO]`.

[124] T. Matsubara, "Integrated Perturbation Theory and One-loop Power Spectra of Biased Tracers," *Phys. Rev.* **D90** no. 4, (2014) 043537, `arXiv:1304.4226 [astro-ph.CO]`.

[125] N. S. Sugiyama and D. N. Spergel, "How does non-linear dynamics affect the baryon acoustic oscillation?," *JCAP* **1402** (2014) 042, `arXiv:1306.6660 [astro-ph.CO]`.

[126] N. S. Sugiyama, "Using Lagrangian perturbation theory for precision cosmology," *Astrophys. J.* **788** (2014) 63, arXiv:1311.0725 [astro-ph.CO].

[127] T. Matsubara, "Recursive Solutions of Lagrangian Perturbation Theory," *Phys. Rev.* **D92** no. 2, (2015) 023534, arXiv:1505.01481 [astro-ph.CO].

[128] A. Yoshisato, M. Morikawa, N. Gouda, and H. Mouri, "Why is the Zel'dovich approximation so accurate?," *Astrophys. J.* **637** (2006) 555–560, arXiv:astro-ph/0510107 [astro-ph].

[129] P. Valageas, "Using the Zeldovich dynamics to test expansion schemes," *Astron. Astrophys.* (2007) , arXiv:0706.2593 [astro-ph]. [Astron. Astrophys.476,31(2007)].

[130] P. Valageas, "Impact of shell crossing and scope of perturbative approaches in real and redshift space," *Astron. Astrophys.* **526** (2011) A67, arXiv:1009.0106 [astro-ph.CO].

[131] S. Tassev and M. Zaldarriaga, "The Mildly Non-Linear Regime of Structure Formation," *JCAP* **1204** (2012) 013, arXiv:1109.4939 [astro-ph.CO].

[132] N. McCullagh and A. S. Szalay, "Nonlinear Behavior of Baryon Acoustic Oscillations from the Zel'dovich Approximation Using a Non-Fourier Perturbation Approach," *Astrophys. J.* **752** (2012) 21, arXiv:1202.1306 [astro-ph.CO].

[133] S. Tassev, "N-point Statistics of Large-Scale Structure in the Zel'dovich Approximation," *JCAP* **1406** (2014) 012, arXiv:1311.6316 [astro-ph.CO].

[134] M. White, "The Zel'dovich approximation," *Mon. Not. Roy. Astron. Soc.* **439** no. 4, (2014) 3630–3640, arXiv:1401.5466 [astro-ph.CO].

[135] M. Bartelmann, F. Fabis, D. Berg, E. Kozlikin, R. Lilow, and C. Viermann, "Non-equilibrium statistical field theory for classical particles: Linear and mildly non-linear evolution of cosmological density power spectra," arXiv:1411.1153 [astro-ph.CO].

[136] N. McCullagh and A. S. Szalay, "Nonlinear Behavior of Baryon Acoustic Oscillations in Redshift Space from the Zel'dovich Approximation," *Astrophys. J.* **798** no. 2, (2015) 137, arXiv:1411.1249 [astro-ph.CO].

[137] U. Seljak and Z. Vlah, "Halo Zeldovich model and perturbation theory: Dark matter power spectrum and correlation function," *Phys. Rev.* **D91** no. 12, (2015) 123516, arXiv:1501.07512 [astro-ph.CO].

[138] J. Carlson, M. White, and N. Padmanabhan, "A critical look at cosmological perturbation theory techniques," *Phys. Rev.* **D80** (2009) 043531, `arXiv:0905.0479 [astro-ph.CO]`.

[139] P. Valageas, "Accuracy of analytical models of the large-scale matter distribution," *Phys. Rev.* **D88** no. 8, (2013) 083524, `arXiv:1308.6755 [astro-ph.CO]`.

[140] S. Tassev, "Lagrangian or Eulerian; Real or Fourier? Not All Approaches to Large-Scale Structure Are Created Equal," *JCAP* **1406** (2014) 008, `arXiv:1311.4884 [astro-ph.CO]`.

[141] Z. Vlah, U. Seljak, and T. Baldauf, "Lagrangian perturbation theory at one loop order: successes, failures, and improvements," *Phys. Rev.* **D91** (2015) 023508, `arXiv:1410.1617 [astro-ph.CO]`.

[142] M. Crocce and R. Scoccimarro, "Renormalized cosmological perturbation theory," *Phys. Rev.* **D73** (2006) 063519, `arXiv:astro-ph/0509418 [astro-ph]`.

[143] M. Crocce and R. Scoccimarro, "Memory of initial conditions in gravitational clustering," *Phys. Rev.* **D73** (2006) 063520, `arXiv:astro-ph/0509419 [astro-ph]`.

[144] M. Crocce and R. Scoccimarro, "Nonlinear Evolution of Baryon Acoustic Oscillations," *Phys. Rev.* **D77** (2008) 023533, `arXiv:0704.2783 [astro-ph]`.

[145] M. Crocce, R. Scoccimarro, and F. Bernardeau, "MPTbreeze: A fast renormalized perturbative scheme," *Mon. Not. Roy. Astron. Soc.* **427** (2012) 2537, `arXiv:1207.1465 [astro-ph.CO]`.

[146] A. Taruya, F. Bernardeau, T. Nishimichi, and S. Codis, "RegPT: Direct and fast calculation of regularized cosmological power spectrum at two-loop order," *Phys. Rev.* **D86** (2012) 103528, `arXiv:1208.1191 [astro-ph.CO]`.

[147] V. L'vov and I. Procaccia, "Exact Resummations in the Theory of Hydrodynamic Turbulence: Line-Resummed Diagrammatic Perturbation Approach," in *eprint arXiv:chao-dyn/9502010*, p. 2010. Feb., 1995.

[148] S. Matarrese and M. Pietroni, "Resumming Cosmic Perturbations," *JCAP* **0706** (2007) 026, `arXiv:astro-ph/0703563 [astro-ph]`.

[149] A. Taruya and T. Hiramatsu, "A Closure Theory for Non-linear Evolution of Cosmological Power Spectra," *Astrophys. J.* **674** (2008) 617, `arXiv:0708.1367 [astro-ph]`.

[150] P. McDonald, "Dark matter clustering: a simple renormalization group approach," *Phys. Rev.* **D75** (2007) 043514, `arXiv:astro-ph/0606028 [astro-ph]`.

[151] P. Valageas, "Dynamics of gravitational clustering I. building perturbative expansions," `arXiv:astro-ph/0107015 [astro-ph]`.

[152] P. Valageas, "Dynamics of gravitational clustering. 2. Steepest-descent method for the quasi-linear regime," *Astron. Astrophys.* **382** (2002) 412, `arXiv:astro-ph/0107126 [astro-ph]`.

[153] P. Valageas, "A new approach to gravitational clustering: a path-integral formalism and large-n expansions," *Astron. Astrophys.* **421** (2004) 23–40, `arXiv:astro-ph/0307008 [astro-ph]`.

[154] P. Valageas, "Large-N expansions applied to gravitational clustering," *Astron. Astrophys.* **465** (2007) 725, `arXiv:astro-ph/0611849 [astro-ph]`.

[155] A. Elia, S. Kulkarni, C. Porciani, M. Pietroni, and S. Matarrese, "Modeling the clustering of dark-matter haloes in resummed perturbation theories," *Mon. Not. Roy. Astron. Soc.* **416** (2011) 1703–1716, `arXiv:1012.4833 [astro-ph.CO]`.

[156] M. Pietroni, "Flowing with Time: a New Approach to Nonlinear Cosmological Perturbations," *JCAP* **0810** (2008) 036, `arXiv:0806.0971 [astro-ph]`.

[157] F. Bernardeau and P. Valageas, "Propagators in Lagrangian space," *Phys. Rev.* **D78** (2008) 083503, `arXiv:0805.0805 [astro-ph]`.

[158] S. Anselmi, S. Matarrese, and M. Pietroni, "Next-to-leading resummations in cosmological perturbation theory," *JCAP* **1106** (2011) 015, `arXiv:1011.4477 [astro-ph.CO]`.

[159] F. Bernardeau, N. Van de Rijt, and F. Vernizzi, "Resummed propagators in multi-component cosmic fluids with the eikonal approximation," *Phys. Rev.* **D85** (2012) 063509, `arXiv:1109.3400 [astro-ph.CO]`.

[160] F. Bernardeau, N. Van de Rijt, and F. Vernizzi, "Power spectra in the eikonal approximation with adiabatic and nonadiabatic modes," *Phys. Rev.* **D87** no. 4, (2013) 043530, `arXiv:1209.3662 [astro-ph.CO]`.

[161] X. Wang, M. Neyrinck, I. Szapudi, A. Szalay, X. Chen, J. Lesgourgues, A. Riotto, and M. Sloth, "Perturbation Theory of the Cosmological Log-Density Field," *Astrophys. J.* **735** (2011) 32, `arXiv:1103.2166 [astro-ph.CO]`.

[162] X. Wang and A. Szalay, "Resummed Perturbation Theory of Galaxy Clustering," *Phys. Rev.* **D86** (2012) 043508, `arXiv:1204.0019 [astro-ph.CO]`.

[163] S. Anselmi and M. Pietroni, "Nonlinear Power Spectrum from Resummed Perturbation Theory: a Leap Beyond the BAO Scale," *JCAP* **1212** (2012) 013, `arXiv:1205.2235 [astro-ph.CO]`.

[164] T. Nishimichi *et al.*, "Modeling Nonlinear Evolution of Baryon Acoustic Oscillations: Convergence Regime of N-body Simulations and Analytic Models," *Publ. Astron. Soc. Jap.* **61** (2009) 321, `arXiv:0810.0813 [astro-ph]`.

[165] T. Baldauf, U. Seljak, L. Senatore, and M. Zaldarriaga, "Galaxy Bias and non-Linear Structure Formation in General Relativity," *JCAP* **1110** (2011) 031, `arXiv:1106.5507 [astro-ph.CO]`.

[166] B. D. Sherwin and M. Zaldarriaga, "The Shift of the Baryon Acoustic Oscillation Scale: A Simple Physical Picture," *Phys. Rev.* **D85** (2012) 103523, `arXiv:1202.3998 [astro-ph.CO]`.

[167] M. Peloso and M. Pietroni, "Galilean invariance and the consistency relation for the nonlinear squeezed bispectrum of large scale structure," *JCAP* **1305** (2013) 031, `arXiv:1302.0223 [astro-ph.CO]`.

[168] A. Kehagias and A. Riotto, "Symmetries and Consistency Relations in the Large Scale Structure of the Universe," *Nucl.Phys.* **B873** (2013) 514–529, `arXiv:1302.0130 [astro-ph.CO]`.

[169] P. Creminelli, J. Norea, M. Simonovic, and F. Vernizzi, "Single-Field Consistency Relations of Large Scale Structure," *JCAP* **1312** (2013) 025, `arXiv:1309.3557 [astro-ph.CO]`.

[170] P. Creminelli, J. Gleyzes, M. Simonovic, and F. Vernizzi, "Single-Field Consistency Relations of Large Scale Structure. Part II: Resummation and Redshift Space," *JCAP* **1402** (2014) 051, `arXiv:1311.0290 [astro-ph.CO]`.

[171] P. Creminelli, J. Gleyzes, L. Hui, M. Simonovic, and F. Vernizzi, "Single-Field Consistency Relations of Large Scale Structure. Part III: Test of the Equivalence Principle," *JCAP* **1406** (2014) 009, `arXiv:1312.6074 [astro-ph.CO]`.

[172] F. Schmidt, E. Pajer, and M. Zaldarriaga, "Large-Scale Structure and Gravitational Waves III: Tidal Effects," *Phys. Rev.* **D89** no. 8, (2014) 083507, `arXiv:1312.5616 [astro-ph.CO]`.

[173] P. Valageas, "Angular averaged consistency relations of large-scale structures," *Phys. Rev.* **D89** no. 12, (2014) 123522, `arXiv:1311.4286 [astro-ph.CO]`.

[174] A. Kehagias, H. Perrier, and A. Riotto, "Equal-time Consistency Relations in the Large-Scale Structure of the Universe," *Mod. Phys. Lett.* **A29** (2014) 1450152, `arXiv:1311.5524 [astro-ph.CO]`.

[175] M. Mirbabayi, M. Simonovic, and M. Zaldarriaga, "Baryon Acoustic Peak and the Squeezed Limit Bispectrum," `arXiv:1412.3796 [astro-ph.CO]`.

[176] T. Baldauf, M. Mirbabayi, M. Simonovic, and M. Zaldarriaga, "Equivalence Principle and the Baryon Acoustic Peak," *Phys. Rev.* **D92** no. 4, (2015) 043514, `arXiv:1504.04366 [astro-ph.CO]`.

[177] T. Baldauf, U. Seljak, L. Senatore, and M. Zaldarriaga, "Linear response to long wavelength fluctuations using curvature simulations," `arXiv:1511.01465 [astro-ph.CO]`.

[178] D. Baumann, A. Nicolis, L. Senatore, and M. Zaldarriaga, "Cosmological Non-Linearities as an Effective Fluid," *JCAP* **1207** (2012) 051, `arXiv:1004.2488 [astro-ph.CO]`.

[179] M. P. Hertzberg, "Effective field theory of dark matter and structure formation: Semianalytical results," *Phys. Rev.* **D89** no. 4, (2014) 043521, `arXiv:1208.0839 [astro-ph.CO]`.

[180] E. Pajer and M. Zaldarriaga, "On the Renormalization of the Effective Field Theory of Large Scale Structures," *JCAP* **1308** (2013) 037, `arXiv:1301.7182 [astro-ph.CO]`.

[181] L. Mercolli and E. Pajer, "On the velocity in the Effective Field Theory of Large Scale Structures," *JCAP* **1403** (2014) 006, `arXiv:1307.3220 [astro-ph.CO]`.

[182] J. J. M. Carrasco, S. Foreman, D. Green, and L. Senatore, "The 2-loop matter power spectrum and the IR-safe integrand," *JCAP* **1407** (2014) 056, `arXiv:1304.4946 [astro-ph.CO]`.

[183] J. J. M. Carrasco, S. Foreman, D. Green, and L. Senatore, "The Effective Field Theory of Large Scale Structures at Two Loops," *JCAP* **1407** (2014) 057, `arXiv:1310.0464 [astro-ph.CO]`.

[184] S. M. Carroll, S. Leichenauer, and J. Pollack, "Consistent effective theory of long-wavelength cosmological perturbations," *Phys. Rev.* **D90** no. 2, (2014) 023518, arXiv:1310.2920 [hep-th].

[185] V. Assassi, D. Baumann, D. Green, and M. Zaldarriaga, "Renormalized Halo Bias," *JCAP* **1408** (2014) 056, arXiv:1402.5916 [astro-ph.CO].

[186] R. E. Angulo, S. Foreman, M. Schmittfull, and L. Senatore, "The One-Loop Matter Bispectrum in the Effective Field Theory of Large Scale Structures," arXiv:1406.4143 [astro-ph.CO].

[187] T. Baldauf, L. Mercolli, M. Mirbabayi, and E. Pajer, "The Bispectrum in the Effective Field Theory of Large Scale Structure," *JCAP* **1505** no. 05, (2015) 007, arXiv:1406.4135 [astro-ph.CO].

[188] L. Senatore, "Bias in the Effective Field Theory of Large Scale Structures," *JCAP* **1511** no. 11, (2015) 007, arXiv:1406.7843 [astro-ph.CO].

[189] L. Senatore and M. Zaldarriaga, "The IR-resummed Effective Field Theory of Large Scale Structures," *JCAP* **1502** no. 02, (2015) 013, arXiv:1404.5954 [astro-ph.CO].

[190] L. Senatore and M. Zaldarriaga, "Redshift Space Distortions in the Effective Field Theory of Large Scale Structures," arXiv:1409.1225 [astro-ph.CO].

[191] M. Lewandowski, A. Perko, and L. Senatore, "Analytic Prediction of Baryonic Effects from the EFT of Large Scale Structures," *JCAP* **1505** no. 05, (2015) 019, arXiv:1412.5049 [astro-ph.CO].

[192] M. Mirbabayi, F. Schmidt, and M. Zaldarriaga, "Biased Tracers and Time Evolution," *JCAP* **1507** no. 07, (2015) 030, arXiv:1412.5169 [astro-ph.CO].

[193] M. McQuinn and M. White, "Cosmological perturbation theory in 1+1 dimensions," arXiv:1502.07389 [astro-ph.CO].

[194] S. Foreman and L. Senatore, "The EFT of Large Scale Structures at All Redshifts: Analytical Predictions for Lensing," arXiv:1503.01775 [astro-ph.CO].

[195] V. Assassi, D. Baumann, E. Pajer, Y. Welling, and D. van der Woude, "Effective Theory of Large-Scale Structure with Primordial Non-Gaussianity," arXiv:1505.06668 [astro-ph.CO].

[196] T. Baldauf, E. Schaan, and M. Zaldarriaga, "On the reach of perturbative descriptions for dark matter displacement fields," `arXiv:1505.07098 [astro-ph.CO]`.

[197] Z. Vlah, M. White, and A. Aviles, "A Lagrangian effective field theory," *JCAP* **1509** no. 09, (2015) 014, `arXiv:1506.05264 [astro-ph.CO]`.

[198] T. Baldauf, E. Schaan, and M. Zaldarriaga, "On the reach of perturbative methods for dark matter density fields," `arXiv:1507.02255 [astro-ph.CO]`.

[199] T. Baldauf, L. Mercolli, and M. Zaldarriaga, "The Effective Field Theory of Large Scale Structure at Two Loops: the apparent scale dependence of the speed of sound," `arXiv:1507.02256 [astro-ph.CO]`.

[200] S. Foreman, H. Perrier, and L. Senatore, "Precision Comparison of the Power Spectrum in the EFTofLSS with Simulations," `arXiv:1507.05326 [astro-ph.CO]`.

[201] Z. Vlah, U. Seljak, M. Y. Chu, and Y. Feng, "Perturbation theory, effective field theory, and oscillations in the power spectrum," *JCAP* **1603** no. 03, (2016) 057, `arXiv:1509.02120 [astro-ph.CO]`.

[202] A. A. Abolhasani, M. Mirbabayi, and E. Pajer, "Systematic Renormalization of the Effective Theory of Large Scale Structure," `arXiv:1509.07886 [hep-th]`.

[203] V. Assassi, D. Baumann, and F. Schmidt, "Galaxy Bias and Primordial Non-Gaussianity," *JCAP* **1512** no. 12, (2015) 043, `arXiv:1510.03723 [astro-ph.CO]`.

[204] M. Zaldarriaga and M. Mirbabayi, "Lagrangian Formulation of the Eulerian-EFT," `arXiv:1511.01889 [astro-ph.CO]`.

[205] M. Lewandowski, L. Senatore, F. Prada, C. Zhao, and C.-H. Chuang, "On the EFT of Large Scale Structures in Redshift Space," `arXiv:1512.06831 [astro-ph.CO]`.

[206] D. Bertolini, K. Schutz, M. P. Solon, J. R. Walsh, and K. M. Zurek, "Non-Gaussian Covariance of the Matter Power Spectrum in the Effective Field Theory of Large Scale Structure," `arXiv:1512.07630 [astro-ph.CO]`.

[207] D. Bertolini, K. Schutz, M. P. Solon, and K. M. Zurek, "The Trispectrum in the Effective Field Theory of Large Scale Structure," `arXiv:1604.01770 [astro-ph.CO]`.

[208] R. A. Porto, L. Senatore, and M. Zaldarriaga, "The Lagrangian-space Effective Field Theory of Large Scale Structures," *JCAP* **1405** (2014) 022, `arXiv:1311.2168 [astro-ph.CO]`.

[209] S. Pueblas and R. Scoccimarro, "Generation of Vorticity and Velocity Dispersion by Orbit Crossing," *Phys. Rev.* **D80** (2009) 043504, `arXiv:0809.4606 [astro-ph]`.

[210] T. Nishimichi, F. Bernardeau, and A. Taruya, "Anomalous coupling of the small-scale structures to the large-scale gravitational growth," `arXiv:1411.2970 [astro-ph.CO]`.

[211] M. Pietroni, G. Mangano, N. Saviano, and M. Viel, "Coarse-Grained Cosmological Perturbation Theory," *JCAP* **1201** (2012) 019, `arXiv:1108.5203 [astro-ph.CO]`.

[212] A. Manzotti, M. Peloso, M. Pietroni, M. Viel, and F. Villaescusa-Navarro, "A coarse grained perturbation theory for the Large Scale Structure, with cosmology and time independence in the UV," *JCAP* **1409** no. 09, (2014) 047, `arXiv:1407.1342 [astro-ph.CO]`.

[213] D. Blas, S. Floerchinger, M. Garny, N. Tetradis, and U. A. Wiedemann, "Large scale structure from viscous dark matter," `arXiv:1507.06665 [astro-ph.CO]`.

[214] F. Führer and G. Rigopoulos, "On Renormalizing Viscous Fluids as Models for Large Scale Structure Formation," `arXiv:1509.03073 [astro-ph.CO]`.

[215] D. Blas, M. Garny, M. M. Ivanov, and S. Sibiryakov, "Time-Sliced Perturbation Theory for Large Scale Structure I: General Formalism," `arXiv:1512.05807 [astro-ph.CO]`.

[216] D. Blas, M. Garny, M. M. Ivanov, and S. Sibiryakov, "Time-Sliced Perturbation Theory II: Baryon Acoustic Oscillations and Infrared Resummation," `arXiv:1605.02149 [astro-ph.CO]`.

[217] P. Creminelli and M. Zaldarriaga, "Single field consistency relation for the 3-point function," *JCAP* **0410** (2004) 006, `arXiv:astro-ph/0407059 [astro-ph]`.

[218] C. Cheung, A. L. Fitzpatrick, J. Kaplan, and L. Senatore, "On the consistency relation of the 3-point function in single field inflation," *JCAP* **0802** (2008) 021, `arXiv:0709.0295 [hep-th]`.

[219] P. Creminelli, J. Norena, and M. Simonovic, "Conformal consistency relations for single-field inflation," *JCAP* **1207** (2012) 052, `arXiv:1203.4595 [hep-th]`.

[220] L. Senatore and M. Zaldarriaga, "A Note on the Consistency Condition of Primordial Fluctuations," *JCAP* **1208** (2012) 001, `arXiv:1203.6884 [astro-ph.CO]`.

[221] K. Hinterbichler, L. Hui, and J. Khoury, "Conformal Symmetries of Adiabatic Modes in Cosmology," *JCAP* **1208** (2012) 017, `arXiv:1203.6351 [hep-th]`.

[222] V. Assassi, D. Baumann, and D. Green, "On Soft Limits of Inflationary Correlation Functions," *JCAP* **1211** (2012) 047, `arXiv:1204.4207 [hep-th]`.

[223] W. D. Goldberger, L. Hui, and A. Nicolis, "One-particle-irreducible consistency relations for cosmological perturbations," *Phys. Rev.* **D87** no. 10, (2013) 103520, `arXiv:1303.1193 [hep-th]`.

[224] P. Creminelli, A. Perko, L. Senatore, M. Simonovic, and G. Trevisan, "The Physical Squeezed Limit: Consistency Relations at Order q^2," *JCAP* **1311** (2013) 015, `arXiv:1307.0503 [astro-ph.CO]`.

[225] K. Hinterbichler, L. Hui, and J. Khoury, "An Infinite Set of Ward Identities for Adiabatic Modes in Cosmology," *JCAP* **1401** (2014) 039, `arXiv:1304.5527 [hep-th]`.

[226] A. Joyce, J. Khoury, and M. Simonovic, "Multiple Soft Limits of Cosmological Correlation Functions," *JCAP* **1501** no. 01, (2015) 012, `arXiv:1409.6318 [hep-th]`.

[227] S. Mooij, G. A. Palma, G. Panotopoulos, and A. Soto, "Consistency relations for sharp inflationary non-Gaussian features," `arXiv:1604.03533 [astro-ph.CO]`.

[228] M. Peloso and M. Pietroni, "Ward identities and consistency relations for the large scale structure with multiple species," *JCAP* **1404** (2014) 011, `arXiv:1310.7915 [astro-ph.CO]`.

[229] A. Kehagias, J. Norea, H. Perrier, and A. Riotto, "Consequences of Symmetries and Consistency Relations in the Large-Scale Structure of the Universe for Non-local bias and Modified Gravity," *Nucl. Phys.* **B883** (2014) 83–106, `arXiv:1311.0786 [astro-ph.CO]`.

[230] P. Valageas, "Kinematic consistency relations of large-scale structures," *Phys. Rev.* **D89** no. 8, (2014) 083534, `arXiv:1311.1236 [astro-ph.CO]`.

[231] T. Nishimichi and P. Valageas, "Testing the equal-time angular-averaged consistency relation of the gravitational dynamics in N-body simulations," *Phys. Rev.* **D90** no. 2, (2014) 023546, `arXiv:1402.3293 [astro-ph.CO]`.

[232] B. Horn, L. Hui, and X. Xiao, "Soft-Pion Theorems for Large Scale Structure," *JCAP* **1409** no. 09, (2014) 044, `arXiv:1406.0842 [hep-th]`.

[233] B. Horn, L. Hui, and X. Xiao, "Lagrangian space consistency relation for large scale structure," *JCAP* **1509** no. 09, (2015) 068, `arXiv:1502.06980 [hep-th]`.

[234] T. Nishimichi and P. Valageas, "Redshift-space equal-time angular-averaged consistency relations of the gravitational dynamics," *Phys. Rev.* **D92** no. 12, (2015) 123510, `arXiv:1503.06036 [astro-ph.CO]`.

[235] J. M. Maldacena and G. L. Pimentel, "On graviton non-Gaussianities during inflation," *JHEP* **09** (2011) 045, `arXiv:1104.2846 [hep-th]`.

[236] R. Scoccimarro, "A new angle on gravitational clustering," *Annals N.Y.Acad.Sci.* **927** (2001) 13, `arXiv:astro-ph/0008277 [astro-ph]`.

[237] B. Jain and E. Bertschinger, "Selfsimilar evolution of cosmological density fluctuations," *Astrophys. J.* **456** (1996) 43, `arXiv:astro-ph/9503025 [astro-ph]`.

[238] C.-T. Chiang, C. Wagner, F. Schmidt, and E. Komatsu, "Position-dependent power spectrum of the large-scale structure: a novel method to measure the squeezed-limit bispectrum," *JCAP* **1405** (2014) 048, `arXiv:1403.3411 [astro-ph.CO]`.

[239] Y. Li, W. Hu, and M. Takada, "Super-Sample Covariance in Simulations," *Phys. Rev.* **D89** no. 8, (2014) 083519, `arXiv:1401.0385 [astro-ph.CO]`.

[240] C. Wagner, F. Schmidt, C.-T. Chiang, and E. Komatsu, "Separate Universe Simulations," *Mon. Not. Roy. Astron. Soc.* **448** no. 1, (2015) L11–L15, `arXiv:1409.6294 [astro-ph.CO]`.

[241] L. Dai, E. Pajer, and F. Schmidt, "On Separate Universes," *JCAP* **1510** no. 10, (2015) 059, `arXiv:1504.00351 [astro-ph.CO]`.

[242] E. P. Hubble, *The observational approach to cosmology*. Clarendon Press Oxford, 1937.

[243] A. R. Liddle and D. H. Lyth, *Cosmological inflation and large scale structure*. 2000.

[244] P. Coles and P. Lucchin, *Cosmology: The Origin and Evolution of Cosmic Structure*. Wiley, 2003.

[245] P. Schneider, *Extragalactic Astronomy and Cosmology: An Introduction*. Springer Berlin Heidelberg, 2014.

[246] A. Cohen, *Numerical Methods for Laplace Transform Inversion*. Numerical Methods and Algorithms. Springer US, 2007.

Bibliography

[247] Homepage of the 2dF Galaxy Redshift Survey, "Galaxy distribution map,".
http://www.2dfgrs.net/.

[248] J. R. G. III, M. Juri, D. Schlegel, F. Hoyle, M. Vogeley, M. Tegmark, N. Bahcall, and
J. Brinkmann, "A map of the universe," *The Astrophysical Journal* **624** no. 2, (2005)
463. http://stacks.iop.org/0004-637X/624/i=2/a=463.

[249] J. A. Peacock *et al.*, "A Measurement of the cosmological mass density from clustering
in the 2dF Galaxy Redshift Survey," *Nature* **410** (2001) 169–173,
arXiv:astro-ph/0103143 [astro-ph].

[250] G. Lemaitre, "The Expanding Universe," *Mon. Not. Roy. Astron. Soc.* **91** (1931)
490–501.

[251] G. Lemaitre, "Evolution of the Expanding Universe," *Proceedings of the National
Academy of Sciences* **20** no. 1, (1934) 12–17.

[252] P. J. E. Peebles, "Large scale background temperature and mass fluctuations due to
scale invariant primeval perturbations," *Astrophys. J.* **263** (1982) L1–L5.

[253] G. R. Blumenthal, S. M. Faber, J. R. Primack, and M. J. Rees, "Formation of Galaxies
and Large Scale Structure with Cold Dark Matter," *Nature* **311** (1984) 517–525.

[254] M. Davis, G. Efstathiou, C. S. Frenk, and S. D. M. White, "The Evolution of Large
Scale Structure in a Universe Dominated by Cold Dark Matter," *Astrophys. J.* **292**
(1985) 371–394.

[255] M. Davis, G. Efstathiou, C. Frenk, and S. White, "The end of cold dark matter?,"
Nature **356** no. 6369, (1992) 489–494.

[256] V. Mukhanov, *Physical Foundations of Cosmology*. Cambridge University Press,
Oxford, 2005.

[257] E. W. Kolb and M. S. Turner, "The Early Universe," *Front. Phys.* **69** (1990) 1–547.

[258] M. J. Benacquista, "Relativistic binaries in globular clusters," *Living Rev. Rel.* **5**
(2002) 2, arXiv:astro-ph/0202056 [astro-ph].

[259] J. Binney, "Discreteness effects in cosmological N-body simulations," *Mon. Not. Roy.
Astron. Soc.* **350** (2004) 939, arXiv:astro-ph/0311155 [astro-ph].

[260] B. Marcos, "Vlasov limit and discreteness effects in cosmological N-body simulations," *Commun. Nonlinear Sci. Numer. Simul.* **13** (2008) 119, `arXiv:0805.1500 [cond-mat.stat-mech]`.

[261] G. Bertone, D. Hooper, and J. Silk, "Particle dark matter: Evidence, candidates and constraints," *Phys. Rept.* **405** (2005) 279–390, `arXiv:hep-ph/0404175 [hep-ph]`.

[262] E. A. Baltz, "Dark matter candidates," *eConf* **C040802** (2004) L002, `arXiv:astro-ph/0412170 [astro-ph]`.

[263] D. S. Gorbunov and V. A. Rubakov, *Introduction to the theory of the early universe: Hot big bang theory.* World Scientific, Hackensack, 2011.

[264] M. Kunz, S. Nesseris, and I. Sawicki, "Constraints on dark-matter properties from large-scale structure," `arXiv:1604.05701 [astro-ph.CO]`.

[265] J. Sommer-Larsen and A. Dolgov, "Formation of disk galaxies: warm dark matter and the angular momentum problem," *Astrophys. J.* **551** (2001) 608–623, `arXiv:astro-ph/9912166 [astro-ph]`.

[266] P. Bode, J. P. Ostriker, and N. Turok, "Halo formation in warm dark matter models," *Astrophys. J.* **556** (2001) 93–107, `arXiv:astro-ph/0010389 [astro-ph]`.

[267] J. J. Mohr, A. E. Evrard, D. G. Fabricant, and M. J. Geller, "Cosmological constraints from cluster x-ray morphologies," *Astrophys. J.* **447** (1995) 8, `arXiv:astro-ph/9501011 [astro-ph]`.

[268] D. N. Spergel and P. J. Steinhardt, "Observational evidence for selfinteracting cold dark matter," *Phys. Rev. Lett.* **84** (2000) 3760–3763, `arXiv:astro-ph/9909386 [astro-ph]`.

[269] B. D. Wandelt, R. Dave, G. R. Farrar, P. C. McGuire, D. N. Spergel, and P. J. Steinhardt, "Selfinteracting dark matter," in *Sources and detection of dark matter and dark energy in the universe. Proceedings, 4th International Symposium, DM 2000, Marina del Rey, USA, February 23-25, 2000*, pp. 263–274. 2000. `arXiv:astro-ph/0006344 [astro-ph]`.

[270] D. Alonso, P. Bull, P. G. Ferreira, R. Maartens, and M. G. Santos, "Ultra-large scale cosmology with next-generation experiments," `arXiv:1505.07596 [astro-ph.CO]`.

[271] J. M. Bardeen, "Gauge Invariant Cosmological Perturbations," *Phys. Rev.* **D22** (1980) 1882–1905.

[272] V. F. Mukhanov, H. A. Feldman, and R. H. Brandenberger, "Theory of cosmological perturbations," *Phys. Rept.* **215** (1992) 203–333.

[273] S. J. Lilly, O. Le Fevre, D. Crampton, F. Hammer, and L. Tresse, "The Canada-France redshift survey. 1. Introduction to the survey, photometric catalogs and surface brightness selection effects," *Astrophys. J.* **455** (1995) 50, arXiv:astro-ph/9507010 [astro-ph].

[274] C. Bonvin, R. Durrer, and M. A. Gasparini, "Fluctuations of the luminosity distance," *Phys. Rev.* **D73** (2006) 023523, arXiv:astro-ph/0511183 [astro-ph]. [Erratum: Phys. Rev.D85,029901(2012)].

[275] J. Yoo, A. L. Fitzpatrick, and M. Zaldarriaga, "A New Perspective on Galaxy Clustering as a Cosmological Probe: General Relativistic Effects," *Phys. Rev.* **D80** (2009) 083514, arXiv:0907.0707 [astro-ph.CO].

[276] J. Yoo, "General Relativistic Description of the Observed Galaxy Power Spectrum: Do We Understand What We Measure?," *Phys. Rev.* **D82** (2010) 083508, arXiv:1009.3021 [astro-ph.CO].

[277] N. E. Chisari and M. Zaldarriaga, "Connection between Newtonian simulations and general relativity," *Phys. Rev.* **D83** (2011) 123505, arXiv:1101.3555 [astro-ph.CO]. [Erratum: Phys. Rev.D84,089901(2011)].

[278] C. Bonvin and R. Durrer, "What galaxy surveys really measure," *Phys. Rev.* **D84** (2011) 063505, arXiv:1105.5280 [astro-ph.CO].

[279] A. Challinor and A. Lewis, "The linear power spectrum of observed source number counts," *Phys. Rev.* **D84** (2011) 043516, arXiv:1105.5292 [astro-ph.CO].

[280] H. Mo, F. van den Bosch, and S. White, *Galaxy Formation and Evolution*. Galaxy Formation and Evolution. Cambridge University Press, 2010.

[281] S. M. Carroll, W. H. Press, and E. L. Turner, "The Cosmological constant," *Ann. Rev. Astron. Astrophys.* **30** (1992) 499–542.

[282] F. R. Bouchet, "Introductory overview of Eulerian and Lagrangian perturbation theories," in *Dark matter in the universe. Proceedings, 132nd course of the International School of Physics *Enrico Fermi*, Varenna, Italy, July 25-August 4, 1995*. 1995. arXiv:astro-ph/9603013 [astro-ph].

[283] M. Hénon, "Vlasov equation," *Astronomy and Astrophysics* **114** (1982) 211.

[284] C.-P. Ma and E. Bertschinger, "Cosmological perturbation theory in the synchronous and conformal Newtonian gauges," *Astrophys. J.* **455** (1995) 7–25, `arXiv:astro-ph/9506072 [astro-ph]`.

[285] E. Toro, *Riemann Solvers and Numerical Methods for Fluid Dynamics: A Practical Introduction.* Springer Berlin Heidelberg, 2009.

[286] L. Landau and E. Lifshitz, *Fluid Mechanics.* Course of Theoretical Physics. Pergamon Press, 1959.

[287] C. Pichon and F. Bernardeau, "Vorticity generation in large scale structure caustics," *Astron. Astrophys.* **343** (1999) 663, `arXiv:astro-ph/9902142 [astro-ph]`.

[288] W. Panofsky and M. Phillips, *Classical Electricity and Magnetism: Second Edition.* Dover Books on Physics. Dover Publications, 2012.

[289] D. J. Heath, "The growth of density perturbations in zero pressure Friedmann-Lemaitre universes," *Monthly Notices of the Royal Astronomical Society* **179** (May, 1977) 351–358.

[290] O. Lahav, P. B. Lilje, J. R. Primack, and M. J. Rees, "Dynamical effects of the cosmological constant," *Mon. Not. Roy. Astron. Soc.* **251** (1991) 128–136.

[291] A. P. Lightman and P. L. Schechter, "The Omega dependence of peculiar velocities induced by spherical density perturbations," *The Astrophysical Journal Supplement Series* **74** (Dec., 1990) 831.

[292] W. J. Percival and M. White, "Testing cosmological structure formation using redshift-space distortions," *Mon. Not. Roy. Astron. Soc.* **393** (2009) 297, `arXiv:0808.0003 [astro-ph]`.

[293] M. B. Wise, "Non-Gaussian Fluctuations," *NATO Sci. Ser. C.* **219** (1988) 215–238.

[294] A. Lazanu, T. Giannantonio, M. Schmittfull, and E. P. S. Shellard, "The matter bispectrum of large-scale structure: three-dimensional comparison between theoretical models and numerical simulations," `arXiv:1510.04075 [astro-ph.CO]`.

[295] F. R. Bouchet, R. Juszkiewicz, S. Colombi, and R. Pellat, "Weakly nonlinear gravitational instability for arbitrary Omega," *Astrophys. J.* **394** (1992) L5–L8.

Bibliography

[296] F. Bernardeau, "Skewness and Kurtosis in large scale cosmic fields," *Astrophys. J.* **433** (1994) 1, `arXiv:astro-ph/9312026 [astro-ph]`.

[297] P. Catelan, F. Lucchin, S. Matarrese, and L. Moscardini, "Eulerian perturbation theory in nonflat universes: Second order approximation," *Mon. Not. Roy. Astron. Soc.* **276** (1995) 39, `arXiv:astro-ph/9411066 [astro-ph]`.

[298] R. Scoccimarro, S. Colombi, J. N. Fry, J. A. Frieman, E. Hivon, and A. Melott, "Nonlinear evolution of the bispectrum of cosmological perturbations," *Astrophys. J.* **496** (1998) 586, `arXiv:astro-ph/9704075 [astro-ph]`.

[299] H. Martel and W. Freudling, "Second-order perturbation theory in Omega is not equal to Friedmann models," *Astrophysical Journal* **371** (Apr., 1991) 1–7.

[300] R. Scoccimarro, "Transients from initial conditions: a perturbative analysis," *Mon. Not. Roy. Astron. Soc.* **299** (1998) 1097, `arXiv:astro-ph/9711187 [astro-ph]`.

[301] J. Lesgourgues, S. Matarrese, M. Pietroni, and A. Riotto, "Non-linear Power Spectrum including Massive Neutrinos: the Time-RG Flow Approach," *JCAP* **0906** (2009) 017, `arXiv:0901.4550 [astro-ph.CO]`.

[302] A. Upadhye, R. Biswas, A. Pope, K. Heitmann, S. Habib, H. Finkel, and N. Frontiere, "Large-Scale Structure Formation with Massive Neutrinos and Dynamical Dark Energy," *Phys. Rev.* **D89** no. 10, (2014) 103515, `arXiv:1309.5872 [astro-ph.CO]`.

[303] D. Blas, M. Garny, T. Konstandin, and J. Lesgourgues, "Structure formation with massive neutrinos: going beyond linear theory," *JCAP* **1411** no. 11, (2014) 039, `arXiv:1408.2995 [astro-ph.CO]`.

[304] S. Matarrese and M. Pietroni, "Baryonic Acoustic Oscillations via the Renormalization Group," *Mod. Phys. Lett.* **A23** (2008) 25–32, `arXiv:astro-ph/0702653 [ASTRO-PH]`.

[305] J. N. Fry, "The Minimal power spectrum: Higher order contributions," *Astrophys. J.* **421** (1994) 21–26.

[306] R. Scoccimarro and J. Frieman, "Loop corrections in nonlinear cosmological perturbation theory," *Astrophys. J. Suppl.* **105** (1996) 37, `arXiv:astro-ph/9509047 [astro-ph]`.

[307] H. W. Jr., "Formulation of the theory of turbulence in an incompressible fluid," *Annals of Physics* **14** (1961) 143 – 165.

[308] P. C. Martin, E. D. Siggia, and H. A. Rose, "Statistical dynamics of classical systems," *Phys. Rev. A* **8** (Jul, 1973) 423–437.

[309] A. Linde, "Inflationary Cosmology after Planck 2013," in *100e Ecole d'Ete de Physique: Post-Planck Cosmology Les Houches, France, July 8-August 2, 2013*, pp. 231–316. 2015. `arXiv:1402.0526 [hep-th]`.

[310] A. D. Linde, "Particle physics and inflationary cosmology," *Contemp. Concepts Phys.* **5** (1990) 1–362, `arXiv:hep-th/0503203 [hep-th]`.

[311] D. H. Lyth and A. Riotto, "Particle physics models of inflation and the cosmological density perturbation," *Phys. Rept.* **314** (1999) 1–146, `arXiv:hep-ph/9807278 [hep-ph]`.

[312] A. J. S. Hamilton, "Linear redshift distortions: A Review," in *Ringberg Workshop on Large Scale Structure Ringberg, Germany, September 23-28, 1996*. 1997. `arXiv:astro-ph/9708102 [astro-ph]`.

[313] P. J. E. Peebles and J. T. Yu, "Primeval adiabatic perturbation in an expanding universe," *Astrophys. J.* **162** (1970) 815–836.

[314] J. R. Bond and G. Efstathiou, "Cosmic background radiation anisotropies in universes dominated by nonbaryonic dark matter," *Astrophys. J.* **285** (1984) L45–L48.

[315] U. Seljak and M. Zaldarriaga, "A Line of sight integration approach to cosmic microwave background anisotropies," *Astrophys. J.* **469** (1996) 437–444, `arXiv:astro-ph/9603033 [astro-ph]`.

[316] W. Hu and N. Sugiyama, "Anisotropies in the cosmic microwave background: An Analytic approach," *Astrophys. J.* **444** (1995) 489–506, `arXiv:astro-ph/9407093 [astro-ph]`.

[317] W. Hu and N. Sugiyama, "Small scale cosmological perturbations: An Analytic approach," *Astrophys. J.* **471** (1996) 542–570, `arXiv:astro-ph/9510117 [astro-ph]`.

[318] J. M. Bardeen, J. R. Bond, N. Kaiser, and A. S. Szalay, "The Statistics of Peaks of Gaussian Random Fields," *Astrophys. J.* **304** (1986) 15–61.

[319] J. Peacock, A. Heavens, and A. Davies, *Physics of the Early Universe: Proceedings of the Thirty Sixth Scottish Universities Summer School in Physics, Edinburgh, July 24 - August 11 1989*. Scottish Graduate Series. Taylor & Francis, 1990.

Bibliography

[320] G. C. Wick, "The Evaluation of the Collision Matrix," *Phys. Rev.* **80** (1950) 268–272.

[321] R. Juszkiewicz, D. H. Sonoda, and J. D. Barrow, "Non-linear gravitational clustering," *Mon. Not. Roy. Astron. Soc.* **209** no. 2, (1984) 139–144.

[322] P. Coles, "Second-order evolution of cold dark matter perturbations," *Mon. Not. Roy. Astron. Soc.* **243** (1990) 171–176.

[323] Y. Suto and M. Sasaki, "Quasinonlinear theory of cosmological self-gravitating systems," *Phys. Rev. Lett.* **66** (Jan, 1991) 264–267.

[324] C. M. Baugh and G. Efstathiou, "A comparison of the evolution of density fields in perturbation theory and numerical simulations i. non-linear evolution of the power spectrum," *Monthly Notices of the Royal Astronomical Society* **270** no. 1, (1994) 183–198.

[325] E. L. Lokas, R. Juszkiewicz, F. R. Bouchet, and E. Hivon, "Previrialization: perturbative and n-body results," *Astrophys. J.* **467** (1996) 1, `arXiv:astro-ph/9508032 [astro-ph]`.

[326] T. Nishimichi, H. Ohmuro, M. Nakamichi, A. Taruya, K. Yahata, A. Shirata, S. Saito, H. Nomura, K. Yamamoto, and Y. Suto, "Characteristic Scales of Baryon Acoustic Oscillations from Perturbation Theory: Non-linearity and Redshift-Space Distortion Effects," *Publ. Astron. Soc. Jap.* **59** (2007) 1049, `arXiv:0705.1589 [astro-ph]`.

[327] H. M. Crocce, *Renormalized cosmological perturbation theory.* PhD thesis, New York University, 2007.

[328] R. Scoccimarro, "Cosmological perturbations: Entering the nonlinear regime," *Astrophys. J.* **487** (1997) 1, `arXiv:astro-ph/9612207 [astro-ph]`.

[329] R. Scoccimarro, "Redshift-space distortions, pairwise velocities and nonlinearities," *Phys. Rev.* **D70** (2004) 083007, `arXiv:astro-ph/0407214 [astro-ph]`.

[330] A. Lewis, A. Challinor, and A. Lasenby, "Efficient computation of CMB anisotropies in closed FRW models," *Astrophys. J.* **538** (2000) 473–476, `arXiv:astro-ph/9911177 [astro-ph]`.

[331] **WMAP** Collaboration, E. Komatsu *et al.*, "Five-Year Wilkinson Microwave Anisotropy Probe (WMAP) Observations: Cosmological Interpretation," *Astrophys. J. Suppl.* **180** (2009) 330–376, `arXiv:0803.0547 [astro-ph]`.

[332] C. M. Bender and S. A. Orszag, "Advanced mathematical methods for scientists and engineers. 1978," *McGrew–Hill, New York* .

[333] D. J. Eisenstein, "Dark energy and cosmic sound [review article]," *New Astronomy Reviews* **49** (Nov., 2005) 360–365.

[334] D. J. Eisenstein, H.-j. Seo, and M. J. White, "On the Robustness of the Acoustic Scale in the Low-Redshift Clustering of Matter," *Astrophys. J.* **664** (2007) 660–674, `arXiv:astro-ph/0604361 [astro-ph]`.

[335] D. H. Weinberg, M. J. Mortonson, D. J. Eisenstein, C. Hirata, A. G. Riess, and E. Rozo, "Observational Probes of Cosmic Acceleration," *Phys. Rept.* **530** (2013) 87–255, `arXiv:1201.2434 [astro-ph.CO]`.

[336] R. Scoccimarro and J. Frieman, "Loop corrections in nonlinear cosmological perturbation theory 2. Two point statistics and selfsimilarity," *Astrophys. J.* **473** (1996) 620, `arXiv:astro-ph/9602070 [astro-ph]`.

[337] F. Bernardeau, M. Crocce, and R. Scoccimarro, "Constructing Regularized Cosmic Propagators," *Phys. Rev.* **D85** (2012) 123519, `arXiv:1112.3895 [astro-ph.CO]`.

[338] F. Bernardeau, A. Taruya, and T. Nishimichi, "Cosmic propagators at two-loop order," *Phys. Rev.* **D89** no. 2, (2014) 023502, `arXiv:1211.1571 [astro-ph.CO]`.

[339] F. Bernardeau, M. Crocce, and R. Scoccimarro, "Multi-Point Propagators in Cosmological Gravitational Instability," *Phys. Rev.* **D78** (2008) 103521, `arXiv:0806.2334 [astro-ph]`.

[340] F. Bernardeau, M. Crocce, and E. Sefusatti, "Multi-Point Propagators for Non-Gaussian Initial Conditions," *Phys. Rev.* **D82** (2010) 083507, `arXiv:1006.4656 [astro-ph.CO]`.

[341] M. Born, "Quantenmechanik der Stoßvorgänge," *Zeitschrift fur Physik* **38** (Nov., 1926) 803–827.

[342] J. Polchinski, "Renormalization and Effective Lagrangians," *Nucl. Phys.* **B231** (1984) 269–295.

[343] M. Bonini, M. D'Attanasio, and G. Marchesini, "Perturbative renormalization and infrared finiteness in the Wilson renormalization group: The Massless scalar case," *Nucl. Phys.* **B409** (1993) 441–464, `arXiv:hep-th/9301114 [hep-th]`.

Bibliography

[344] T. R. Morris, "The Exact renormalization group and approximate solutions," *Int. J. Mod. Phys.* **A9** (1994) 2411–2450, `arXiv:hep-ph/9308265 [hep-ph]`.

[345] M. D'Attanasio and M. Pietroni, "Wilson renormalization group formulation of real time thermal field theories," *Nucl. Phys.* **B472** (1996) 711–737, `arXiv:hep-ph/9601375 [hep-ph]`.

[346] J. Berges, N. Tetradis, and C. Wetterich, "Nonperturbative renormalization flow in quantum field theory and statistical physics," *Phys. Rept.* **363** (2002) 223–386, `arXiv:hep-ph/0005122 [hep-ph]`.

[347] N. Bartolo, J. P. B. Almeida, S. Matarrese, M. Pietroni, and A. Riotto, "Signatures of Primordial non-Gaussianities in the Matter Power-Spectrum and Bispectrum: the Time-RG Approach," *JCAP* **1003** (2010) 011, `arXiv:0912.4276 [astro-ph.CO]`.

[348] B. Audren and J. Lesgourgues, "Non-linear matter power spectrum from Time Renormalisation Group: efficient computation and comparison with one-loop," *JCAP* **1110** (2011) 037, `arXiv:1106.2607 [astro-ph.CO]`.

[349] G. Juergens and M. Bartelmann, "Perturbation Theory Trispectrum in the Time Renormalisation Approach," `arXiv:1204.6524 [astro-ph.CO]`.

[350] A. Vollmer, L. Amendola, and R. Catena, "Efficient implementation of the Time Renormalization Group," *Phys. Rev.* **D93** no. 4, (2016) 043526, `arXiv:1412.1650 [astro-ph.CO]`.

[351] P. Valageas, T. Nishimichi, and A. Taruya, "Matter power spectrum from a Lagrangian-space regularization of perturbation theory," *Phys. Rev.* **D87** (2013) 083522, `arXiv:1302.4533 [astro-ph.CO]`.

[352] D. J. Eisenstein and W. Hu, "Baryonic features in the matter transfer function," *Astrophys. J.* **496** (1998) 605, `arXiv:astro-ph/9709112 [astro-ph]`.

[353] F. J. Dyson, "The S matrix in quantum electrodynamics," *Phys. Rev.* **75** (1949) 1736–1755.

[354] N. S. Sugiyama and T. Futamase, "Relation between standard perturbation theory and regularized multi-point propagator method," *Astrophys. J.* **769** (2013) 106, `arXiv:1303.2748 [astro-ph.CO]`.

[355] P. Valageas, "Expansion schemes for gravitational clustering: computing two-point and three-point functions," *Astron. Astrophys.* **484** (2008) 79, `arXiv:0711.3407 [astro-ph]`.

[356] H. D. I. Abarbanel and C. Itzykson, "Relativistic eikonal expansion," *Phys. Rev. Lett.* **23** (1969) 53.

[357] M. Levy and J. Sucher, "Eikonal approximation in quantum field theory," *Phys. Rev.* **186** (1969) 1656–1670.

[358] H. Bruns, *Das Eikonal.* No. Bd. 21,Nr. 5 in Abhandlungen der Königlich-Sächsischen Gesellschaft der Wissenschaften. S. Hirzel, 1895.

[359] L. Evans, *Partial Differential Equations.* Graduate studies in mathematics. American Mathematical Society, 2010.

[360] D. Tseliakhovich and C. Hirata, "Relative velocity of dark matter and baryonic fluids and the formation of the first structures," *Phys. Rev.* **D82** (2010) 083520, `arXiv:1005.2416 [astro-ph.CO]`.

[361] S. Ma, *Statistical Mechanics.* World Scientific, 1985.

[362] N. Bogoliubov, "Problems of a dynamical theory in statistical physics [in russian], gostekhizdat, moscow (1946)," *English transl., North-Holland, Amsterdam* (1962) .

[363] J. Lesgourgues and S. Pastor, "Massive neutrinos and cosmology," *Phys. Rept.* **429** (2006) 307–379, `arXiv:astro-ph/0603494 [astro-ph]`.

[364] S. Saito, M. Takada, and A. Taruya, "Impact of massive neutrinos on nonlinear matter power spectrum," *Phys. Rev. Lett.* **100** (2008) 191301, `arXiv:0801.0607 [astro-ph]`.

[365] Y. Y. Y. Wong, "Higher order corrections to the large scale matter power spectrum in the presence of massive neutrinos," *JCAP* **0810** (2008) 035, `arXiv:0809.0693 [astro-ph]`.

[366] S. Matarrese, M. Pietroni, and C. Schimd, "Nonlinear gravitational clustering in scalar field cosmologies," *JCAP* **0308** (2003) 005, `arXiv:astro-ph/0305224 [astro-ph]`.

[367] E. Fermi, "Sopra i fenomeni che avvengono in vicinanza di una linea oraria," *Atti R. Accad. Lincei Rend, Cl. Fis. Mat. Nat* **31** (1922) 101–3.

[368] F. K. Manasse and C. W. Misner, "Fermi normal coordinates and some basic concepts in differential geometry," *Journal of Mathematical Physics* **4** no. 6, (1963) 735–745.

[369] L. Dai, E. Pajer, and F. Schmidt, "Conformal Fermi Coordinates," `arXiv:1502.02011 [gr-qc]`.

[370] W. D. Goldberger and I. Z. Rothstein, "An Effective field theory of gravity for extended objects," *Phys. Rev.* **D73** (2006) 104029, `arXiv:hep-th/0409156 [hep-th]`.

[371] K. G. Wilson, "Nonlagrangian models of current algebra," *Phys. Rev.* **179** (1969) 1499–1512.

[372] P. Breitenlohner and D. Maison, "Dimensional Renormalization and the Action Principle," *Commun. Math. Phys.* **52** (1977) 11–38.

[373] W. Zimmermann, "Local operator products and renormalization in quantum field theory, lectures on elementary particles and quantum field theory," 1970.

[374] W. Zimmermann, "Normal products and the short distance expansion in the perturbation theory of renormalizable interactions," *Annals Phys.* **77** (1973) 570–601.

[375] S. Pokorski, *Gauge Field Theories*. Cambridge Monographs on Mathematical Physics. Cambridge University Press, 2000.

[376] M. D. Schwartz, *Quantum Field Theory and the Standard Model*. Cambridge University Press, 2014.

[377] R. Courant and D. Hilbert, *Methods of Mathematical Physics*. No. Bd. 1 in Methods of Mathematical Physics. Wiley, 2008.

[378] O. Hahn, R. E. Angulo, and T. Abel, "The Properties of Cosmic Velocity Fields," *Mon. Not. Roy. Astron. Soc.* **454** (2015) 3920, `arXiv:1404.2280 [astro-ph.CO]`.

[379] **WMAP** Collaboration, E. Komatsu *et al.*, "Seven-Year Wilkinson Microwave Anisotropy Probe (WMAP) Observations: Cosmological Interpretation," *Astrophys. J. Suppl.* **192** (2011) 18, `arXiv:1001.4538 [astro-ph.CO]`.

[380] C. Wagner, F. Schmidt, C.-T. Chiang, and E. Komatsu, "The angle-averaged squeezed limit of nonlinear matter N-point functions," *JCAP* **1508** no. 08, (2015) 042, `arXiv:1503.03487 [astro-ph.CO]`.

[381] U. Seljak, "Analytic model for galaxy and dark matter clustering," *Mon. Not. Roy. Astron. Soc.* **318** (2000) 203, `arXiv:astro-ph/0001493 [astro-ph]`.

[382] C.-P. Ma and J. N. Fry, "Deriving the nonlinear cosmological power spectrum and bispectrum from analytic dark matter halo profiles and mass functions," *Astrophys. J.* **543** (2000) 503–513, arXiv:astro-ph/0003343 [astro-ph].

[383] J. A. Peacock and R. E. Smith, "Halo occupation numbers and galaxy bias," *Mon. Not. Roy. Astron. Soc.* **318** (2000) 1144, arXiv:astro-ph/0005010 [astro-ph].

[384] A. Cooray and R. K. Sheth, "Halo models of large scale structure," *Phys. Rept.* **372** (2002) 1–129, arXiv:astro-ph/0206508 [astro-ph].

[385] R. E. Smith, J. A. Peacock, A. Jenkins, S. D. M. White, C. S. Frenk, F. R. Pearce, P. A. Thomas, G. Efstathiou, and H. M. P. Couchman, "Stable clustering, the halo model and non-linear cosmological power spectra," *Monthly Notices of the Royal Astronomical Society* **341** no. 4, (2003) 1311–1332.

[386] R. Takahashi, M. Sato, T. Nishimichi, A. Taruya, and M. Oguri, "Revising the Halofit Model for the Nonlinear Matter Power Spectrum," *Astrophys. J.* **761** (2012) 152, arXiv:1208.2701 [astro-ph.CO].

[387] C. J. Hogan, N. Kaiser, M. J. Rees, R. Fabbri and W. H. McCrea, "Interpretation of Anisotropy in the Cosmic Background Radiation," *Phil. Trans. R. Soc. Lond. A* **307** (1982) 97–110.

Acknowledgments

First of all, I would like to express my sincere appreciation and gratitude to my supervisor Thomas Konstandin. I am very grateful to him not only for giving me the possibility to work on the highly interesting topic of large-scale structure formation during my time as a PhD student, but also for being such a great, motivating and encouraging advisor! Thank you, Thomas, for many hours of discussions and comparing calculations, for always taking the time to give good advice, for the patient guidance as well as for the continuous support.

In addition, I would like to thank Günter Sigl who kindly agreed to act as second referee of my dissertation, and Dieter Horns, Kai Schmidt-Hoberg as well as Géraldine Servant for being the referees in the examination committee for my disputation. Furthermore, I am particularly grateful to Ido Ben-Dayan, Mathias Garny and Rafael A. Porto both for a very enjoyable and fruitful collaboration.

I highly appreciate that I had the possibility to carry out my PhD project at DESY. Throughout my time as a PhD student, I profited from the high level of expertise and the stimulating environment on the DESY campus. Many thanks to all members of the DESY Theory Group for the inspiring working atmosphere, and to the team of the PIER Helmholtz Graduate School as well as the PhD representative DOIT for making the campus such a lively community! Furthermore, I would like to thank Iason Baldes, Elina Fuchs, Felix Kahlhöfer, Leonardo de Lima, Ingo Rues, Matthias Schlaffer and Pedro Schwaller for sharing many enjoyable hours. Special thanks go to Bijan Chokoufe Nejad, Glàuber Carvalho Dorsch, Michael Dürr, Julian Schweizer, Benedict von Harling and Christian Weiss for proofreading the manuscript of this thesis, and to Markus Dierigl both for proofreading and for our great time as DOIT speakers. Besides, I would like to express my particular gratitude to my marvelous present and former office mates, Sebastian Bruggisser, Nayara Fonseca, Janis Kummer, Vàclav Tlapàk and Clemens Wieck, for their support in all circumstances and for the fantastic time we spent together!

Finally and foremost, I wish to thank my amazing family. I am especially grateful to my younger brothers, Lennart and Yannik, for always standing by my side. My warmest gratitude goes to my (future) parents-in-law, Brigitte and Rolf, for giving me the feeling of having a second home in Hessia. Moreover, I am more than thankful to my parents, Barbara and Holger, for their love, understanding, boundless optimism and catching joy of life, and to my boyfriend Timo for his incredible support and encouragement, for all his love and for making me so happy every day. I love you.

Eidesstattliche Erklärung

Hiermit erkläre ich an Eides statt, dass ich die vorliegende Dissertationsschrift selbst verfasst und keine anderen als die angegebenen Quellen und Hilfsmittel benutzt habe.

Hamburg, den 26. August 2016   Laura Sagunski